Lampiran 20

UTM/RMC/F/0024 (1998)

UNIVERSITI TEKNOLOGI MALAYSIA

BORANG PENGESAHAN
LAPORAN AKHIR PENYELIDIKAN

TAJUK PROJEK : PERFORMANCE INVESTIGATION OF ENERGY TRANSPORT MEDIA AS INFLUENCED BY CROP BASED PROPERTIES

Saya _____WAN MOHD NORSANI WAN NIK_____
(HURUF BESAR)

Mengaku membenarkan **Laporan Akhir Penyelidikan** ini disimpan di Perpustakaan Universiti Teknologi Malaysia dengan syarat-syarat kegunaan seperti berikut :

1. Laporan Akhir Penyelidikan ini adalah hakmilik Universiti Teknologi Malaysia.
2. Perpustakaan Universiti Teknologi Malaysia dibenarkan membuat salinan untuk tujuan rujukan sahaja.
3. Perpustakaan dibenarkan membuat penjualan salinan Laporan Akhir Penyelidikan ini bagi kategori TIDAK TERHAD.
4. * Sila tandakan (/)

☐	SULIT	(Mengandungi maklumat yang berdarjah keselamatan atau Kepentingan Malaysia seperti yang termaktub di dalam AKTA RAHSIA RASMI 1972).
☐	TERHAD	(Mengandungi maklumat TERHAD yang telah ditentukan oleh Organisasi/badan di mana penyelidikan dijalankan).
☑	TIDAK TERHAD	

TANDATANGAN KETUA PENYELIDIK

_____
Nama & Cop Ketua Penyelidik

Tarikh : _____

CATATAN : ***** *Jika Laporan Akhir Penyelidikan ini SULIT atau TERHAD, sila lampirkan surat daripada pihak berkuasa/organisasi berkenaan dengan menyatakan sekali sebab dan tempoh laporan ini perlu dikelaskan sebagai SULIT dan TERHAD.*

ABSTRACT

Todays concern of protecting the environment has encouraged the research and the use of environmental friendly products. This project initiates the experimental investigation of using palm based oil as hydraulic fluid. This research was aimed at obtaining a better understanding of short term performance and long term durability of palm based oil working as hydraulic fluid. A vane pump test rig was designed and built. The instantaneous data were recorded in a computer using an analog-to-digital data acquisition system. The rig was integrated with LabVIEW software version 6.1. Among the data stored are reservoir and return line temperatures, suction and delivery pressures, instantaneous flow rate, total flow, total running time and torque. Test rig performance running on palm oil was determined and monitored. In order to predict the oil performance in the test rig operation, bench tests were also conducted in evaluating the thermal and rheological performance of the oil. The bench tests gave useful insight to the performance of the actual test rig. Some improvement of the oil was made and tested on the hydraulic test rig. The results indicate that ageing process was significantly improved by the additived oil. The investigation also indicates that flow slip, viscous friction, and coulomb friction coefficients were affected by oil and hydraulic component conditions. Non-Newtonian behavior of the oil had been analyzed using five rheological models. It was found that Cross and Carreau rheological models provided best correlation coefficient ($R^2 > 0.999$) to the oil under investigation. The palm oil had relatively strong shear thinning behavior with flow behavior index (n) lower than 0.8 compared to mineral hydraulic oil (n>0.9). However this effect was less pronounced at high temperatures. Modified power law and generalized models were proposed to study variation of Newtonian level of the oil with temperature and shear rate. Thermal stability of the oils was also investigated using thermogravimetry analysis (TGA). Based on thermodynamic activation energy (E_a), onset temperature and acid value, the recommended treat level for F10 additive is between 1.5% to 2% (wt/wt) while for L135 additive is 1.5% (wt/wt). In the aspect of tribology, more than 60% wear occurred during the first 500 hours of operation. In general, the results show that the additived palm oil is comparable if not better than the commercial biodegradable hydraulic fluid that is derived from rapeseed oil.

ABSTRAK

Keperihatinan untuk menjaga alam sekitar telah menggalakkan penyelidikan dan penggunaan bahan mesra alam. Projek ini mengetuai penyelidikan penggunaan minyak asas sawit sebagai bendalir hidraulik. Projek ini bermatlamat untuk mendapatkan pemahaman prestasi jangka pendek dan ketahanan jangka panjang minyak asas sawit bekerja sebagai bendalir hidraulik. Rig pengujian pam ram telah direka dan dibina. Data semasa disimpan dalam komputer menerusi sistem perolehan data analog-ke-digital. Rig dilengkapkan dengan perisian LabVIEW versi 6.1. Di antara data yang disimpan adalah suhu takungan dan talian kembali, tekanan sedutan dan hantaran, kadar alir semasa, jumlah masa operasi dan daya kilas. Prestasi rig menggunakan minyak sawit ditentukan dan diawasi. Untuk menjangkakan prestasi minyak dalam rig ujian, ujian meja dijalankan untuk menilai prestasi terma dan reologi minyak. Pengujian ini memberikan maklumat berguna terhadap prestasi dalam rig sebenar. Pembaikan ke atas minyak telah dibuat dan diuji dalam rig ujian hidraulik. Keputusan menunjukkan bahawa kadar penuaan banyak diperbaiki oleh minyak beraditif. Kajian ini juga menunjukkan bahawa pekali gelincir aliran, geseran likat dan geseran coulomb dipengaruhi oleh keadaan minyak dan komponen hidraulik. Kelakuan tak-Newtonian minyak telah dianalisakan menggunakan lima model reologi. Model reologi Cross dan Carreau telah didapati memberikan pekali perkaitan terbaik (R^2>0.999) kepada minyak yang dikaji. Minyak sawit mempunyai kelakuan penipisan tegasan yang agak ketara dengan indeks kelakuan aliran (n) kurang dari 0.8 berbanding dengan minyak hidraulik mineral (n>0.9). Bagaimanapun, kesan ini kurang nyata pada suhu tinggi. Model hukum kuasa terubahsuai dan umum telah dicadangkan untuk mengkaji perubahan tahap Newtonian minyak terhadap suhu dan terikan ricih. Kestabilan terma minyak juga dikaji menggunakan analisa termogravimetri (TGA). Berdasarkan tenaga aktiviti termodinamik (E_a), suhu onset dan tahap acid, kadar campuran yang dicadangkan bagi aditif F10 adalah di antara 1.5% ke 2.0% (berat/berat), dan untuk aditif L135 adalah 1.5% (berat/berat). Dari aspek tribologi, lebih dari 60% kehausan berlaku semasa 500 jam pertama operasi. Secara umum, keputusan menunjukkan minyak sawit beraditif adalah setara, jika tidak lebih baik, dari bendalir hidraulik boleh biorosot komersial yang dihasilkan dari minyak biji sesawi.

TABLE OF CONTENTS

LIST OF TABLES

LIST OF FIGURES

LIST OF SYMBOLS

SYMBOL	DESCRIPTION	UNIT
A	Arrhenius factor	-
C_c	Coulomb friction coefficient	-
C_s	Flow slip coefficient	-
C_{st}	Turbulent slip coefficient	-
C_v	Viscous coefficient	-
D_p	Pump displacement	cm^3/rev
E_a	Activation energy	J/mol
g	Gravitational acceleration	m/s^2
H_{input}	Input power to pump	kW
k	Consistency index	$Pa.s^n$
k_H	Herschel-Bulkley consistency index	$Pa.s^n$
k_m	Modified Power Law consistency index	$Pa.s^n$
L	Load	N
m	Cross flow index	-
n	Dimensionless flow behavior index	-
n_H	Herschel-Bulkley flow behavior index	-
n_m	Modified Power Law flow behavior index	-
P	Pressure	bar, Pa
P_p	Pump pressure	bar, Pa
Q	Flow rate	m^3/s
Q_a	Actual flow rate	l/min, m^3/s
Q_R	Compressed flow rate	l/min
Q_t	Theoretical flow rate	l/min, m^3/s
R	Universal gas constant	$J\ mol^{-1}K^{-1}$

T	Temperature	^{o}C, K
T_1	Temperature at 1% weight loss	^{o}C
T_f	Final temperature	^{o}C
T_{off}	Offset temperature	^{o}C
T_{on}	Onset temperature	^{o}C
T_a	Actual torque	N.m
T_c	Coulomb torque	N.m
T_p	Pump torque	N.m
T_t	Theoretical torque	N.m
W	Power	Watt
W_p	Pump speed	rpm
v_x	Velocity of fluid in x direction	m/s
w	Specific weight	N/m³
γ	Shear rate	s^{-1}
μ	Apparent or dynamic viscosity	Pa.s, N.s/m^2, cP
μ_o	Apparent viscosity at zero shear rate	Pa.s
μ_∞	Apparent viscosity at infinite shear rate	Pa.s
η	Efficiency	%
η_{mp}	Mechanical efficiency	%
η_o	Overall efficiency	%
η_{vp}	Volumetric efficiency	%
ν	Kinematic viscosity	m²/s
π	Pi	3.142
ρ	Mass density	kg/m³
σ	Relative density	-
τ	Shear stress	N/m^2, dyne/cm^2
τ_m	Meter-Bird shear stress	N/m^2, dyne/cm^2
du/dy	Shear rate	s^{-1}

LIST OF ABBREVIATIONS

SYMBOL	DESCRIPTION
AOCS	American Oil Chemists' Society
AOM	Active oxygen method
ASTM	American Society of Testing Materials
BS	British Standard
DIN	Deutsche Standard
DSC	Differential scanning calorimetry
IP	Industrial Practice
IV	Iodine value
I/O	Input/output
KI	Potassium iodide
KOH	Potassium hydroxide
KUSTEM	Kolej Universiti Sains dan Teknologi Malaysia
MSE	Mean square error
OSI	Oil stability instrument
PO	Palm oil (RBD grade)
POME	Palm oil methyl ester
PV	Peroxide value
RBD	Refined bleached and deodorized
RO	Commercial rapeseed hydraulic oil
SEM	Scanning electron microscope
SV	Saponification value
TAN	Total acid value
TGA	Thermogravimetric analysis
USA	United States of America
VI	Virtual instrument

LIST OF APPENDICES

CHAPTER 1

INTRODUCTION

1.1 Introduction

Plant or vegetable based hydraulic fluid represents breakthrough and interesting technology and products in the aspect of being biodegradable, environmental friendly and fire resistance. Several European and American based crop oils have been researched and converted to commercial hydraulic fluid. The challenge now is to investigate another potential plant oil that is also a main source of oils and fats: Palm Oil. Even several vegetable based oils have been used as hydraulic fluid, but not much is reported on the performance of hydraulic system when this type of oil is used. Thus this project investigates and evaluates the palm oil as hydraulic fluid in actual test rig and bench tests.

1.2 Background of Research

The usage of environmentally benign product as lubricants and hydraulic fluid has many advantages. Some of the positive points are high biodegradability, non-toxic to living organism and non-pollutant to water, soil and air. The good choice for benign raw material is vegetable oil. This base material is derived from renewable resource. Vegetable oils were already considered as potential industrial fluid as early as 1900s. The early use of vegetable as industrial component includes coolant in power capacitors and electrical transformers in 1990s. However the use was merely experimental than commercial (Oommen and Claiborne, 1999). The interest to use this type of oils decreases due to several disadvantages in industrial

applications such as oxidative and thermal stability. Furthermore, these oils have less economic advantages since the price is at least twice as much as petroleum based oil. Thus later these oils were used mainly as foodstuff.

Due to increase in environmental awareness lately, research in converting vegetable based oil into non-food application has revived. The research includes the potential use of this base oil as hydraulic fluid, surfactants, solvents, drilling fluid, transmission fluid and lubricants. The base oil can also be converted to oleochemical product before being tested in engine or industrial machines (Demirbas, 2002; Antolinm *et al*., 2002; Demirbas, 2003; Rao and Mohan, 2003; da Silva *et al*., 2003). Vegetable or plant oil is considered the most likely candidate for a fully biodegradable hydraulic fluid. Plant oil is a natural resource available in abundance. It is a good power transmission media, lubricating agent and corrosion protection agent.

The hydraulic fluid is always considered as a major component in a hydraulic system. The fluid can be regarded as the system blood, an element that connects the whole parts together. The main functions of hydraulic fluid are transmitting power efficiently, lubricating moving parts and absorbing, transporting and transferring heat from heat source back to reservoir or heat exchanger.

As there are growing concerns in some regions over the use of mineral-based hydraulic oils in several types of hydraulic systems, the vegetable oil-based hydraulic oils serve as the alternative solution to the environmental problems caused by the mineral-based oils (Kassfeldt and Dave, 1997). From the viewpoint of natural environmental requirement, the vegetable oil is non-toxic and environmental benign. Other reasons for their contribution in future hydraulic fluid are:

i. Vegetable oil is of renewable resource, plentiful in supply and relatively low cost.
ii. The oil is non-toxic and biodegradable.
iii. The oil has good lubricating performance (Ohno *et al*., 1997).
iv. No significant adverse effects on unit performance characteristics (Cheng *et al*., 1994).

v. Inherently high viscosity index.

However, it is well known that vegetable oils have poor low-temperature fluidity and rapid oxidation at elevated temperatures. Besides, vegetable oils are limited to their naturally inherent viscosity (dynamic viscosity at 40ºC is around 30 to 45 cP depending on oil type) (Cheng *et al*., 1994). Some other disadvantages of the vegetable-based hydraulic oils are:

i. Unmodified or non-additive oil cannot provide adequate long-term performance.
ii. Low oxidation resistance especially at elevated temperatures.
iii. More expensive than conventional mineral oil for those with capable of meeting required temperature and oxidation performance.
iv. Cause excessive swelling of nitrite rubbers (NBR), which are generally used in hydraulic system (Ohkawa, 1979). This especially occurs due to high acidic value when the oil is oxidized.

Due to several natural advantages and disadvantages, continuous efforts are being made to further investigate and improve the vegetable based fluid (Honary, 1996; Krzan and Vizintin, 2003). Most of the vegetable oils studied are canola, soy, sunflower and crambe oils. No technical report has been published on the use of palm oil as hydraulic fluid. However, several reports have been made on the use of palm based materials such as biodiesel and lubricant (Masjuki and Maleque, 1996b, 1997; Masjuki *et al*., 1999; Maleque *et al*., 2000; Yunus *et al*., 2003; Yaacob, 2004).

1.3 Objectives

The major objectives of this work were to investigate the thermal and rheological properties of palm oil as hydraulic fluid. The work includes:

i) To design and set up an integrated laboratory scale hydraulic test rig which can measure hydraulic performance in addition to wear performance of pump.
ii) To test and analyze thermal performance and rheological behavior of palm based oils, in bench tests and when used in the built hydraulic system.
iii) To determine suitable additives to be incorporated into palm oil for improving its thermal oxidative performance.
iv) To identify and propose suitable mathematical rheological models for the oil under investigation.
v) To investigate the influence of fluid properties on major hydraulic components.

1.4 Scope and Limitation

The study is subjected to the following scopes and limitations:

i) The performance investigation for bench test was limited to thermal and rheological performance. These two areas are interrelated. The thermal stability will affect the rheological performance.
ii) The crop oil under study was limited to palm oil. Other oil data and results were also be used for comparison purposes.
iii) The work includes the design, fabrication, instrumentation, system improvement, data collection and data analysis.

iv) The performance investigations are limited to bench tests and hydraulic test rig test, where the former has to be conducted prior to the latter test. Several standard tests were performed at some accredited testing institutions.

In the present study the palm oil supply was obtained from a refinery in Pasir Gudang, Johor. Otherwise stated, the oil was obtained from local retailer. In the bench test, several heating temperatures were used. Commercial and basic additives were tested. Seven types of oils were evaluated in low temperature and pressure hydraulic test.

1.5 Significance and Contribution of Work

The major contributions of this work can be summarized as follows:

i. A suitable test rig to evaluate palm based hydraulic fluid has been designed, fabricated and set-up. The test rig as stipulated in BS and ASTM standards can only measure wear performance. The rig built in this study incorporated novel instrumentation and data acquisition system. Thus using this rig not only wear performance can be evaluated but also hydraulic performance.
ii. Various rheological models have been used for representing rheological properties of various oils. However, no such report has been made for palm oil. In this study two best models were identified to represent palm oil rheological properties. The widely used power law model was found to be less accurate to represent palm oil rheological properties. A modified rheological model was proposed to study the effect temperature on flow behavior. A generalized rheological model which can include the effect of both temperature and shear rate was also proposed.
iii. Thermal study of palm oil blends was compared and evaluated by several means. Additives to improve palm oil thermal stability have been optimized.
iv. Extensive experimental results from the hydraulic system prototype were obtained, analyzed and presented. Variation of flow and friction coefficients with several operating conditions was observed. Wear on hydraulic components was studied.

1.6 Work Flow Chart

Figure 1.1 summarizes the work flow of the research study. Initially, various hydraulic models were produced. Then the work proceed with the test rig detailed design and fabrication. Parallel to the test rig development, different grades of palm oils were evaluated in bench tests. The purpose of the bench tests is to predict the palm oil performance when used in hydraulic system.

1.7 Thesis Outline

This thesis contains five chapters. The first chapter contains a general introduction and background of the thesis. Objective, scope and importance of work are outlined. The rest of the chapters are described below.

Chapter 2 starts by quoting several researches work in hydraulic fluid, lubricant and related areas. It then provides the review of literature of the thermal-oxidation, rheological and hydraulic study performed by past researchers. Important theoretical background is included in this chapter. This chapter discusses the theory of viscosity and rheology. Viscosity and rheological models are provided.

Chapter 3 presents the research methodology and describes the equipment used in this study. Development and important features of hydraulic test rig are described. This chapter also includes computer programs used in analyzing the data.

Chapter 4 presents the bench and hydraulic test rig data. This includes the basic properties of palm oil blends, rheological and thermal performances obtained from both bench tests and hydraulic test rig, and test rig performances when palm oils were used in continuous and intermittent operation. It then analyzes and discusses all the results obtained.

Finally, Chapter 5 is the concluding chapter. This chapter summarizes and concludes the research that has been carried out in this study. Future work is suggested at the end of this chapter.

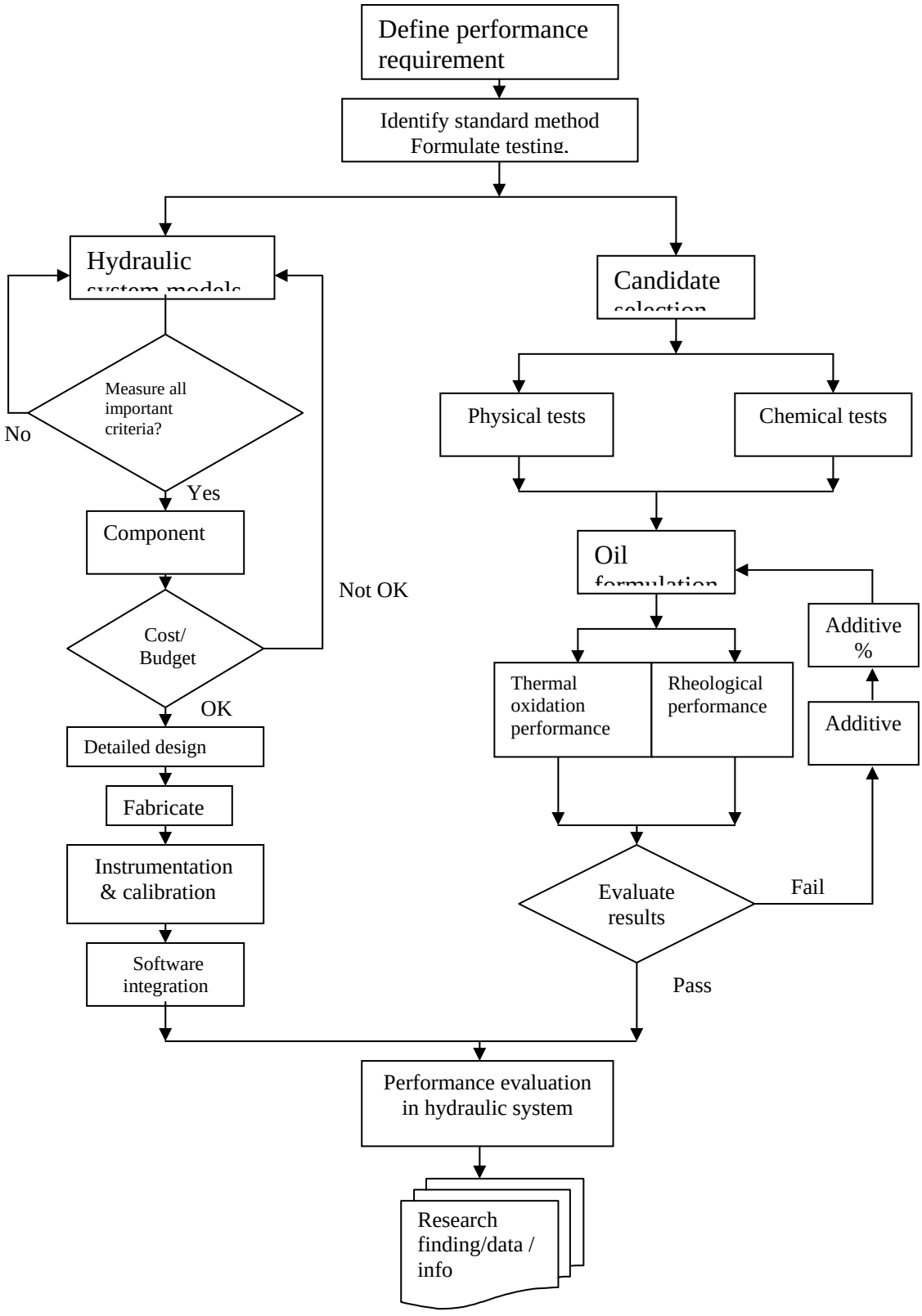

Figure 1.1: Work flow chart.

CHAPTER 2

LITERATURE AND THEORETICAL BACKGROUND

2.1 Introduction

Due to problems of petroleum based fluid such as toxicity, water and land pollutant, fire risk, non-biodegradability and limited resource there is a unique opportunity to produce new environmental acceptable lubricants derived from natural ester like vegetable oils. It is reported that world production of 17 major oils and fat are over 100 billion tones and out of this 79% are from vegetable oils (Hamm and Hamilton, 2000).

Research, development and application of vegetable based oil in industrial and automotive sectors are rapidly increasing. The attractive part of vegetable oils is they are natural, non-toxic, biodegradable, relatively non-polluting and derived from renewable raw material (Wilson, 1998). During the last decade due to strict government and environmental regulations, there has been a constant demand for environmentally friendly lubricants (Rhee, 1996). Most of lubricants originate from petroleum stock, which is toxic to environment and difficult to dispose. Vegetable oils are preferred over synthetic and mineral based fluids because they are renewable resources and cheaper. Vegetable oils with high oleic content are considered to be potential candidates to substitute conventional mineral oil based lubricating oils and synthetic esters (Randles and Wright, 1992; Asadauskas *et al*., 1996).

Most of the properties of vegetable oils are similar to commercial mineral hydraulic fluids. However, according to Randles and Wright (1992) and Battersby *et al*. (1998), vegetable oils as lubricants are preferred because they are biodegradable

and non-toxic, unlike mineral based oil. Basically vegetable oils have lower volatility than mineral oil (low evaporation and high flash point), higher bulk modulus (stiff hydraulic system), better fire resistance and better additives solvency (Wilson, 1998). Vegetable oils have very low volatility due to the high molecular weight of the triacylcerol molecule. In addition, vegetable oils have high solubilizing power for polar contaminants and additive molecules (Adhvaryu *et al*., 2005).

Vegetable oils when used as industrial or automotive applications show excellent lubricity. It has better inherent lubricity (good boundary lubricating properties), higher viscosity index (relatively small change in viscosity with temperature) compared to petroleum oil (Sivasankaran *et al*., 1988). These advantages are mainly due to the polar ester structure and high molecular weight in comparison to all non-polar petroleum derive hydrocarbon. Polar ester groups are able to adhere to metal surfaces, and therefore, possess good boundary lubrication properties (Bisht *et al.*, 1993).

Nevertheless, vegetable oils have been slow to gain wide acceptance in engineering application, mainly it is because of their variable quality, higher production cost when compare to mineral oils and significant performance limitation. It has low thermal and oxidative stability (Asadauskas *et al*., 1996) and thus has limited resistance to oxidation in storage and in service. The low hydrolytic stability renders the oil to hydrolysis susceptibility in the presence of water to produce corrosive acidic breakdown products. The oil also has poor low temperature behavior and high pour point and has some problem with component compatibility, tendency to clog filters, poor resistance to foaming, causing swelling and softening of seals (Wilson, 1998).

Polar oxy compounds produced during oxidation process result in insoluble deposits and increases in oil acidity and viscosity. The presence of ester functionality renders the vegetable oil to further hydrolytic breakdown (Rhodes *et al*., 1995). Ohkawa *et al*. (1995) shows that aged vegetable oils have poor corrosion protection.

Due to the above weaknesses, only small portion of vegetable oil is converted into lubricant. According to Sraj *et al*. (2000), only 2% of vegetable oil is used for

energy production and transportation in today market while mineral based oil has 83% share. The balance is synthetic based lubricant. However, the prognosis for the next ten years foresees that hydraulic fluids based on vegetable oils could reach about 8% of market share.

2.2 Research in Related Areas

Large amount of money and great effort have been put on investigating the use of vegetable oil-diesel blends and vegetable oil esters as biofuel (Ziejewski and Kaufman, 1983; Mittelbach and Trillhart, 1988; Hermmerlein *et al*., 1991; Altin *et al*., 2001; Kalam and Masjuki, 2002). Much of the work involves esterification of the oil while others involve in testing the fuel in engines. Other efforts are involved in vegetable based-lubricant and hydraulic fluid.

Stoffa, J.V. (1995) has patented functional fluids from vegetable oil triglyceride. The base oil comprises of genetically modified sunflower, rapeseed, lesquerella or meadowform oil. However, Gapinski *et al*. (1994) and Becker and Knorr (1996) pointed out that vegetable oils have poor oxidative stability. This is primarily due to the presence of bis allylic protons. The vegetable oils are also susceptible to radical attack and subsequently undergo oxidative degradation to form polar oxy compounds.

Joint research work between University of Delaware, University of Illinois and DuPont Company has developed a high oleic soybean oil-based hydraulic fluid (Glancey *et al*, 1996). The research suggests that the development of competitive vegetable oil-based industrial products should involve a combination approach of additives as well as alterations of fatty acid composition via genetic modifications. Several additives should be used to enhance oxidative stability and anti-wear characteristics.

According to Carnes (2004), North American Caterpillar has teamed up with Agricultural Research Services National Center developing and testing several new

fluids such as biolubricant, hydraulic fluid and other industrial applications derived from vegetable oils including soybean, corn and sunflower.

2.2.1 Lubricants

The main and general function of a lubricant is to lubricate moving parts in order to reduce friction and wear. In general, lubricants can be categorized as liquid, semisolid and solid lubricant. Majority of the lubricants fall under liquid category, either oil based or water based (Booser, 1994). Bearing, hydraulic and engine oils are examples of liquid lubricants. Synthetic lubricant researchers, Yao (1997) used sodium acetylacetonate while Huang *et al*. (2000) used sulfurone-benzothiazole methyl ester as their synthetic additives. However synthetic lubricants are expensive and have high toxicity (Adhvaryu, 2005). At present majority of the liquid lubricants are petroleum based. However, special machines require special lubricants. For example if the machine has high external leakage or come into contact with food or drinking water source, the machine requires high degree of biodegradable lubricant.

According to Glaeser *et al*. (1992), the most worthy liquid lubricant is the engine oil. This is due to the regular change of the oil as recommended by the vehicle manufacturer. If wear occurs due to improper lubrication, such as in automotive industry, the cost can be estimated to be more than $40 billion annually. Due to this factor, research in engine oil is tremendous (Godfrey, 1991; Tomita *et al*., 1995; Bartz, 1998; Gautam *et al*., 1999; Priest and Taylor, 2000; Cerny *et al*., 2001; Weller and Perez, 2001). There is increasing interest to investigate biodegradable and environmentally friendly engine oils (Sivasankaran *et al.*, 1988). Basic research involves studying tribological aspects of this lubricant.

Recently there is increasing interest to investigate and produce synthetic lubricant from epoxidized vegetable oil. Adhvaryu *et al*. (2005) come up with synthetic approach for chemical modification of vegetable oils to improve their thermo-oxidative and low-temperature stability. The bio-fluids from this chemical modification offer great potential for the development of industrial fluid such as hydraulic fluid and engine oil.

Great interest in engine oil research is also available in Malaysia. Most of the work done was by Masjuki *et al*.. The main interest is in palm based lubricants (Masjuki and Maleque, 1996b; Masjuki *et al*., 1999; Maleque *et al.*, 2000). The research on using palm based lubricant was also conducted by Castrol at Paddington, United Kingdom (Surina, 1995). An European patent has been produced based on this research. The company produces motorcycle 2T oil but the research is not made known to others. Researchers in Universiti Putra Malaysia have produced lubricants that can reduce wear in engine up to 15% (Yaacob, 2004).

2.2.2 Hydraulic Fluid

Hydraulic fluid can be regarded as the 'blood' for hydraulic systems. As the blood in human body, the fluid travels to all parts in hydraulic systems. The functions of hydraulic fluid can be outlined as follows (Busch and Baske, 1993):

- As media for power transmission (power transfer efficiency)
- Lubricates the moving parts (lubricity)
- Work as cooling media (heat capacity)
- Transport of contaminants (compatibility, stability)

However, contrary to human blood, the fluid degrades with time. The degradation is accelerated due to a number of factors. Thus the fluid performance for the above four functions decreases. The performance decrease depends on types of hydraulic fluid. So it is a challenge for power hydraulic researcher and oil producer to formulate new and better hydraulic fluid to meet more stringent regulation and demanding usage. At present there are several types of hydraulic fluid used in hydraulic systems. The most widely used is petroleum-based fluid which cater around 80% of the consumption (Pinches and Ashby, 1989). Petroleum is nonrenewable resource. For instance, with the current findings, Malaysia oil reserve can last for another 20 years. Thus the consumption rate of the oil should be reduced and alternatives to the petroleum based oil must be searched.

It has been estimated that European Economic Community (EEC) countries are producing approximately 400 million liters of hydraulic fluid a year. This fluid at the end of its operational life time has to be disposed. This mineral based oil when exposed can pose serious potential damage to the environment. It is worth to stress that the additives used in present lubricant not only pose danger to the environment but also poisonous if the oil leaks out from system and gets into our water drinking systems. Improper disposal, even if it is incidental, may be the source of large penalties or even litigations.

Van der Waal and Kenbeek (1993) point out that there is a need for the hydraulic fluid supplier and user to think of a new hydraulic fluid that is less hazardous to the environment. Considerable effort has been made in turning vegetable oils into potential hydraulic fluid. Different researchers research different crops as hydraulic fluid. Lazzeri *et al*. (1997) studied the use of crambe oil as hydraulic oil and quenchant. Honary (1998) studied soybean oil in several bench tests and hydraulic systems. Willing (2001) dealt with several plant oils, fats and tallow.

In Finland, researchers at Institute of Hydraulics, Tempere University of Technology studied the use of vegetable oil as hydraulic fluid using two units of hydraulic system (Lappalainen and Jokinen, 1984). Other institutions are Lulea University of Sweden (Kassfeldt and Dave, 1997) and Technische Universitat Hamburg, Germany (Feldmann and Kessler (1998)). The most common vegetable oils that have been researched for hydraulic fluid are canola oil or rapeseed oil, soybean oil and high oleic sunflower oil. Brief results of the researches are cited respectively in corresponding papers. The advantage of vegetable oil over water based fluid as hydraulic fluid is that the vegetable oil has similar viscosity as mineral oil. Researchers in Engineering Department of Maine studied the use of animal oil as hydraulic fluid (Christensen and Bimbo, 1996).

2.3 Oil Thermal Oxidation

Thermal oxidation is the major concern that limits the use of vegetable oils as lubricating fluid. Thermal oxidation leads to polymerisation and degradation. Polymerisation increases the viscosity that reduces the functionality of lubricating fluids. Further degradation leads to breakdown products that are volatile, corrosive and diminish the structure and properties of the lubricant. Several alternatives are available to improve the vegetable oil thermal oxidation stability: genetic modification, chemical processing and use of additives (Kodali, 2002).

Additives were used to retard the degradation of thermal degradation (Yao, 1997; El-Qurashi and Ali, 1997). Some additives interfere with free radicals by a chain breaking mechanism during initiation or propagation stage of oxidation. Butylated hydroxyanisole (BHA), butylated hydroxyl toluene (BHT) and tertiary butyl hydroquinone (TBHQ) are the examples of this additive type. Thus the presence of additive in oil can improve or lengthen the oil life time.

The factors that affect the lubricant stability are oxygen, contamination with water and corrosive acids, which limit the useful life of lubricant. Besides that, oxidation is also accelerated by increasing the exposed temperature. All lubricating oils react with oxygen in air, eventually forming acids or sludge products. These products could cause surface corrosion or blocking of component clearance (Maleque *et al*., 2000).

Oxidation process is the most important reaction of oils resulting in increased acidity, corrosion, viscosity and volatility when used as lubricant based oils. Oxidative stability depends on the presence of unsaturated fatty acids in the triacyglycerol molecule due to the double bond (C=C) in fatty acids (Adhvaryu *et al*, 2000). For example, the lower the unsaturation the better the oxidative stability, but with higher pour point.

Reaction of the double bond includes hydrogen abstraction, addition reaction, fragmentation, rearrangement, disproportionate reaction and polymerisation. Unsaturated fatty acyl chains react with molecular oxygen to form free radical that

lead to polymerisation and fragmentation. The rate of oxidation depends on the degree of unsaturation of fatty acyl chain as shown in Figure 2.1.

Oil oxidation can occur in three stages which includes initiation, propagation and termination (Figure 2.2). Hydroperoxides are primary products of oxidation. Due to their unstable nature, the hydroperoxides will break down and produce free radicals, aldehydes, ketones and alcohols (Adhvaryu *et al*., 1999; Erhan and Asadauskas, 2000; Adhvaryu and Erhan, 2002; Sharma and Stipanovic, 2003; Gomez-Rico *et al*., 2003; Rehman *et al*., 2004). At this point decomposition compounds can undergo further oxidation to produce carboxylic acids or they may polymerize. When the carboxylic acid is produced, the acid number of the oil is increased (Figure 2.3). Thus one of the tests that can be used to study the oil condition after heating is the total acid number test. If the oil polymerize, then viscosity test can be used to check the oil deterioration condition.

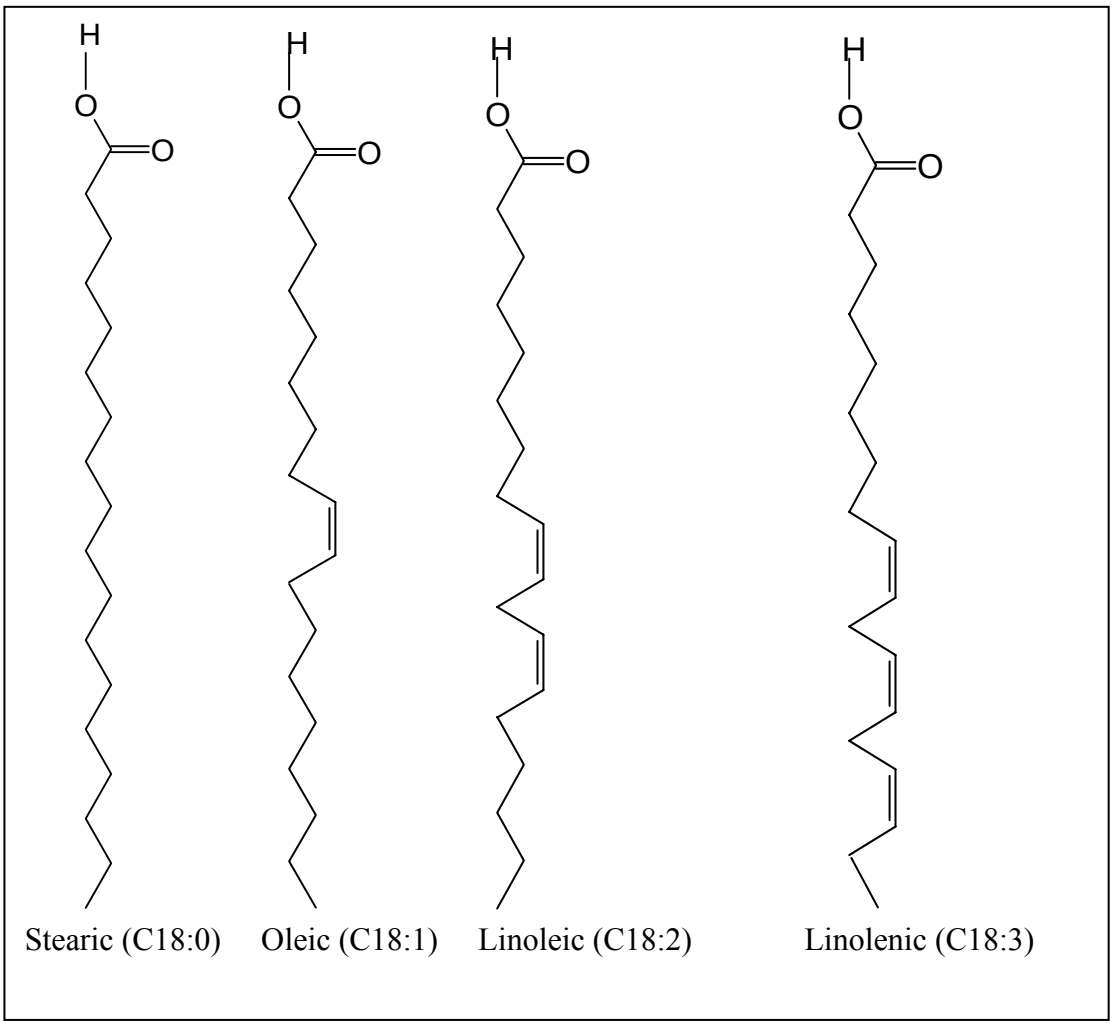

Figure 2.1: Fatty acids – rate of oxidation (Kodali, 2002).

Initiation	:	$RH \rightarrow R\bullet + H\bullet$	
Propagation	:	$R\bullet + O_2 \rightarrow ROO\bullet$	(fast reaction)
		$RO_2\bullet + RH \rightarrow ROOH + R\bullet$	(rate-determining step)
		$ROOH \rightarrow RO\bullet + \bullet OH$	
		$RO\bullet + RH \rightarrow ROH + R\bullet$	
		$\bullet OH + RH \rightarrow OH2 + R\bullet$	
Termination	:	$ROO\bullet + ROO\bullet \rightarrow O_2 + ROOR$	
		$ROO\bullet + R\bullet \rightarrow ROOR$	
		$R\bullet + R\bullet \rightarrow R\text{–}R$	

Figure 2.2: Initiation, propagation and termination of triglycerides oxidation process (Solomons and Fryhle, 2000).

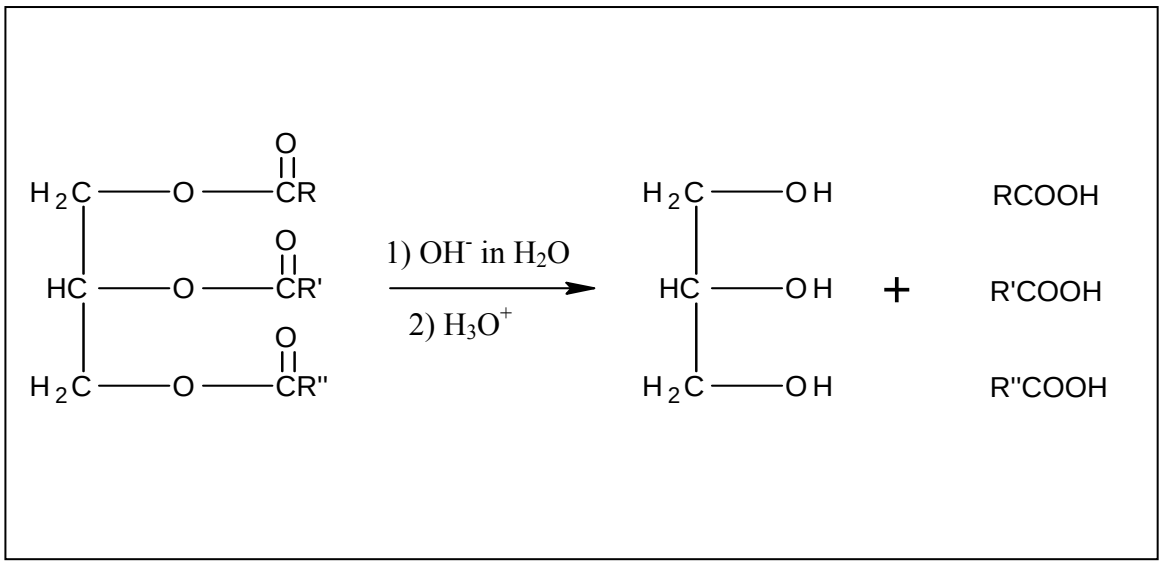

Figure 2.3: The hydrolysis of oil produces glycerols and fatty acids (Solomons and Fryhle, 2000).

2.3.1 Oil Thermal Degradation Tests in Oil and Fat Industries

Oil will oxidize when exposed to various environmental conditions, especially heat and air. The oxidative product can influence further oil degradation process (catalyze the process). Thus the oxidation status of the oil has to be monitored or checked. In oil and fat industries, there are several methods to determine the oil condition and to determine the oil thermal and oxidative stability.

The methods used to determine the rate at which the oxidation process advances are related to the measurement of the concentration of primary and secondary oxidation products. Rate of oxygen consumed during this process also can be used as an indicator for oxidation level. Some of the indicators that can be used to determine rate of oxidation are PV which measures hydroperoxide concentration and TAN which measures acid level. Among other tests are Schall oven, active oxygen method (AOM), oxidative stability indeed (OSI), thermal gravimetric analysis (TGA) and differential scanning calorimetry (DSC).

2.3.1.1 Schaal Oven Test

This test measures the oil stability both physically and chemically. 100g oil sample is sealed in a bottle and placed in a dry compartment at 65^{o}C. The sample is monitored periodically. The induction time is indicated by first sign of rancid odor and PV increase. This method is labor intensive and time consuming.

2.3.1.2 Active Oxygen Method (AOM)

This method measures the oil stability in terms of time (in hour) required for a sample to reach a predetermined peroxide value (PV 100 meq/kg) under specific condition. 5 g oil sample is bubbled with dried air at a flow rate of 140 ml/min at a temperature of 96.7^{o}C. Similar to Schaal oven test, the progress of oxidation is monitored periodically in terms of PV.

2.3.1.3 Oil Stability Instrument (OSI)

Rancimat method is a widely used method in evaluating oxidative stability of vegetable oil. Induction time is the indicator for oil oxidative stability. OSI is an improved version of Rancimat method. This method measures the conductivity in deionized water as it increases due to the absorption of volatile acids and the decomposed products of oil oxidation. Increasing conductivity is an indication of peroxide breakdown that occurs at the same time as peroxide value increases (AOCS, 1993).

Tan *et al*. (2002) had studied the comparative between the differential scanning calorimetry (DSC) and oxidative stability index (OSI) methods to determine the oxidative study of twelve different edible oils. The OSI instrument temperature was set at 110°C while the DSC was set at four different temperatures (110, 120, 130, 140 ºC) and air was passed through the sample enclosure at 50 ml/min. The samples used were 5.0 $\pm$ 0.5 mg. They conclude that DSC provides a convenient way to determine the oxidative stability of various edible oils.

Besides that, Tan and Che Man (1999, 2002) also used the DSC to monitor the oxidation of heated oils. The DSC method was based on the cooling thermogram of oil samples at a scanning rate of 1ºC/min from –30 to –85ºC. Besides DSC method the deterioration of heated oils was also quantified by other chemical methods. They were total polar compounds, iodine value, free fatty acids, anisidine value, peroxide value and ratio of linoleic acid/palmitic acid (C18:2/C16:0). They conclude that there is good correlation between the DSC method an other standard chemical methods. This result is as same as the literature studied by Tan *et al*. (2002) in their research on the effects of microwave heating on the quality characteristic and thermal properties of RBD palm olein.

Kinetic parameter can be determined by using TGA and DSC curves. Adhvaryu *et al.* (2000) studied the oxidative stability of vegetable oils derived from genetically modified vegetable oils using pressure DSC and found that the complexity of vegetable oil oxidation was primary due to the involvement of different structural parameter in the fatty acid chain. Statistical methods developed on the start and onset temperature and kinetic parameter like activation energy (E_a) can be used as predictive tools for quick assessment of vegetable oil oxidation.

2.3.2 ASTM Oil Thermal Oxidation Tests

ASTM, BS, IP and DIN have established several standard methods in assessing oil performance. Different tests were designed to evaluate particular performance parameter. The most relevant testing standards in evaluating hydraulic fluid and lubricating oils according to ASTM are:

- Oxidation characteristics of inhibited mineral oils - ASTM D943.

- Thermal stability of hydraulic oils - ASTM D2070.
- Thermal stability of hydraulic fluids - ASTM D2160.
- Hydrolytic stability of hydraulic fluids - ASTM D2619.
- Oxidation characteristics of extreme pressure lubrication oils - ASTM D2893.
- Oxidation stability of steam turbine oils by rotating bomb (RBOT) - ASTM D2272.
- Oxidation stability of distillate fuel oil/inhibited mineral oils - ASTM D2274.
- Oxidation stability of gasoline automotive engine oils by thin-film oxygen uptake (TFOUT) - ASTM D4742.
- Corrosiveness and oxidation stability of hydraulic oils - ASTM D4636.
- Determination of the ageing behaviour of steam turbine oils and hydraulic oils (TOST) - ASTM D4310.
- Preliminary examination of hydraulic fluid - ASTM D2271.
- Indicating wear characteristics of petroleum and non-petroleum hydraulic fluids in a constant volume vane pump - ASTM D2882.

Table 2.1 summarizes and compares some of the standard methods mentioned above. The suggested heating temperature, heating time, sample amount and experimental condition are compared. This comparison was the basis for the condition made in this study.

Only few of these standard methods have established correlations to actual or field test results. ASTM D943 is the most standard referred by hydraulic fluid manufacturer.

Table 2.1: ASTM standards concerning oil stability test

Test code	Heating temperature (^{o}C)	Heating time (hour)	Sample volume (ml)	Note
ASTM D943	95	1000	-	Water, Fe and Cu as catalyst Indicator: time to TAN 2 mg KOH/g
ASTM D2070	135	168	200	Convection oven Cu and iron as catalyst Indicator: weight of sludge
ASTM D2160	260-316	6	20	Glass container No catalyst Indicator: visual, TAN, viscosity
ASTM D2619	93	48	75g	Oven Indicator: viscosity and TAN change
ASTM D2893	95	312	300	Tube container No catalyst Indicator: precipitation, viscosity Dry air 10 l/hr
ASTM D2272	150	Time to reach pressure drop	50	Oil bath No catalyst Indicator: pressure drop Oxygen at 90 psi
ASTM D2274	95	16	350	Heating bath or hot plate Oxygen bubble at 3 l/hr Indicator: insolubles filtered
ASTM D2271	70	1000	18 liter	Pressure 70 bar Pump speed 1200 rpm Indicator: cam ring and vane weight loss
ASTM D2882	65.6	100	11.4 liter	Pressure 140 bar Pump speed 1200 rpm Indicator: cam ring and vane weight loss

2.3.3 TGA Activation Energy

Thermogravimetric data is used in characterizing the oil as well as in investigating the thermodynamics and kinetics of the reaction and transitions that

results from the application to oil samples. Currently several methods were available in the literature that can be used to calculate kinetic parameters (Jaber and Probert, 2000).

The rate of conversion, dx/dt, for the oil conversion is expressed by

$$\frac{dx}{dt} = k\ \mathrm{f}(x) = k(1\text{-}x)^n \qquad 2.1$$

where n is the order of reaction, k is constant and x is the extend of conversion or fractional weight loss and is given by

$$x = \frac{w_o - w_t}{w_o - w_\infty}$$

where w_o, w_t, w_∞ are the original, current and final weights (mg), respectively. For $n = 1$, Equation 2.1 is simplified to

$$\frac{dx}{dt} = k(1\text{-}x)\ .$$

For the non-isothermal case, the above equation can be further modified to

$$\frac{dx}{dT} . \frac{dT}{dt} = k(1\text{-}x) \qquad 2.2$$

where $\frac{dT}{dt}$ is the heating rate B.

According to Arrhenius relationship, the reaction rate constant k in Equation 2.2 can be expressed as

$$k = A \exp(-E_a/RT) \qquad 2.3$$

2.4 Theory of Viscosity and Rheology

Viscosity is an important parameter for fluid rheology. This fundamental knowledge and data are vital to study the performance of palm oil in hydraulic system or can be the guide for designing future palm based oil lubricant. Sufficient viscosity is required to provide proper lubrication to moving parts in hydraulic system such as in pump, actuators and valves. Too high viscosity will reduce

mechanical efficiency while too low viscosity will reduce volumetric efficiency of hydraulic system. In other words, improper lubrication can affect system performance and reliability.

Variation of physical properties with temperature can affect the heat and power transfer considerably. For liquids, temperature dependence viscosity is of major importance (Kreith and Bohn, 1993). In this study it would be expected that the effect of lubrication would affect the pump and system overall efficiency. According to Thoma and Wilson theory (discussed in Section 2.71 and 2.7.2), the volumetric efficiency is directly related to oil viscosity. Since some hydraulic system is operating in wide range of temperature, the effect of temperature on oil viscosity will be studied first.

Viscosity is the measure of fluid resistance to flow. It is one of the rheological parameters that describe the flow properties of some transport fluids such as bio oils. Bio oil is the oil derived from animal or vegetable and known also as agriculturally derived products (Goodrum *et al*., 2003). The viscosity is related to the energy dissipated during flow primarily due to sliding activities in pipes and expansion and contraction at control valves, pumps and actuators.

Viscosity is defined as the ratio of shear stress and shear rate in a fluid. For a Newtonian fluid, shear stress τ is related to shear rate du/dy and apparent or dynamic viscosity,

$$\tau = \mu \, du/dy \qquad 2.4$$

Oil viscosity is an important parameter that influences hydrodynamic and elastohydrodynamic lubrication in hydraulic system. The oil viscosity will affect the shearing level in components that have relative motions and all restriction in a hydraulic system. Based on viscosity behavior, the oil can be categorized either Newtonian or non-Newtonian fluid. If the viscosity of the oil decreases with increasing shear rate, it is categorized as non-Newtonian (Goodrum *et al*., 2003). The non-Newtonian behavior is common in oils and some polymers (Munson *et al*., 2002).

2.4.1 Viscosity Temperature Dependency

The effect of temperature on the viscosity of palm oil must be known as in most hydraulic system the oil will be subjected to a range of temperatures. The relationship between viscosity and hydraulic performance is given by Equations 2.38b and 2.39b.The effect will be more significant if the hydraulic system uses a low viscosity index fluid. In this section, the common relationships between temperature and viscosity are presented. The symbols and units used may differ and best be referred in corresponding references.

Published viscosities at different temperatures, have limited value when viscosities are needed at temperatures other than those published ones (Fisher, 1998). Beside published data, equations are needed to represent the experimental data.

Several estimation methods have been proposed to represent the temperature effect on the oil viscosity at atmospheric pressure. Most of the methods are empirical in nature as no fundamental theory exists for the transport phenomena of oils. Among the famous viscosity-temperature law is the Vogel-Fulcher relationship (Cameron, 1981; Coy, 1998)

$$\mu = \mu_o \exp [B/(T-T_\infty)] \qquad 2.5$$

where μ_o (mPa.s) and B (K) are the fluid constants, T (K) is the oil absolute temperature and T_∞ (K) is the temperature at which viscosity would become infinite.

For most liquids at temperatures below the normal boiling point, the plot of ln μ versus 1/T or ln μ versus ln T is approximately linear (Noureddini *et al*., 1992). One of the proposed equations is Arrhenius type relation (Igwe, 2004):

$$\mu = Ae^{\frac{E_a}{RT}} \qquad 2.6$$

where μ is the dynamic viscosity (mPa s), A is a pre-exponential constant or known also as Arrhenius factor, R is a constant (8.314 J $mol^{-1}K^{-1}$), T is the absolute temperature (K) and E_a is the activity or viscous activation energy (J/mol). This equation can be linearized into the following forms:

$$\ln \mu = \ln A + \frac{E_a}{RT} \quad 2.7$$

The Arrhenius relationship has been used by many recent researchers (Vlad and Oprea, 2001; Barreto *et al*., 2003; Perez-Alonso *et al*., 2004; Ahmed *et al*., 2004) to describe the temperature dependency of rheological parameters. Equation 2.4 is in equivalent to the following Andrade's equation, where ln A= A_1 and E_a/R=B,

$$\ln \mu = A_1 + \frac{B}{T}. \quad 2.8$$

This Andrade's equation can be further modified from a first-order to higher-order polynomial in 1/T to give a better accuracy:

$$\ln \mu = A + \frac{B}{T} + \frac{C}{T^2} + \frac{D}{T^3} + \frac{E}{T^4} + \ ..... \quad 2.9$$

where A, B, C, D, E… are the liquid specific parameters.

Equation 2.8 (Andrade equation) is similar to Vogel equation (2.10). Several researchers use Vogel type equation to describe the effect of temperature on oil rheology (Coy, 1998). Vogel's equation has been further modified by Noureddini *et al*. (1992) and Coy (1998) to the term as shown below:

$$\ln \mu = A + \frac{B}{(C_1 + T)} \quad 2.10$$

where C_1 is a constant. Other logarithmic equation to correlate viscosity with temperature was used by Cameron (Cameron, 1981):

$$\log \mu = A + \frac{B}{T} + C_2 T + D_1 T^2 \quad 2.11$$

where C_2 and D_1 are constants. The above relations (Equations 2.7 - 2.10) show that most of the proposed models suggest the logarithm of viscosity is inversely proportional to the absolute temperature of the fluid. On the other hand, McCabe *et al*. (2001) and other researchers use Walther equation to describe the viscosity-temperature dependence of lubricants:

$$\log (\log \mu + c) = A + B \log T \quad 2.12$$

where A, B and c are Walther equation's constants. The Walther model is a two parameter correlation that is used widely for lubricating oils of moderate operating viscosity. The required properties are viscosities at two temperatures, normally at 40 and 100^{o}C. The variation of viscosity over temperature range of most mineral oils can be represented by a straight line using Walther equation. However this model cannot predict the viscosity data for several oils such as polymer-blended and synthetic oils.

Viscosity behavior is similar to a "rate-controlled process". It shows the same temperature dependence as other processes (such as reaction rate process). Thus Arrhenius dependence on temperature (Equation 2.6) can be used to determine viscous activation energy. The E_a, viscosity activation energy, is a characteristic of a flow and indicates the amount of energy necessary to move the fluid.

This Arrhenius type equation is used to be applied to Newtonian fluids only. However nowadays this Arrhenius equation has been widely used to explain rheological property dependence on temperature over limited temperature range.

2.4.2 Newtonian and non-Newtonian Fluid

Fluid is defined as a substance that does not resist shear. It will keep on flowing or changing shape if shear or force is applied. Fluid consists of liquid and gas (Figure 2.4). Liquid can be categorized as viscous fluid and inviscid fluid. Inviscid means that the liquid does not pose viscosity or no internal friction. Viscous liquid falls either Newtonian or non-Newtonian. By definition Newtonian fluid is the fluid of which shear stress is proportional to shear rate (Figure 2.5), as indicated in Equation 2.4. According to the Newton's law of viscosity, the diagram relating shear stress and shear rate of a Newtonian is a straight line through the origin. The slope of this line is equal to the viscosity of the fluid. The flow index (n), the indication of Newtonian level, for this type of fluid is unity.

Most of the fluids used in industry are non-Newtonian fluid and do not follow Newtonian equation (Equation 2.4). They are included in pseudoplastic, bingham,

dilatant, rheopectic or thixotropic categories. Irrespective of categories the viscosity of each fluid is a function of pressure, temperature, shear, base material, type and composition of mixture (Dexheimer *et al*., 2001) but the temperature plays the most important role. In general, viscosity of oil decreases with increasing operating temperature.

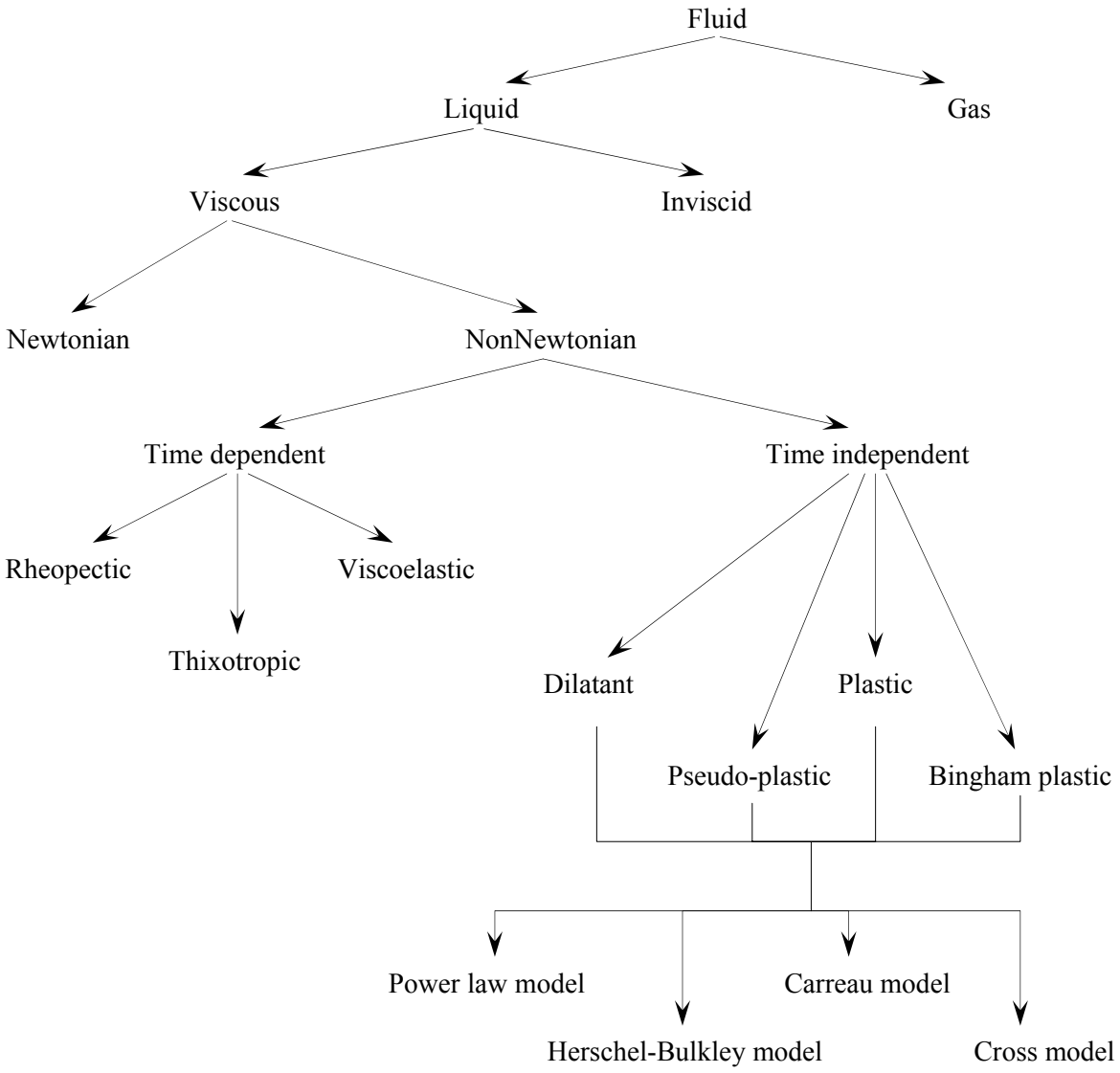

Figure 2.4: Fluid classification.

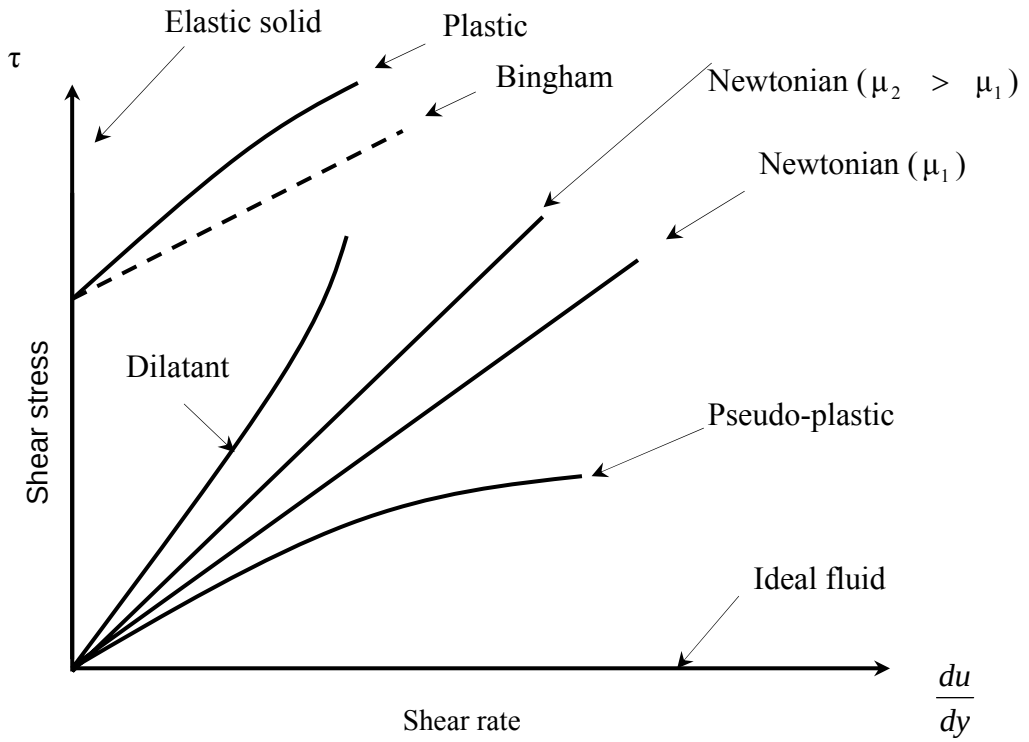

Figure 2.5: Variation of shear stress with shear rate.

2.5 Rheology Study of Palm Oil and Mineral Oil

This project investigates the transport performance of vegetable oil in hydraulic system. Since the 'crude' palm oil is still in monograde form, variation of oil with temperature and shear is crucial to be investigated. In this project, it was found that the palm oil used behaves as non-Newtonian material in low shear region.

In order to understand the influence of fluid property on hydraulic system performance, it is necessary to understand the fluid rheology. The chemical and mechanical properties of intermolecular interaction have to be well studied and understood. Some basic property studies of palm oil and its relation to the design of process equipment had been studied (Morad, 1995). It is well known that pressurized lubricant rheology at certain shear rates has a major influence on power loss. This power loss occurs at contacts of pumps, valves and pipings.

The use of rheology to evaluate the performance characteristics of lubricating oil is nothing new. However, the use of rheology for plant or vegetable oil analysis is

scarcely found in the literature. The study of the dependence of η on γ of vegetable oil was scarce except by Goodrum *et al*. (2003). This is due to their low viscosity. Most of the time, for the purpose of simplicity, the vegetable oil was assumed to be Newtonian.

Since no investigation is available to relate palm oil or other vegetable oil viscosity with power law and other models, this study pioneers the investigation of palm oil non-Newtonian behavior, even though the Newtonian approximation can be justified for many applications.

In order to understand and control the hydraulic system performance, this research investigates of how the viscometric property changes under different shear rates and temperatures. In real application, movement of fluid will involve heat generation and stress to both fluid hydraulic system components. Thus rheological study is necessary to investigate the fluid behaviors at various operating conditions.

2.5.1 Viscosity Shear Dependency - Rheological Modeling

All fluids for which the shear stress-shear rate curve is not linear through the origin (Figure 2.5) at a given temperature and pressure are said to be non-Newtonian. The viscous properties of fluids without a yield stress are described by curves type. If the shear stress increases less than in proportion to the shear rate, the fluid is called pseudoplastic or shear thinning. On the other hand, if the shear stress increases more than in proportion to the shear rate then it is a dilatant or shear thickening fluid. The simplest model for Newtonian, pseudoplastic or dilatant fluid is power law model.

Sometimes more than one model may be necessary to present the rheological data. To this date there are several models, which mostly empirical formula, that describe the viscosity of fluid with shear. Some of the relationships are valid only for certain applications since they can be used for a limited range of shear rate. Furthermore, model parameters are affected by other state variables, such as composition and temperature.

2.5.2 Ostwald de-Waele Model

The pioneer model for shear dependence of viscosity is the famous Ostwald-de Waele model which was proposed in 1925. This model is known better as Power Law model. It is used extensively in handling most engineering applications (Bair and Qureshi, 2003; Li and Zhang, 2003). It is used to describe both shear-thickening and shear-thinning fluids. This model has only two parameters, *n* and *k*. Basic relationship of power law,

$$\tau = k\,\mu^{n} \qquad 2.13$$

where *n* is the power law index or flow behavior index. *n* is a dimensionless exponent and reflects the closeness to Newtonian flow. *k* is the consistency index ($Pa.s^n$) and τ is the shear stress at a shear rate of 1.0 s^{-1}. In this work, the power law index and consistency index are obtained using a computer program. The computer program, Statistical non-Linear Fit of Mathematica 4.2 provides statistically best values of *k* and *n*.

Combining Equations 2.13 and 2.4, the power law can be written in terms of absolute viscosity (μ) and shear rate (γ)

$$\mu = k\,\gamma^{n}/\gamma. \qquad 2.14$$

Thus it can be shown that, taken the ratio of shear stress to rate of strain, an expression for the absolute viscosity can be shown as

$$\mu = k\,\gamma^{n-1} \qquad 2.15$$

According to Equation 2.15, the viscosity decreases with increasing of shear rate for $n<1$ (shear thinning fluids) and increases with increasing shear rate for $n>1$ (shear thickening fluids). The equation for power law can be linearized into the following forms (ln or log):

$$\log \mu = \log k + (n-1)\log \gamma \qquad 2.16$$

The disadvantage of power law model is that it does not explain the low shear and high shear rate viscosity constant. Several researchers such as Sharman *et al*. (1978), Chauvetaau (1982) and Bewersdorff and Singh (1988) improved the

Ostwald-de Waele power law model to suit aqueous, polymer and gum material applications.

2.5.3 Cross Model

Two famous model functions that relate viscosity of non-Newtonian fluid and shear are given by Cross model and Carreau model. In general, the Cross model is widely used in Europe while the Carreau model in North America (Rao, 1999). In general, the relationship between absolute viscosity and shear rate can be shown as,

$$\mu = \mu_\infty + (\mu_o - \mu_\infty)\, f(\gamma) \qquad 2.17$$

According to Cross model, the relationship between absolute viscosity and shear rate can be shown as,

$$\mu = \mu_{\infty,\gamma} + \frac{\mu_{o,\gamma} - \mu_{\infty,\gamma}}{1 + (\alpha_c \gamma)^m} \qquad 2.18a$$

where

$\mu_{\infty,\gamma}$ - limiting viscosity at infinite shear rate (Pa.s)

$\mu_{o,\gamma}$ - limiting viscosity at zero shear rate (Pa.s)

m - exponent (dimensionless)

α_c – Cross consistency index (dimensionless)

Cross model has been used widely to describe the shear thinning of non-Newtonian fluid in a number of scientific publications (Sharman *et al*., 1978; Cuvelier and Launay, 1984; Vlad and Oprea, 2001; Gonzalez-Reyes *et al*., 2003) and have been found suitable to model several polymers and solutions. However it is found that no study has been done to relate Cross model or any of the above relationships in palm oil or plant oil rheological analysis. Some researchers, such as Gonzalez-Reyes *et al*., (2003), use simplified Cross model in their analysis. The simplified Cross model can be shown as

$$\mu = \mu_o / k_1 (\gamma)^m \qquad 2.18b$$

where k_1 is constant.

2.5.4 Carreau Model

The most common function used for Carreau model has the following form:

$$f(\gamma) = 1 / [1 + (\lambda_c\gamma)^2]^{(1-n)/2}. \quad 2.19$$

Applying this Careau function to the general form (Equation 2.17), the relationship becomes

$$\mu = \mu_\infty + (\mu_o - \mu_\infty) / [1 + (\lambda_c\gamma)^2]^{(1-n)/2} . \quad 2.20a$$

This equation has been applied by Chauveteau (1982), Bewersforff and Singh (1988) and Tam and Tiu (1989) and has been found suitable to model their samples. The equation is sometimes written in the following form,

$$\mu = \mu_{\infty,\gamma} + \frac{\mu_{o,\gamma} - \mu_{\infty,\gamma}}{\left[1 + (\lambda_c\gamma)^2\right]^N} \quad 2.20b$$

where

$\mu_{\infty,\gamma}$ - limiting viscosity at infinite shear rate (Pa.s)

$\mu_{o,\gamma}$ - limiting viscosity at zero shear rate (Pa.s)

N, n - exponent (dimensionless)

λ_c – Carreau consistency index (dimensionless)

$N = (1-n)/2$.

2.5.5 Herschel-Bulkley Model

Herschel-Bulkley model is different from power law model since in addition to two parameters of n and k, this model also introduces yield stress parameter. So it is a three-parameter rheological model. It is therefore suitable for fluids having a significant yield stress, or the yield stress is measurable. The yield stress the yield at zero shear rate. According to Figure 2.5, plastic and Bingham materials have some measurable value of yield stress. Writing in term of viscometric parameters, the model can be written as

$$\mu = k_H \gamma^{n_H - 1} + \mu_{\infty,\gamma}. \quad 2.21a$$

Many researchers relate the term yield stresses to shear stress,

$$\tau - \tau_o = k_H (\gamma)^{n_H} \quad 2.21b$$

where τ is shear stress (Pa), τ_o is the yield stress, γ is the shear rate (s^{-1}), n_H is the Herschel-Bulkley flow behavior index and k_H is the Herschel-Bulkley consistency index. It is more useful for viscoplastic fluid (Figure 2.5).

2.5.6 Other Models

There are other rheological models available in the literature to suit different applications as in Table 2.2. These models are not very famous. Thus they are not applied in this work.

Table 2.2: Other rheological models

Model	Mathematical relationship
Meter-Bird	$\mu = \mu_\infty + (\mu_o - \mu_\infty) / (\tau/\tau_m)^{(1-n)/n}$
Chang-Ollis	$\mu = \mu (1 + k\gamma)^{n-1}$
Sisko	$\mu = \mu_o + k(1/\gamma)^m$
Ellis	$1/\mu = (1/\mu_o) + K(\tau)^{(1-n)/n}$

2.5.7 Generalized Viscosity Model for Waxy Oil

Al-Zahrani and Al-Fariss (1998) have proposed an empirical general model for the viscosity of waxy oils. The model describes the non-Newtonian behavior of the oils in the following form:

$$\mu = \frac{B}{\gamma}\left[\left(\frac{\gamma + A}{A}\right)^n - 1\right]^{\frac{1}{n}} e^{\frac{C}{T}+D+W} \quad 2.22a$$

where μ is the viscosity, γ is the shear rate, T is the temperature, W is the wax percentage and A, B, C and D are the model parameters.

A nonlinear regression analysis was used to determine the model parameters. The proposed viscosity model yields was found to fit the experimental data well as

demonstrated by a high coefficient of correlation 97.5% (Al-Zahrani and Al-Fariss, 1998). If wax concentration was not taken into account, Equation 2.27a can be reduced to

$$\mu = \frac{B}{\gamma}\left[\left(\frac{\gamma + A}{A}\right)^{n} - 1\right]^{\frac{1}{n}} e^{\frac{C}{T}+D}. \qquad 2.22b$$

2.6 Viscosity of Oil Mixtures

Theories suggested that viscosity and relative viscosity of oil and polymeric blends depend on the base material. Some models such as Rouse model (Daivis *et al*., 2003) suggest that viscosity is a linear function of relative volume fraction, while other models suggest that the viscosity is a linear function of relative weight fraction.

In order to determine the viscosity of blends, some researchers suggested that physical and chemical properties of blended oil to be measured. From these physical and chemical properties, the viscosity of the blend can be determined. For example Toro-Vazquez and Infante-Guerrero (1993) suggested saponification value and iodine value of the mixture to be measured. Based on these values, the dynamic viscosity of the mixture at particular temperature can be calculated using the following mathematical relationship

$$\ln \mu = -4.8 + 2526 / T + (SV / T)^2 - IV^2 \times 10^{-5} \qquad 2.23$$

where T, SV and IV are temperature, saponification and iodine value of the blend.

This method is not straight forward. Few measurements have to be made. It is of interest (more convenient) if the blended viscosity can be calculated based on viscosities of the base oils. Follows are some expressions used by previous researchers and proposed models to predict the viscosity of blended oils:

Dow (1935, 1956)

Dow used simple expression to predict viscosity of mixture of liquid A and B. Using x_A and x_B to represent wt% of A and B, respectively :

$$\mu_{AB}{}^{1/3} = x_A * \mu_A{}^{1/3} + x_B * \mu_B{}^{1/3} \quad 2.24$$

Goodrum and Eiteman (1996)

Goodrum and Eiteman (1996) proposed a model to calculate the viscosity of mixture as follows

$$\mu_{AB}{}^{1/2} = x_A * \mu_A{}^{1/2} + x_B * \mu_B{}^{1/2} \quad 2.25$$

He has tested the model for low molecular weight triglycerides blended with diesel.

Lederer Equation (Kokal and Sayegh, 1993)

$$\ln \mu_{AB} = (x_A)/ (x_A + S * x_B)\ln \mu_A + (S * x_B)/ (x_A + S * x_B)\ln \mu_B \quad 2.26$$

where S is the correction factor. Lederer equation is used to predict viscosity values for mineral oils and their constitutive fractions.

Rahmes and Nelson (1948)

Rahmes and Nelson (1948) used viscosity reciprocal to expressed the viscosity of mixture

$$(\mu_{AB})^{-1} = (x_A) * \mu_A{}^{-1} + (x_B) * \mu_B{}^{-1} \quad 2.27$$

2.7 Flow and Torque Models for Pump

Theoretically, there are two major losses involve in the test rig study. They are flow loss and torque loss, which are outlined in Section 2.7.1 and 2.7.2, respectively. The losses will result in volumetric and mechanical inefficiencies, respectively.

2.7.1 Flow Mathematical Models

Theoretical pump flow rate, Q_t, is determined by the pump speed, W_p, and size, D_p (Pinches and Ashby, 1989),

$$Q_t = D_p W_p . \qquad 2.28$$

When the pump rotates, the velocity induces the flow from the low pressure side to high pressure side. The rotation of the rotor will not affect the internal leakage. Only the pressure induced flow that causes the fluid to flow from high pressure side to the low pressure side of the vane pocket. Most of flow losses is due to leakage, either internal or external. The major factors that influence both leakages are pressure and viscosity. The higher the pressure the higher is the leakage. On the other hand, the flow leakage will be greater for lower viscosity fluid (Dong *et al*., 2001):

$$Q_l \alpha \frac{P_p}{\mu} . \qquad 2.29$$

Another flow loss is due to compressibility, Q_R. This loss occurs when the system operates at high pressure. Because of these losses, the actual flow that returns to the reservoir is always less that the ideal flow. Combining Equations 2.28, 2.29 and Q_R term gives actual flow rate, Q_a, as;

$$Q_a = Q_t - Q_l - Q_R . \qquad 2.30a$$

After taking into account the correct dimension, leakage flow rate can be written as $C_s \frac{D_p P_p}{2\pi\mu}$. Thus the actual flow rate that flows through the system can be written as

$$Q_a = D_p W_p - C_s \frac{D_p P_p}{2\pi\mu} - Q_R . \qquad 2.30b$$

Other flow models produced by Wilson (1946), Schlosser (1969), Thoma (1969), Zarotti and Nevegna (1981), Dorey (1988), and Huhtala (1996) are shown in Table 2.3. Thoma neglected compressibility effect in his model. Other researchers introduced compressibility factor at different positions in their flow models.

Table 2.3: Flow models produced by respective researchers

Researcher	Flow model
Huhtala	$Q_a = D_p W_p - \left[Q_{v_{n,p}} + f_v(\mu) + f_v(\beta)\right]$
Dorey	$Q_a = D_p W_p - C_s \frac{D_p P_p}{\mu} - \frac{D_p P_p W_p}{\beta}\left(D_r + \frac{1}{2}\right)$
Zarotti and Nevegna	$Q_a = D_p W_p - C_1 P_p - C_2 P_p^2 - C_3 P_p^2 W_p^{3/2} - C_4 P_p W_n (C_5 + D_p)$
Schlosser	$Q_a = D_p W_p - C_s \frac{D_p P_p}{2\pi\mu} - C_{st} D_p^{2/3} \sqrt{\frac{2P_p}{\rho}}$
Thoma	$Q_a = D_p W_p - C_s \frac{D_p P_p}{2\pi\mu}$
Wilson	$Q_a = D_p W_p - C_s \frac{D_p P_p}{2\pi\mu} - Q_R$

2.7.2 Torque Mathematical Models

The torque required to drive the hydraulic mover (pump) depends on the pump size and the pump pressure. The theoretical torque, T_t, is given by (Pinches and Ashby, 1989),

$$T_t = \frac{D_p P_p}{2\pi}. \qquad 2.31$$

However, the actual torque to drive the system is higher than the theoretical due to torque loss. Torque loss is the result of friction, either viscous or coulomb. Viscous or speed dependent torque, T_v, is proportional to speed and to fluid viscosity but is independent of load,

$$T_v = C_v \mu D_p W_p. \qquad 2.32$$

Coulomb friction torque, T_c, is proportional to pressure,

$$T_c = C_c \frac{D_p P_p}{2\pi} \qquad 2.33$$

where C_v and C_c are viscous and coulomb friction coefficients, respectively. Thus the actual torque, T_a, can be written as the summation of the theoretical torque and all the torque loss,

$$T_a = T_t + T_c + T_v \qquad 2.34$$

$$T_a = \frac{D_p P_p}{2\pi} + C_c \frac{D_p P_p}{2\pi} + C_v \mu D_p W_p \quad . \qquad 2.35$$

The C_v and C_c coefficients in Equation 2.35 can vary with pressure, temperature, shear rate and surface finish. Due to stiction of the oil, the coefficient of friction increases sharply at very low speed. This can be understood also in term of oil rheology.

Other torque models are shown in Table 2.4.

Table 2.4: Torque models produced by respective researchers

Researcher	Torque model
Huhtala	$T_{pa} = \frac{D_p}{2\pi} P_p + T_{h_{n,p}} + f_h(\mu)$
Dorey	$T_{pa} = D_p P_p + \dot{C}_v \mu W_p D_p + \dot{C}_f D_p P_p$
Zarotti and Nevegna	$T_{pa} = D_p P_p + W_p\left(C_1 + C_2 W_p\right) + C_3\left(1 + \frac{C_4}{\sqrt{P_p}} + \frac{C_5 + C_6}{W_p + C_7}\right) + \frac{C_8}{W_p + C_9}$
Schlosser	$T_{pa} = D_p P_p + C_c \frac{D_p P_p}{2\pi} + C_d \mu D_p W_p + C_h \frac{\rho D_p^{5/3} W_p^2}{4\pi}$
Thoma	$T_{pa} = D_p P_p + C_c \frac{D_p P_p}{2\pi} + C_d \mu D_p W_p + C_h \frac{\rho D_p^{5/3} W_p^2}{4\pi} + \frac{D_p P_c}{2\pi}$
Wilson	$T_{pa} = \frac{D_p P_p}{2\pi} + C_c \frac{D_p P_p}{2\pi} + C_d \mu D_p W_p + T_s$

2.8 System Efficiency

High system efficiency is of primary importance for any system. The total system efficiency can be determined from the products of individual efficiencies. The overall system efficiency of the test rig under study depends on two main efficiencies i.e., volumetric and mechanical efficiencies. These efficiencies can be determined by measuring flow and torque loss values.

2.8.1 Power

The input power for a hydraulic system is defined as the product of torque required to drive a hydraulic pump with the pump speed,

$$H_{input} = T_p W_p \ . \qquad 2.36$$

This input power is known also as shaft power. On the other hand, the output power is the fluid power. The output power is calculated as

$$H_{output} = P_p Q . \qquad 2.37$$

2.8.2 Volumetric Efficiency

The flow through hydraulic component especially a pump, can be categorized as main flow and the leakage flow, as already described in Section 2.7.1. The main flow is extremely complex. It is neither steady nor uniform. This can be due to the motion of vane and non-uniform hydraulic flow path. However the nature of the leakage flow is relatively simple. It can be treated as a laminar flow in a narrow passage. There are two types of leakage flow in a narrow passage, pressure induced (Poiseuille) and velocity induced (Couette) flow.

The volumetric efficiency is the ratio of the actual flow rate to the ideal flow rate. Dividing Equation 2.30b with the ideal flow term (Equation 2.28), the volumetric efficiency can be written as

$$\eta_{vp} = \frac{Q_a}{D_p W_p} \qquad 2.38a$$

or

$$\eta_{vp} = 1 - C_s \frac{P_p}{2\pi\mu W_p} - \frac{Q_R}{D_p W_p} \ . \qquad 2.38b$$

It should be noted that the second term of Equation 2.38b is the losses due to leakages and the last term is due to the compressibility effect.

2.8.3 Mechanical Efficiency

Mechanical efficiency and mechanical losses are due to viscous friction and coulomb friction. The mechanical efficiency is defined as the ideal torque divided by the actual torque:

$$\eta_{mp} = \frac{D_p P_p}{T_a} . \qquad 2.39a$$

Taking into account all the torque losses explained in Section 2.7.2, mechanical efficiency can be expressed as

$$\eta_{mp} = \frac{P_p}{P_p / 2\pi + C_c \, P_p / 2\pi + C_v \mu W_p} \ . \qquad 2.39b$$

The viscous and coulomb friction coefficients in Equation 2.39b can vary with pressure, temperature, shear rate and surface finish.

2.8.4 Overall Efficiency

The overall efficiency of the pump is the ratio of output power to the input power at a given flow rate for a given shaft speed. In all cases, the output power is simply the fluid power. The input and output powers are calculated as in Equations 2.36 and 2.37, respectively.

The overall efficiency could also be considered as the ratio of the actual performance to an ideal performance that would have been achieved. From the definition of this efficiency, the overall efficiency can be written as (Pinches and Ashby, 1989),

$$\eta_{op} = \frac{Q_p P_p}{T_p W_p}. \qquad 2.40$$

CHAPTER 3

MATERIAL, EQUIPMENT, TEST RIG AND METHOD

3.1 Introduction

The aim of this research is to investigate performance of palm based oils when used as hydraulic fluid. Prior to the testing in the real hydraulic test rig, the oil performance was investigated in 'simulated' bench tests. The simulation results (rheological work and thermal tests) then can be compared with the real results from hydraulic test rig. In this chapter the test fluids, apparatus and methods used are described. This is followed by description of hydraulic test rig set up.

3.2 Test Fluids and Additives

3.2.1 Test Fluids

The proposed test oil for this research was the refined bleached and deodorized (RBD) palm oil. Several types of vegetable oils were also used in the beginning of the research as comparison. To complete the research objective, commercial vegetable based hydraulic fluid, mineral based hydraulic fluid and palm oil methyl ester (POME) were also tested. The rheological and thermal stabilities of the oils were investigated to determine the best candidate for further study. Several grades of RBD palm oils were obtained from refineries in Johor and local retailers.

The fatty acid composition for RBD palm oil is shown in Table 3.1. The palm oil has large amount of palmitic and oleic acids. The high content of palmitic acid in

palm oil compared to pure corn or rapeseed oils results in the palm oil being more oxidatively stable than corn or rapeseed oils. Fatty acid composition of commercial vegetable based hydraulic fluid is also shown in Table 3.1.

For the mineral oil, a commercial hydraulic fluid (Shell Tellus) was used. Commercial vegetable based hydraulic fluid was imported from the United States. The basic oil properties for both commercial mineral and vegetable based hydraulic fluid are shown in Table 3.2.

3.2.2 Additives

Among the additives used in this study were Ciba L135, L74, L06, F10 and Lubrizol 7652. Lubrizol 7652 additive was found effective to work as antioxidant in vegetable oils (Adhvaryu and Erhan, 2002). Details of the Ciba L135, L06 and F10 additives are shown in Figure 3.1. This study also used some other additives for comparison purposes, which the author specifically noted in Results and Discussion section.

Table 3.1: Fatty acid composition of RBD palm and vegetable based hydraulic oils used

Common name	Systematic name	Symbol	% of total weight (RBD palm oil)	% of total weight (Superolein palm oil)	% of total weight (Vege. hyd. oil)
Saturated acids					
Lauric	n-Dodecanoic	C12:0	0.4	0.5	0.0
Myristic	n-Tetradecanoic	C14:0	1.0	1.2	1.3
Palmitic	n-Hexadecanoic	C16:0	38.3	34.8	4.0
Stearic	n-Octadecanoic	C18:0	4.0	3.3	2.2
Arachidic	n-Eicosanoic	C20:0	0.7	0.5	-
Mono-unsaturated acids					
Palmitoleic	n-Hexadec-9-enoic	C16:1	0.4	0.4	0.3
Oleic	n-Octadec-9-enoic	C18:1	43.1	45.5	60.7
Gadoleic	n-Eicos-9-enoic	C20:1	0.1	-	1.6
Poly-unsaturated acids					
Linoleic	n-Octadec-9, 12-dienoic	C18:2	11.6	13.8	18.9
Linolenic	n-Octadec-9, 12, 15-trienoic	C18:3	0.2	0.1	0.0
Others		C20-C22	-	-	11.8

Table 3.2: Properties of commercial mineral and vegetable based hydraulic fluid used

Properties	Standard method		
Type		Mineral	Vegetable
Grade		HM 100	VG 46
Flash point (^{o}C)	ASTM D92	228	220
Pour point (^{o}C)	ASTM D97	-24	-28
Total acid number (mg KOH/g)	ASTM D664	0.64	1.05
Density (kg/m^3)	ASTM D1298	885	922
Kinematic viscosity at 40^{o}C (cSt)	ASTM D2196	106	37
Kinematic viscosity at 100^{o}C (cSt)	ASTM D2196	11.4	8.4
Viscosity index	ASTM D2270	93	213

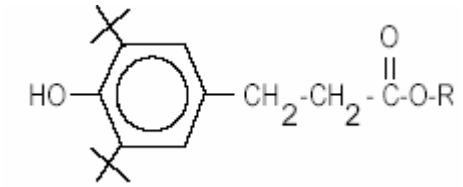

a) Ciba Irganox L135

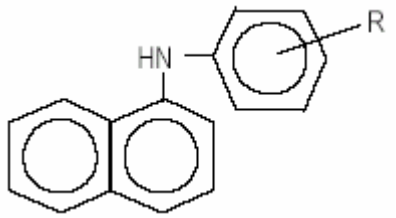

b) Ciba Irganox L06

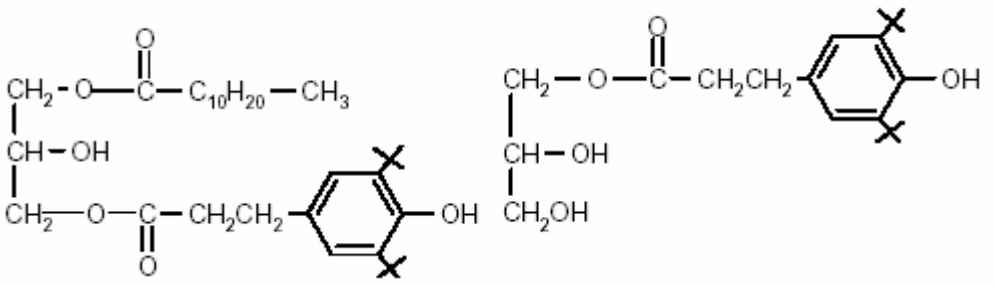

c) Ciba Irgalube F10

Figure 3.1: Molecular structure of additives used.

POME was obtained from a local oleochemical company. The POME properties are as in Table 3.3.

Table 3.3: Basic properties of POME

Properties	Standard method	Value
Total acid number (mg KOH/g)	ASTM D664	0.2167
Iodine value (cg I_2/g)	AOCS Cd 1b	59.6
Kinematic viscosity at 40^{o}C (cSt)	ASTM D2196	7.02
Kinematic viscosity at 100^{o}C (cSt)	ASTM D2196	3.42

3.2.3 Blending Preparation

The blending ratios for palm oil - mineral and palm oil - POME blends are shown in Table 3.4. Different percentage levels of commercial additives were blended to the RBD palm oil for bench test (Table 3.5). The samples were blended according to these ratios and mixed thoroughly in beaker using magnetic stirrer on hot plate at 40^{o}C for one hour before being subjected to continuous heating. Vigorous stirring was made in order to make sure homogeneous mixture was obtained.

Table 3.4: Palm oil – mineral and palm oil - POME blending ratio

Notation	RBD palm oil (%wt/wt)	Mineral oil (%wt/wt)	Notation	RBD palm oil (%wt/wt)	POME (%wt/wt)
100P0M	100	0	100P0ME	100	0
75P25M	75	25	80P20ME	80	20
50P50M	50	50	60P40ME	60	40
25P75M	25	75	40P60ME	40	60
0P100M	0	100	20P80ME	20	80
			0P100ME	0	100

Table 3.5: Percentage level of additives to RBD

Additives	Percentage (%wt/wt)				
L74	0.0	0.5	1.0	1.5	2.0
L06	0.0	0.1	0.5	2.0	4.0
Lubrizol 7652	0.0	3.0	4.0	5.0	6.0
L135	0.0	0.2	0.6	0.8	1.5
F10	0.0	0.5	1.0	1.5	2.0

3.3 Apparatus and Experimental Set-up

Before the oil was tested in hydraulic system, it was tested in bench tests. The purpose of the bench tests was to predict the oil condition when it was exposed to heat in hydraulic system.

3.3.1 Heating Facilities

250 ml oil sample contained in Erlenmeyer flask was heated either in electric oven or oil bath. Temperature of 95ºC was used for the initial simulation tests. Other temperatures (55, 70 and 135ºC) were also used for selected good additives. These temperatures were selected based on standard methods mentioned in Sections 2.3.1 and 2.3.2 and to simulate the running temperatures in hydraulic test rig. To study the effect of aeration, compressed air was supplied by a compressor and the flow rate was controlled by flow control valves. The oils were sampled out at sampling period as mentioned in respective sections in Chapter 4. The samples were then subjected to several property tests such as in Sections 3.3.2 – 3.3.5.

3.3.2 Thermogravimetric Analyzer (TGA)

Thermogravimetric measurements were performed using Perkin-Elmer Pyris 6 TGA at a heating rates of 5 and 10 ºC/min. Samples of approximately 15 mg were heated from 50ºC to 500ºC in pure nitrogen flow of 20 ml/min. This TGA test involves weight change as the oil was heated. The weight loss data of the sample was logged using the in-situ computer.

3.3.3 Fourier Transform Infrared (FTIR) Spectroscopy

Infrared spectroscopic (IR) studies were performed using Perkin Elmer FTIR System Spectrum GX. Small amount of oil sample was deposited on a round KBr cell. Prior to that N-hexane solution was used for cell cleaning. The oil layer was scanned for wavelength from 4000 to 400 cm^{-1}. Number of scan for each sample was 16 times. The spectra obtained were used to observe the structural bond and functional groups of samples. The chemical structural of organic molecules was analyzed qualitatively and quantitatively.

3.3.4 Total Acid Number Analysis

This analysis is applicable to crude and refined vegetables, marine fats and oils, and various products derived from them (Eisentrager *et al.*, 2002). The acid value number (TAN) is the milligrams of potassium hydroxide (KOH) necessary to neutralize the free acids in 1 gram of sample. About 3 ml of sample was weighed into a 250 ml Erlenmeyer flask. Then 25 ml of diethyl ether, 25 ml of ethanol analar and 1 ml of phenolphthalein indicator solution 1% were added into the sample. The sample was shaken gently for 10 minutes until the entire solution was well mixed. The solution was then titrated with KOH 0.05M. It was swirled vigorously at the end point, but by avoiding dissolving carbon dioxide (CO_2) in the solvent. The end point was considered definite if the color change persists for 15 seconds. The amount of KOH used was recorded. The calculation for the acid value is as follow (ASTM D974):

$$\text{The acid number, mg KOH / g oil} = \frac{(A-B) \times N \times 56.1}{W} \quad 3.1$$

where, A = ml KOH used in titration

B = ml KOH used in titrating the blank

N = normality of KOH (0.05)

W = weight of sample (g)

3.3.5 Iodine Value

The iodine value was determined according to AOCS Cd 1b-87 method. The method involves similar procedure as TAN determination except for the chemicals used.

3.4 Rheological Measuring Instrument

3.4.1 Rheological Measurement

In conducting viscometric or rheology measurement, great care was made to ensure the flow between the spindle and carousel chamber was fully developed laminar flow and the oil properties did not change with time (steady flow). A thermosel was used to ensure that the temperature of the test sample was maintained uniformly.

The Newtonian and non-Newtonian behavior of oil samples was investigated. Several data was obtained at different spindle speeds. The equipment used in this experiment is of concentric cylinder type. Thus suitable shear stress and shear rate terms had to be derived.

Appendix A shows the derivation of shear rate and shear stress for the cylindrical viscometer used in this study. The derivation of the shear rate expression required solution of the continuity and momentum equations with the application of

boundary conditions. There is no pressure gradient in the θ direction (direction of rotation – Equation 1 of Appendix A). The derived expression shows that geometrical measurements play important role in determining shear rate. Using the derived expression, the shear stress and shear rate were determined from viscometric values and dimensions of the test geometry.

3.4.2 Brookfield Viscometer (model DV-I+) and Measurement Procedure

The viscosity measurement was carried out using Brookfield viscometer model DV-I+. The rotational viscometer is constructed from two concentric cylinders. The OD of inner cylinder is 17.48 mm and the ID of the outer cylinder is19.06 mm. The height of the outer cylinder is 35.53 mm.

Sample of 8 ml was placed in a carousel. The measurement was carried out using spindle SP-18 with a concentric cylinder. The spindle was attached to the motor above via a rigid connecting wire. Then the spindle was lowered to the indicated point for measurement purposes. Shear rate was calculated using Equation 11 of Appendix B or by the following simplified relationship:

$$\gamma = 1.318 \times N \qquad 3.2$$

where N is the spindle speed (rpm).

The viscosity of the samples was measured in triplicate at particular shear rates with spindle speed ranging from 3 rpm to 100 rpm (ten discrete shear rates altogether: 3.9, 6.6, 7.9, 13.2, 15.8, 26.3, 39.5, 65.8, 79.0, 131.6 s^{-1}).

In order to achieve the consistency of the measurement readings, measurement was recorded ninety seconds after rotating of the spindle. The temperature was increased by means of Brookfield thermosel from 30^{o}C to 100^{o}C with 10^{o}C increment. After each temperature increment, the filled sample chamber and spindle were temperature-equilibrated for 10 minutes. The measurement was made only after this duration in order to make sure that steady state heat transfer could be achieved. In order to ensure reproducibility was good, the test was

duplicated for each temperature setting. Then the average values were used. When the two results show significant difference, another run was made. Small differences sometimes noticed at low shear rate. At this rate, it was observed that the outer spindle surface sometimes touched the inner surface of sample chamber.

3.5 Hydraulic Test Facility

The main objective of this investigation was the development of an experimental facility for testing of hydraulic fluid and the efficiencies of the system when palm based oil was used as hydraulic fluid. Then the rheological and thermal test results from bench tests could be compared.

The main objective of the study is to produce model, design, fabricate and instrumented a hydraulic test rig that can evaluate the palm oil performance in real running condition. In other words, the design and development of the test rig is the heart of this research work. Two identical units of hydraulic test rig were built in Fluid Mechanics laboratory, KUSTEM for this purpose. Two identical units were built in order to directly compare the performance of hydraulic system running on palm oil and commercial hydraulic oil. The following sections describe the development of the test rig, starting with the development of models, engineering drawings and the novel design features of the test rig. The data acquisition comprised of hardware and software was used to collect and manipulate the required data. High speed PC logger was possible with the use of ADAM hardware and the LabVIEW from the National Instruments. Industrial sensors were used in this project.

3.5.1 Design of Hydraulic Test Rig

Several models were produced during hydraulic modeling work (Wan Nik *et al*., 2003b). The best model was selected based on the design criteria and specifications. The design procedures for the design of hydraulic test rig are as follows:

1. The pump type and size were determined based on rheological properties of the test oil.
2. The prime mover power was determined.
3. The control valve type and size was selected.
4. Other miscellaneous components such as reservoirs, piping, filter and cooling system were selected.
5. The overall system cost was calculated.

This procedure was repeated several times until the best system was obtained. Assistance from component suppliers and experienced fabricators was sought through out the study. This is to ensure cost effectiveness, since any subsequent modification would require hardware changes and could result in cost constraint.

3.5.2 Design Consideration and Specification

The fluid operating temperature of 70^{o}C was selected based on ASTM D2271 recommendation. However different operating temperatures were also possible to evaluate the dependence of performance on temperature and oil viscosity. Overload temperature can be set to protect the test facility components.

Pressure of 210 bar was selected to reflect the maximum practical pressure of several hydraulic systems these days. The selected test pressure is higher than those specified in ASTM D2271 and ASTM D2882 standards.

3.5.3 Hydraulic System Layout

Figures 3.2 and 3.3 show the final hydraulic system model and layout, respectively. Round reservoir is located at the corner edge of the 1m x 1.5m base. The inlet pipe starts from this reservoir. A manually operated shutoff valve is located 10 cm from the reservoir. The purpose of this shuttle valve is to block the fluid especially during the pump dismantlement. Vane pump is located underneath the

electrical motor. Pressure control was used to control the pressure in the main line. Several transducers were used to measure flow parameters.

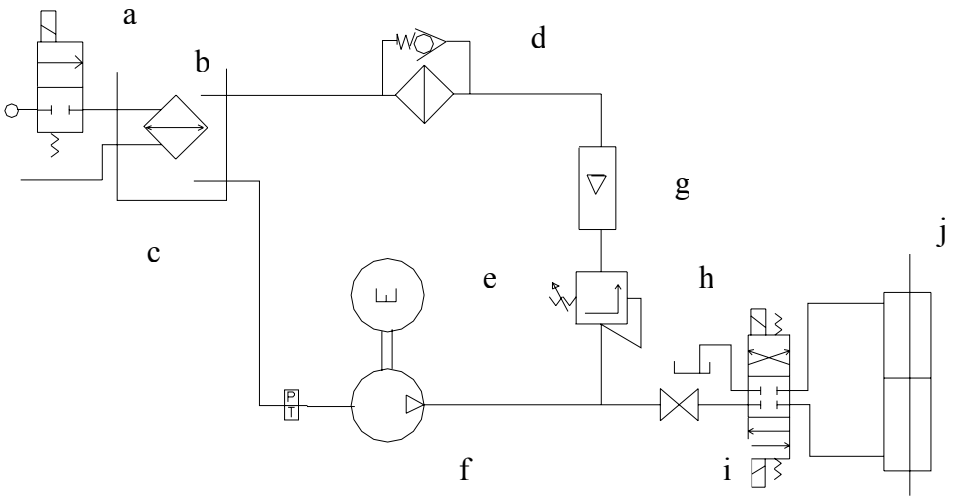

a – cooling solenod valve; b – cooler; c – hydraulic reservoir
d – safety filter; e – 3 phase electrical motor; f – pump
g – flowmeter; h – pressure relief valve;
i – directional control valve; j – actuator

Figure 3.2: Final test rig model.

3.5.4 Mechanical Component Description

3.5.4.1 Hydraulic Pump

Since the pump is the most expensive component and the most affected by the palm based hydraulic fluid, this section gives some overview of the pump used in this project. Hydraulic pump used in this project can be classified as positive displacement type. The hydraulic pump is the source of hydraulic power. The pump converts mechanical energy received from the electric motor to fluid flow and pressure. It operates by forcing a certain volume of fluid from the suction side to the discharge side of the pump.

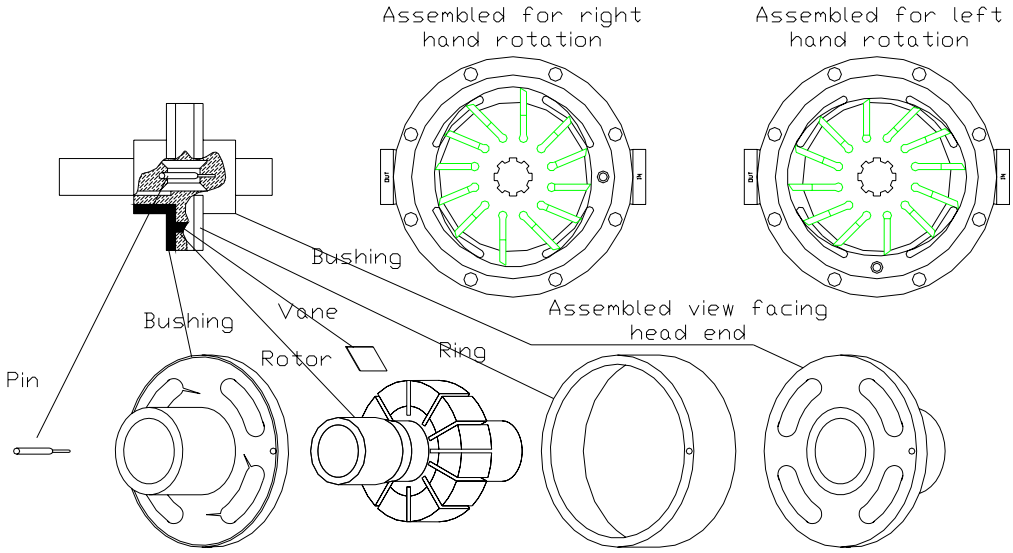

Figure 3.4: Illustration of the vane pump.

Figure 3.4 shows the exploded view of the vane pump used. The figure shows the position of rotor, vane, side plate and cam ring. The pump shaft is coupled to the motor shaft located on the upper side. This pump, being a positive displacement pump, is suitable for high pressure applications and fluid of relatively high viscosity.

3.5.4.2 Pump and Motor Assembly

The pump and motor are mounted along a vertical axis to facilitate alignment. Strong support was fabricated for safety reason. Figure 3.5 shows photograph of pump-motor assembly.

Figure 3.5: Photograph of pump-motor assembly.

3.5.5 Electrical Components

3.5.5.1 Electric Motor

The prime mover of the hydraulic test rig is a 4 pole AC electric motor which is controlled by an inverter. The motor is of three phase type with 5.5 kW power. It is FOCUS brand 3VZ 132S 4 series. The maximum speed is 1500 rpm, frequency 50

Hz with current supply of 10.8A and 415V. Table 3.6 shows the relationship between the motor speed in rpm and Hz. Standard operating temperature is up to 40°C. It is equipped with IP 55 protection. Electrical circuit diagram for motor and cooling system is shown in Figure 3.6.

Table 3.6: Relationship between the motor speed in rpm and Hz

rpm	1440	1350	1290	1200	1140	1050	900	840	750	600
Hz	48	45	43	40	38	35	30	28	25	20

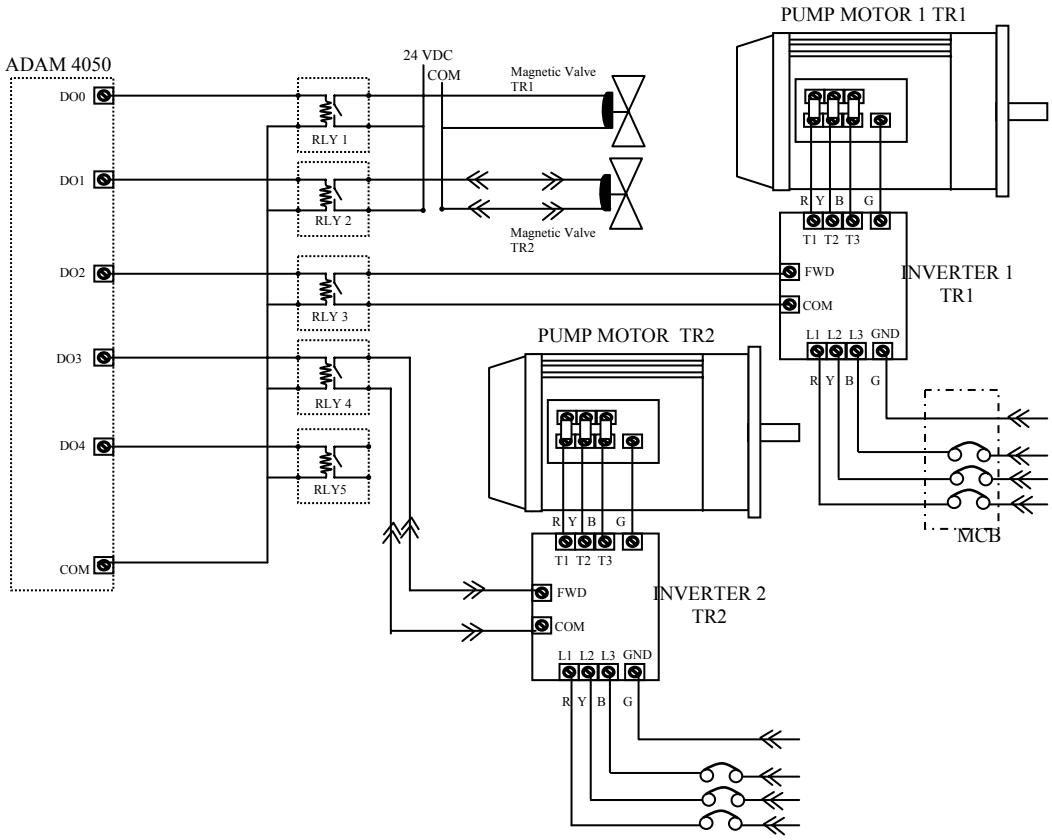

Figure 3.6: Motor and solenoid valve circuit drawing.

3.5.5.2 Watt Tronic 55H3 Frequency Inverter

Details of the inverter are as follow:

Type: FUWTG0055H3

Input: 50/60Hz +-5%

Output: 3X 0-380/460V

0.1 – 400 Hz

9.9kVA, 5.5kW, 13A

3.5.6 Sensors and Transducers

3.5.6.1 Pressure

The pressure transducer that measures upstream and downstream pipe pressure was purchased from Keller Instrument. The transducer working pressure is from 0 bar to 250 bar. The accuracy is +- 0.25%. The transducer works on current principle. The output signal is 4-20 mA which corresponds to 0-250 bar. Each pressure transducer is connected to individual power supply (Figure 3.7a). The supply current for this transducer is 8-28 VDC. After about 2000 hours running, missing signal problem occurred. The problem was overcome by installing a flexible adapter. As shown in Figure 3.7b, the pressure sensor was screwed into a mounting adapter, which in turn is fastened to pressure port.

Figure 3.7a: Individual power supply for pressure transducer.

Figure 3.7b: Pressure transducer installation via flexible adapter.

3.5.6.2 Thermocouple

The reservoir temperature was measured using K type thermocouple. The thermocouple reading was used as active input to energize or deenergize the operation of solenoid valve. The solenoid valve in turn connects or disconnects cooling water to the heat exchanger. The second thermocouple located in the return pipe acts as indicator for heat generation in the system.

3.5.7 Calibration Method

Flowmeter, pressure sensors, thermocouples and strain gauge were calibrated to verify their measurements. Thermocouple and pressure sensor were calibrated both offsite and in-situ.

3.5.7.1 Flow rate

Calibration of flowmeter is necessary since it will affect the volumetric performance. In calibrating the flowmeter, the rig was run at zero loading for several speeds (rpm). The flowmeter was calibrated by capturing oil reentering the hydraulic reservoir using jug and beakers. Stop watch was used to indicate the amount of time

required to fill certain volume. The actual volume divide with time required was taken as actual flow rate (lit/min).

3.5.7.2 Torque

The torque calibration was made when the rig was in idle condition. Two deadweights of 20 kg each were used. Torque loading was applied at 0.18m from shaft center (measured at motor casing). Gravitational force was taken into account. 0, 20 and 40 kg_f loading was applied. With a certain loading, corresponding mA reading was recorded.

3.5.7.3 Temperature

A digital thermometer was used to calibrate the thermocouples. The thermocouples and thermometer give the same temperature reading in hot water and atmospheric air.

3.5.7.4 Pressure

The pressure sensor and gauge calibration was performed by putting known weights on the dead-weight tester platform. Pressure gauge reading was made. The dead weight pressure calculation was made by dividing the dead load with the platform area. It was found that this calculated pressure was linear with the pressure gauge reading. For the in-situ calibration, the rig was run at constant speed of 40 Hz. Certain pressures were applied using pressure relief valve. Corresponding mV was obtained. Test was repeated at several pressures from 20 to 150 bar.

3.5.8 Data Acquisition System

Data acquisition system is shown in Figures 3.8a and 3.8b. The signal acquired by each transducer was transmitted through respective ADAM conditioner units (through RS485 data interface cable) before being transmitted to PC through RS232 cable.

The analog data were converted to digital data using this ADAM acquisition hardware. When the data was transmitted to the PC, the LabVIEW software, with the conditioned set by the built programs, conditioned and saved the data in basic Excel text file. The number of samples and the sampling rate could be adjusted according to the author's requirement. A Pentium III–550MHz computer with 64Mb SDRAM 6.4GB hard disk was used in the PC logger system.

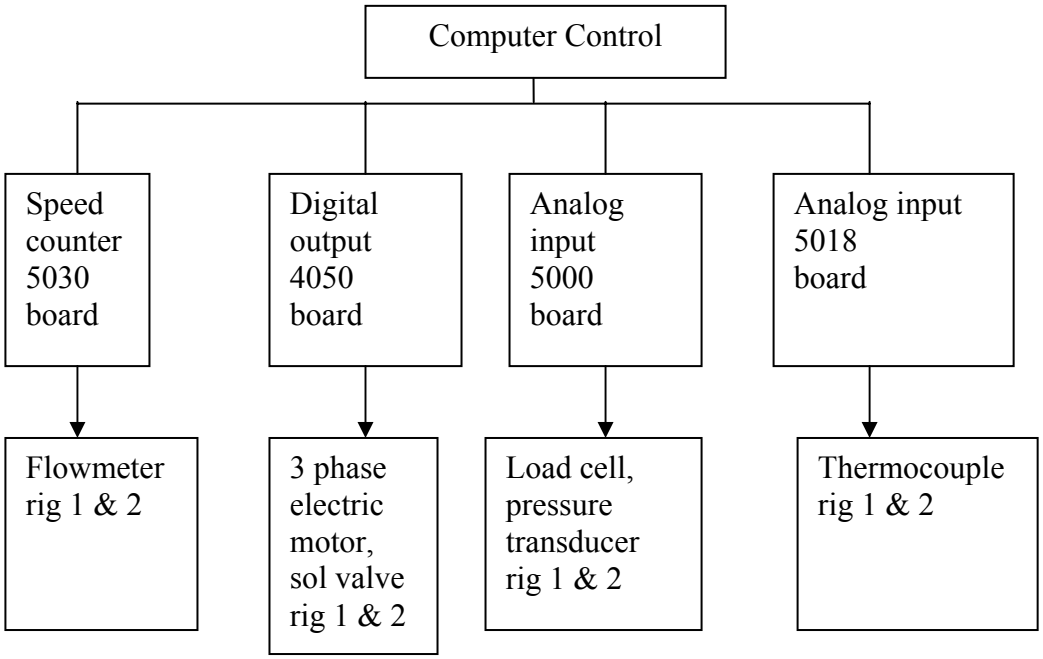

Figure 3.8a: Architecture of data acquisition system.

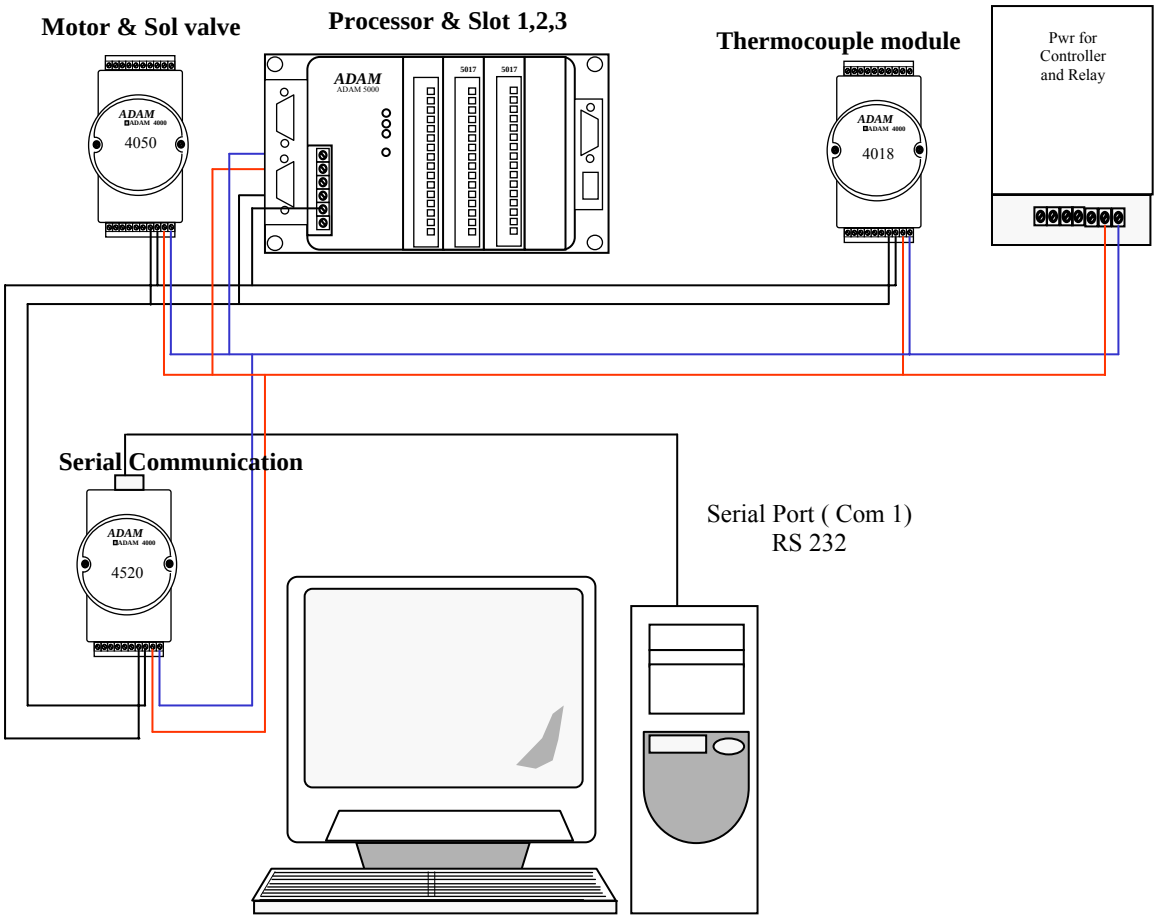

Figure 3.8b: Layout of data acquisition system.

3.5.8.1 Basis for Software Selection

LabVIEW is an excellent choice of software programs for data acquisition (Well and Travis, 1997). LabVIEW is graphical programming software that is produced by National Instrument. The software uses numerical techniques to solve problems. The fascinating feature of the software is that its ability to write the language code in a flow chart manner. There are many programs, which are called VIs, which can be used for a particular process.

LabVIEW was the choice for this project due to its visual representation and user friendly. On computer screen it shows visual depictions of input and output parameters. There are add-on toolkits which can be used to represent detailed graphics of a process. The LabVIEW has the ability to perform actual data acquisition as required in this project. In addition the software also can be used to simulate a process and redisplay the process using the stored data.

3.5.8.2 LabVIEW

LabVIEW Full Development Systems for Windows version 6.1 was used as the software for the data acquisition system. It is a very powerful and provides almost unlimited flexibility. However, it is quite complex and a reasonably long learning time was spent to become proficient with it.

Debugging of the software was conducted using LabVIEW's execution highlighting feature. Execution highlighting displays the code execution in a very slow mode, allowing the author to see the data flow and the value of the variables in the software.

The software was used to acquire data, process data and present the results. It handled not only analogue but also digital I/O. It was decided that the digital control would also be implemented using LabVIEW. Thus the software was also used to run the motor and to activate the cooling solenoid valve. The software is not only flexible but also compatible with all National Instruments and most ADAM hardware. Thus not much problem was encountered in acquiring complex data with hydraulic system continuous running.

For transient data, the data acquisition system failed to capture data less than 3 seconds interval. This is due to bottlenecking at the 4520 ADAM hardware. For the steady state data, the data acquisition system collected data at prespecified time interval and converted the voltages to engineering parameters with correct units. The built programs then calculated the volumetric and mechanical efficiencies. The data was then formatted and saved in a spreadsheet for later use. The data was exported and further manipulation was performed in Microsoft Excel. Besides, the system also plots real-time graphs for immediate analysis.

3.5.8.3 Program Algorithm

i. Open communication port
ii. Initialize data array

iii. Create data file with detailed time information
iv. Read data T,P,Q, L
v. ON/Off pump
vi. Confirm step iv logic min/max allowable data
vii. Calculate performance, etc
viii. Check and calculate total Q
ix. Alert T_{max}, blinking for safety
x. Export parameter values to array
xi. Make needed variables visible/hide
xii. Exit – close serial communication

3.5.8.4 LabVIEW Programming

Figure 3.9a shows LabVIEW front panel outlook and its respective block diagram (Figure 3.9b) before entering this hydraulic program. It gave 3.5 seconds for user to decide either to really enter this program or not. Figure 3.10a show display front panel using 'main menu2.vi'. This panel gives choice to the user either to:

- get some information related to the system,
- set the system safety features,
- run the system or
- exit from the system.

The block diagram in Figure 3.10b uses WHILE loop for the user to decide either to stay with 'main menu2.vi' or to exit.

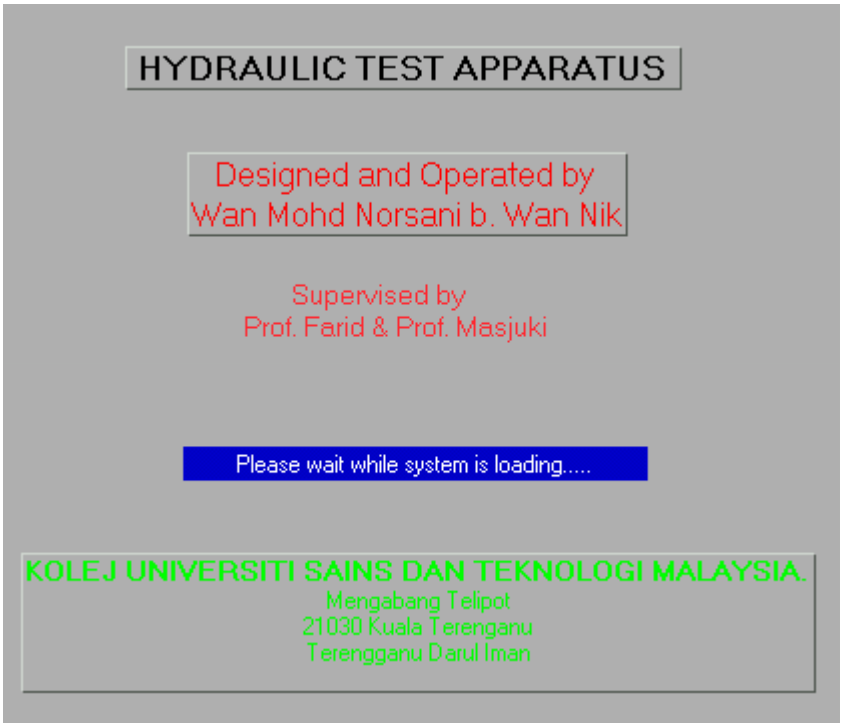

Figure 3.9a: LabVIEW front panel outlook.

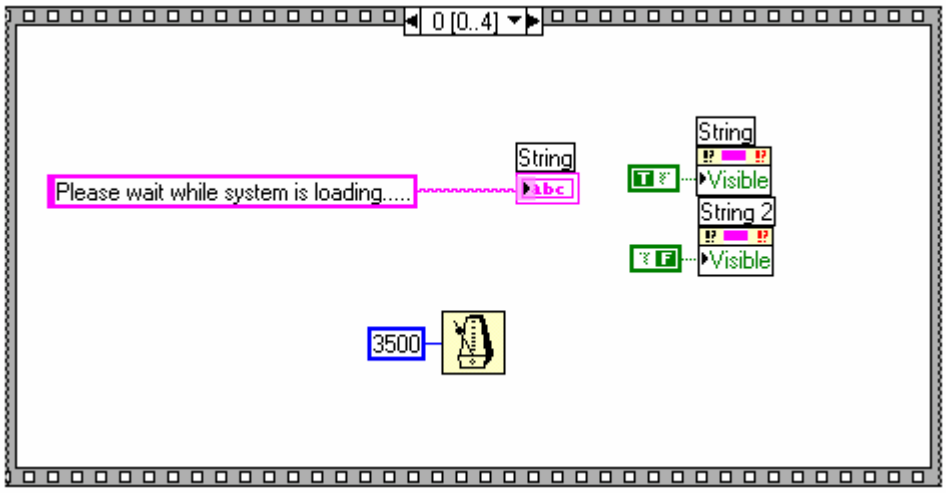

Figure 3.9b. LabVIEW front panel program (block diagram).

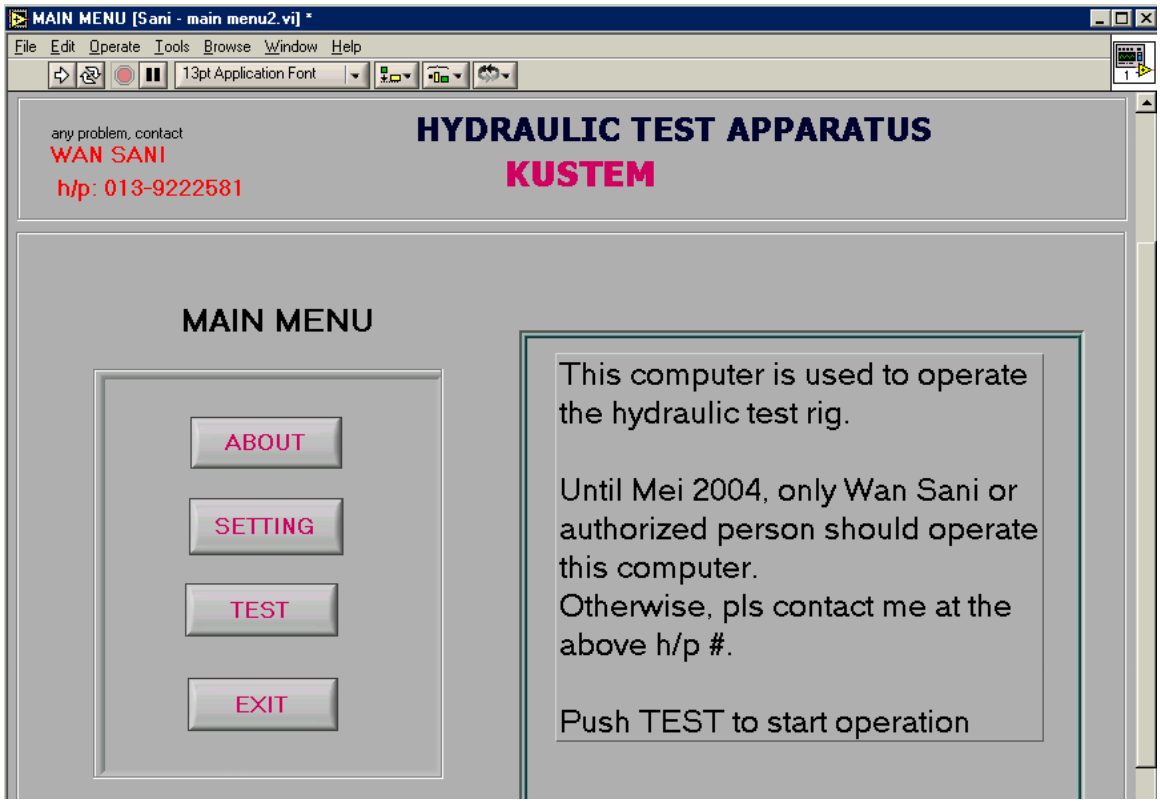

Figure 3.10a: Front panel of 'main menu2.vi'

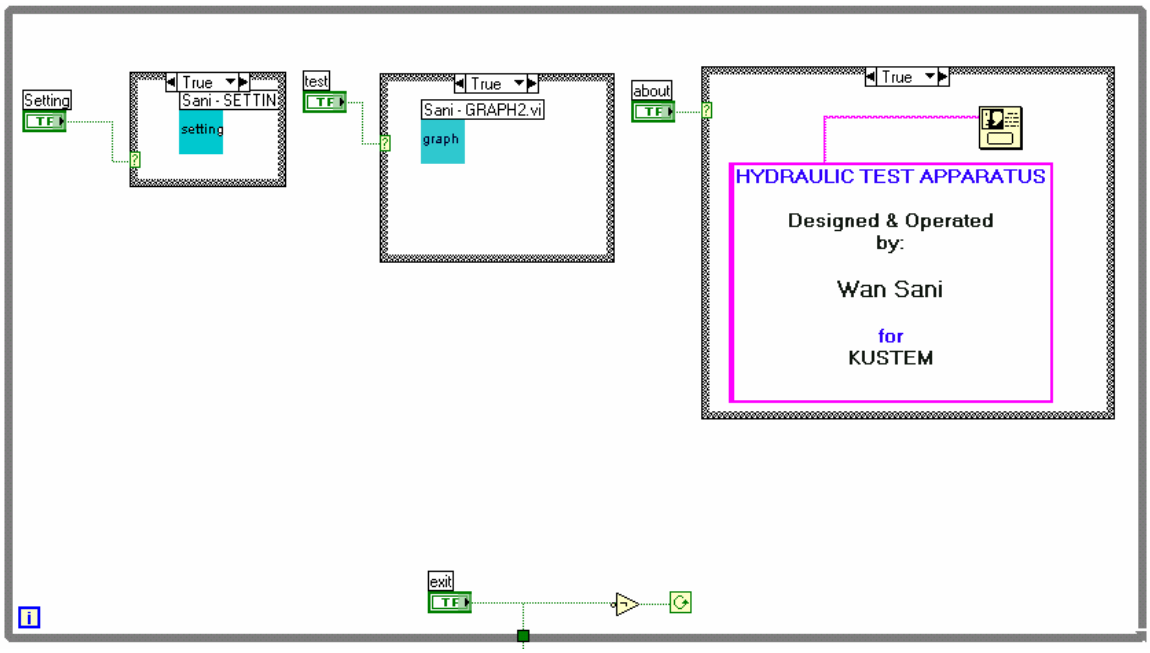

Figure 3.10b: Condition program of 'main menu2.vi'

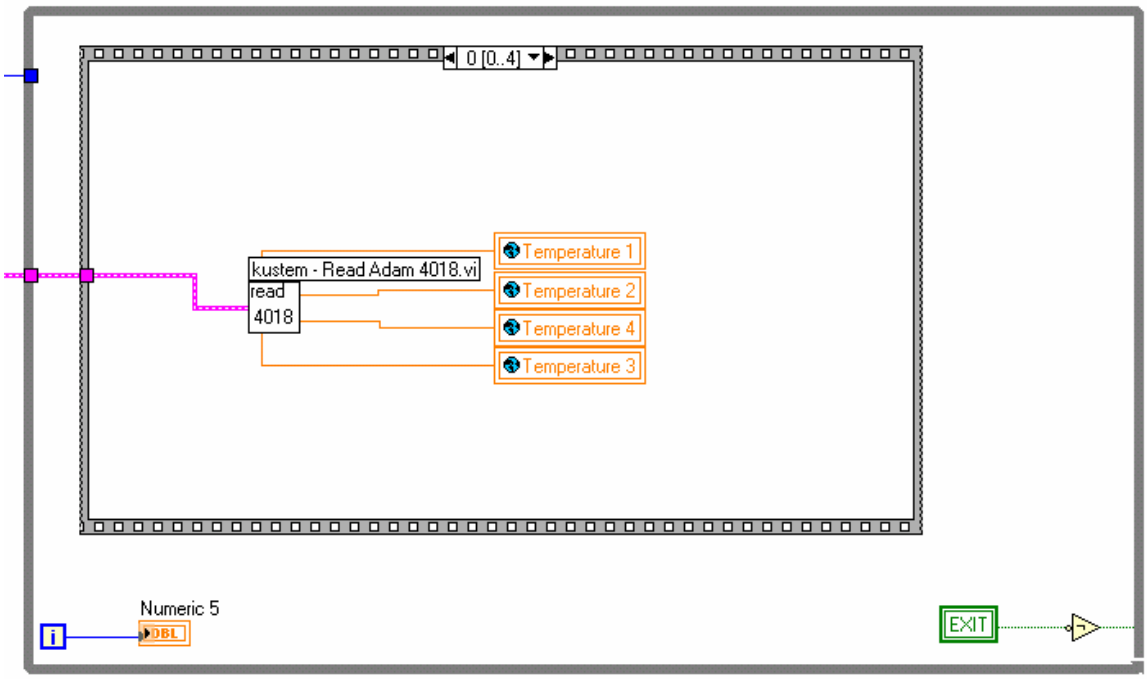

Figure 3.11: WHILE loop to acquire flow data.

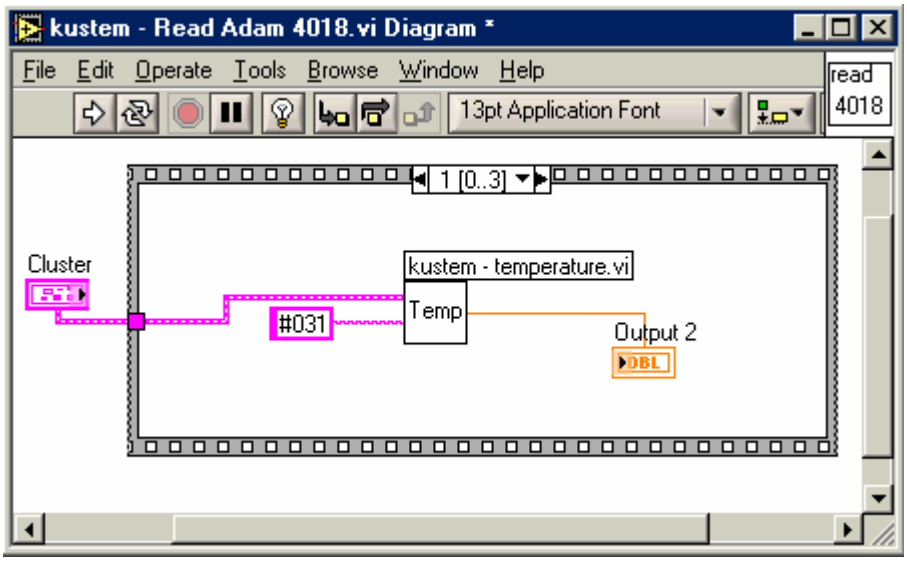

Figure 3.12: Acquiring temperature values from port no. 31.

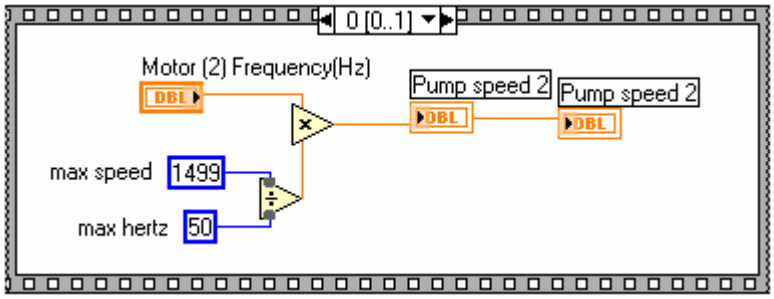

Figure 3.13: Case structure loop to calculate pump speed.

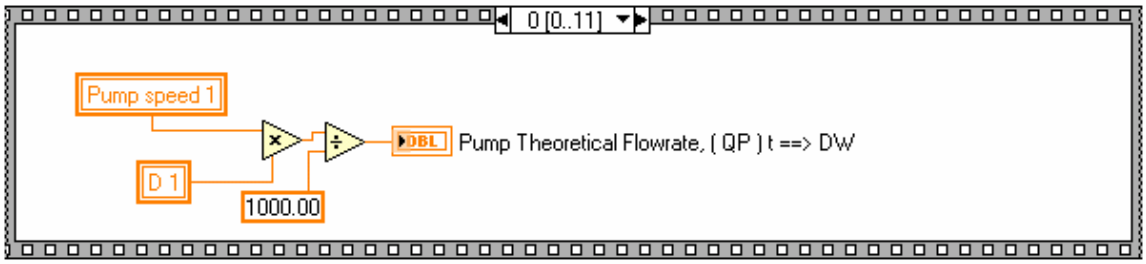

Figure 3.14: Program to calculate pump theoretical flow rate.

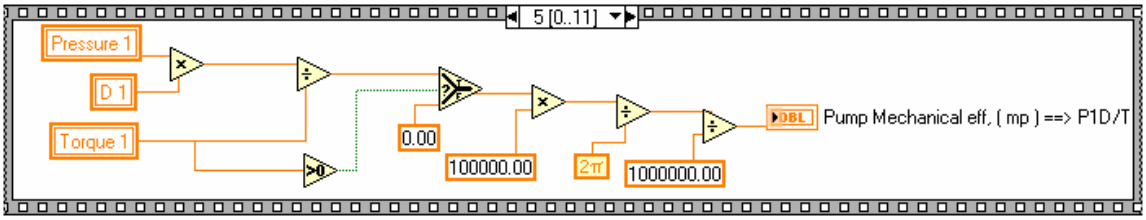

Figures 3.15: Program to calculate pump mechanical efficiency.

Figure 3.11 shows a WHILE loop so that hydraulic flow parameters can be acquired and monitored. The data is acquired until the EXIT button is pressed. Within the while loop, a case structure loop contains five operations. Figure 3.12 shows how the sub VI commands the computer to read data from port #31, in this case, temperature values. Similar sub VIs were developed for acquiring flow rate, torque and pressure data. The case structure also contains condition for the pump to be ON or OFF.

Figure 3.13 shows a case structure loop which contains two operations. Each operation calculates pump speed for each rig, given the Hz reading. As given in the inverter manual, maximum motor speed is 1499 rpm which corresponds to 50 Hz. Thus, in converting frequency reading to rotational speed, ratio of 1499/50 was used as multiplication factor to motor frequency input at the control panel. Figures 3.14 and 3.15 depict of how pump theoretical flow rate and mechanical efficiency were calculated automatically in this project.

With the aid of many tools the author was able to formulate the equations, mathematical operators, loops and built-in subroutines. The main program for running the hydraulic system is integrated in Graph2.vi (Appendix B).

3.5.9 Running of Hydraulic System

The procedure started with switch ON power supply and activation of data acquisition system. Using Advantech software, the communication port was searched and identified. When the respective addresses for pump and cooler activation, pressure, temperature, flow rate and load cell were identified, then the LabVIEW program was activated.

When all the PC work was done, manual check at the test rig was made. Shutoff valve was opened, peculiar sign (such as leakage) was observed and setting of loading valve was checked. Cooling system was checked. When everything was in good condition, the hydraulic system was ready to be operated.

PUMP icon was clicked and the pump was running. The speed of the pump was adjusted manually. So does the system pressure. System pressure was increased to the desired operating pressure by rotating the knob at the loading valve. When the system operation was judged satisfactory, all the operational data was saved via the computer data acquisition system in the local hard disk for further analysis. Before the accomplishment of the 'Graph2.vi' program, the data was recorded manually.

Sections 3.5.9.1 and 3.5.9.2 outline the hydraulic test procedures. Detailed test procedures and conditions are specifically noted in Sections 4.7 – 4.9.

3.5.9.1 Static Endurance Test

Static endurance test involves heating and shearing the palm oil in hydraulic test rig at particular temperature and load. Two phases of endurance tests were performed. The earlier phase involved circulating the oil at minimum loading and the oil temperature was maintained at 55^{o}C. The rig was run continuously at 600 rpm and minimal pressure. The total investigation period was 600 hours. Palm oil, with and without additives were used. The additives used were F10 (1.5% and 2.0%) and L135 (1.5%). Commercial rapeseed hydraulic oil was used as comparison. The

rheological and thermal test results are presented and discussed in Sections 4.4.1 and 4.6, respectively.

The latter phase involves operating the system at 70 bar, 1200 rpm and maintaining the oil temperature at 70^{o}C. The rig was run about 14 hours a day. Palm oil without additive was used in this test. Total flow and running hours were recorded manually and automatically by the LabVIEW. At about every 100 hour, 30 ml oil sample was retrieved from the rig for TGA, IR, TAN, IV and rheological tests as explained in Sections 3.3.2, 3.3.3, 3.3.4, 3.3.5 and 3.4.2, respectively.

3.5.9.2 Performance Test

During the high pressure (70 bar) operation phase, system performance test was performed at every 100 hour interval. The test conditions were:

Temperature: 30^{o}C to 70^{o}C
Pump speed: 600 rpm to 1440 rpm
Pressure: 0 bar to 210 bar.

At any particular test, only one parameter was varied. Basic performance and system efficiencies when running on palm oil with out additive are presented and discussed in Sections 4.7 – 4.9, respectively.

3.6 Data Collection and Analysis

3.6.1 TGA Activation energy determination

The thermogravimetric data from TGA test was used to determine rate of conversion. Using Excel Spreadsheet, plots of $\ln[(1/(1-x)(dx/dT)]$ versus $1/T$ and $\ln[-\ln(1-x)]$ versus $1/T$ were produced to determine activation energy based on direct Arhenius method (Equation 2 of Appendix C) and integration method (Equation 3 of Appendix C).

3.6.2 Determination of Order

Lately a number of researchers study the kinetic order of their samples (Gomez-Rico *et al*., 2003; Vuthaluru, 2004; Li and Yue, 2004) but none of the report shows the effect of aging on sample kinetic order. In this study a technique based on the Arrhenius equation, used by Mansaray and Ghaly (1999), was utilized to determine the kinetic parameters from typical curves of TGA data over an entire temperature range in a continuous manner. For the purpose of *n* order determination, the linearized form of the Arrhenius equation was used. Then multiple linear regressions were applied. The multiple regression analysis was done using Minitab statistical software. The simplified form of the linearized rate equation is as follows:

$$y = B + Cx + Dz \qquad 3.3$$

The parameters y, x, B, C and D in Equation 3.3 are defined as follows:

$y = \ln\{[-1/(w_o - w_\infty)][dw/dT]\}$

$x = 1/(RT)$

$z = \ln[(w_t - w_\infty)/(w_o - w_\infty)]$

$B = \ln A$

$C = -E_a$

$D = n$

3.6.3 Determination of Rheological Properties

3.6.3.1 Mathematica Program for Andrade Constants

Oil viscosity is a function of temperature. In addition, viscosity is also a function of shear rate and so the values of the four parameters (A, B, C and D) in Equation 2.9 change with shear rate. Therefore, program made using Mathematica software has to make sure these parameters were to be determined at constant shear rate for a range of temperature.

Program #D1 of Appendix D shows the Mathematica 4.2 program to determine the Andrade constants. The polynomial curve-fitting program was applied to each oil samples at eight different shear rates. The temperature range represented the range of temperature used, where the modified Andrade's equation was fitted into the experimental data. Regression correlation (R^2) and mean square error (MSE) were also calculated to determine the appropriateness of the fitted data. MSE stands for the mean of how much of the data spread unaccounted for by equation. The MSE and R^2 equations are based on predicted and experimental values as shown below:

$$\mathrm{MSE} = \frac{\sum \left(\eta_{\mathrm{pred}} - \eta_{\mathrm{exp}}\right)^2}{\text{number of data}} \qquad 3.4$$

$$R^2 = 1 - \frac{\sum \left(\eta_{\mathrm{pred}} - \eta_{\mathrm{exp}}\right)^2}{\sum \left(\eta_{\mathrm{ave}} - \eta_{\mathrm{exp}}\right)^2} \qquad 3.5$$

3.6.3.2 Mathematica Programs for Rheological Models

Some rheological parameters were obtained using Microsoft Excel. Some models could not be solved using the Excel. In order to determine the equation constants, nonlinear fit programs were made for Ostwald de-Waele, proposed modified power law, Cross, Carreau, Herschel-Bulkley and Casson models. Sample of the programs are included in Appendix D.

In general, the following steps were performed in the Mathematica programs:

- Experimental data, title, x-label, y-label were input and the required equation was set.
- The experimental data was transposed to matrix form.
- The non-linear regression package was loaded.
- Non-linear regression was performed and ANOVA table was produced.
- Experimental data and best fitted curve were plotted.
- The mean square error and coefficient of determination were calculated.

- The best-fitted equation constants were produced

3.6.4 Dimensionless Parameter

In many hydraulic models dealing with efficiencies, the parameters viscosity, speed and pressure seem to play important roles (Section 2.8). For this reason, it is of great interest to relate the efficiencies with these parameters. In fluid mechanics study, a technique which has proven very useful in reducing to a minimum number of experiments required is known as dimensional analysis (Massey, 1997).

Thus, in this study parameters viscosity, speed and pressure were lumped together, with the effect of units were taken into account. Volumetric, mechanical and overall efficiencies of the hydraulic system as function of dimensionless parameters were calculated and the relationship between efficiencies and dimensionless parameters were studied.

Information extracted from the resultant figures can help researchers to determine various efficiencies given important parameters such as oil viscosity or temperature, pump speed and operating pressure. This method can save the researchers' time in determining the system efficiencies and parameter coefficients.

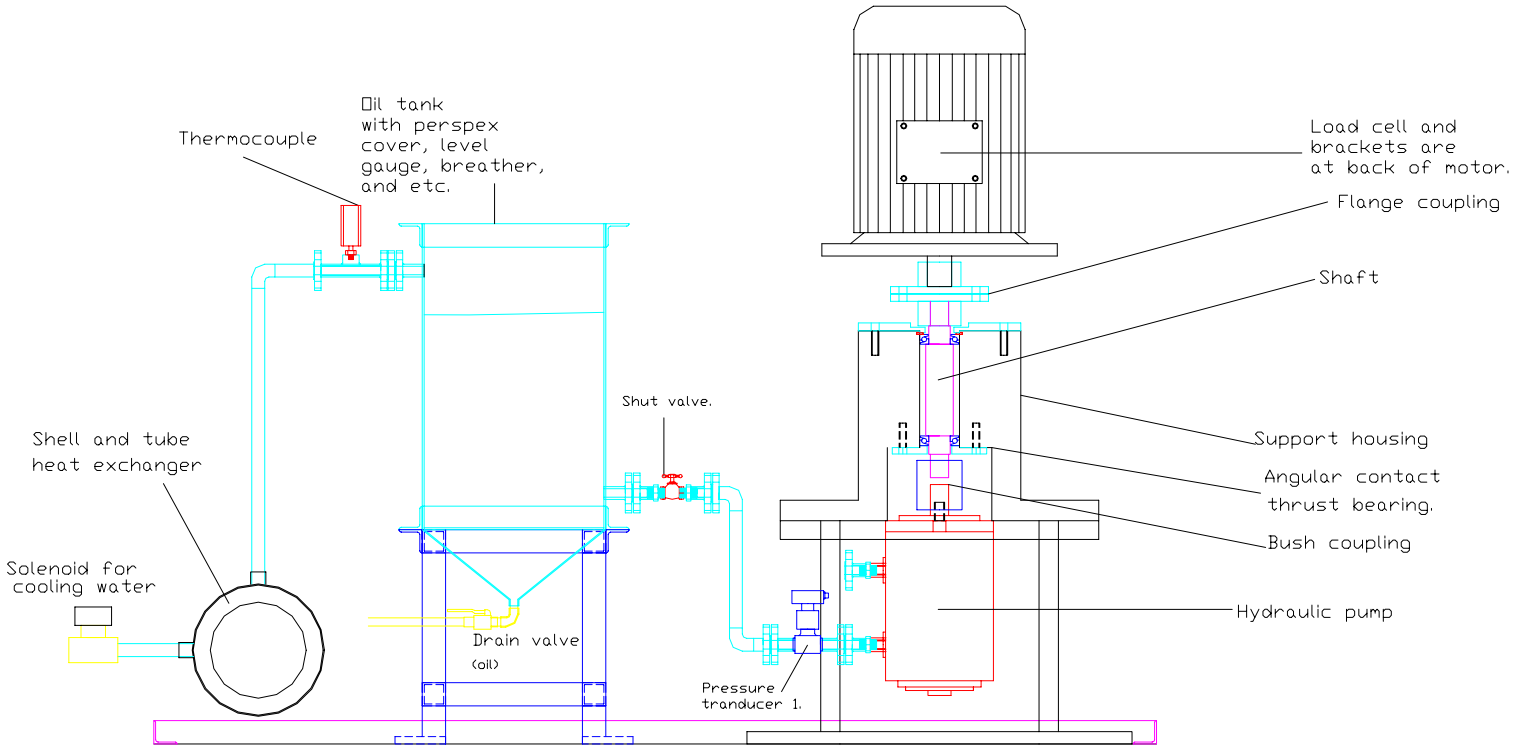

Figure 3.3a: Front view of test rig latest layout.

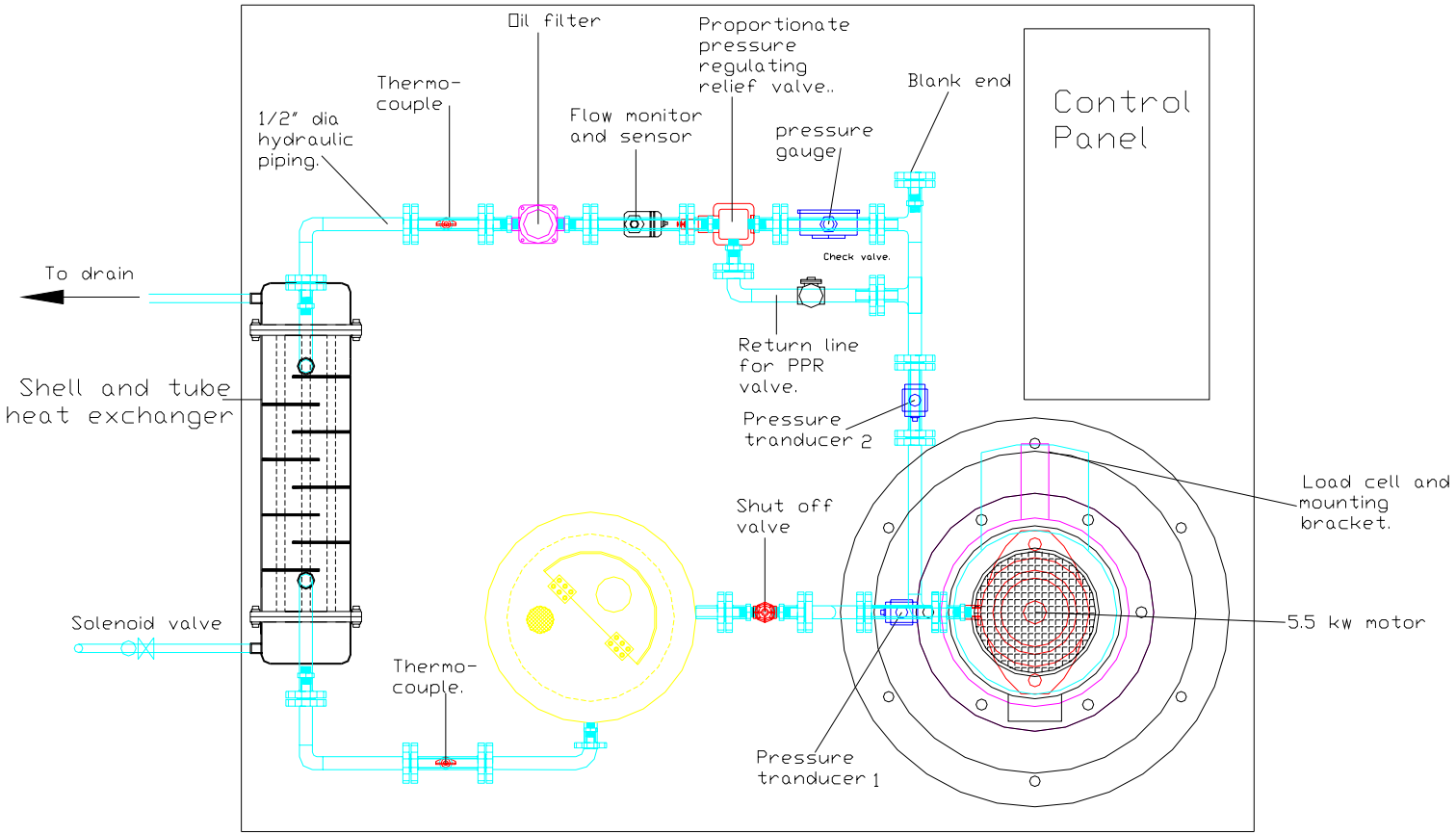

Figure 3.3b: Top view of test rig latest layout.

CHAPTER 4

RESULTS AND DISCUSSION

4.1 Introduction

In this chapter, all test results will be presented and discussed. In Section 4.2 basic rheological properties of oils are presented. This includes the effect of temperature, shear rates and blends. Section 4.3 discusses the effect of blends with mineral oil, aging time, aging temperature and aeration on rheological properties of palm oil when the oil was exposed to heat in bench test. Section 4.4 studies the rheological properties of palm oil when it was used in the built hydraulic test rig.

Section 4.5 presents the thermal performance of palm oils in bench tests. The performances of blended oils are compared. Section 4.6 presents the thermal performance of palm oils when it was operated in hydraulic test rig at 55^{o}C and minimum load. Sections 4.7 – 4.10 discuss performance of hydraulic system from various aspects. The results are based on hydraulic test rig running intermittently using unadditived palm oil.

4.2 Effect of Blending on Viscometric Properties and Rheological Behavior of Oils

4.2.1 RBD Palm Oil and Shell Tellus 100

Figure 4.1 shows the variation of dynamic viscosity with temperature when 100% RBD palm oil was sheared at speed of 60 rpm. Figure 4.2 shows the effect of changing viscometer rotational speed ranging from 3 to 100 rpm in measuring viscosity

of RBD palm oil. It was noticed that different viscosity values were obtained when different spindle speeds were used.

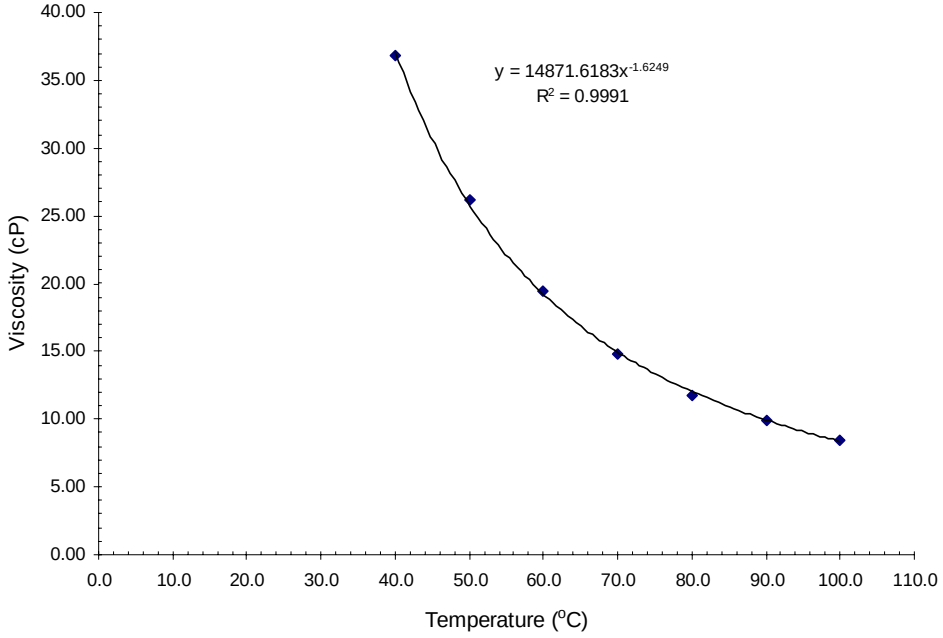

Figure 4.1: Dynamic viscosity of RBD palm oil at 60 rpm.

Figure 4.3 shows the variation of dynamic viscosity of Tellus100 with increasing temperature. Comparing with Figure 4.2., the variation of dynamic viscosity with temperature of Shell Tellus is larger. Another observation was that, effect of changing the viscometer speed was not very significant.

In order to study variation of viscosity of RBD palm oil at particular shear rate, Figure 4.4 was plotted. The figure shows the variation of dynamic viscosity with shear rate ranging from 30^{o}C to 100^{o}C for RBD palm oil. The apparent viscosity was found to decrease by approximately 250% with the increase in temperature from 40^{o}C to 100^{o}C at 60s^{-1}. All lines show that viscosity decreases with increasing shear rate until around 40s^{-1}, indicating a shear thinning behavior (as mentioned in Section 2.4).

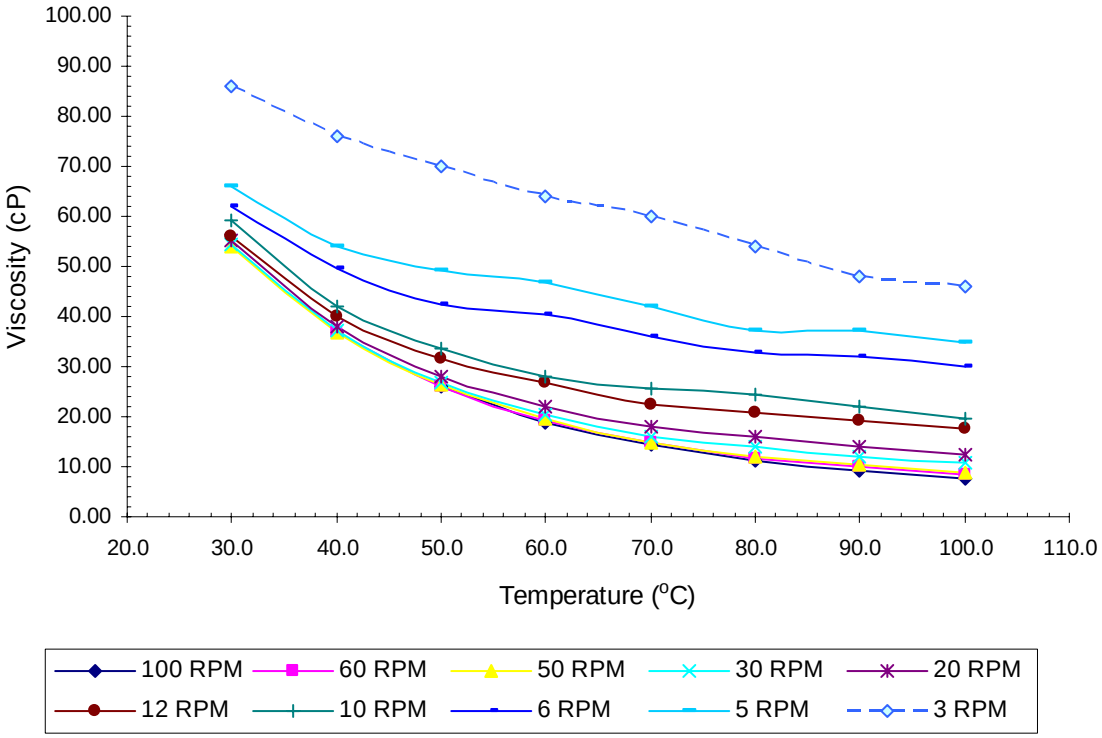

Figure 4.2: Viscosity as a function of temperature at constant shear rate of RBD palm oil.

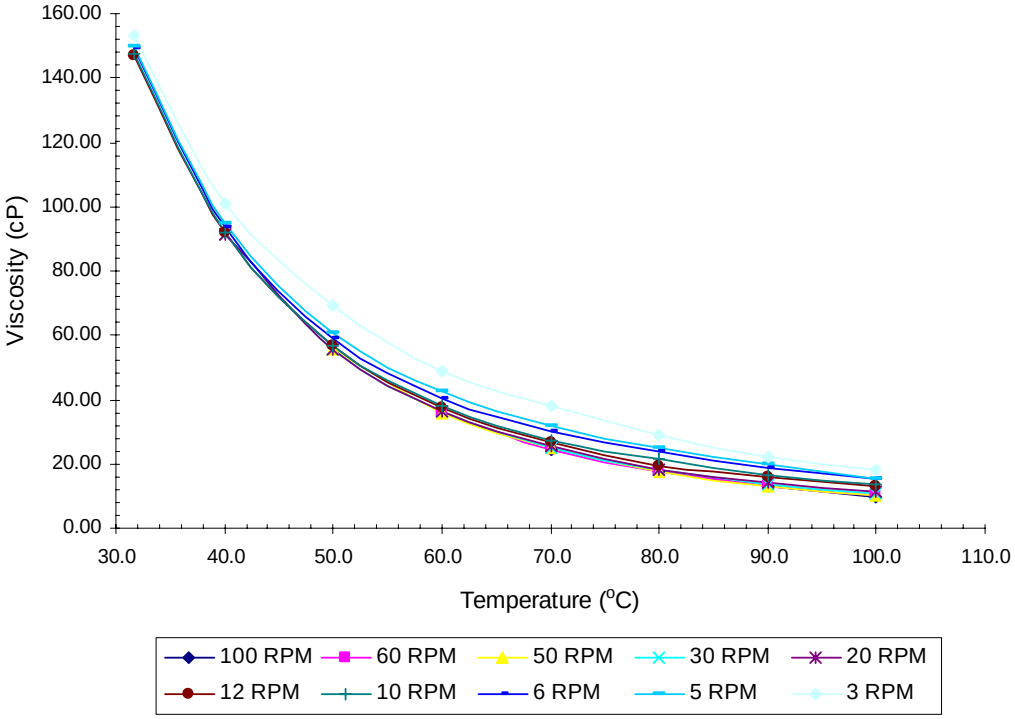

Figure 4.3: Viscosity as a function of temperature at constant shear rate of Shell Tellus 100.

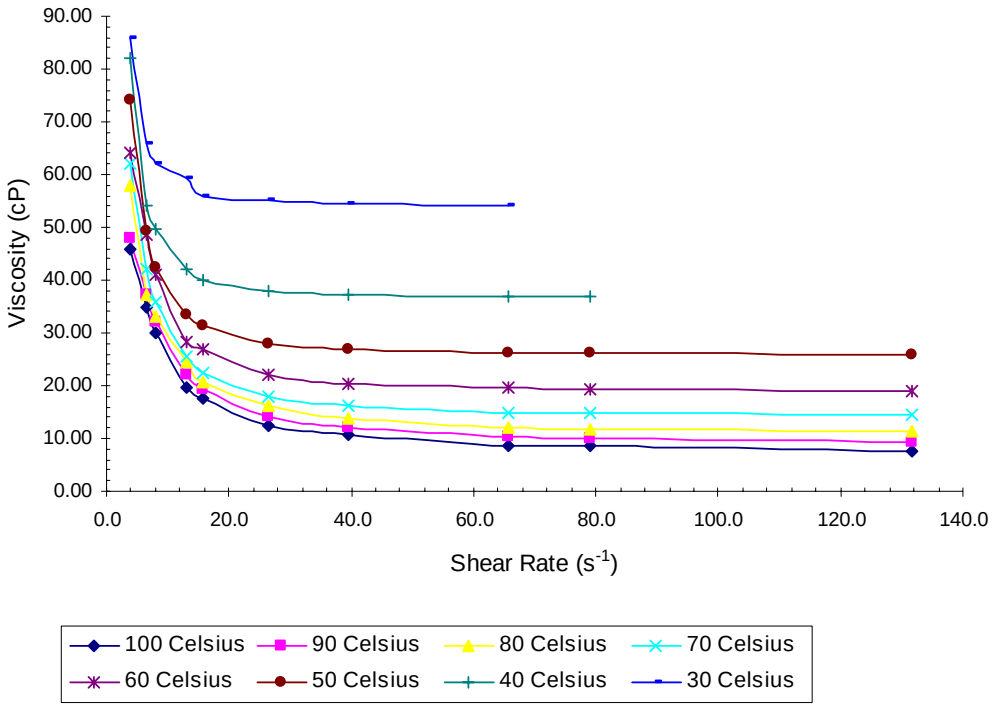

Figure 4.4: Flow diagram of RBD palm oil.

Figure 4.5 shows the variation of dynamic viscosity with shear rate ranging from around 30°C to 100°C for Shell Tellus. The deviation of viscosity with shear rate is not that significant compared to RBD palm oil. This might be attributed to the refined material of the Shell Tellus. Similar phenomena can also be seen from Figure 4.3.

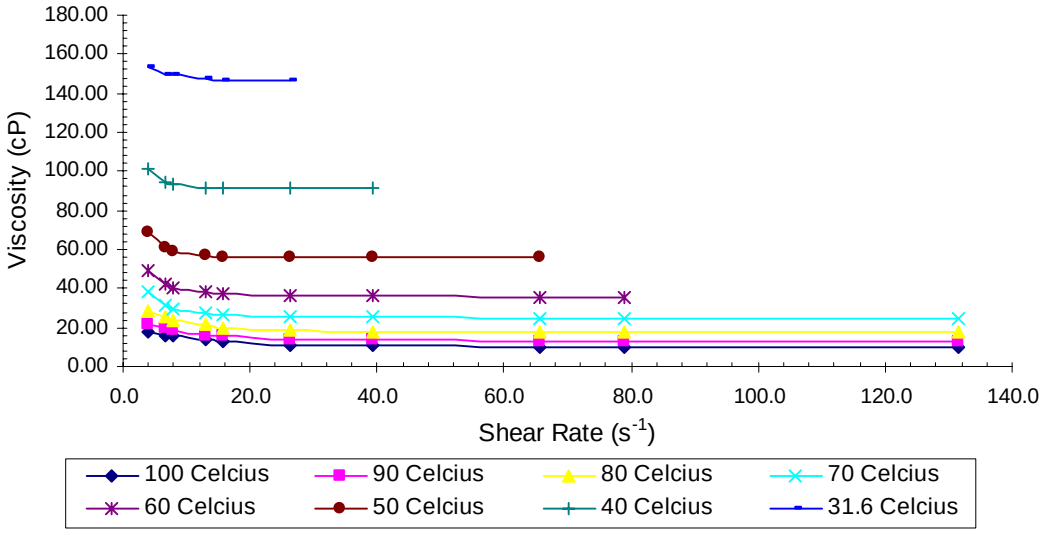

Figure 4.5: Flow diagram of Shell Tellus 100.

4.2.2 Superolein Palm Oil

Figure 4.6 shows variation of palm superolein viscosity with temperature when it was measured at different spindle speeds. There was no significant viscosity difference when it was measured at different speeds.

Figure 4.7 shows the variation of superolein with shear rate. The main difference between this oil with RBD type (Figure 4.4) is that viscosity of superolein does not change much with shear rate. The result shows that this oil has better Newtonian characteristics compared to RBD type. The result also may indicate that the more refined the oil, with less impurity and less saturated fatty acid, the higher Newtonian level.

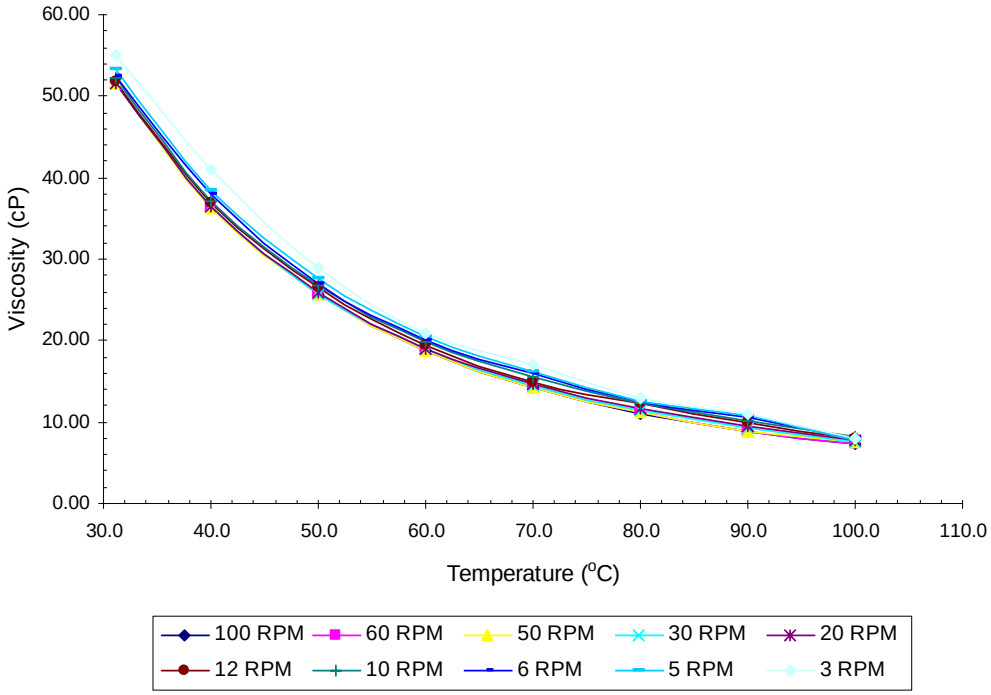

Figure 4.6: Flow diagram of superolein palm oil.

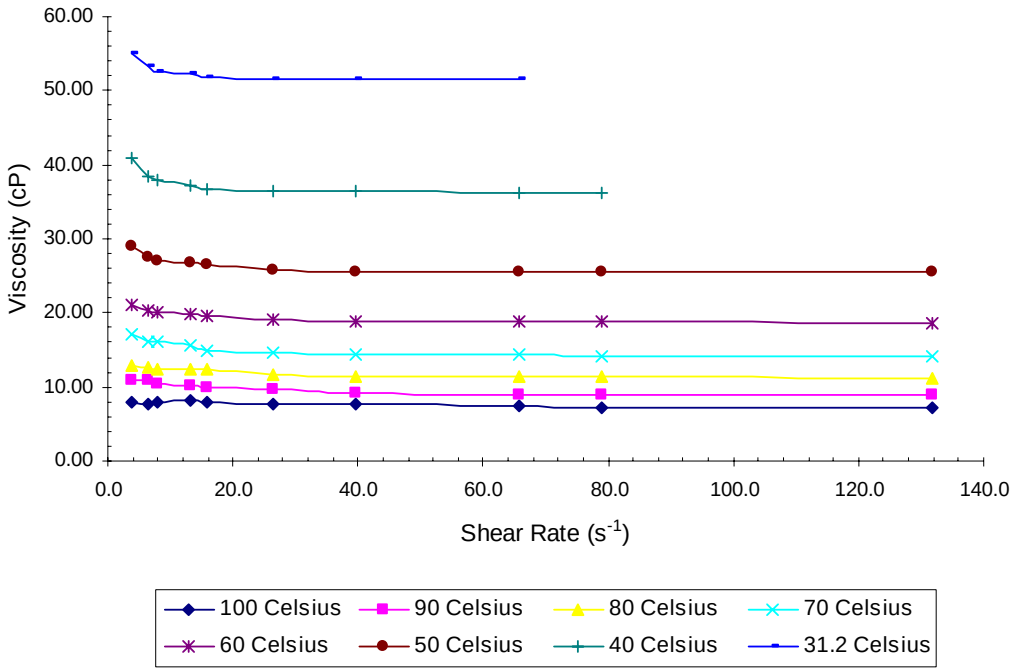

Figure 4.7: Dynamic viscosity for pure superolein with temperature and shear rate range of 31.2 - 100^{o}C and 3.9 - 131.6s^{-1}, respectively.

Figure 4.8 shows the relationship of shear stress and shear rate for superolein oil sample tested from 31.2^{o}C to 100^{o}C. Shear stress and shear rate were calculated using Equations 9 and 11 of Appendix B, respectively. Linear relationship between shear stress and shear rate was found for this sample (Figure 4.8). This result supports the result in Figures 4.6 and 4.7 that the more refined the palm oil, the better the Newtonian level. Interestingly, the correlation coefficients for all temperatures are above 0.998.

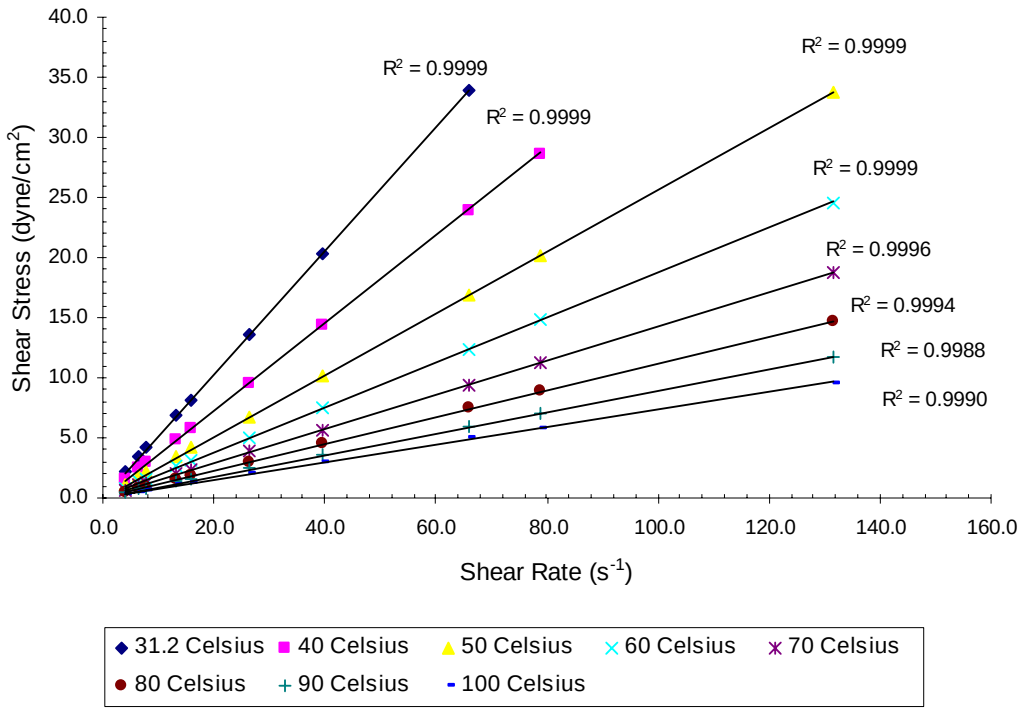

Figure 4.8: Plot of shear stress versus rate of shear for superolein.

4.2.3 Effect of Blend on Rheological Properties

Figure 4.9 presents the flow curves of RBD palm - mineral oils at the various blending ratio measured at 40°C. The figure shows that the palm oil sample and the blends behave as shear thinning fluid. The viscosity is high (82 cP) at low shear rate (3.9 s^{-1}). As the shear rate increases, the viscosity decreases until reaching a steady value. It means that the oil poses non-Newtonian behavior at low shear rate. The apparent viscosity is seen to be reasonably insensitive above shear rate of 26.3 s^{-1}. This means that the oil approaches Newtonian behavior as shear rate increases above this value. The non-Newtonian behavior of this plant oil might be attributed to the dissolved molecules (foreign molecules), mixed with the base oil molecules. According to the oil fatty acid composition, the oil is consisted of 44.4% saturated and 55.4% unsaturated fatty acid composition. The interaction between the small molecular sizes of the saturated fatty acid with the larger unsaturated molecules might give rise to the non-Newtonian oil structure.

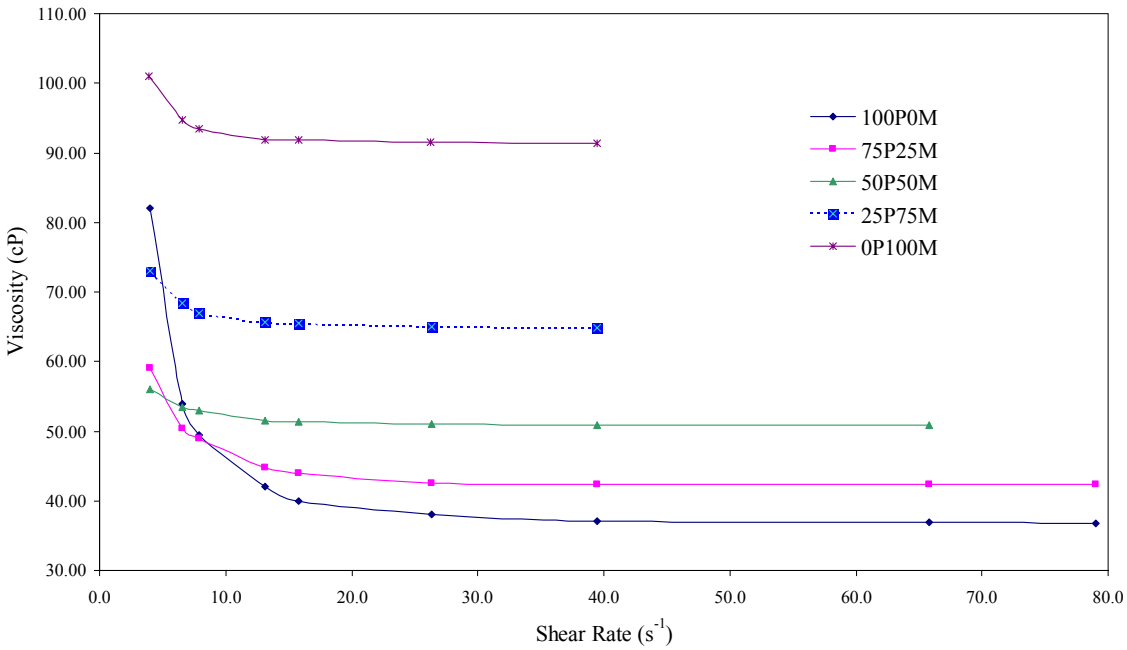

Figure 4.9: Flow curves of RBD palm - mineral oil blends at 40°C.

In short it can be said that the shear thinning effect is more obvious for palm oil compared to mineral oil. If this oil is further refined, reducing the amount of saturated fatty acid, the oil might approach Newtonian behavior.

This decrease viscosity phenomenon was not very significant for the mineral oil sample. The oil shows more Newtonian behavior. The oil with Newtonian behavior is preferred since the oil poses consistent internal resistance irrespective of shear rate. For the blended samples, their Newtonian behavior is very much improved when the mineral oil was introduced except for the 75P25M sample. Interestingly, the 50P50M sample is slightly better in terms of viscosity compared to 25P75M sample. The 50P50M curvature is less than 25P75M. This shows that this 50P50M blend behaves most Newtonian behavior compared to other samples including pure mineral oil. During the experiment, no separation of the two oils was noticed.

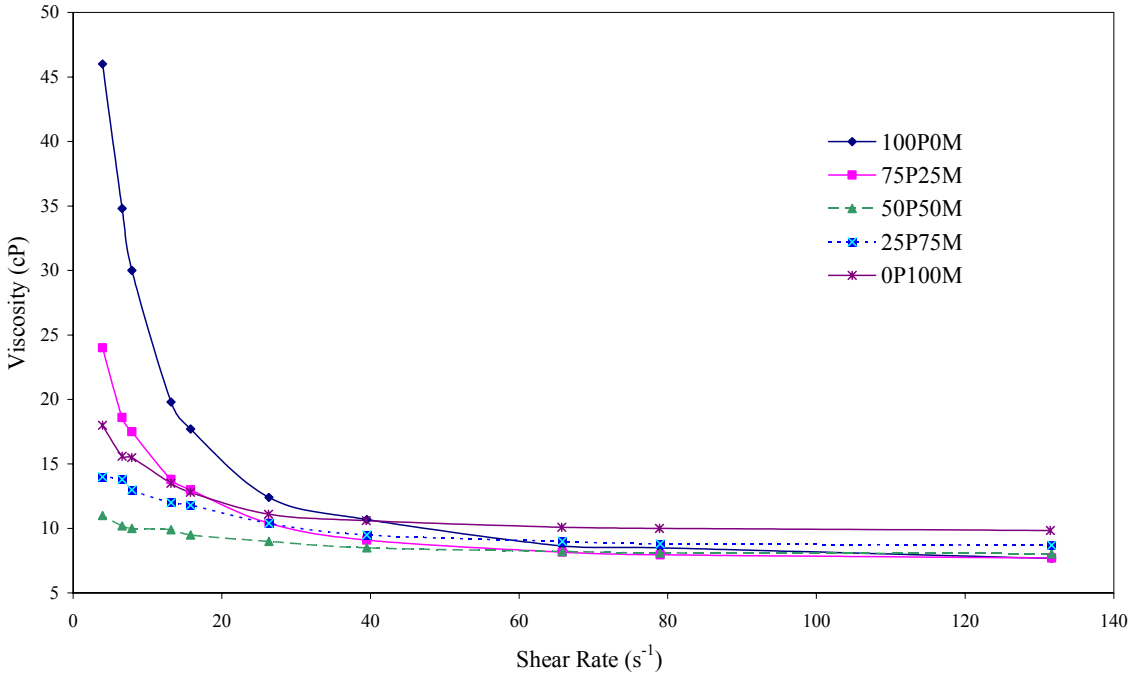

Figure 4.10: Flow curves of RBD palm - mineral oil blends at 100^{o}C.

Figure 4.10 shows the effect of shear rate of oils viscosity at 100^{o}C. Similar pattern was observed as in Figure 4.9, except the viscosity of oil samples at high shear rate is quite close together compared to significant difference for 40^{o}C case.

Shear thinning effect was observed for all samples as shear rate increases. However, comparing Figure 4.9 and Figure 4.10, it was observed that the shear thinning effect was less obvious for high temperature sample where the apparent viscosity is less dependent on shear rate. This statement is true for all palm, mineral and the blended samples. Investigation on bitumen (Ukwuoma and Ademodi, 1999) also shows that bitumen became more Newtonian in the higher temperature region.

The decreased value of viscosity with increasing shear rate, either at 40^{o}C or 100^{o}C, might also be due to rearrangement of oil molecular structure that decrease the value of flow resistance with increasing shear rate. The non-Newtonian behavior at lower shear rate is the property of pseudoplastic material. Due to limited capability at very high shear rate, it is not possible to measure the viscosity greater than 131.6 s^{-1}. However, it is expected that the viscosity value is maintained at this value.

4.2.4 Effect of Temperature and Blending on Flow Behavior

In order to better understand the pseudoplastic level of the samples, several rheological models as discussed in Section 2.6 were applied. Empirical constants were calculated. For Ostwald de-Waele model flow index, *n*, consistency coefficient, *k,* and correlation coefficient, R^2, were calculated using Excel 2000 and Mathematica 4.2 (Appendix D). Using the least square regression analysis, not only R^2, mean square error was also calculated.

Figure 4.11 shows log of viscosity versus log shear rate for RBD palm oil at 40, 60, 80, 100^{o}C. Equation 2.16 was used to determine rheological parameters using Microsoft Excel. From the best fit line, *n* and *k* values were calculated.

Table 4.1 shows that *n* value at 40^{o}C for 100% palm oil and Tellus samples are 0.7820 and 0.9626, respectively. The value less than unity shows that the oils exhibit pseudoplastic behavior. The higher value for Shell Tellus sample shows that Shell Tellus is more Newtonian than palm oil. Graphically, the *n* value is reflected by significant curve and horizontal straight lines in Figures 4.4 and 4.5, respectively.

In general Table 4.1 shows that with increasing of the mineral oil content, the value of the flow behavior index approaches to unity. This indicates that the level of the Newtonian increases with addition of mineral oil. The 50P50M blend has the highest *n* values. This shows that the maximum Newtonian level (least pseudoplasticity) occurs for 50% palm and 50% mineral blend. Again the value of *n* reflects directly the curvature of viscosity-shear rate in Figures 4.9 and 4.10. The highest *n* value of 50P50M blend (0.9689) was reflected by the smallest curvature while the lowest *n* value of 100P0M (0.7820) was corresponded to the largest upward viscosity slope (Figure 4.9).

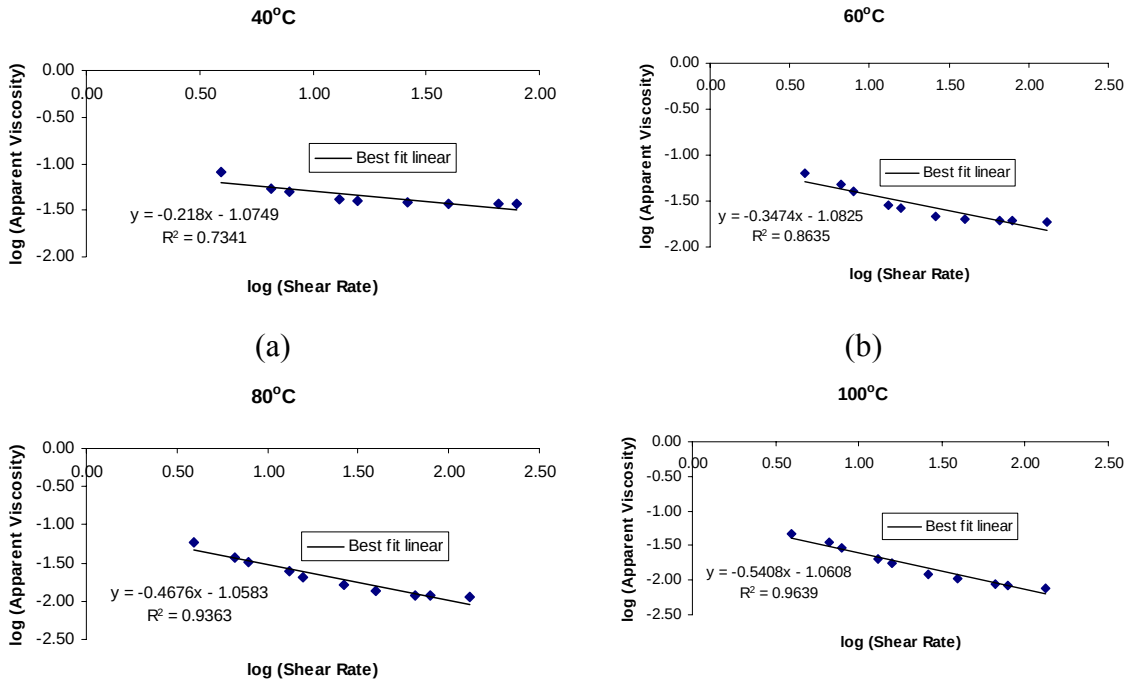

Figure 4.11: Plot of viscosity - shear rate in log form.

In general, from Table 4.1 consistency coefficient, *k*, for 75P25M, 50P50M, 25P75M and 0P100M samples for 100°C is lower than that of 40°C. This reflects the dependency of consistency index on temperature which influenced the oil viscosity. Decrease in consistency index with increasing temperature is also found in other samples (Hernandez *et al*., 1995; Goodrum *et al*., 2003).

Figure 4.12 shows experimental data and best flow curves produced using Mathematica 4.2 for RBD palm oil at 40, 60, 80, 100°C. The nonlinear program calculated and output the value of *n* and *k*. The rheological properties together with the R^2 are shown in Table 4.2. The value of *n* decreases with the increase in temperature. This observation was also reported by Kaur *et al*. (2002) who studied rheology of molasses.

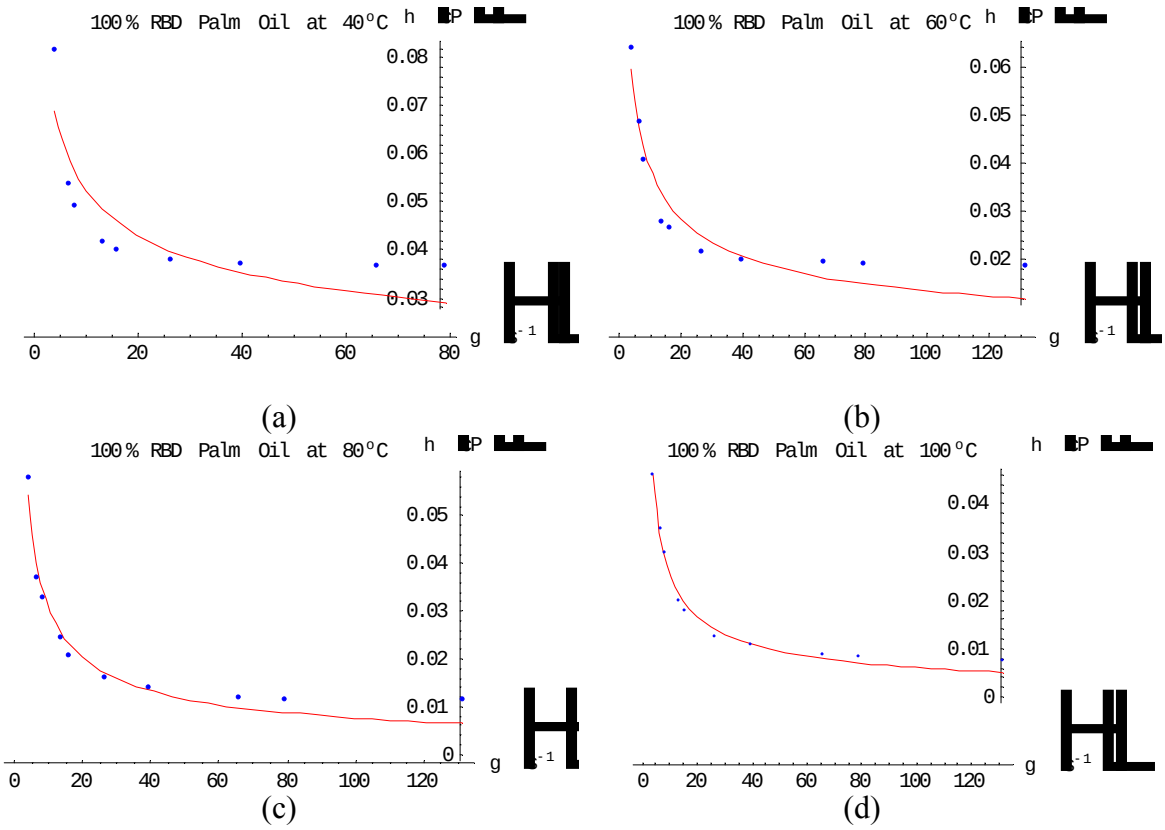

Figure 4.12: Experimental data and Ostwald de-Waele plot as output by Mathematica 4.2.

Comparing the correlation coefficients for data analyzed using Excel 2000 and Mathematica 4.2 for Ostwald de-Waele model, the latter gives better correlation compared to the former. This shows that analysis using dedicated Mathematica software can yield better accuracy compared to normal processing software. Variation of R^2 with temperature for Ostwald de-Waele model is shown in Figures 4.13a and 4.13b. The R^2 in Figure 4.13b is slightly higher than in Figure 4.13a.

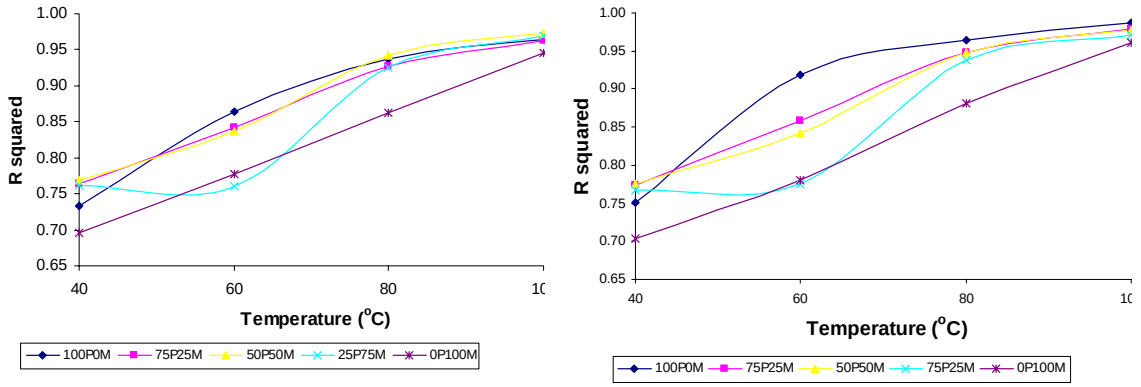

Figure 4.13: Variation of R^2 and MSE using (a) Excel 2000 and (b) Mathematica 4.2.

The next model attempted was the Simplified Cross model (Equation 2.18b). Using this form of simplified Cross model, the analysis cannot be performed using Excel 2000. In order to used Excel, Cross models had been simplified and linearized into the following form

$$\log (\mu/\mu_o) = \log (1/k_1) + m\ [\log (1/\gamma)] \qquad 4.1$$

Cross model of the Equation 2.18b form was also solved using Mathematica (Program #D3, Appendix D). Empirical constants for Simplified Cross, using both Excel 2000 and Mathematica 4.2 were summarized in Tables 4.3 and 4.4, respectively. Similar pattern is shown between m result for simplified Cross and *n* result for power law. This might be due to simplified Cross model which has the same form as the Power Law model. Since m=1-n, the result is basically reversed. Improved correlation coefficients were observed when the simplified Cross model was analyzed using Mathematica compared to Excel (Table 4.4 compared to Table 4.3).

Rheological properties of RBD palm oil, Tellus 100 and their blends were also analyzed using full Cross model (Equation 2.18a) and the linearized form of full Cross model, which are presented in Tables 4.5 and 4.6, respectively. Full Cross model gives better R^2 than Power Law and simplified Cross model indicates that full Cross model better fits the oils rheological data. Better fit of Cross model may be attributed to four additional parameters in the model compared to Power Law model which has only two parameters, *n* and *k*.

4.2.5 Modified Power Law Model

By comparing Figures 4.9 and 4.10, it is clear that shear thinning is more prominent for 40^{o}C than 100^{o}C case. The same observation was made for palm superolein (Figure 4.7). It can be concluded that the oils are more Newtonian at high temperature compared to low temperature. Thus it is expected that the flow index will increase with temperature. However Ostwald de-Waele model yields reducing flow index with increasing temperature (Tables 4.1 and 4.2). Contradiction between flow index of Ostwald de-Waele model and graphical flow curve pattern was observed. Thus

this model is not suitable to be used to visualize Newtonian level at different temperatures.

In order to better visualize the Newtonian level of the fluid at different temperatures, a modified power law model is proposed

$$\eta - \eta' = K\gamma^{n_m - 1} \qquad 4.2$$

where

$$\eta' = \eta_{100\,\mathrm{rpm}} - 0.010$$

The flow and consistency indices of this model were calculated using Program #D4 (Appendix D). The new flow behavior index and consistency coefficient were calculated and are shown in Table 4.7. As temperature increases, n_m increases while k_m decreases. Similar results are reported for some other plant oils (Wan Nik *et al*., 2004).

4.2.6 Andrade Constants

Figure 4.14 shows the graphical output of Program #A1 (Appendix A). Beside the best-fit curve, the program also calculated the Andrade constants and statistical results of the analysis. The results of RBD palm, superolein, Shell Tellus 100 and RBD palm – Shell Tellus 100 blends are summarized in Tables 4.8a to 4.8f.

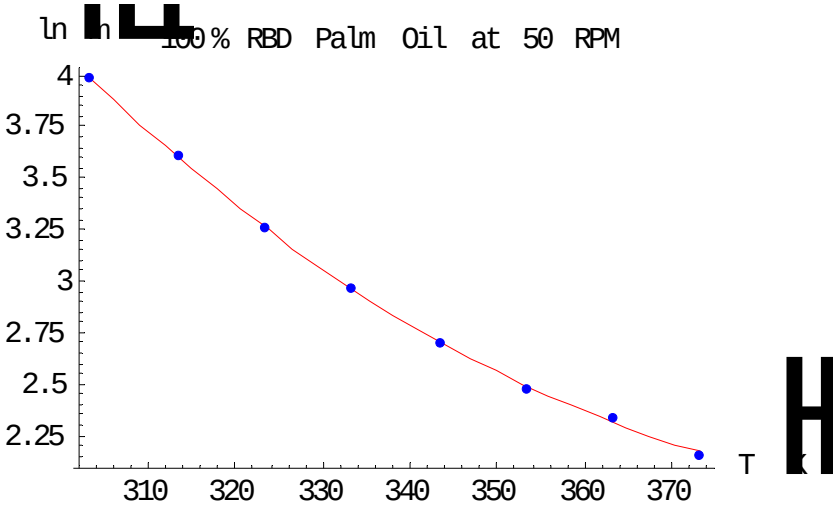

Figure 4.14: Best-fit curve for Andrade equation produced by Mathematica software.

Table 4.1: Ostwald de-Waele using Excel 2000 (Equation 2.16)

100% RBD Palm Oil					
Temp. (^oC)	n - 1	log k	n	k	R^2
40	-0.2180	-1.0749	0.7820	0.0842	0.7341
60	-0.3474	-1.0825	0.6526	0.0827	0.8635
80	-0.4676	-1.0583	0.5324	0.0874	0.9363
100	-0.5408	-1.0608	0.4592	0.0869	0.9639
75% RBD Palm Oil and 25% Tellus 100					
Temp. (^oC)	n - 1	log k	n	k	R^2
40	-0.0954	-1.2166	0.9046	0.0607	0.7646
60	-0.1864	-1.3409	0.8136	0.0456	0.8422
80	-0.2645	-1.4209	0.7355	0.0379	0.9268
100	-0.3377	-1.4625	0.6623	0.0345	0.9618
50% RBD Palm Oil and 50% Tellus 100					
Temp. (^oC)	n - 1	log k	n	k	R^2
40	-0.0311	-1.2453	0.9689	0.0568	0.7695
60	-0.0534	-1.5271	0.9466	0.0297	0.8363
80	-0.0803	-1.7333	0.9197	0.0185	0.9414
100	-0.0934	-1.9105	0.9066	0.0123	0.9722
25% RBD Palm Oil and 75% Tellus 100					
Temp. (^oC)	n - 1	log k	n	k	R^2
40	-0.0454	-1.1241	0.9546	0.0751	0.7616
60	-0.0859	-1.3955	0.9141	0.0402	0.7596
80	-0.1385	-1.5737	0.8615	0.0267	0.9252
100	-0.1591	-1.7471	0.8409	0.0179	0.9700
100% Tellus 100					
Temp. (^oC)	n - 1	log k	n	k	R^2
40	-0.0374	-0.9878	0.9626	0.1028	0.6964
60	-0.0881	-1.2985	0.9119	0.0503	0.7774
80	-0.1442	-1.4944	0.8558	0.0320	0.8623
100	-0.1819	-1.6605	0.8181	0.0219	0.9449

Table 4.2: Ostwald de-Waele using Mathematica 4.2 (Equation 2.15)

100% RBD Palm Oil

Temp. (^oC)	*k*	*n*	R^2
40	0.1021	0.7123	0.7516
60	0.1116	0.5413	0.9192
80	0.1238	0.3946	0.9649
100	0.1081	0.3742	0.9872

75% RBD Palm Oil and 25% Tellus 100

Temp. (^oC)	*k*	*n*	R^2
40	0.0625	0.8946	0.7742
60	0.0506	0.7783	0.8582
80	0.0425	0.6949	0.9475
100	0.0386	0.6213	0.9786

50% RBD Palm Oil and 50% Tellus 100

Temp. (^oC)	*k*	*n*	R^2
40	0.0570	0.9680	0.7753
60	0.0300	0.9441	0.8424
80	0.0186	0.9169	0.9471
100	0.0124	0.9046	0.9765

25% RBD Palm Oil and 75% Tellus 100

Temp. (^oC)	*k*	*n*	R^2
40	0.0755	0.9529	0.7679
60	0.0413	0.9054	0.7752
80	0.0274	0.8524	0.9386
100	0.0180	0.8401	0.9715

100% Tellus 100

Temp. (^oC)	*k*	*n*	R^2
40	0.1032	0.9612	0.7031
60	0.0515	0.9038	0.7800
80	0.0337	0.8389	0.8818
100	0.0227	0.8044	0.9603

Table 4.3: Simplified Cross model using Excel 2000 (Equation 4.1)

100% RBD Palm Oil

Temp. (^oC)	m	log ($1/k_1$)	k_1	R^2
40	0.2180	-0.1683	1.4733	0.7341
60	0.3474	-0.0220	1.0520	0.8635
80	0.4676	0.0072	0.9836	0.9363
100	0.5408	0.1468	0.7132	0.9639

75% RBD Palm Oil and 25% Tellus 100

Temp. (^oC)	m	log ($1/k_1$)	k_1	R^2
40	0.0954	-0.0800	1.2023	0.7646
60	0.1864	-0.1043	1.2715	0.8422
80	0.2645	-0.0229	1.0541	0.9268
100	0.3377	0.0190	0.9572	0.9618

50% RBD Palm Oil and 50% Tellus 100

Temp. (^oC)	m	log ($1/k_1$)	k_1	R^2
40	0.0311	-0.0234	1.0554	0.7695
60	0.0534	-0.0322	1.0770	0.8363
80	0.0803	-0.0121	1.0283	0.9414
100	0.0934	0.0103	0.9766	0.9722

25% RBD Palm Oil and 75% Tellus 100

Temp. (^oC)	m	log ($1/k_1$)	k_1	R^2
40	0.0454	-0.0272	1.0646	0.7616
60	0.0859	-0.0582	1.1434	0.7596
80	0.1385	0.0113	0.9743	0.9252
100	0.1591	0.0488	0.8937	0.9700

100% Tellus 100

Temp. (^oC)	m	log ($1/k_1$)	k_1	R^2
40	0.0374	-0.0370	1.0889	0.6964
60	0.0881	-0.0767	1.1932	0.7774
80	0.1442	-0.0507	1.1238	0.8623
100	0.1819	-0.0029	1.0067	0.9449

Table 4.4: Simplified Cross model using Mathematica 4.2 (Equation 2.18b)

100% RBD Palm Oil

Temp. (^oC)	k_1	m	R^2
40	1.2148	0.2877	0.7516
60	0.7794	0.4587	0.9192
80	0.6948	0.6055	0.9649
100	0.5737	0.6258	0.9872

75% RBD Palm Oil and 25% Tellus 100

Temp. (^oC)	k_1	m	R^2
40	1.1675	0.1054	0.7742
60	1.1459	0.2217	0.8582
80	0.9403	0.3051	0.9475
100	0.8556	0.3787	0.9786

50% RBD Palm Oil and 50% Tellus 100

Temp. (^oC)	k_1	m	R^2
40	1.0528	0.0320	0.7753
60	1.0684	0.0559	0.8424
80	1.0197	0.0831	0.9471
100	0.9713	0.0954	0.9765

25% RBD Palm Oil and 75% Tellus 100

Temp. (^oC)	k_1	m	R^2
40	1.0600	0.0471	0.7679
60	1.1128	0.0946	0.7752
80	0.9478	0.1476	0.9386
100	0.8913	0.1599	0.9715

100% Tellus 100

Temp. (^oC)	k_1	m	R^2
40	1.0850	0.0388	0.7031
60	1.1649	0.0962	0.7800
80	1.0680	0.1612	0.8818
100	0.9672	0.1956	0.9603

Table 4.5: Full Cross model using Mathematica 4.2 (Equation 2.18a)

100% RBD Palm Oil

Temp. (^oC)	α_c	*m*	R^2
40	0.2508	2.4683	0.9936
60	0.1772	1.9073	0.9968
80	0.2021	1.6938	0.9922
100	0.1516	1.6293	0.9986

75% RBD Palm Oil and 25% Tellus 100

Temp. (^oC)	α_c	*m*	R^2
40	0.2354	2.0828	0.9982
60	0.2187	1.4021	0.9778
80	0.1786	1.4980	0.9972
100	0.1678	1.2912	0.9973

50% RBD Palm Oil and 50% Tellus 100

Temp. (^oC)	α_c	*m*	R^2
40	0.2172	1.4472	0.9506
60	0.1821	1.5180	0.9922
80	0.1272	1.0821	0.9904
100	0.1029	1.1449	0.9745

25% RBD Palm Oil and 75% Tellus 100

Temp. (^oC)	α_c	*m*	R^2
40	0.2375	1.9626	0.9652
60	0.1931	1.9402	0.9849
80	0.1155	1.3899	0.9917
100	0.0772	1.1517	0.9887

100% Tellus 100

Temp. (^oC)	α_c	*m*	R^2
40	0.2673	2.6047	0.9945
60	0.2353	1.7591	0.9806
80	0.1808	1.5631	0.9947
100	0.1348	1.1575	0.9931

Table 4.6: Linearized Full Cross model using Mathematica 4.2

100% RBD Palm Oil

Temp. (^oC)	α_c	*m*	R^2
40	1.6840	0.9682	0.9576
60	0.8957	0.8982	0.9770
80	0.2354	1.3735	0.9873
100	0.0809	1.4119	0.9969

75% RBD Palm Oil and 25% Tellus 100

Temp. (^oC)	α_c	*m*	R^2
40	2.0308	0.9236	0.9147
60	1.2938	0.5937	0.8968
80	0.0280	1.7441	0.9983
100	0.3377	0.9668	0.9798

50% RBD Palm Oil and 50% Tellus 100

Temp. (^oC)	α_c	*m*	R^2
40	1.1319	0.5609	0.8359
60	1.2736	0.6699	0.8648
80	0.3819	0.7275	0.9518
100	0.0759	1.2214	0.9766

25% RBD Palm Oil and 75% Tellus 100

Temp. (^oC)	α_c	*m*	R^2
40	0.8486	0.8279	0.9487
60	2.1422	0.7200	0.8780
80	0.4760	0.7538	0.9084
100	0.1699	0.8639	0.9558

100% Tellus 100

Temp. (^oC)	α_c	*m*	R^2
40	1.5969	0.9628	0.9363
60	0.9104	0.8085	0.9799
80	0.7053	0.8742	0.9683
100	0.4151	0.7470	0.9616

Table 4.7: 100% RBD using modified power law model

Temp. (^oC)	n_m	k	R^2	MSE
40	0.1529	0.1627	0.8928	2.06298x10-6
60	0.3096	0.1385	0.9607	8.37305x10-6
80	0.3475	0.1304	0.9697	6.17831x10-6
100	0.4397	0.1029	0.9811	2.93832x10-6

Table 4.8a: Predicted parameters and statistics for 100% Shell Tellus 100

rpm	Constants for modified Andrade's equation				R^2	MSE	Temp. Range (^oC)
	A	B	C	D			
3	-7.4495000E+01	7.6183500E+04	-2.5775338E+07	3.0303613E+09	9.9963E-01	1.8103E-04	31.6 - 100
6	-6.0453300E+01	6.5512100E+04	-2.3493202E+07	2.9281249E+09	9.9987E-01	6.9534E-05	31.6 - 100
12	2.2643500E+01	-1.9698200E+04	5.3965705E+06	-3.1482066E+08	9.9989E-01	7.1483E-05	31.6 - 100
20	1.0010600E+01	-8.7840100E+03	2.2571457E+06	-1.4172891E+07	9.9998E-01	1.1447E-05	31.6 - 100
50	-1.5854900E+00	1.5772300E+03	-8.2964900E+05	2.9247091E+08	9.9999E-01	3.8165E-06	50 - 100

Table 4.8b: Predicted parameters and statistics for 100% RBD palm oil

rpm	Constants for modified Andrade's equation				R^2	MSE	Temp. Range (^oC)
	A	B	C	D			
3	1.7150000E+00	-1.3128700E+03	1.3551165E+06	-2.1360291E+08	9.8014E-01	9.2330E-04	30 - 100
6	-4.7809400E+01	5.2959600E+04	-1.8475848E+07	2.1806846E+09	9.9163E-01	4.4151E-04	30 - 100
12	-3.1614000E+01	3.7924000E+04	-1.4230426E+07	1.8215816E+09	9.9921E-01	1.0958E-04	30 - 100
20	-3.9010000E+01	4.4283600E+04	-1.6241299E+07	2.0526377E+09	9.9900E-01	2.3252E-04	30 - 100
50	3.4403900E+01	-3.2989300E+04	1.0486322E+07	-9.9443427E+08	9.9952E-01	1.7373E-04	30 - 100
100	-7.4996800E-01	1.3221400E+03	-7.2792000E+05	2.3240576E+08	1.0000E+00	5.1692E-07	50 - 100

Table 4.8c: Predicted parameters and statistics for 25% Shell Tellus 100 - 75% RBD palm oil

rpm	Constants for modified Andrade's equation				R^2	MSE	Temp. Range (^oC)
	A	B	C	D			
3	-5.7308400E+00	7.7820000E+03	-2.6713924E+06	3.7539203E+08	9.9813E-01	2.7713E-04	30 - 100
6	-3.8299100E+01	4.2068900E+04	-1.4824249E+07	1.8123726E+09	9.9984E-01	3.0645E-05	30 - 100
12	-6.9724100E+00	1.1386100E+04	-5.0610978E+06	7.9857520E+08	9.9997E-01	8.5608E-06	30 - 100
20	9.6599100E+00	-6.8472500E+03	1.3823984E+06	5.7226746E+07	9.9995E-01	1.9105E-05	30 - 100
50	-6.1964300E+00	6.5233300E+03	-2.3854204E+06	4.1258707E+08	9.9979E-01	6.4617E-05	40 - 100
100	-6.5804000E+00	6.7063900E+03	-2.4279210E+06	4.2019155E+08	9.9999E-01	2.5518E-06	50 - 100

Table 4.8d: Predicted parameters and statistics for 50% Shell Tellus 100 - 50% RBD palm oil

rpm	Constants for modified Andrade's equation				R^2	MSE	Temp. Range (^oC)
	A	B	C	D			
3	6.0097600E+00	-5.9604700E+03	1.9677699E+06	-9.2438740E+07	9.9946E-01	2.3629E-04	30.9 - 100
6	-2.6839300E+01	2.7362600E+04	-9.3078070E+06	1.1775410E+09	9.9997E-01	1.3794E-05	30.9 - 100
12	-1.9027200E+01	2.0512700E+04	-7.3968804E+06	1.0098363E+09	9.9992E-01	3.6540E-05	30.9 - 100
20	2.5828700E+00	-1.7137000E+03	1.5246500E+05	1.6171789E+08	1.0000E+00	3.9686E-07	30.9 - 100
50	3.0042200E+00	-3.2763600E+03	9.9878400E+05	3.6965484E+07	9.9999E-01	5.3506E-06	40 - 100
100	-4.3214000E+01	4.5333800E+04	-1.6056342E+07	2.0326998E+09	1.0000E+00	3.5587E-07	60 - 100

Table 4.8e: Predicted parameters and statistics for 75% Shell Tellus 100 - 25% RBD palm oil

rpm	Constants for modified Andrade's equation				R^2	MSE	Temp. Range (^oC)
	A	B	C	D			
3	-1.0652300E+02	1.0654900E+05	-3.5297612E+07	4.0078471E+09	9.9946E-01	2.3180E-04	30.2 - 100
6	-7.4884800E+01	7.7940200E+04	-2.6887482E+07	3.2052295E+09	9.9979E-01	9.4723E-05	30.2 - 100
12	-5.6451200E-01	4.0513700E+03	-2.5729939E+06	5.5397555E+08	9.9985E-01	7.6487E-05	30.2 - 100
20	9.6904600E+00	-7.5855100E+03	1.6740698E+06	5.0137814E+07	9.9986E-01	8.0803E-05	30.2 - 100
50	-3.2411200E+01	3.3856800E+04	-1.2004074E+07	1.5633198E+09	9.9997E-01	8.4451E-06	50 - 100
100	-7.7146600E+01	8.0812200E+04	-2.8463014E+07	3.4893666E+09	1.0000E+00	1.5002E-08	60 - 100

Table 8f: Predicted parameters and statistics for 100% superolein

rpm	Constants for modified Andrade's equation				R^2	MSE	Temp. Range (^oC)
	A	B	C	D			
3	-6.8882095E+01	6.5964943E+04	-2.1067938E+07	2.3562967E+09	9.9948E-01	2.3871E-04	30 - 100
6	-1.7742505E+01	1.6596177E+04	-5.2287638E+06	6.6638674E+08	9.9947E-01	2.2704E-04	30 - 100
12	1.9310498E+00	-3.1718527E+03	1.3539813E+06	-6.0932989E+07	9.9994E-01	2.7505E-05	30 - 100
20	4.5919705E+00	-5.2514356E+03	1.8699028E+06	-1.0042377E+08	9.9998E-01	7.9494E-06	30 - 100
50	6.1754045E-02	-7.5177016E+02	3.8492238E+05	6.2175483E+07	9.9999E-01	4.3477E-06	30 - 100
100	-2.0471859E+01	2.0668035E+04	-7.0509280E+06	9.2112773E+08	9.9999E-01	2.4935E-06	50 - 100

As shown from Tables 4.8a to 4.8f, the polynomial curve-fitting software was applied to each oil samples at 6 different shear rates. The temperature range was representing the range of temperature, where the modified Andrade's equation was fitted into the experimental data.

The experiment has proven that the behavior of Shell Tellus 100, RBD palm, superolein and their blends exhibited more linear viscosity-shear rate relationship (Newtonian behavior) at high temperature (100^oC) which indicates that the shear rate has less effect on viscosity and the viscosity of the oils depend heavily on the changes of temperature. However, at low temperature (30^oC) the shear rate has a larger effect on changes of viscosity of all the oils being investigated. Noticeable curve was seen at low shear rate region on viscosity-shear rate graph. Shear rate contributes to the changes of viscosity of the oils, but this effect was less pronounced for pure Shell Tellus 100 and pure superolein when compared to pure RBD palm oil.

From the results of regression tabulated in Tables 4.8a - 4.8f the lowest coefficient of determination and the highest mean square error are 0.98014 and 9.2330×10^{-4}, respectively. As a rule of thumb, a good fit accounts for at least 99 percent of the data variation, where this value corresponds to $R^2 \geq 0.99000$ (Palm, 2001). Overall, there was only one reading of coefficient of determination less than 0.99000,

which was happened at 3 rpm for 100% RBD palm oil. The variation of R^2 and MSE is shown in Figures 4.15a and 4.15b, respectively. Therefore, by referring to these coefficients of determination and mean square error values, a concrete statement can be made that superolein, RBD palm oil and their blends with Shell Tellus 100 were very well fitted to the modified Andrade's equation.

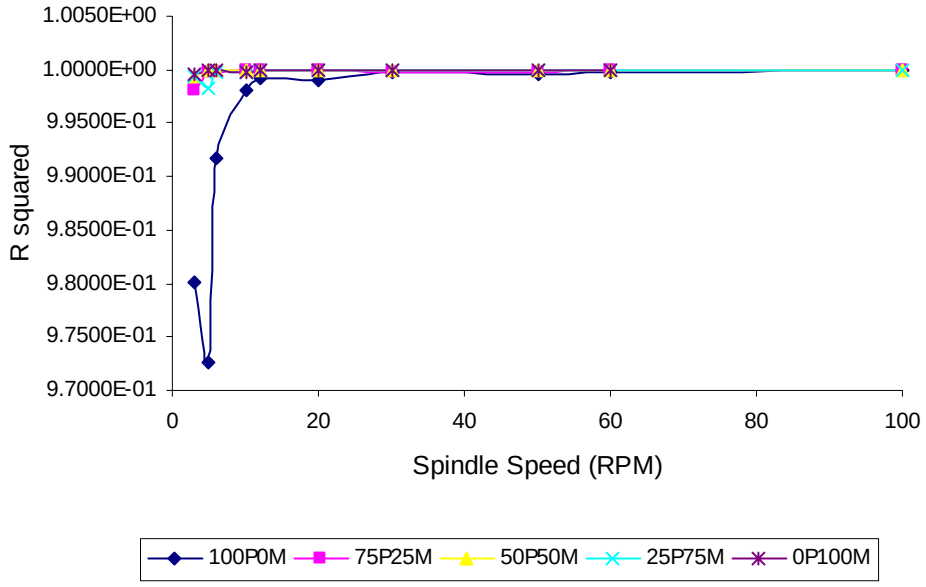

Figure 4.15a: R^2 for Andrade equation using Mathematica 4.2.

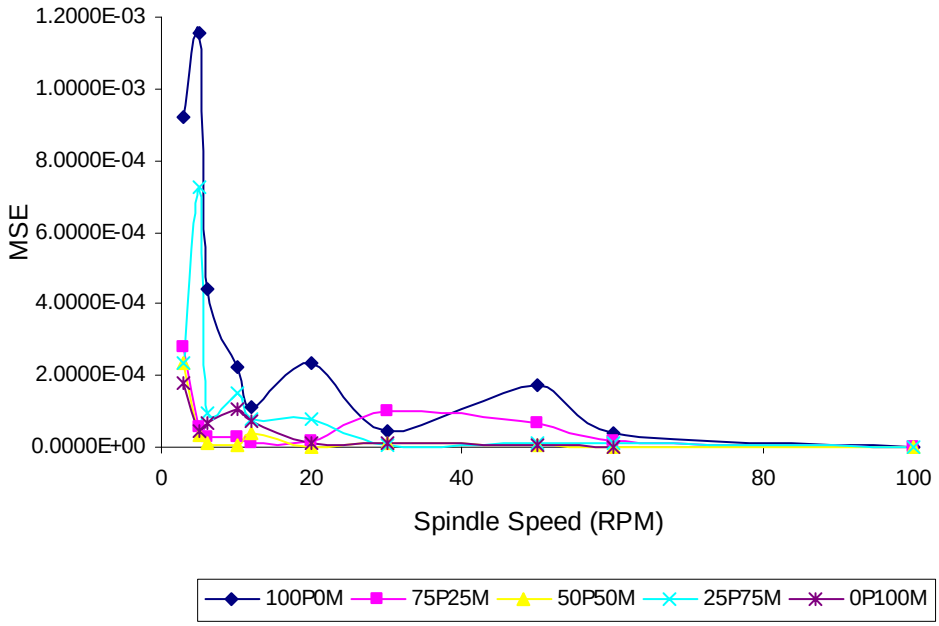

Figure 4.15b: MSE for Andrade equation using Mathematica 4.2.

4.2.7 Effect of Blending on Viscosity, Viscosity Index and Density

Previous studies (Adhvaryu *et al*., 2000; Wan Nik *et al*., 2002, 2003a) show that vegetable oil is not oxidatively stable. Using unadditive or unformulated vegetable oil, the oil can deteriorate after short time. When deterioration occurs, the oil is changed at shorter interval. Some user may blend or top-up the oil with other oil types of different viscosity grades.

When the oil was changed or top-up, the oil properties would change. Important oil properties such as viscosity and density would also change. These changes would have significant effect on system performance. Because of the above reasons, it is of importance to determine the viscosity and density of oil mixtures. There is no direct relation between oil viscosity and oil oxidative stability.

Figure 4.16 shows the viscosity relationship of RBD palm oil with the percentage addition of Shell Tellus 100 when the viscosity was measured at 50^{o}C and spindle speed of 50 rpm. The relationship between viscosity and percentage of Tellus can be written as

$$\eta = 0.0028\%^2 + 0.0021\% + 26.709 \qquad 4.3$$

The viscosity does not increase linearly with amount of Shell Tellus added but with the above relationship. This interesting observation is further studied in this section and theoretical relationships in Section 2.6 are used.

Figure 4.17 shows the effect of blending Shell Tellus and RBD palm oil at shear rate of 50 rpm for temperatures from 30^{o}C up to 100^{o}C. For case study, kinematic viscosities at 50^{o}C were used to predict the viscosity of the blends.

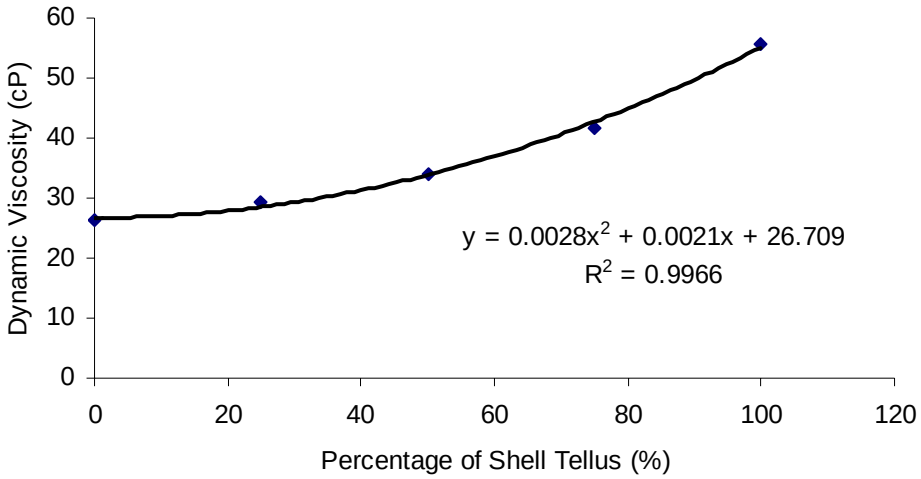

Figure 4.16: Viscosity variation of palm with the addition of Shell Tellus.

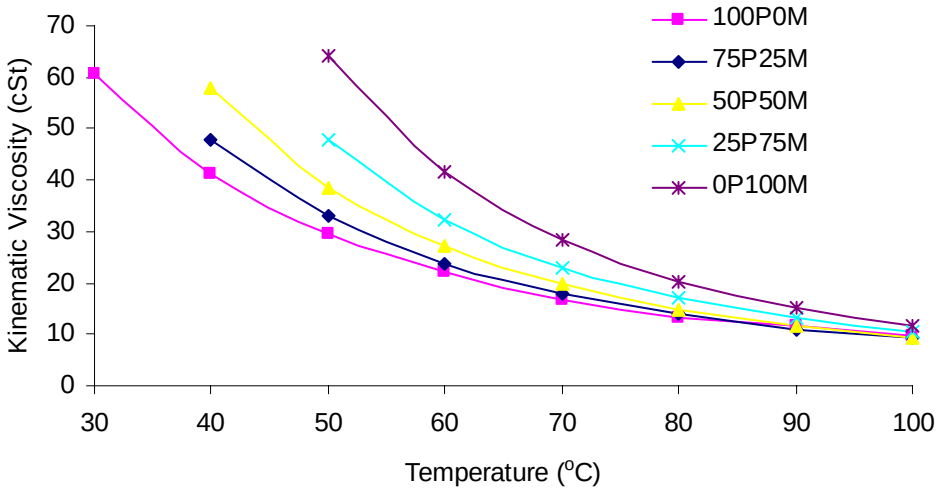

Figure 4.17: Effect of blending on viscosity – temperature variation (at shear rate of 50 rpm).

Section 2.6 discusses several models to predict viscosity of mixtures. Based on these models, another three models are proposed to predict the viscosity of mixtures.

Model 1:

$$\mu_{AB} = \mu_A * x_A + \mu_B * x_B \qquad 4.4$$

or in general,

$$\mu_{AB} = \Sigma\, \mu_i\, x_i$$

where x_i is the wt% of individual element

Model 2:

$$\mu_{AB} = \mu_A^{xA} + \mu_B^{xB} \quad 4.5$$

or making this into general equation,

$\eta_{AB} = \Sigma\, \eta_i^{xi}$.

Model 3:

$$\mu_{AB} = \mu_A^{xA} * \mu_B^{xB} \quad 4.6$$

or making this into general equation,

$\mu_{AB} = \Pi \mu_i^{xi}$.

The proposed Model 1 was based on mixing type rule used in lubricating oil blends (Diaz *et al*., 1996). The proposed Model 2 and 3 were based on Arrhenius form of relationship.

Tables 4.9 – 4.11 shows the comparison of experimental and predicted dynamic viscosity, kinematic viscosity and viscosity index of oil blends. S in ninth column is the factor in Equation 2.26 to be determined by trial and error. With the dynamic viscosities of RBD and Shell Tellus 100 at 26.3 cP, 55.6 cP respectively, Table 4.9 shows that Lederer equation is the best model to predict the dynamic viscosity of mixture. Very small error percentage suggests that the accuracy is high and this model is very suited to predict the dynamic viscosity of the blends. The next best model to predict the dynamic viscosity of the palm and mineral blends are Rahmes model, Model 3, Dow model, Goodrum model and Model 1. Model 2 is not suitable to predict the dynamic viscosity of mixtures.

Even though Lederer equation gives the least error in predicting the mixture viscosity, the troublesome is that the correction factor S has to be determined by trial and error. This suggests that experimental work still needed to be conducted in the case where different blending ratios or different oils types are used.

The work in using different models to predict properties of oil mixtures was extended to kinematic viscosity (Table 4.10). Same ranking was observed as in Table 4.9. However the accuracy of the models was different. Rahmes model in predicting kinematic viscosity results in better accuracy compared to predicting dynamic viscosity.

Based on the smaller error results in Table 4.10 compared to Table 4.9, this study suggest that when using Rahmes model in predicting the viscosity of the blends, kinematic viscosity is better to be used compared to dynamic viscosity. On the other hand, when using Model 3 in predicting mixture viscosity, it is better to deal with dynamic viscosity. Dow and Goodrum model results also suggest that dynamic viscosity is to be used, instead of kinematic viscosity.

Viscosity index (VI) was calculated according to ASTM D2271. Figure 4.18 shows the variation of VI of blend when Shell Tellus was blended with RBD palm oil. The viscosity index for the Shell Tellus is 93. The viscosity index for the Tellus increases linearly with the addition of RBD palm oil.

The models were also used to predict viscosity index of the oil blends. The results are shown in Table 4.11. Similar to the dynamic and kinematic viscosity results, Lederer equation can give the least error, but after some effort in manipulating the correction factor. Based on the results, next best models are Dow, Model 3, Goodrum and Model 1.

Surprisingly, Rahmes model gives significant error. This might be due to unlinearity of the model while Figure 4.18 shows that the viscosity index of the blends is linear with respect to blending ratio. On the other hand, Dow, Model 3, Goodrum and Model 1 predict the viscosity index better compared to Rahmes model.

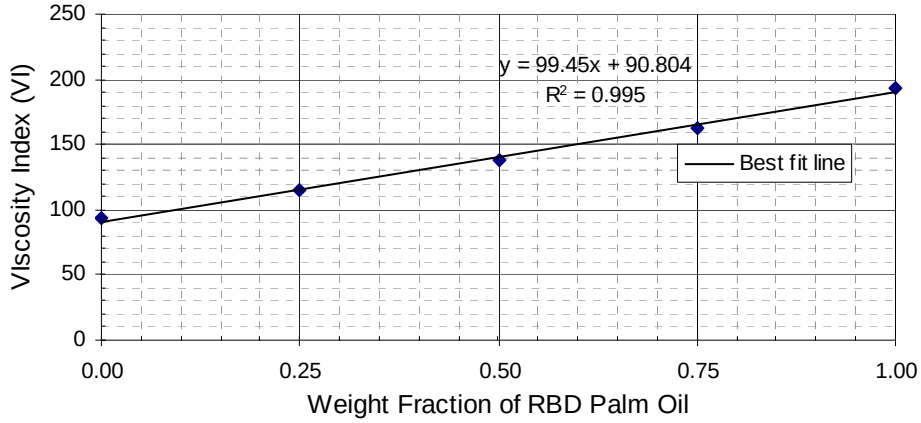

Figure 4.18: Variation of viscosity index with weight fraction of palm oil.

Figures 4.19 and 4.20 show the variation of specific gravity, as measured using a hydrometer and pycnometers, of RBD palm, Shell Tellus and their blends. Figure 4.19 shows that the specific gravity for all oils is linearly decreasing with temperature. In another aspect, Figure 4.20 shows that the specific gravity for Shell Tellus increases linearly with the addition of RBD palm oil for all temperature cases.

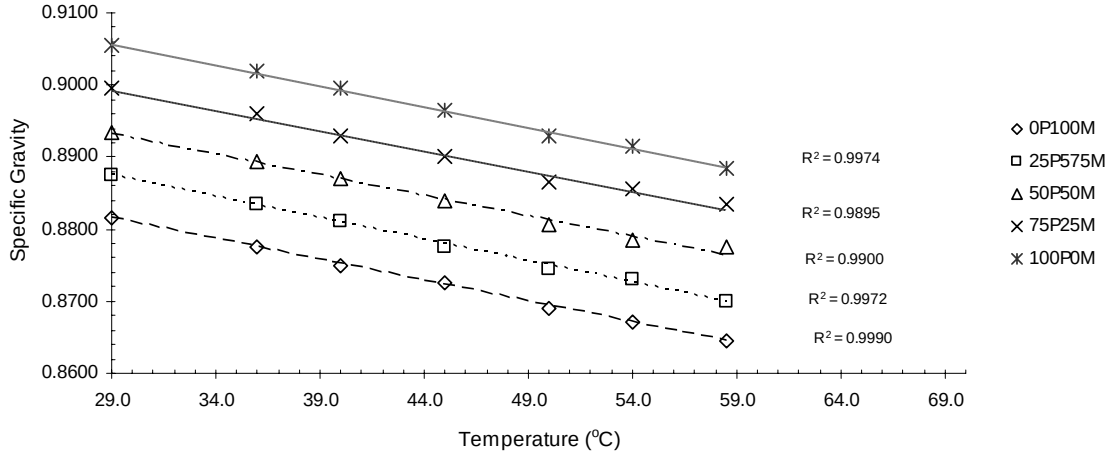

Figure 4.19: Variation of specific gravity of blends with temperature.

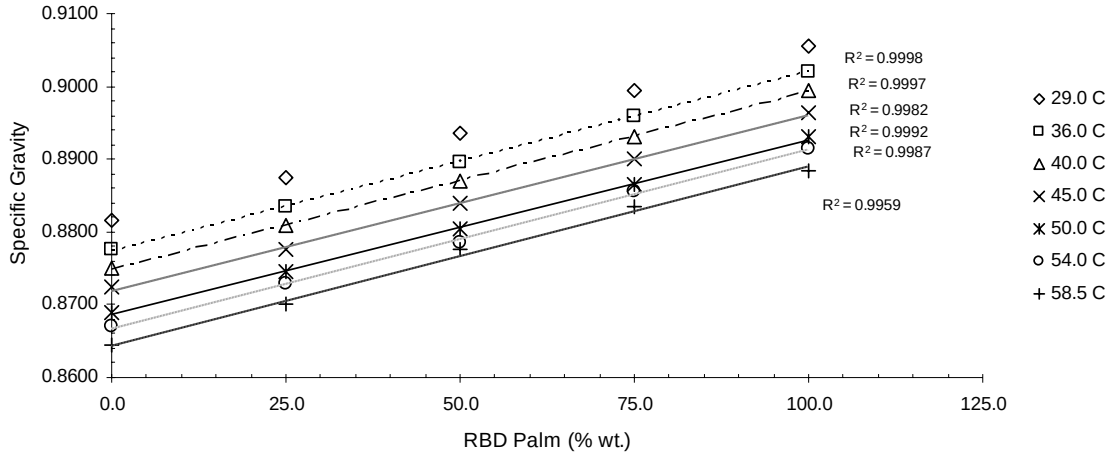

Figure 4.20: Variation of specific gravity of RBD palm, Shell Tellus and their blends.

Specific gravity refers to ratio of oil density to water density. This means that density of oils under study is linearly decreasing and increasing with temperature and RBD palm blending ratio, respectively. This is similar to viscosity index versus blending ratio relationship. Thus simulation work using the above models was not performed on density. It is expected that the best and worse models to simulate density would be similar to that of viscosity index.

4.3 Rheological Performance from Bench Tests

4.3.1 Effect of Aging Time on Rheological Properties of Palm – Mineral Blends

Figure 4.21 shows the changes of oil dynamic viscosity with heating time for palm oil and its blends with mineral oil when heated at 95^{o}C in bench test. Considerable viscosity change occurred to the pure palm oil, while very minimal change occurred to the Shell Tellus 100. Intermediate effect was observed for the blends. Interesting phenomena was observed between 0 hour and 48 hour. Slight viscosity decrease was observed at 48 hours. Some oil structure change might occur to the oil components that results in reduced viscosity. Similar result was observed to the palm oil ran in hydraulic system at 70 bar and 70^{o}C (Section 4.4.2).

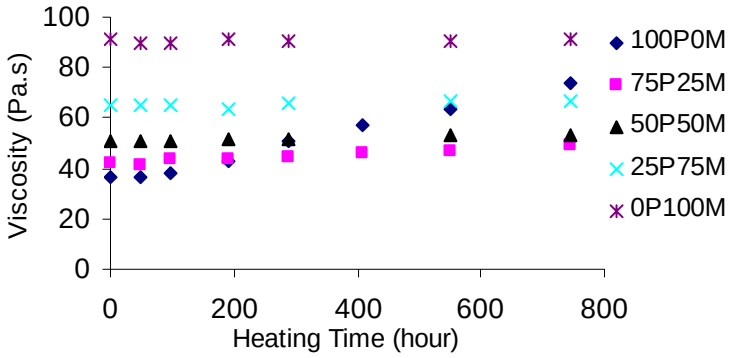

Figure 4.21: Changes of palm – mineral blends viscosity with heating time.

Figure 4.22 shows the flow diagram of palm oil at 48, 96, 192 and 288 hours. The figure suggests that the oil samples are becoming more Newtonian as heating progresses. In order to confirm this observation, the flow properties for selected sample and sampling hour were calculated. Flow property of RBD palm oil when heated at 95^{o}C for 48, 96 and 192 hours, as analyzed by Ostwald de-Waele model is presented in Table 4.12. Almost all cases, flow index decreases consistently with increasing temperature, except n_{192} for 70^{o}C is higher than for 60^{o}C. The decrease in n with the increase of temperature is similar to result of Tables 4.1 and 4.2. It is expected that n should be closer to unity as temperature increases. However the opposite results were obtained using Ostwald de-Waele model. This model may not suitable to be used to visualize Newtonian level at different temperatures.

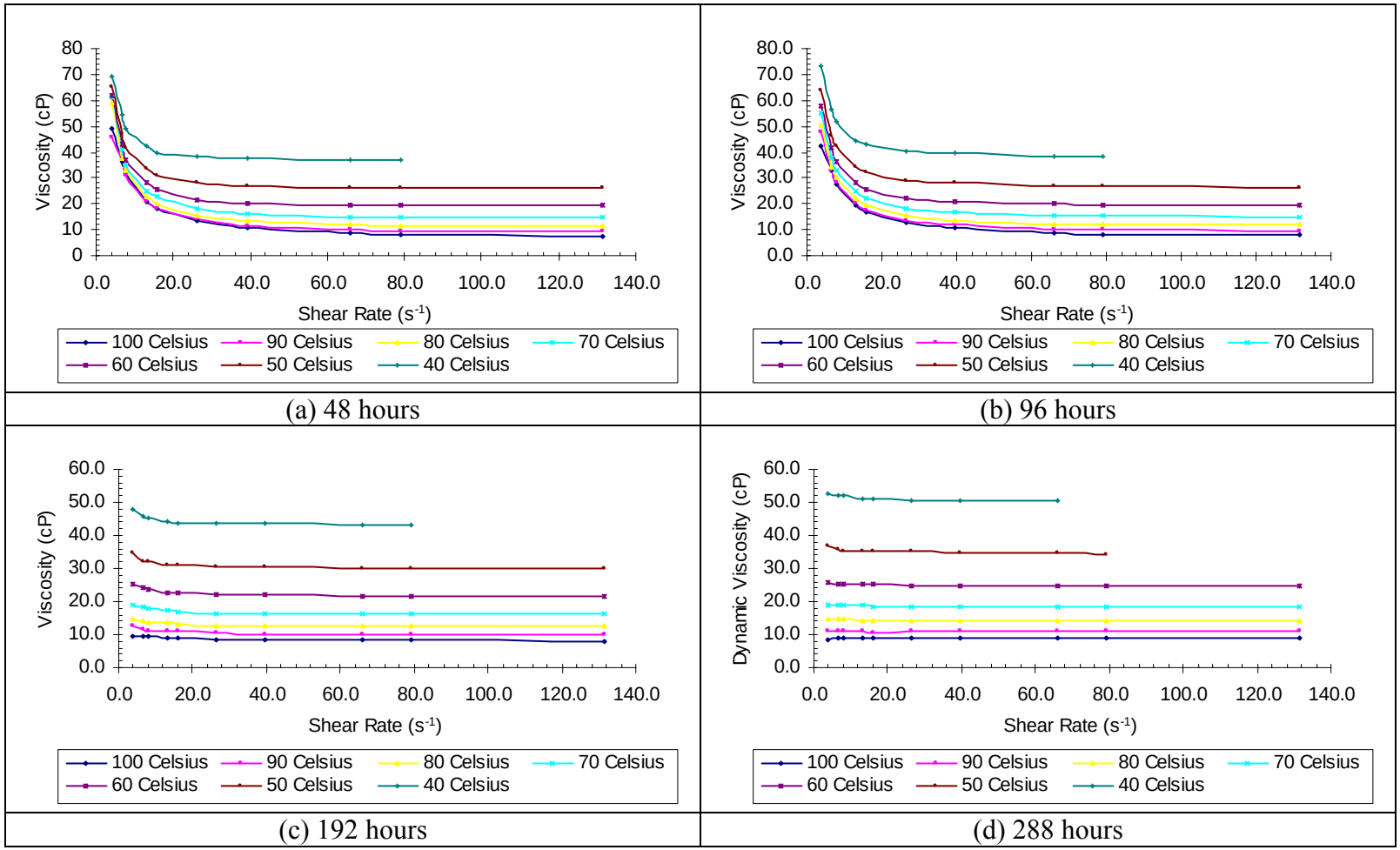

Figure 4.22: Flow diagram of palm oil at different heating time in bench test.

Table 4.12: Flow index of RBD palm at n_{48}, n_{96} and n_{192} using Ostwald de-Waele model

Temperature °C	Flow index		
	n_{48}	n_{96}	n_{192}
40	0.6880	0.7706	0.9703
50	0.6537	0.7096	0.9652
60	0.5663	0.6153	0.9550
70	0.4834	0.5208	0.9559
80	0.4452	0.4603	0.9507
90	0.4068	0.4248	0.9490
100	0.3636	0.4045	0.9373

It was expected that when the oil damaged, the Newtonian level decreases. Interestingly, results in Table 4.12 show the reverse. The flow index increases with heating time ($n_{192} > n_{96} > n_{48}$), applied to all temperatures. This confirms the observation seen in Figure 4.22. The Newtonian level increases with heating period. The explanation to this phenomenon might be in the aspect of triglyceride molecular chains. As the oil was heated, the chain broke. With the short chain condition, the oil internal resistance remains low even at low shear rate.

Table 4.13: Consistency index of RBD palm at 192 and 408 hour using Ostwald de-Waele model

	192 hour			408 hour		
Temp. (°C)	*k*	R^2	MSE	*k*	R^2	MSE
40	0.0485	0.7841	4.5153×10^{-7}	0.0665	0.8100	1.0081×10^{-6}
60	0.0262	0.8657	1.9683×10^{-7}	0.0358	0.7954	1.0076×10^{-6}
80	0.0155	0.8497	9.0787×10^{-9}	0.0232	0.9074	3.1382×10^{-7}
100	0.0102	0.9686	8.0016×10^{-9}	0.0156	0.9722	5.0082×10^{-8}

Table 4.13 shows the consistency index for 192 and 408 hour cases. For each temperature, the *k* value for 408 hour case is higher than the 208 hour case. This is due to increase in viscosity with aging period, since *k* is the viscosity related constant. The high R^2 and low MSE at higher temperature indicates that the data fitted better for the Ostwald de-Waele model at higher temperatures.

4.3.2 Effect of Aeration Level on Rheological Properties

This bench test was conducted mainly in order to study the effect of aeration in hydraulic reservoir. When hydraulic oil returns to the reservoir, bubbling and aeration occurs (Figure 4.23). The severity depends on the oil flow rate and breather condition. Figure 4.24 shows the effect of aeration on viscosity level of the palm oil in a bench test at 95°C. The oil was heated up to 400 hours. The oil viscosity was measured every 100 hours. The viscosity ratio is the ratio of current viscosity to the initial viscosity. Without aeration (A), the viscosity increased at almost constant rate. The figure shows that when the aeration was introduced the viscosity level exponentially increased with heating time. Doubling the aeration rate increased the viscosity level much further. In other words, with the presence of aeration, oil degradation rate increases.

Figure 4.23: Bubbling and aeration in hydraulic system.

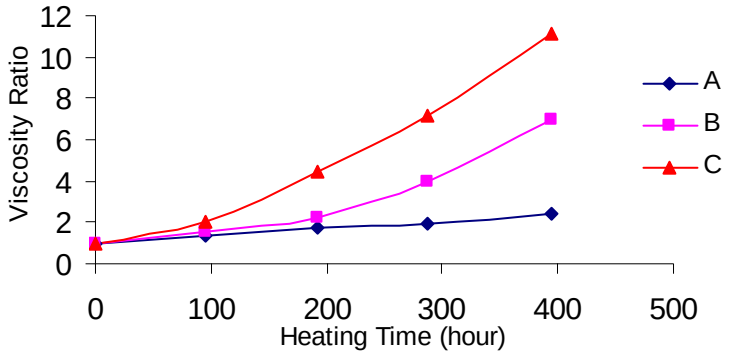

Figure 4.24: Effect of aeration on viscosity at 95°C: A – without aeration; B – 15 ml/min aeration; C – 30 ml/min aeration.

This bench result has significant importance on the oil condition when it is operated in real hydraulic system. Beside aeration in hydraulic reservoir as mentioned above, in real operation the oil passes several hydraulic components

where mixing the oil with air trapped in the system is possible. When the oil enters a hydraulic reservoir from a long piping system, it is allowed to rest and mixed with the contained air in the reservoir. According to this bench result, the resultant is the increased viscosity after prolong use. The increased viscosity is then sucked by the pump. If the pump starts from rest, i.e., running from low rpm, the pseudoplastic behavior of this increased viscosity oil can cause significant problems. In term of pump power, significant input pump is required to run the pump or will reduce mechanical and overall efficiencies. Often cavitation can occur, although a pump could cope with the sheared oil. Cavitation can take place when there is not enough oil in suction chamber. The pump might be unable to initiate flow of oil if the oil has been rested for some time and significant viscosity increase occurs. Based on the results from this bench test, it is expected that the oxidation of oil in real hydraulic system will be much severe compared to the pure heating condition in bench test (Section 4.3.1).

4.3.3 Effect Aging of Oil due to Temperatures on Viscosity

Figure 4.25 shows the bench test results of viscosity variation with heating temperatures. Temperature of 55^{o}C was used since the normal operating temperature of well-conditioned hydraulic system is 35-55^{o}C. In the bench test, the increase in viscosity was minimal when heated statically at 55^{o}C. The 70^{o}C environment was used since the recommended temperature for evaluating hydraulic fluid is 70^{o}C. Minimal viscosity increase was also observed when heated at temperature of 70^{o}C.

The 95^{o}C and 135^{o}C test temperatures were used since there are testing standards use these temperatures as the testing condition in evaluating functional fluids (Section 2.3.2). Significant viscosity increased occurred when the palm oil was heated at 95^{o}C. The rate doubled when the heating temperature of 135^{o}C was used. It can be summarized that, based on heating temperature only, the normal grade of palm oil can be used without significant viscosity increase if run up to 70^{o}C (no other degrading factors involved.

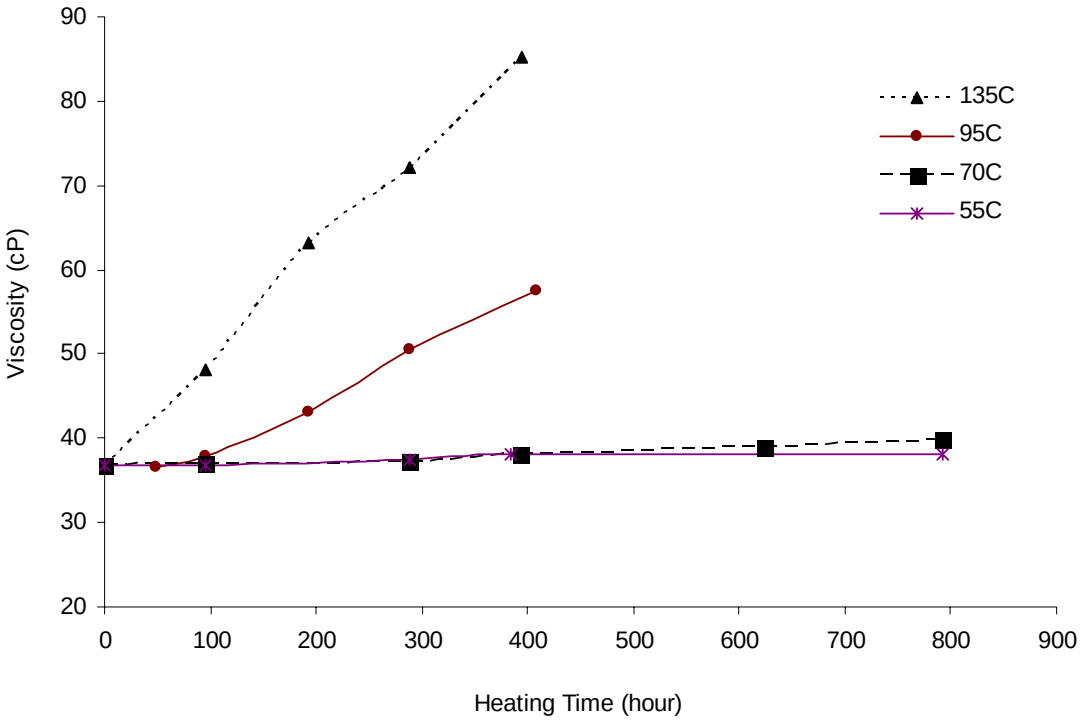

Figure 4.25: Effect aging of oil due to temperatures on viscosity.

4.3.4 Effect of Aging on Viscous Activation Energy

Table 4.14 shows the variation of viscous activation energy with heating time when it was heated at 135°C. The viscous activation energy and Arrhenius factor were calculated as Equation 2.3. Activation energy (E_a) could be treated as potential energy barrier in that molecules of the oil require achieving this energy before it could flow freely in the applied shear rate direction and Arrhenius factor (A) relates to the viscosity of oil. The results show that as viscometer spindle speed increases, the activation energy increases while the Arrhenius factor decreases. It can be seen also that as heating time progresses, the activation energy increases. This is due to the increased energy required to move the oil molecules.

Table 4.14: Activation energy of RBD palm oil after heating at 135 °C

(a) after 96 hours

rpm	E_a	A	R^2
3	7895.6	3.3380	0.9915
5	12663.1	0.4833	0.9933
6	13322.4	0.3352	0.9762
12	18143.6	0.0435	0.9669
20	20487.4	0.0160	0.9776
50	23550.2	0.0047	0.9888
60	23990.1	0.0038	0.9990
100	24402.4	0.0032	0.9986

(b) after 384 hours

rpm	E_a	A	R^2
3	21118.4	0.0260	0.9990
5	21855.8	0.0176	0.9944
6	31255.7	0.0109	0.9953
12	24743.3	0.0050	0.9937
20	26833.4	0.0022	0.9967
50	26841.8	0.0020	0.9996
60	26897.5	0.0020	0.9999
100	26929.9	0.0019	1.0000

(c) after 864 hours

rpm	E_a	A	R^2
3	27349.7	0.0059	0.9832
5	28452.2	0.0037	0.9897
6	30021.9	0.0020	0.9943
12	31203.3	0.0012	0.9960
20	31211.6	0.0012	0.9968
50	31367.1	0.0011	1.0000
60	31342.1	0.0011	1.0000
100	N/A	N/A	N/A

4.4 Rheological Performance from Hydraulic Test Rig

4.4.1 Continuous Operation

Effect of aging time and heat when palm oil was subjected to aging process in hydraulic test rig running continuously at 55^{o}C, 600 rpm and minimum load is shown in Figure 4.26. The figure shows the variation of viscosity with temperature when tested at different shear rates. Due to thermal degradation and oxidation, the viscosity at 600 hours is always higher than of 288 hours and 96 hours, irrespective of shear rates applied.

Testing at 3 rpm indicates higher viscosity compared to other speeds, similar to results in Section 4.3 (bench test). This viscosity increase can have significant impact on hydraulic system performance especially during starting where low rpm is involved. Besides being dependent on pressure and speed, the performance of hydraulic test rig is significantly affected by viscosity property (results discussed in Section 4.8).

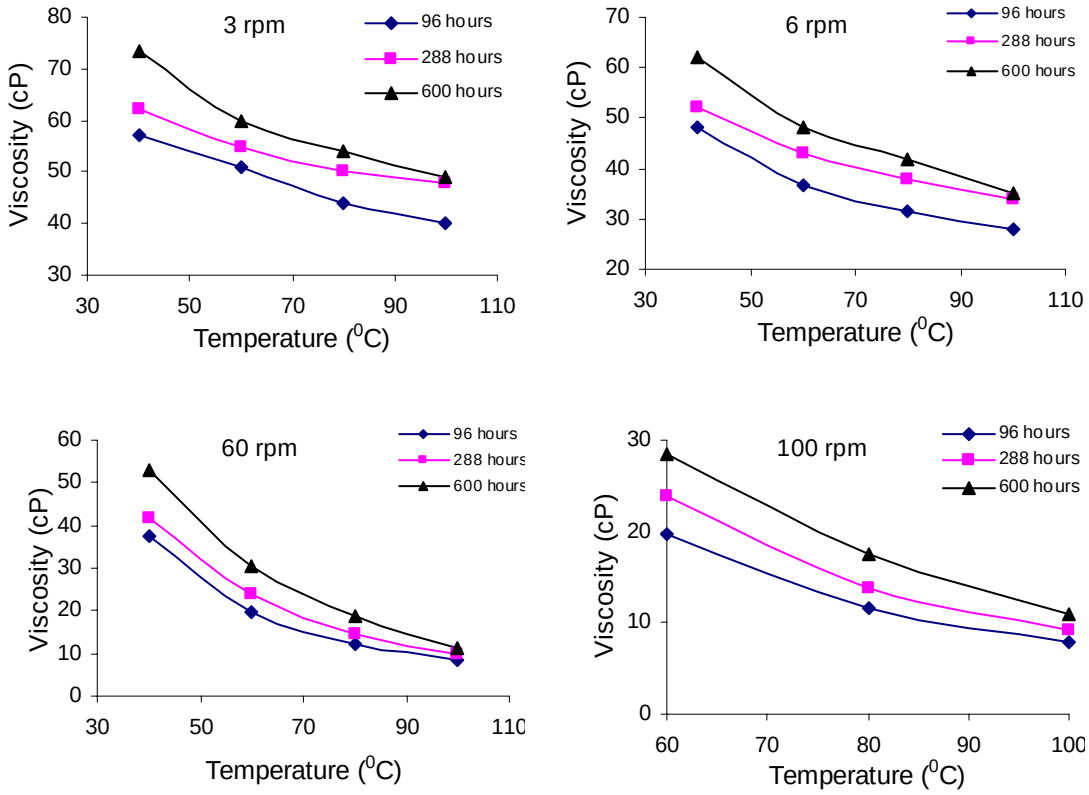

Figure 4.26: Viscosity versus temperature for palm oil without additive at different running time and spindle speeds.

Similar pattern was observed from the oil flow curves (Figure 4.27). The results show that palm oil experienced significant viscosity increase when used without additive in the hydraulic system. All samples show pseudoplastic behavior at all temperatures.

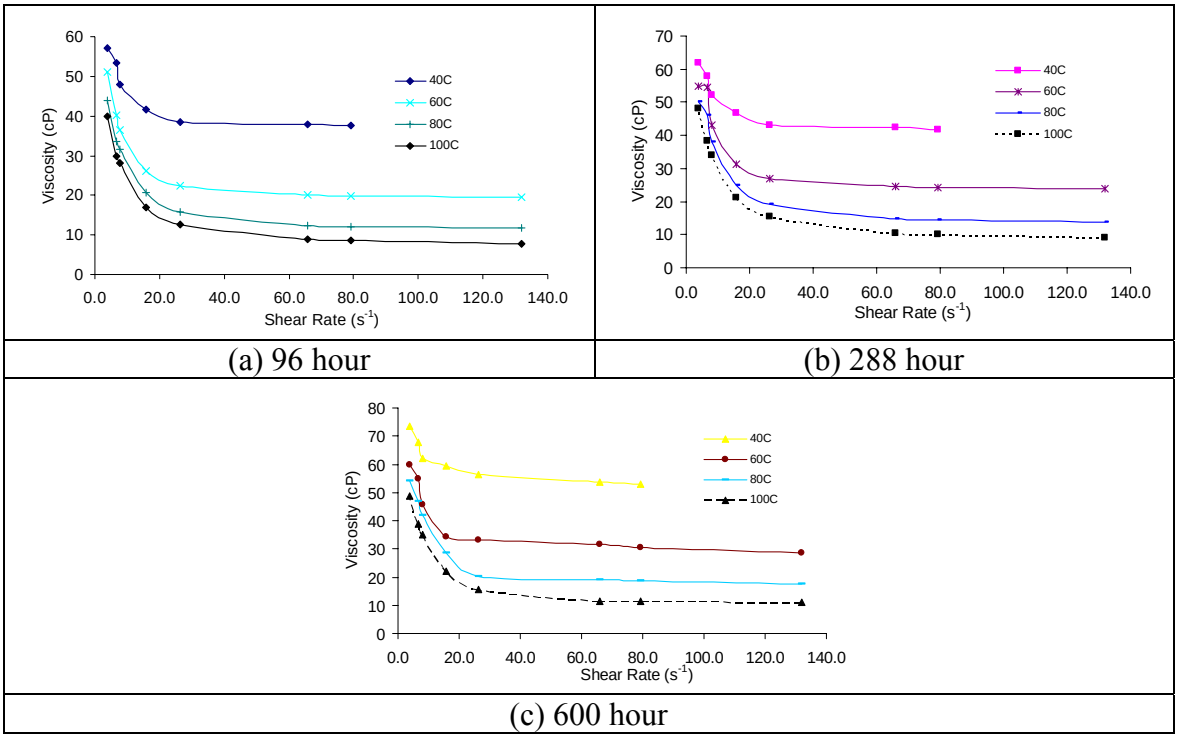

Figure 4.27: Flow curve for palm oil without additive at different running time.

Figure 4.28 compares the effect of additive on viscosity level. As already explained in previous figures, the viscosity of the oil increased with running time. At 96 hours, the effect of additive is not very clear. At 288 hours, the F10 and L135 additives managed to reduce the oil viscosity to a certain level. The ability of additive to prevent the oil viscosity from increasing was very clear based on 600 hour results. The inhibited oil was very much increase in term of viscosity. The effect of additive type and percentage used was not very significant. The possible reason is that these additives are antioxidant, not viscosity improver. However these additives managed to suppress the viscosity increase by reducing the oil oxidation rate (acidic value of oils is discussed in Section 4.6.1).

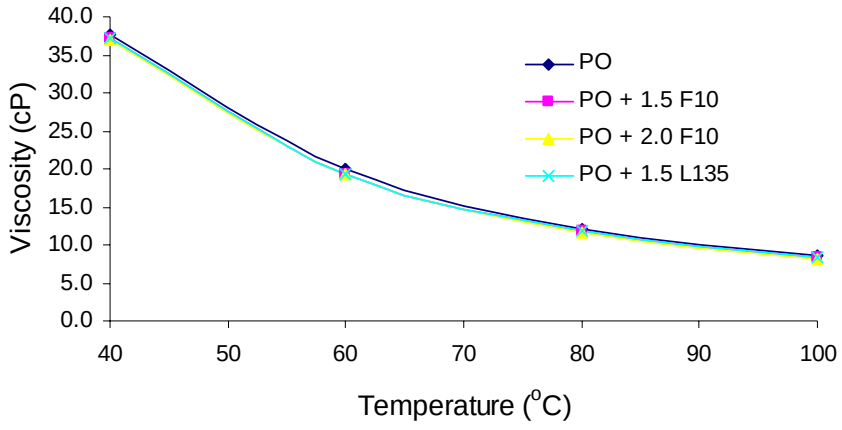

(a)

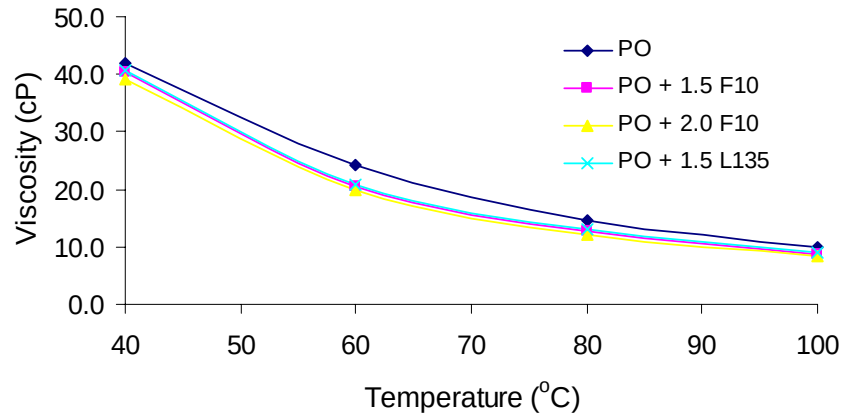

(b)

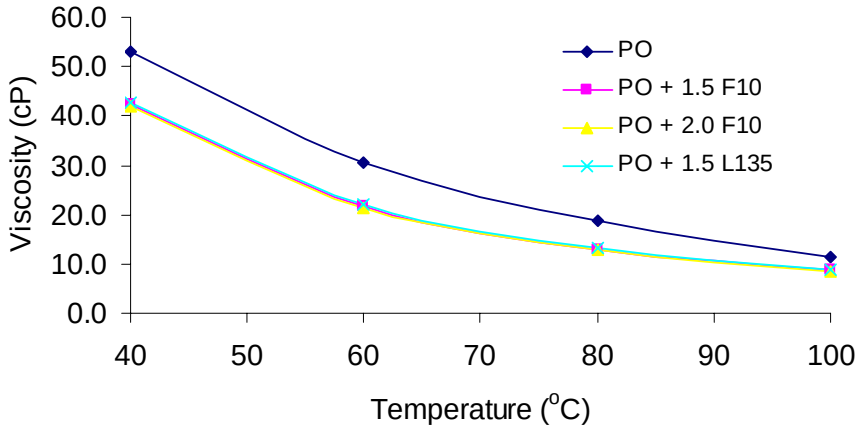

Figure 4.28: Effect of additives on viscosity at (a) 96, (b) 288 and (c) 600 hours.

Figure 4.29 compares the viscosity of RBD palm oil (PO) and commercial rapeseed based hydraulic oil (RO). The two oils have similar viscometric property

level, even after operated up to 600 hours. It is worth to remember that the commercial RO might have been fortified with several types of additives. Surprisingly the viscometric property of the PO was not much different from that of RO. Based on higher mono-unsaturated acids (C18:1) of RO compared to PO, RO should be more thermally stable than PO. The drawback of RO maybe due to high polyunsaturated acids (Table 3.1).

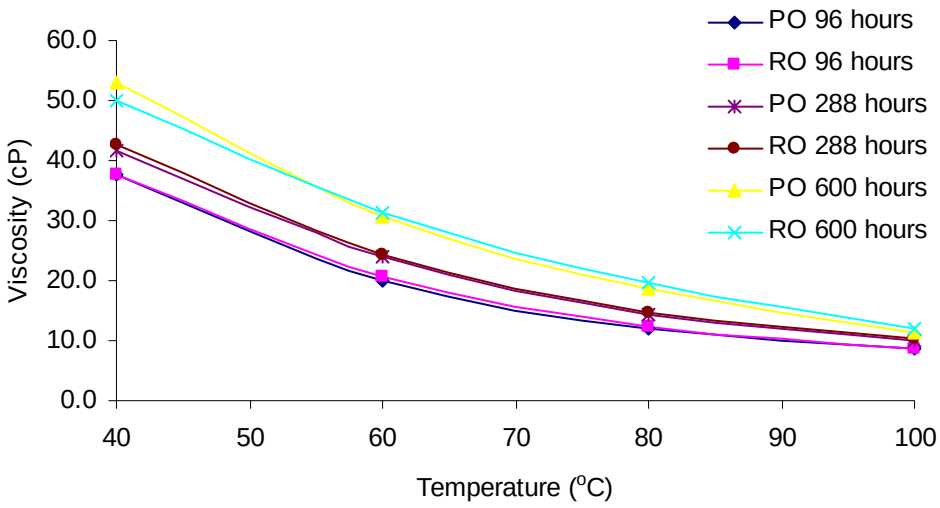

Figure 4.29: Viscosity comparison between palm oil and commercial rapeseed oil.

Figure 4.30 plots the viscosity versus shear rate in log form for the palm oil at 96 hours operation at viscometric properties of 40°C and 100°C. From the best fitted line, the slope and the intercept were noted. The values were used to determine the oil rheological properties according to Ostwald de-Waele model.

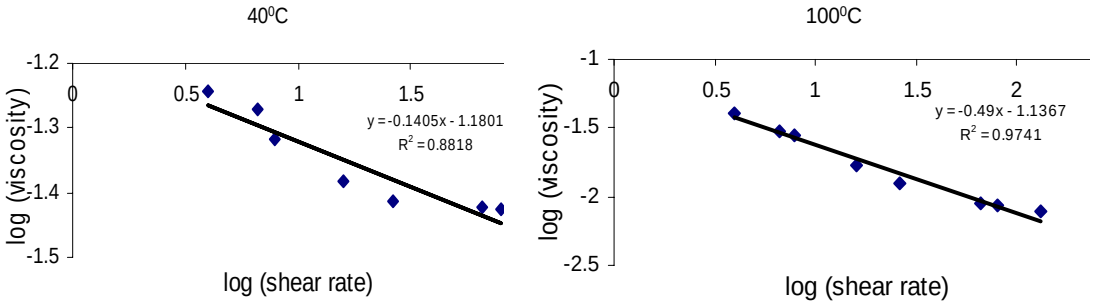

Figure 4.30: Determination of rheological parameters according to Ostwald de-Waele model.

Table 4.15 shows the calculated flow behavior index for oil samples at 96 hours running. At 96 hours, the palm oil was always more Newtonian than rapeseed oil. As in previous sections, when analyzed using Ostwald de-Waele model, the flow behavior index decreases with viscometric temperatures.

Table 4.15: Flow behavior index at 96 hours according Ostwald de-Waele model

Temp(^{0}C)	PO	PO+1.5F10	PO+2F10	PO+1.5L135	RO
40	0.8595	0.8635	0.8710	0.8565	0.8534
60	0.7251	0.7290	0.7516	0.7236	0.7213
80	0.6017	0.6047	0.6114	0.6100	0.5954
100	0.5100	0.5087	0.5096	0.5123	0.5075

Figure 4.31 shows the effect of test rig running time and additive on the oil flow behavior index. It compares the *n* values at viscometric temperature of 40^{o}C for inhibited and additived oil when it was aged at 96, 288 and 600 hours. The result shows that the *n* increases with ageing time. Flow index becomes closer to unity suggest that the oil samples become more Newtonian. Interestingly, this is similar to test results from bench test (Section 4.3.1) but contradicted with the result of oil running 15 hours a day at higher pressure (Section 4.4.2).

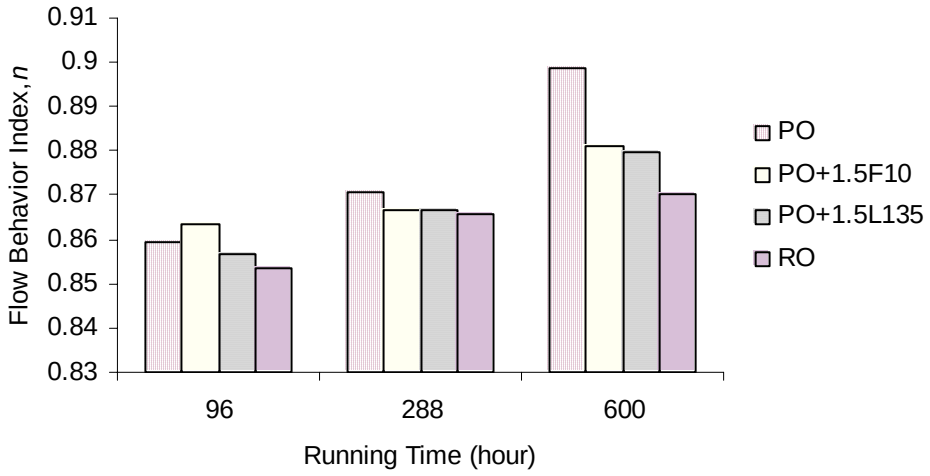

Figure 4.31: Variation of flow index for different oils at three running time.

The increase occurs to all palm and rapeseed oil samples. However the amount of increase depends on the oil sample. The result shows a large increase of *n* for inhibited palm oil. This suggests that this inhibited oil had gone significant molecular structural change during heating in the hydraulic system, thus modify

significantly its flow behavior. Similar observation was made by Shenoy (2002) where many asphalt materials experienced increased flow index when aged in Rolling Thin Film Test.

The results in the figure also suggest that the increase in *n* was suppressed with the presence of the additive. The presence of additive has protected the oil from degradation and thus reduced the structural change as suggested by less *n* change. Effect of different additive type, of same concentration (1.5% F10 and 1.5%L135), on the value of *n* was not significant.

In order to confirm that the *n* increases with running time, palm and rapeseed oil samples were analyzed for other viscometric temperatures (60, 80, 100^{o}C). Table 4.16 shows that in general for palm oil *n* increases with running time. The same goes for rapeseed oil. Based on *n* value, it can be said that rapeseed oil is always slightly more pseudoplastic compared to palm oil ($n_{rapeseed} < n_{palm}$).

Table 4.16: Changes of *n* with running time for (a) palm and (b) rapeseed oils

	Running time(hour)		
Temp(^{0}C)	96	288	600
40	0.8595	0.8705	0.8988
60	0.7251	0.7348	0.7926
80	0.5936	0.6017	0.6545
100	0.4912	0.5100	0.5362

(a)

	Running time(hour)		
Temp(^{0}C)	96	288	600
40	0.8534	0.8657	0.8702
60	0.7213	0.7273	0.8035
80	0.5785	0.5954	0.6675
100	0.5042	0.5075	0.5447

(b)

Based on the above results, it was confirmed that the flow behavior index increases with running time. The reason is not very clear. The hypothesis that can be made is that, when the oil is heated over time, the long triglycerides chains of the vegetable oils become broken. The break down of the chain results in short chains, thus less resistance exists at low shear rate. This can be understood when considering commercial mineral hydraulic fluid which has shorter hydrocarbon chain. Due to short carbon chain, Shell Tellus 100 behaves Newtonian like.

Table 4.17 compares the consistency index with running time for palm oil added with additive F10 with concentration of 1.5%. Consistency index for each temperature was calculated. The table shows that for each temperature case, except

for 40°C of 288 hour case, the consistency index increases with heating time. This can be another indication that the viscosity value increases with heating time.

Table 4.17: Consistency index for palm oil blended with 1.5% F10

Temp(°C)	96 hour		288 hour		600 hour	
	k	R^2	*k*	R^2	*k*	R^2
40	0.0642	0.8756	0.0686	0.8524	0.0677	0.8185
60	0.0627	0.9070	0.0648	0.9241	0.0677	0.9035
80	0.0659	0.9390	0.0895	0.9587	0.0906	0.9622
100	0.0714	0.9688	0.0912	0.9793	0.0912	0.9785

Figure 4.32 shows the linearity of viscosity in natural logarithmic form with temperature reciprocal of unadditived palm oil at 96 hours at two different spindle speeds. From the best fit line, the slope and the intercept were noted. The slope of the plot is equal to E_a/R of Equation 2.4 from which activation energy, E_a, was evaluated. The values of E_a and A are given in Table 4.18.

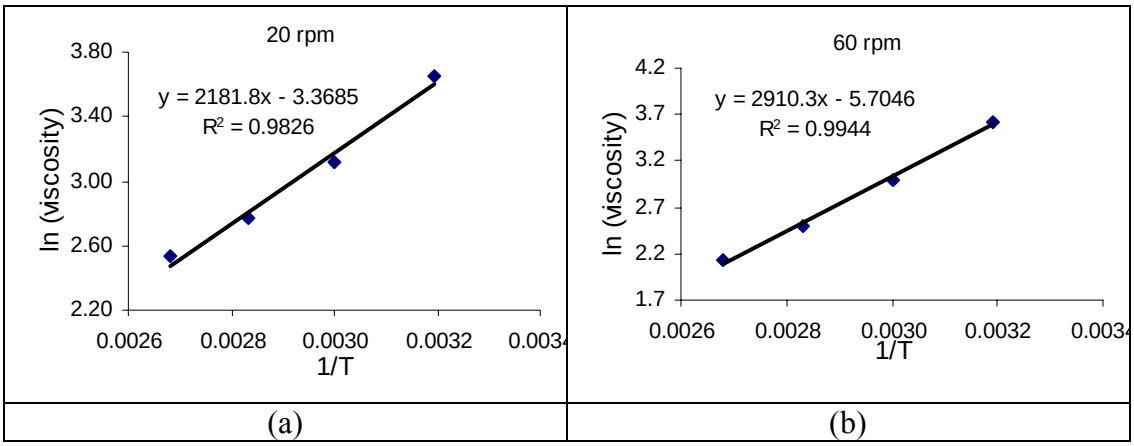

(a) (b)

Figure 4.32: Determination of activation energy and Arrhenius factor for (a) 20 rpm and (b) 60 rpm cases.

Table 4.18: Activation energy and Arrhenius factor for different spindle speeds

rpm	E_a/R	E_a	ln*A*	*A*
3	650.2	5406.3	1.9808	7.2485
5	1124.8	9352.1	0.3549	1.4260
12	1716.6	14272.6	-1.8103	0.1636
20	2181.8	18140.5	-3.3685	0.0344
50	2854.5	23733.7	-5.5248	0.0039
60	2910.3	24197.6	-5.7046	0.0033

It is observed that the value of activation energy increases with spindle speed. In another words, the activation energy increases with shear rate. It reveals the relationship between shear rate and energy of the oil. The shear rate was actually acting as an input of energy, which continuously supplied to given oil under shear. Eventually oil that was subjected to high shear rate would obtain high activation energy.

Table 4.18 also shows that as the shear rate increased, the Arrhenius factor decreased. This is directly due to the energy supplied by shear was actually used to free the oil molecules from attraction force between adjacent molecules.

4.4.2 15 Hours Intermittent Operation

After the palm oil was thermally and sheared degraded in hydraulic test rig at 70^{o}C and 70 bar for about 15 hours a day, the rheological property change of oil were analyzed and evaluated. The total running hour was 920 hour. The oil did not exhibit time-dependency during shearing at 3.9 - 131.6 s^{-1}. Figure 4.33 shows the variation of viscosity versus temperature at 65.8 s^{-1} and 3.9 s^{-1} for 100 hour sample. Similar increased viscosity was also observed as in continuous operation case (Section 4.4.1) and bench tests (Section 4.3). The increased viscosity at low shear rate would render low mechanical performance to hydraulic test rig during starting.

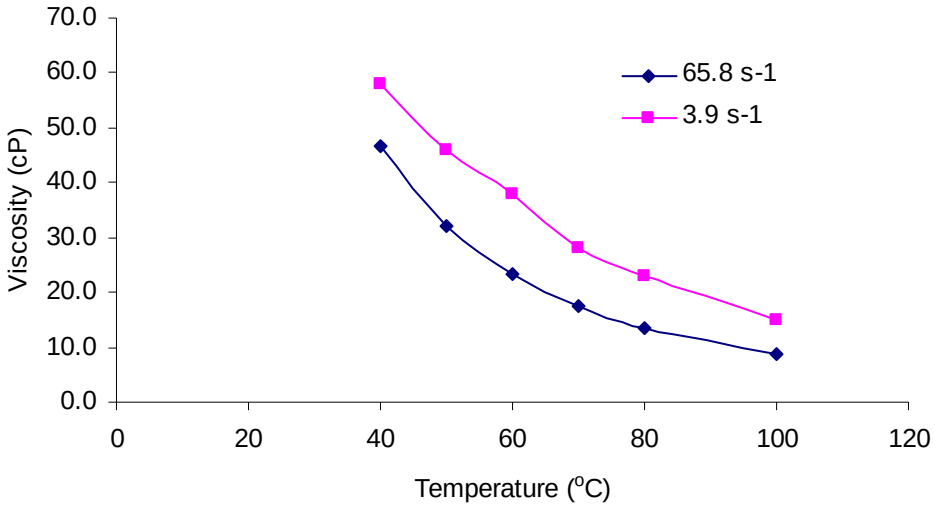

Figure 4.33: Viscosity versus temperature of PO from test rig at two shear rates.

Figure 4.34 shows the flow curves for 0, 100, 300, 400, 500 and 600 hour samples. The figure shows that the viscosity constantly increases from 0 to 100, 300, 400, 500 and 600 hours. As operating hour increases, less and less viscometric values were available for high shear rates and at lower temperature (eg. 40^{o}C). This is due to increased viscosity which resulted in higher torque to rotate spindle. All samples behaved as pseudoplastic fluid with different degrees.

In order to perform a qualitative comparison of oil properties, various rheological models as discussed in Section 2.5 were used. They were empirical Ostwald de-Waele, proposed modified power law, Cross, Carreau and Herschel-Bulkley using programs made in Mathematica 4.2. Best fit model was suggested based on the basis of standard errors (R^2 and MSE).

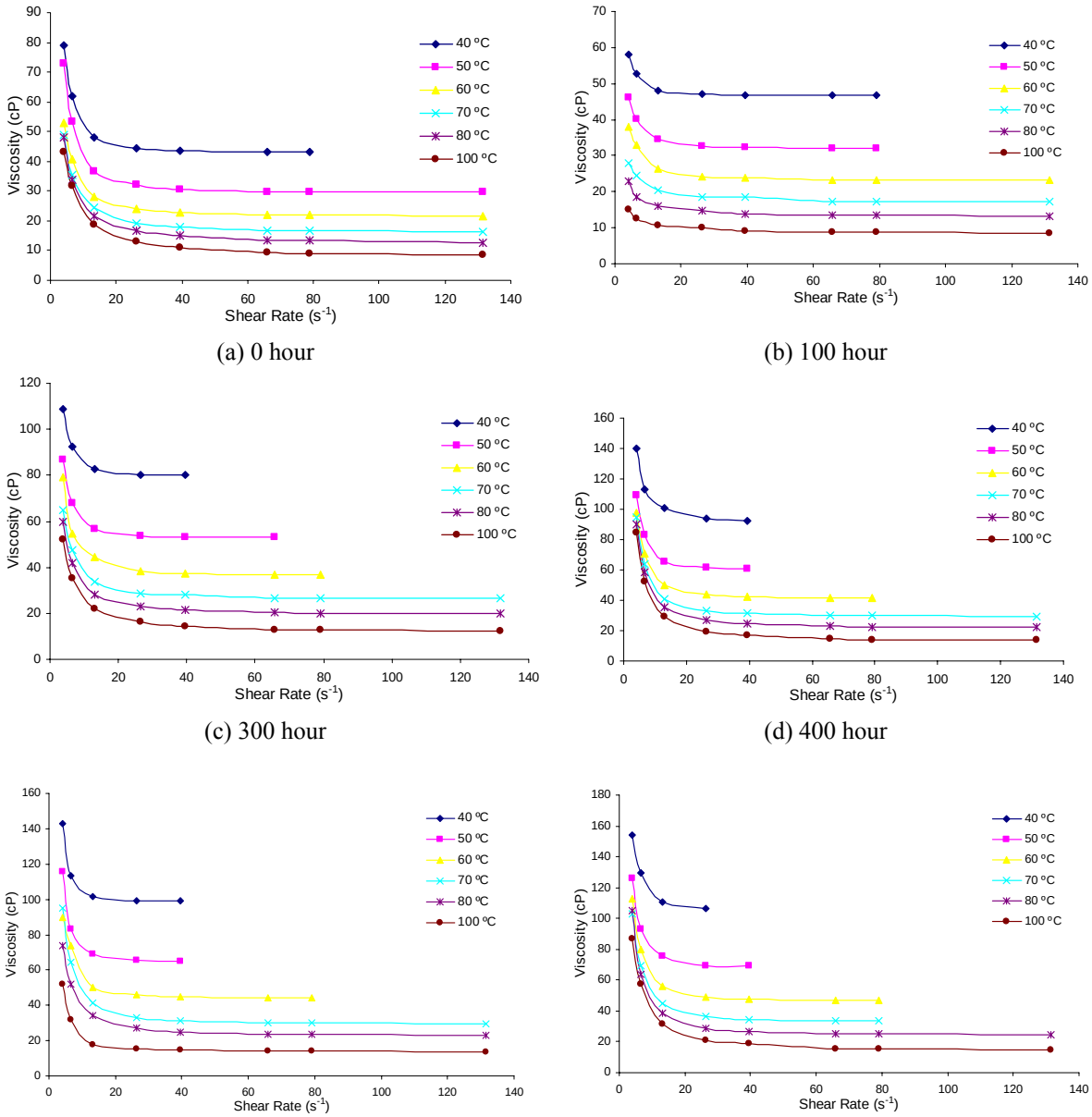

(a) 0 hour (b) 100 hour

(c) 300 hour (d) 400 hour

(e) 500 hour (f) 600 hour

Figure 4.34: Flow curves for palm oil samples at different operating hours.

Figure 4.35 shows variation of experimental dynamic viscosity at 60°C with shear rate for oil at 200 hour running. With an enlarged y-axis scale, a sharp viscosity drop from above 0.07 Pa.s to below 0.055 Pa.s can be observed. This corresponds to a strong shear thinning behavior of the oil. A strong fatty acid chain might have broken down under an applied shear field.

The simulated plots using proposed modified power law, Cross, Carreau and Herschel-Bulkley models are also shown. Among the four models, Cross and

Carreau were very well fitted to the experimental data with the correlation coefficient of 0.9999. It was followed by Herschel-Bulkley and modified power law with 0.9996 and 0.9572, respectively. Plot of Ostwald de-Waele is not shown in Figure 4.35 since the R^2 is less than 0.9. Similar results were also obtained for basic palm oil data, where Cross model always gives higher R^2 compared to Ostwald de-Waele model (Results in Table 4.2 versus Table 4.5).

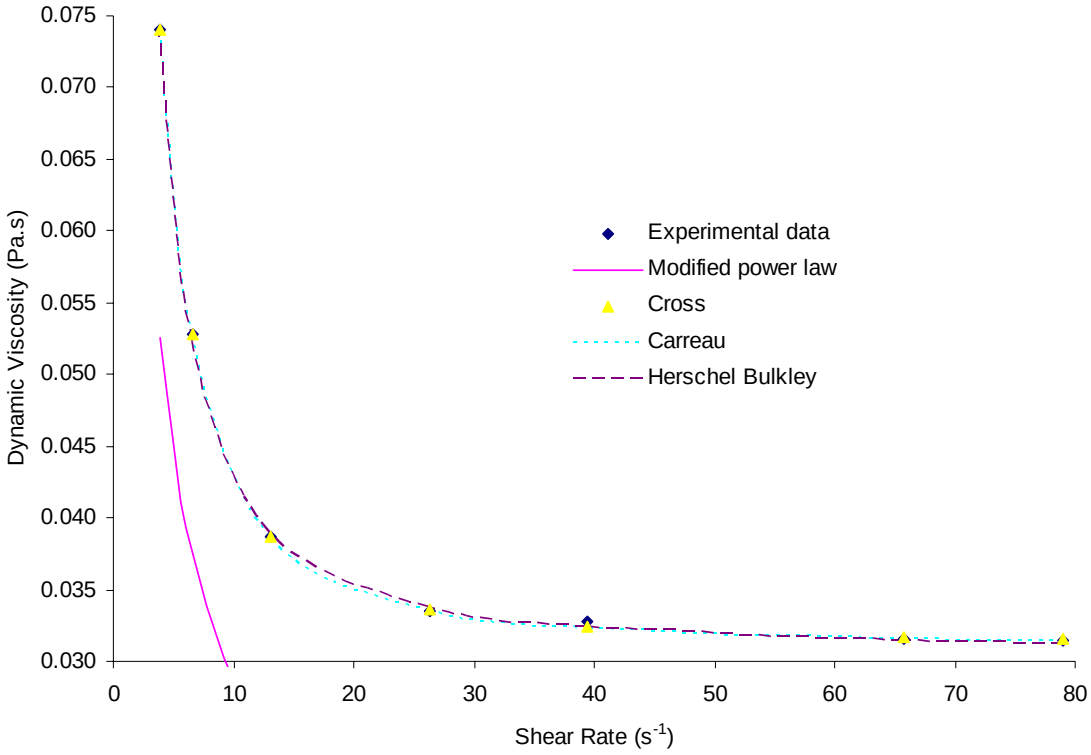

Figure 4.35: Variation of viscosity of experimental and predicted data.

From the results of multiple non-linear regressions, the variation of consistency index and flow behavior was of main interest. Figure 4.36 shows the variation of *n* with increasing temperature for 100, 300 and 400 hour cases as determined by Ostwald de-Waele model.

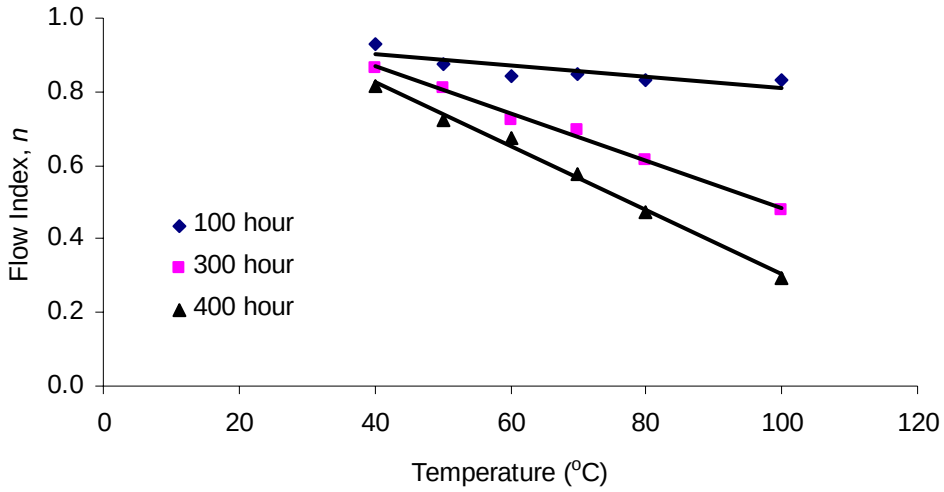

Figure 4.36: Variation of *n* with increasing temperature as determined by Ostwald de-Waele model.

The figure shows that as running time increases the flow index decreases. The decrease in flow index indicates that the oil is becoming more pseudoplastic. The non-Newtonian behavior of the oil increases. This might be due to crosslinking or bridging of the oil molecular structure. The relationship between flow index and temperature for 100, 300 and 400 cases can be fitted to Equation 4.7a-c:

$$n_{100} = -0.0015T + 0.9600 \quad (4.7a)$$

$$n_{300} = -0.0064T + 1.1256 \quad (4.7b)$$

$$n_{400} = -0.0087T - 1.1711 \quad (4.7c)$$

The correlation coefficients for 100, 300 and 400 hour cases are 0.6962, 0.9923 and 0.9931, respectively. Interestingly as running time increases the R^2 increases, indicating better linearity.

The contradiction of *n* trend between this test and test discussed in Section 4.4.1 (Table 4.16) might be due to experimental condition. In Section 4.4.1 test, the thermal (55°C) and shear condition (less than 15 bar) is less severe than the test in Section 4.4.2. Another difference is that the test in Section 4.4.2 imposed 15 hours heating and 9 hours cooling periods and sometimes subjected the oil to higher pressures (up to 210 bar). The harsher environment might polymerize the oil. Another possibility is that the short chains produced during the heating and shearing

processes (Section 4.4.2) might entangle again to produce some other form of long chain molecular structure, which is related to polymerization process.

Figure 4.37 shows the decrease in consistency index with temperature which is similar to the results discussed in Section 4.3 and 4.4.1. It is also commonly reported by other researchers on plant oil blends (Ma and Barbosa-Canovas, 1995; Maskan and Gogus, 2000). Consistency index increases with ageing time indicates that the oil is becoming more viscous, thus giving greater resistance to flow. The changes in flow and consistency indices compares well with Figure 4.34.

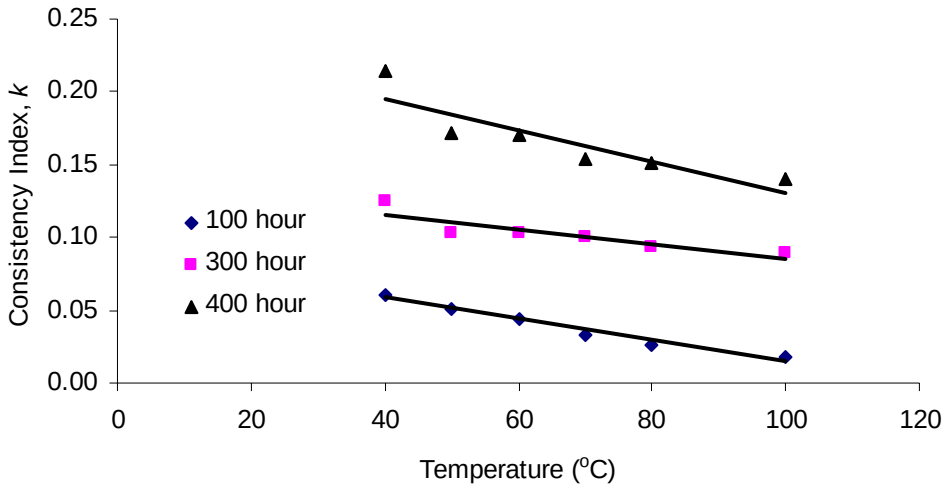

Figure 4.37: Variation of *k* with increasing temperature as determined by Ostwald de-Waele model.

Table 4.19 shows the rheological properties of the oil samples at 100 hour as analyzed using Cross model. This table contains the viscometric properties at zero shear rate ($\eta_{o,\gamma}$), and at infinite shear rates ($\eta_{\infty,\gamma}$), Cross flow index (m), and Cross consistency index (α_c). This model suitably explains the experimental data. It is better than the previous Ostwald de-Waele model. The correlation coefficient values range from 0.9973 to 0.9999 while the MSE is very small with the highest value is 3.79×10^{-8}.

Table 4.19: Rheological properties of 100 hour oil according to Cross Model

Temp. °C	$\eta_{o,\gamma}$	$\eta_{\infty,\gamma}$	m	α_c	R^2	MSE
40	0.0632057	0.0467564	2.61513	0.188207	0.9995	8.02028E-09
50	0.0529472	0.0320863	2.25081	0.185931	0.9999	2.21194E-09
60	0.0430132	0.0231841	2.20878	0.1545265	0.9992	2.10837E-08
70	0.0363001	0.0171546	1.48370	0.2102287	0.9973	3.79035E-08

Table 4.20 shows the rheological properties of the oil as analyzed using Carreau model. $\eta_{\infty,\gamma}$, λ_c and N values were obtained direct from the Mathematica output. In the case of 300 hour oil, the R^2 values were greater than 0.994 and MSE were less than $2.5x10^{-8}$.

Table 4.20: Rheological properties of 300 hour oil according to Carreau model

Temp. °C	$\eta_{o,\gamma}$	$\eta_{\infty,\gamma}$	λ_c	N	R^2	MSE
50	0.0543177	0.0320968	0.175959	1.18913	0.9999	2.81303E-09
60	0.0440769	0.0231688	0.150992	1.11882	0.9991	2.39700E-08
70	0.0334655	0.0170886	0.232812	0.65798	0.9975	3.41799E-08
100	0.2584383	0.0079533	0.365101	0.36039	0.9947	2.44421E-08

Table 4.21 shows the rheological properties of oil sample at 100 hour according to Herschel-Bulkley model. Based on R^2 and MSE values, it is clear that Herschel-Bulkley is not as good as Cross and Carreau models to be applied to palm oil samples.

Table 4.21: Rheological properties according to Herschel-Bulkley model

Temp. °C	K_H $x10^{-3}$	n_H	$\eta_{\infty,\gamma}$ $x10^{-3}$	R^2	MSE
40	78.7245	-0.3828	46.3858	0.9917	1.34039E-05
50	73.6612	-0.1681	31.3982	0.9947	1.32065E-05
60	60.9375	0.0445	21.9408	0.9908	2.66574E-05
70	37.3066	0.1596	16.4307	0.9945	7.63939E-06
100	18.7327	0.2792	7.9533	0.9947	2.44408E-07

In overall, the extremity viscosities ($\eta_{\infty,\gamma}$ and $\eta_{o,\gamma}$) were determined through Herschel-Bulkley, Cross and Carreau models. Most of the zero-shear rate viscosity ($\eta_{o,\gamma}$) estimated by Cross was greater than Carreau and value estimated by Carreau was greater than Herschel-Bulkley. Not much different of the infinite-shear rate

viscosity ($\eta_{\infty,\gamma}$) estimated by different models were observed and therefore the result of $\eta_{\infty,\gamma}$ was considered acceptable. The $\eta_{\infty,\gamma}$ was found decreased as the temperature increased, which suggests that less friction was encountered as the temperature increased.

In summary, Figure 4.38 shows the flow diagram for all oil samples taken from the hydraulic test rig and as measured at 60°C. The flow diagram clearly depicts the viscosity change throughout the rig operation. The overall increased oil viscosity is due to the oxidation and build up sludge. Prolong usage of the oil at high temperature eventually degraded the palm oil.

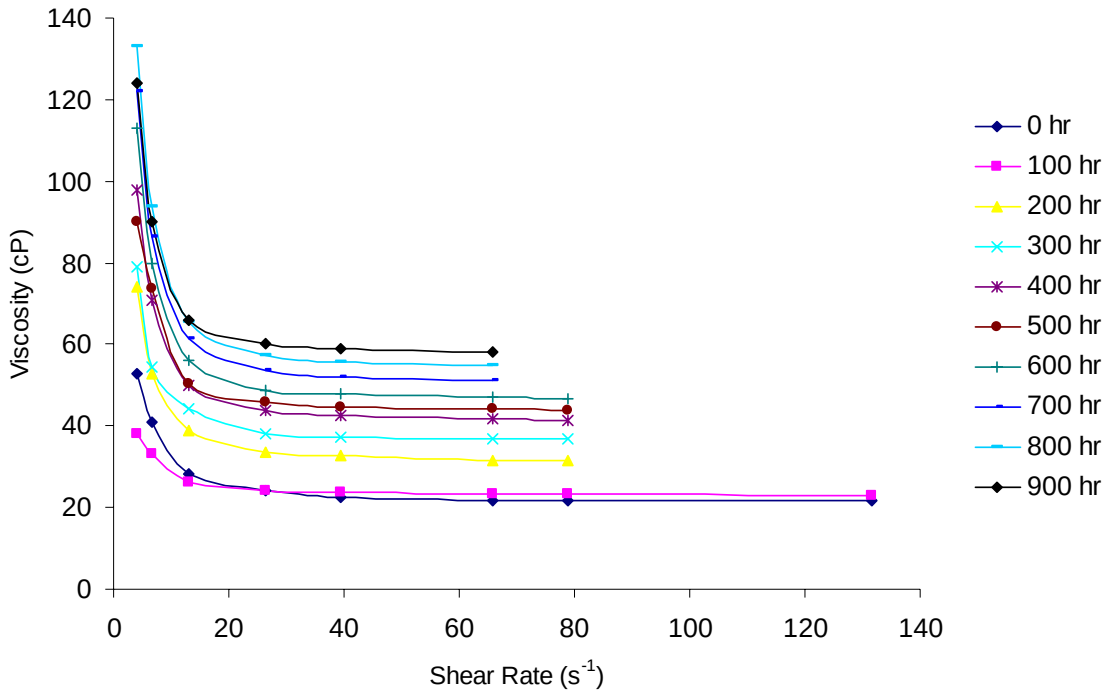

Figure 4.38: Flow diagram for all oil samples from hydraulic test rig running at 60°C, 70 bar and 15 hours a day.

4.4.3 Proposed Generalized Rheological Model

Rheological data for oils under study have been applied to rheological model proposed by Al-Zahrani and Al-Fariss (1998). Parameter constants of this empirical model were calculated using Mathematica 4.1 program. Statistical analysis to determine the suitability of the model was performed.

Based on observation of palm oil data pattern and Arrhenius type relation, the author proposed the following model for the palm oil under study.

$$\eta = a + 100\left(1+\frac{1}{T}\right)^{n_T}\left(1+\frac{1}{\gamma}\right)^{m_\gamma} \qquad 4.8$$

where a, n_T and m_γ are constants. This model has only 3 constants to be determined compared to Al-Zahrani and Al-Fariss's model which has 4 constants. The non-linear regression analysis was used to determine the model parameters a, n_T and m_γ (Appendix D – Program #D5). Using the contants output by the Mathematica program, the predicted viscosity value as determined by the above model was calculated using Excel spreadsheet (Appendix E). The R^2 and MSE were calculated using Equations 3.4 and 3.5, respectively.

The fittings to Al-Zahrani and Al-Fariss's and proposed generalized models were applied to several palm oil data sets (both bench test and hydraulic test). Based on higher coefficient correlation and lower mean square error, the proposed model was found to fit the experimental data better than Al-Zahrani and Al-Fariss's model. For the data set as shown in Appendix E, the R^2 and MSE for proposed model and Al-Zahrani and Al-Fariss's model are 0.9646, 8.2158×10^{-6}, 0.9175 and 1.9133×10^{-5}, respectively.

The proposed model includes the dependency of viscosity on shear rate and temperature in one expression. Graphically, for the data used in Appendix E, this dependency is shown as in Figure 4.39. Figure 4.40 shows the closeness of viscosity data predicted by the proposed model and Al-Zahrani and Al-Fariss's model to the actual experimental data. The closeness of 'proposed' points to the 45^o line (Figure 4.40) shows the good fit of proposed model to the experimental data.

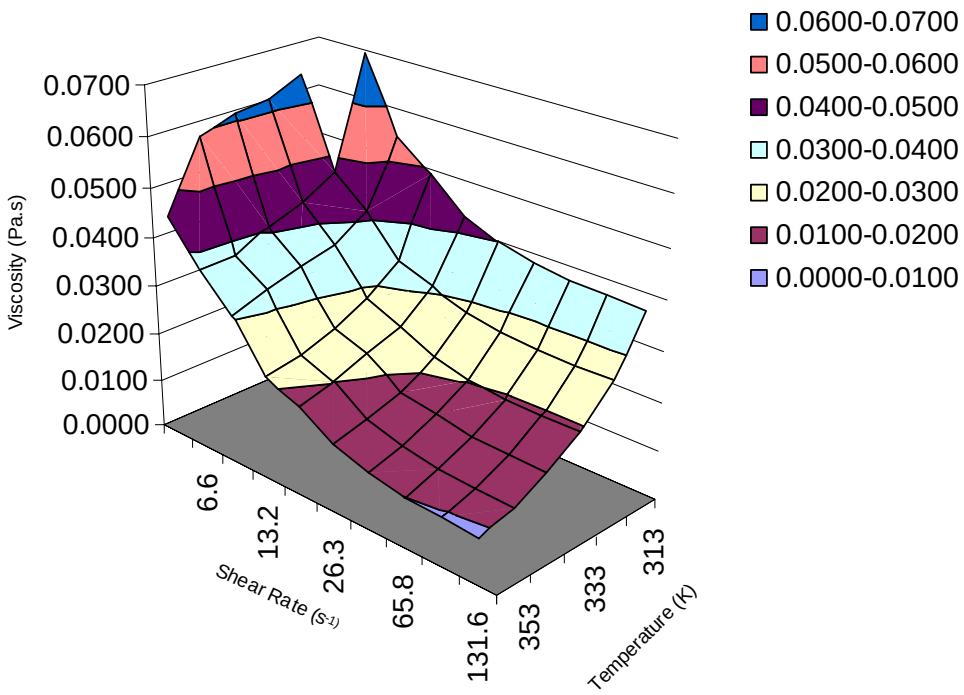

Figure 4.39: Graphical variation of viscosity with shear rate and temperature.

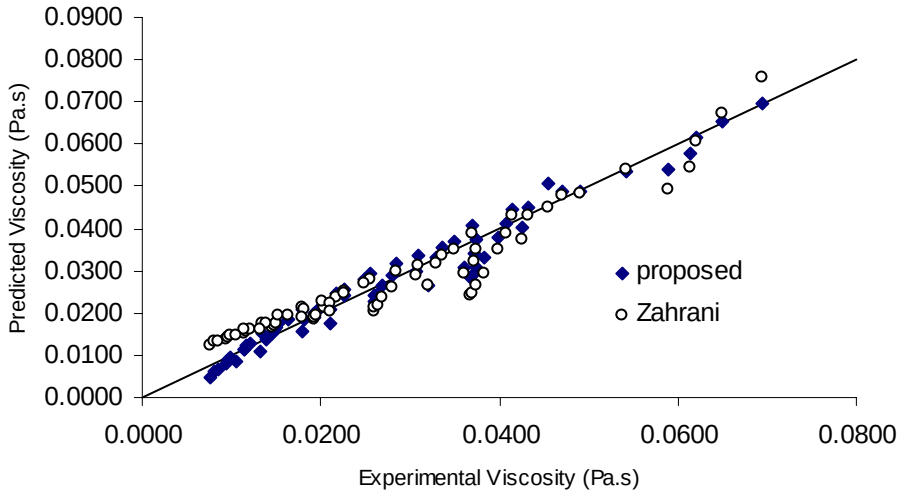

Figure 4.40: Comparison between measured and predicted viscosities according to the proposed model and Al-Zahrani and Al-Fariss's model.

4.5 Thermal Performance of Blended RBD Palm Oil in Bench Tests

The purpose of the bench test in this chapter was to forecast the oil condition when it was exposed to heat in hydraulic system. The good oil blends for further study are primarily based on TAN and viscosity values.

4.5.1 RBD Palm - POME Blend

Many researchers in biodiesel field blend ester to their diesel. For instance Masjuki and Maleque (1996b) used POME in their engine. In another application Yunus *et al*. (2003a) had transesterified POME into environmentally acceptable lubricant. Other lubricant researchers also studied the use of vegetable ester (Erhan and Asadauskas, 2000; Adhvaryu and Erhan, 2002). In this investigation the thermal stability of palm oil blended with POME when heated up to 792 hours has been investigated. The palm-POME blends were attempted in order to investigate if the POME can improve the thermal stability of the palm oil.

Figure 4.41 shows the increase of TAN for palm oil, POME and their blends when heated in an electric oven at 95^{o}C. The result shows that POME is less stable thermally compared to palm oil. The TAN values indicated that in the early stages of oil oxidation, the rate of reaction was very slow. It is obviously known that the rate of this process at this stage is dependent on the amount of free radical produced in the reaction environment. As the heating process continues, a higher rate increase of TAN was detected. This was due to the rapid formation of hydroperoxide and hydroperoxide products such as aldehyde, ketone and peracid with short alcohol chains (mentioned in Section 2.3).

The results show that the more the amount of POME added to palm oil, the higher the acid generation during the heating process. Figure 4.42 shows the percentage TAN increase for all blends at 792 hours. The y-axis is the percentage increase, taking the TAN increase of pure palm oil as 100%. Based on percentage increase of TAN of the used sample, TAN increased exponentially with the amount of POME used. It can be concluded that the ability of the blends to contribute to the

TAN depends on the percentage of the methyl ester in the oil samples because the structure of methyl ester is shorter than the palm oil and thus, it is easier to oxidize in a shorter period of exposure. Thus it was not recommended to include POME into the oil for hydraulic test rig testing.

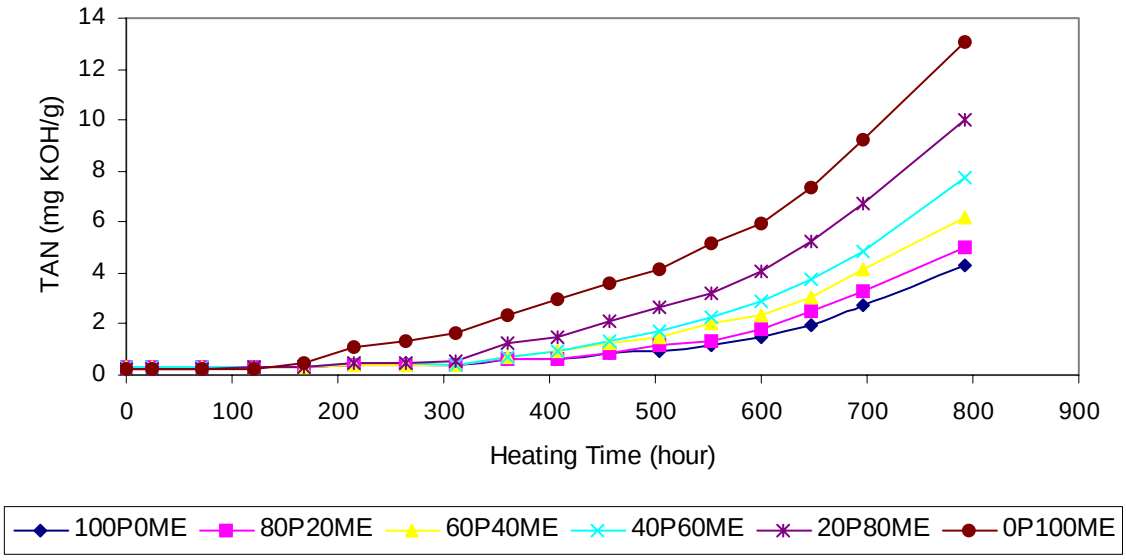

Figure 4.41: Variation of TAN for palm oil - POME blends.

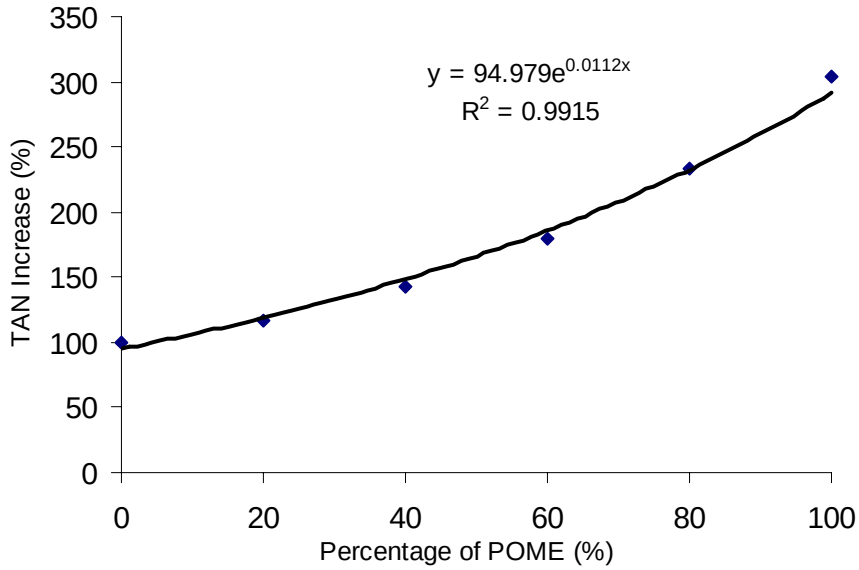

Figure 4.42: Percentage increase of TAN for palm - POME blends.

Table 4.22 shows the summary of IV of palm oil, methyl ester and the blends. An iodine value analysis shows the decrease of the double bond in the oil samples

after 792 hours of heating. For example the IV of palm oil before heating process was 59.63 cg I_2/g but after 792 hours of heating the IV of palm oil decreased to 46.38 cg I_2/g. During heating, thermal energy was supplied to excite the atoms in the bonding molecules. After a certain stage, the atoms had enough energy to break the double bond in the chain. Mostly this mechanism occurred in the unsaturated parts. The result is that the saturated structure was formed. Beside this, reaction of the hydrogen allylic in the oil during oxidation formed a diperoxide, which caused the decrease of the double bond in the oil samples (Yeshajahu and Clifton, 1994). The decrease in IV amount for 100P0ME, 80P20ME, 60P40ME, 40P60ME, 20P80ME and 0P100ME is 13.25, 13.87, 14.38, 17.32, 18.13 and 17.82 cg I_2/g, respectively. In general, the higher the POME content the larger the decrease of IV. This shows that the blend will be less thermally stable when more POME was added to the palm oil. This result complements the acid value result in Figures 4.41 and 4.42.

Table 4.22: Summary of the IV for palm oil, methyl ester and oil blends

Oil Samples	Iodine Value (cg I_2/g)	
	0 hour	792 hours
100P0ME	59.63	46.38
80P20ME	58.57	44.70
60P40ME	56.63	42.25
40P60ME	56.05	38.73
20P80ME	55.69	37.56
0P100ME	51.70	33.88

4.5.2 RBD Palm - Mineral Blend

Two bench tests using palm - mineral (Shell Tellus) oil blend were conducted at 95°C. The first test was conducted in an electric oven and the second test conducted in an oil bath. The TAN result for the former test is shown in Figure 4.43 and the latter is shown in Figure 4.44.

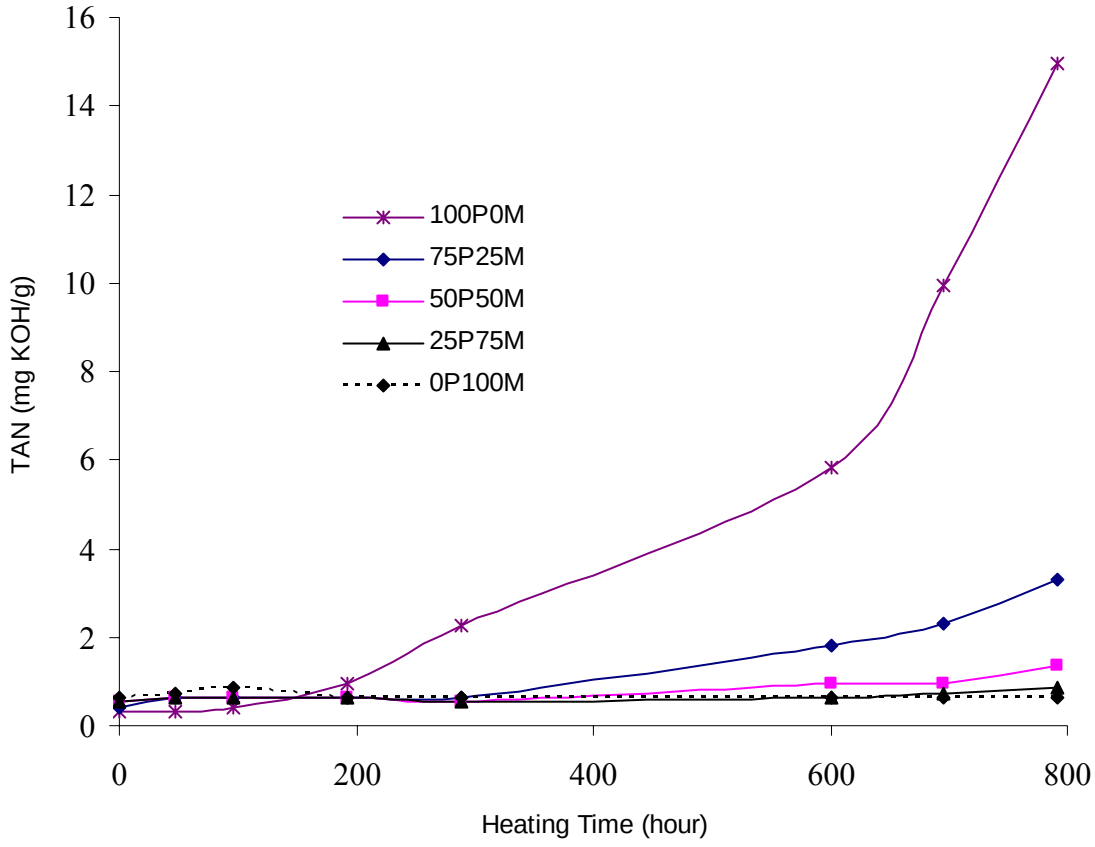

Figure 4.43: Variation of TAN for palm – Shell Tellus blends – in oven.

In the early stage of heating (up to 300 hours), only a small increase of TAN occurred. Significant increase in TAN occurred after 300 hours especially to pure palm oil. The increase in TAN was closely related to thermal and oxidative degradation of the oils. During the oxidation process, an active oxygen or a radical attacks the oil double bonds to form hydroperoxide (Kodali, 2002). As already been mentioned and shown in Section 2.3 and Figure 2.1, respectively, the rate of degradation depends on the amount of olein (C18:1), linoleic (C18:2) and linolenic (C18:3). The significant increase in instability is due to the high content of

polyunsaturated acid of the palm oil (Table 3.1). For blended sample, the sample that has higher content of the mineral oil has lower TAN increase.

Similar result was obtained when the oil was heated in open oil bath at 95°C (Figure 4.44). Oil bath should better simulate the hydraulic system built since the oil in hydraulic reservoir is in contact with atmospheric air. Shell Tellus is different from palm oil in which Shell Tellus is hydrocarbon base ($CH_3(CH_2)_x CH_3$) whereas palm is ester base. Shell Tellus oil did not experience much degradation since the mineral oil consists of liquid polymer like structures which can withstand high temperature condition (Lehrle *et al.*, 2002). The presence of additives in the oil also protected the oil from severe oxidation (Strochkova *et al.*, 1999). The change in chemical structure of the palm and mineral oil was also reflected by the IR spectra (Figure 4.45). Relatively unchanged in the IR spectra of mineral oil (Figure 4.45b) indicates that the mineral oil undergone less deterioration compared to palm oil which has noticeable IR change (Figure 4.45a).

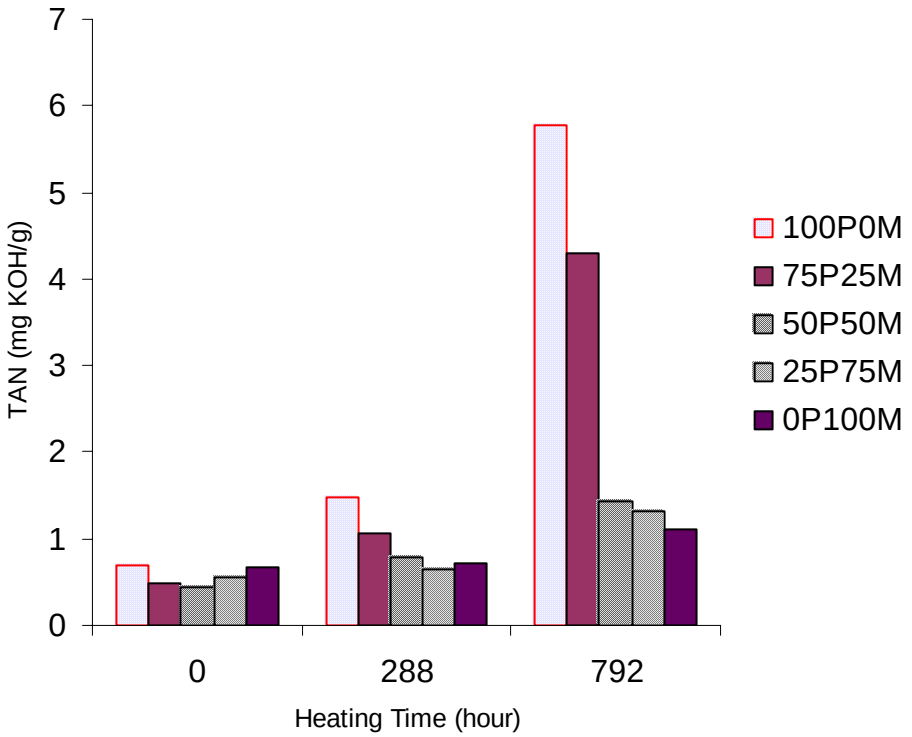

Figure 4.44: Variation of TAN for palm – Shell Tellus blends – in oil bath.

Even though blending with mineral Shell Tellus yields much improved thermal oxidative stability, it was decided not to use palm oil – Shell Tellus blends in hydraulic test rig. Blending palm oil with Shell Tellus will diminish the benign

properties of plant oil and will introduce the negative effects as pointed out in Sections 2.1 and 2.2.

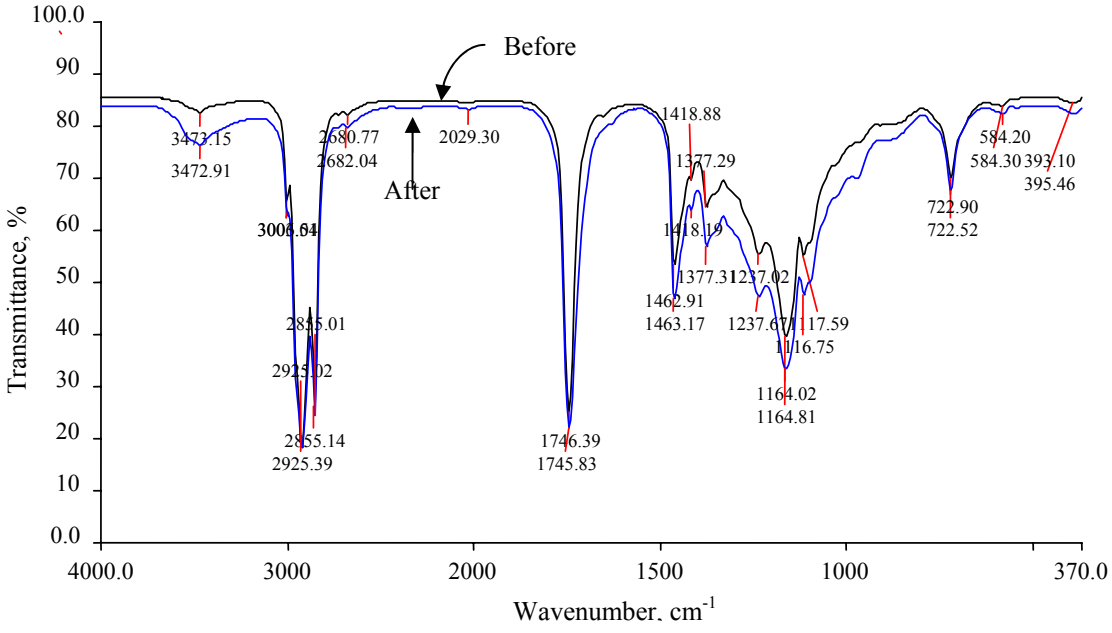

(a)

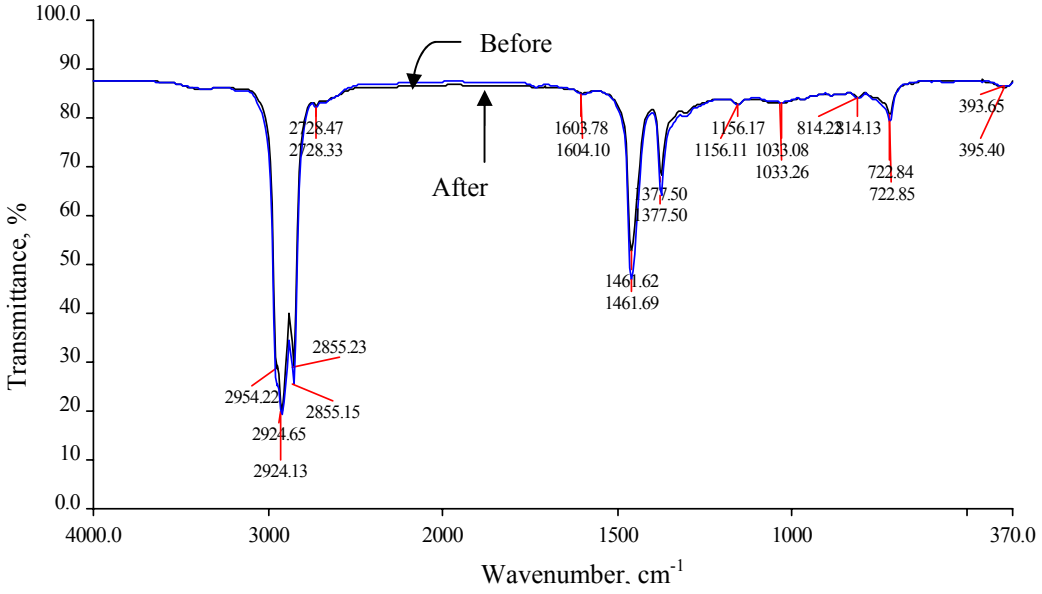

(b)

Figure 4.45: IR spectra for (a) palm oil and (b) mineral oil before and after 800 hour heating.

4.5.3 RBD Palm - Additives Blend

Figure 4.46 shows the increase of TAN of palm oil when it was blended with L74 additive. Based on the TAN result, it was decided that the palm oil - L74 blends were not worth to proceed since the acid value was high for the first 700 hours. The additived oil only became advantage after 700 hours. Only then the acid value was already very high.

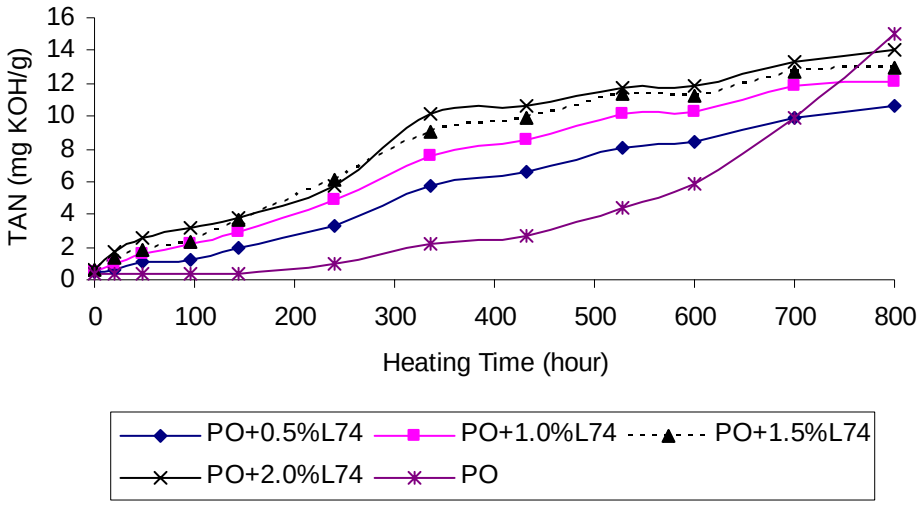

Figure 4.46: Variation of TAN for palm - L74 blends.

Figure 4.47 shows the increase of TAN of palm oil when it was blended with L06 additive. The result shows that 0.1 and 0.5% additive L06 did not much improve the TAN of the blends. 2% and 4% additive level managed to improve the TAN to 1.9 and 1.6 mg KOH/g, respectively. Based on recommendation and practical use of additive level, 4% is considered high amount. Thus it was not recommended to use this additive at 4% or higher.

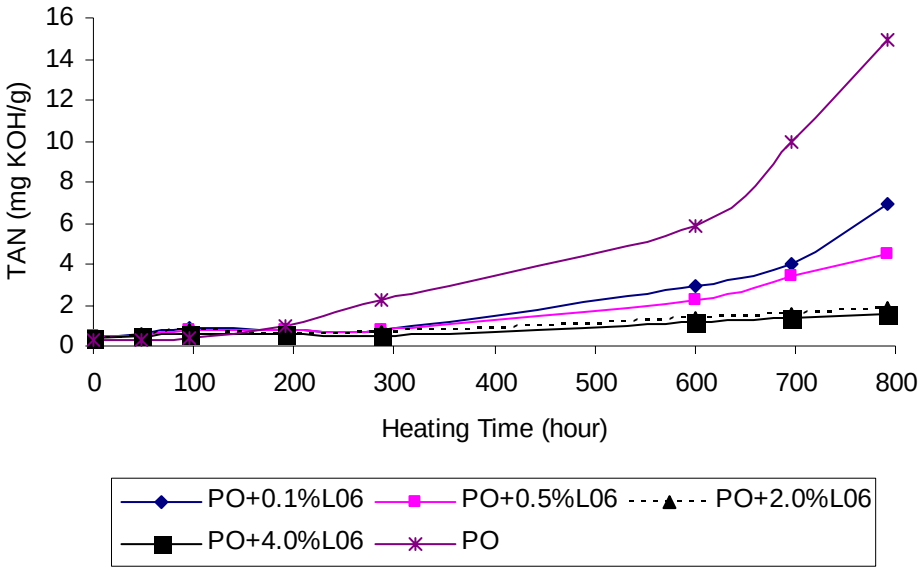

Figure 4.47: Variation of TAN for palm - L06 blends.

Figure 4.48 shows the increase of TAN of palm oil when it was blended with Lubrizol 7652 additive. For the first 500 hours, there was no advantage of using this additive. The additive used only managed to show its advantage only after 600 hours. However, the acid value already high. Furthermore, amount of additive used in this study was already high.

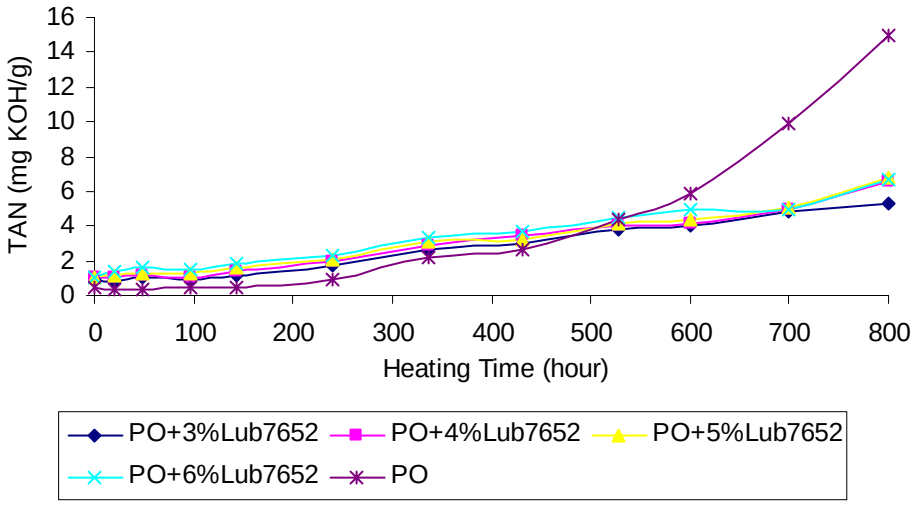

Figure 4.48: Variation of TAN for palm - Lubrizol7652 blends.

Very small percentages of L135 additive were used in these blends (Figure 4.49). It was proposed to use this type of additive, of this amount or higher, for

consecutive tests since the bench test results as depicted in Figure 4.49 show that 1.5% L135 managed drastically reduced the TAN to 2 mg KOH/g.

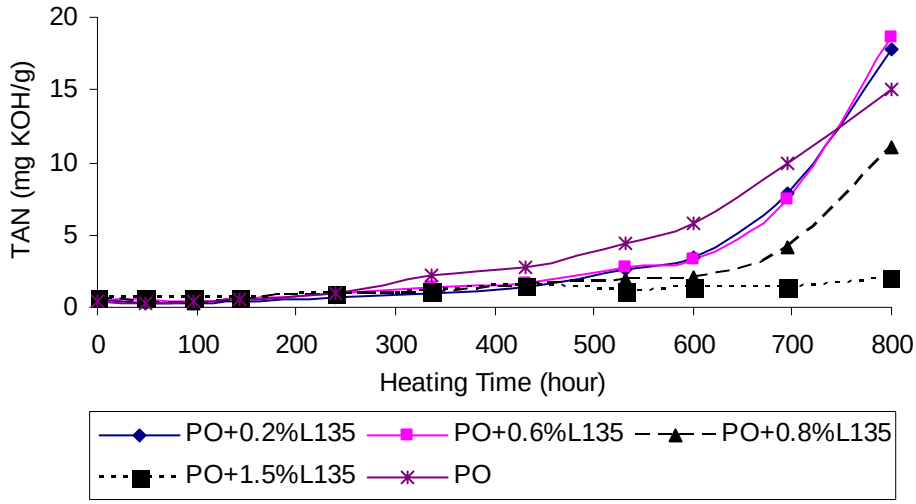

Figure 4.49: Variation of TAN for palm - L135 blends.

Small percentages of F10 additive were used in the blends (Figure 4.50). F10 additive managed drastically reduced the TAN below 2 mg KOH/g. Based on small TAN increase, it was proposed to use this additive for hydraulic and other tests.

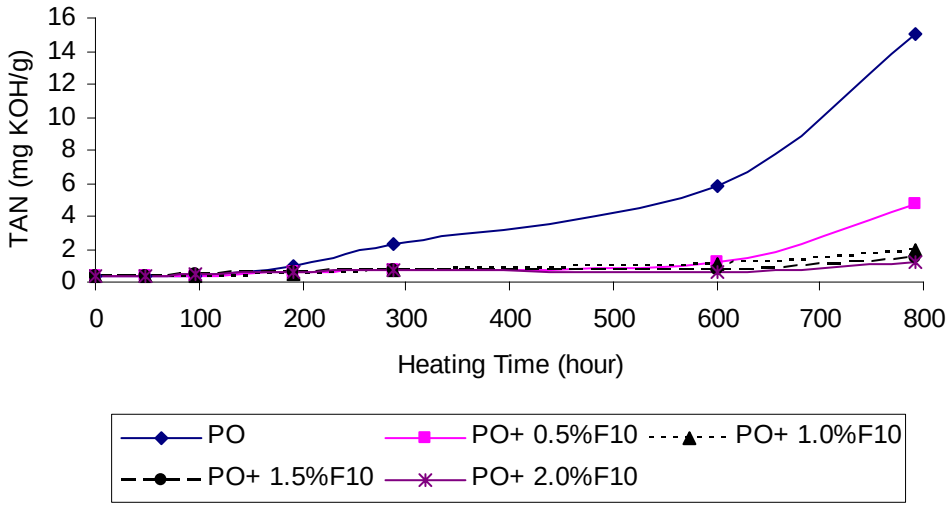

Figure 4.50: Variation of TAN for palm - F10 blends.

Beside the chemical properties, the color of the oil samples was also monitored. There were changes to all samples after 800 hours of heating. For palm oil, the color of the oil becomes clearer. This is due to the decomposition of natural carotene found in the oil. For palm oil blended with additive L135, the color of the oil tends to be clearer (Figures 4.51a and 4.51b). When higher amount of L135 additives were used, the palm oil color was preserved better. For other blends the color becomes darker. For palm - Lubrizol 7652 blends, the color of the oil changes to reddish brown (Figures 4.52a and 4.52b).

Figure 4.51a: Appearance of palm oil with additive L135; from left: 0.2%L135, 0.6%L135, 0.8%L135 and 1.5%L135 (0 hour).

Figure 4.51b: Appearance of palm oil with additive L135; from left: 0.2%L135, 0.6%L135, 0.8%L135 and 1.5%L135 (800 hour).

Figure 4.52a: Appearance of palm oil with additive Lubrizol 7652; from left: 0.5%Lubrizol 7562, 1.5 %Lubrizol 7652, 2.0%Lubrizol 7562 and 3.0%Lubrizol 7652 (0 hour).

Figure 4.52b: Appearance of palm oil with additive Lubrizol 7652; from left: 0.5%Lubrizol 7562, 1.5 %Lubrizol 7652, 2.0%Lubrizol 7562 and 3.0%Lubrizol 7652 (800 hour).

4.6 Thermal Performance of Palm and Commercial Hydraulic Oils in Actual Hydraulic Test Rig

Oil circulated in the built hydraulic system was heated due to friction at the pump, loading valve and 418 cm length piping (as explained in Section 3.5.9.1). The friction gave rise to temperature of 55°C or more. Excess heat was taken away by cooling system, so as to maintain the oil in the hydraulic reservoir at 55°C at all times. The rig was operated continuously for 600 hours.

4.6.1 Total Acid Number

About 8 ml of oil sample was taken at 0, 50, 100, 200, 300, 400, 450, 500, 550 and 600 hours. Figure 4.53 shows the increase of TAN with test rig operation time. Similar patterns were observed as in bench tests (Section 4.5.3). Additived palm oils (PO+1.5%F10, PO+2.0%F10 and PO+1.5%L135) managed to keep the TAN low. After 200 hours, unadditived palm oil could not maintain its TAN and shot up to 12.6 mg KOH/g at 600 hours. Strangely, commercial rapeseed oil also could not maintain its TAN and reached 8.5 mg KOH/g at 600 hours.

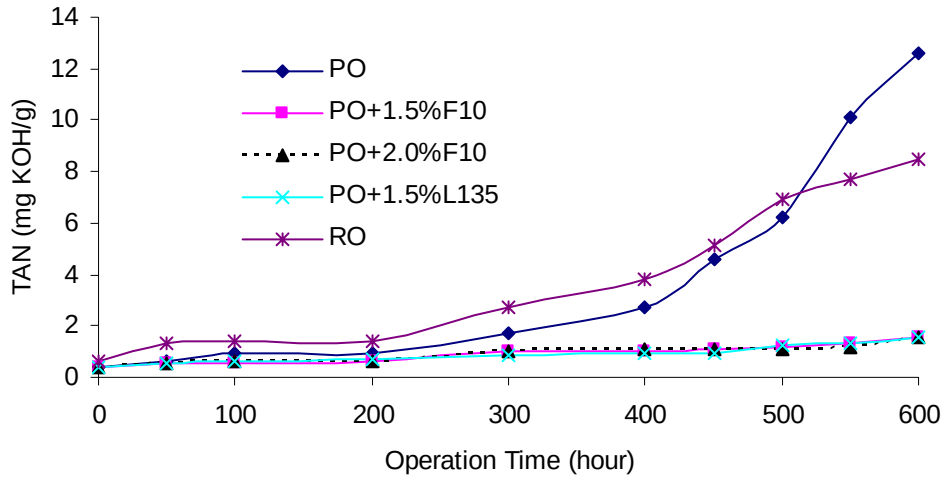

Figure 4.53: TAN variation of oil samples with test rig running time.

4.6.2 TGA Thermogram

Before the oil was introduced into the hydraulic system and at the end of test period (600 hour), the oils samples were characterized and quantified using TGA method. Kinetics of palm oil samples was studied non-isothermally under conditions of sample temperature increasing at the rate of 5 ^{o}C/min. Figure 4.54 shows the temperature scan of pure palm oil sample in nitrogen atmospheric heating. It shows the decomposition and weight loss of oil samples and derivative weight (DTG) with the corresponding temperature. It reveals that the thermal degradation of the oil occurred in a single-step reaction. Other samples also gave similar TG-DTG curves.

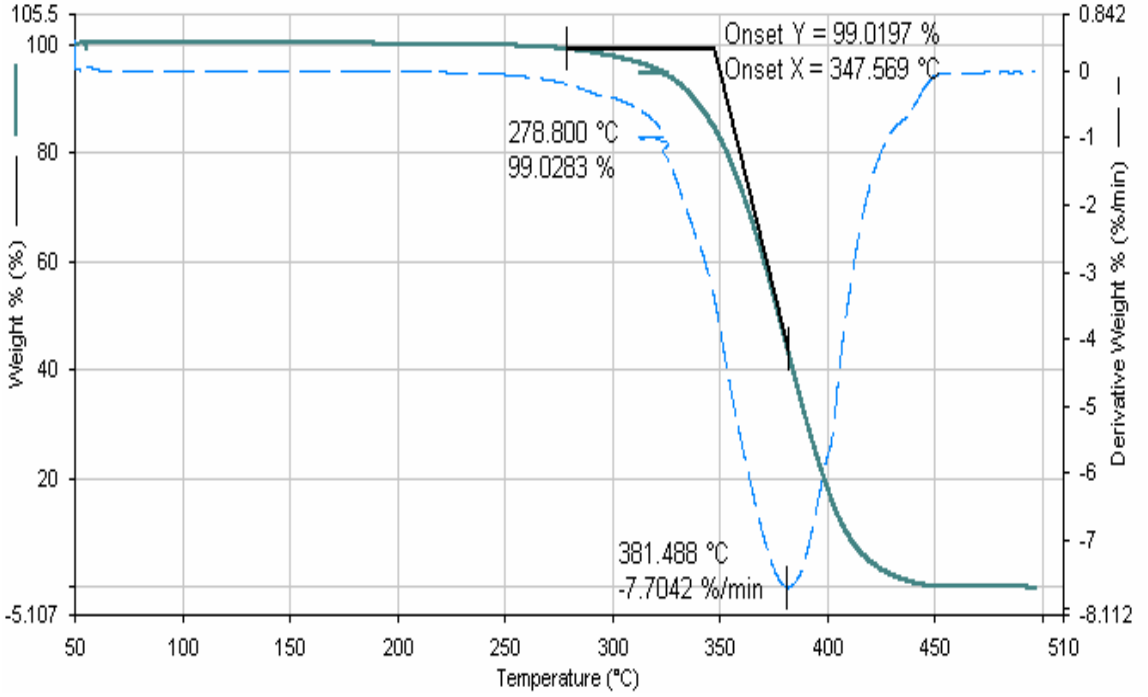

Figure 4.54: TGA thermogram of palm oil.

The oil thermogram as shown in Figure 4.54 consists of three phases. During the first phase, only minimal weight change was observed during this induction period. The thermogram shows that 1% weight loss of the pure palm oil sample in the inert atmosphere occurs around 279^{o}C. 46 minutes was taken before it changes to second phase. Rapid weight change was observed during the second phase. Maximum degradation rate temperature occurs at 381^{o}C, where the rate of weight decrease increases to the maximum up to this point. Slower weight decrease was observed over this temperature. The curve flattering at 466^{o}C shows that there was

no further conversion occurred. The differential weight loss (DTG) curve shows a clear evidence for the three degradation steps. The TG curves and the negative first derivative of the oil decomposition suggest that the overall process occurs in first order kinetics.

4.6.3 Onset and Degrading Temperatures

Onset temperatures (T_{on}) can be used to indicate the resistance of the oil to thermal degradation. It is determined by extrapolating the horizontal baseline at 1% degradation. The intercept of this line with the tangent of downward portion of the weight curve is defined as onset temperature.

Table 4.23 shows the detailed temperatures for the point of 1% weight loss, onset temperature, offset and final temperatures. The onset temperature for the fresh unadditived palm oil is significantly lower than the additived palm oils. This shows that these types of additive and percentages well protected the oil from oxidation. Hindered phenol is among the earliest oxidation inhibitor packages suggested in history. In this case the author used L135, a phenolic anti oxidant. It works as free radical scavengers. However, the onset of oil with L135 additive is lower than the oil with F10 additive. The onset temperatures for palm and rapeseed of aged cases are very similar while for additived palm oils are slightly higher.

Surprisingly the T_1 for rapeseed oil both fresh and aged samples were significantly low. This may indicate the presence of small amount of volatile components in the oil. The T_1 of A_{600} sample was greatly reduced compared to A_0. This may indicate that volatile components were produced during the ageing process.

Comparing the 0 and 600 hour values, it can be seen that T_{on} values for all fresh samples were 2-16^{o}C higher than the aged oil. This is as expected. Degraded oil may have higher volatile components that lead to earlier decomposition. Naturally, the higher the degradation product, the lower the onset temperature. Similar result occurs for polyfilms that were degraded for several weeks (Pezzin and Duek, 2002).

Table 4.23: The 1% weight loss, onset, offset and final temperatures for different samples at 0 and 600 hours

Sample Id.	Additive type and amount	Temperature at 1% weight loss T_1 (^oC)	Onset temperature T_{on} (^oC)	Offset temperature T_{off} (^oC)	Final temperature T_f (^oC)
A_0	PO, no additive	278.80	347.57	426.55	465.92
B_0	1.5% F10	215.09	384.48	435.84	469.85
C_0	2% F10	266.56	384.64	430.98	464.78
D_0	1.5% L135	244.505	375.99	433.00	466.50
E_0	RO	176.22	376.47	436.28	473.29
A_{600}	PO, no additive	134.23	331.94	434.02	465.04
B_{600}	1.5% F10	224.87	377.78	433.77	460.59
C_{600}	2% F10	242.81	375.84	435.90	462.56
D_{600}	1.5% L135	258.46	373.51	436.35	466.54
E_{600}	RO	49.575	363.03	443.12	478.22

4.6.4 Oil Conversion and Decomposition Rate

Figure 4.55 shows the extend of conversion of fresh and aged palm oil at corresponding temperatures. Significant difference of the conversion curve for fresh and aged palm oil exists. The aged oil starts to paralyze at lower temperature than the fresh oil. This corresponds to lower T_1 and T_{on} as discussed in the Section 4.6.3. Another reason might be due to water content vaporization. The aged oil has 1758 ppm water content when measured according to ASTM D4377. Fresh oil has only 994 ppm of water. At elevated temperatures also the aged oil has higher fractional weight loss. This is due to pyrolysis of volatile secondary product that was produced during the 600 hour ageing period.

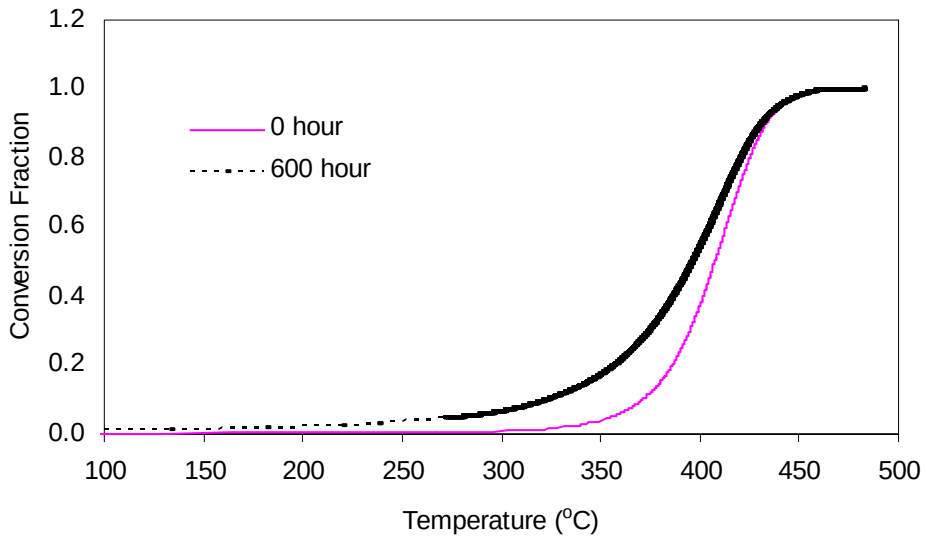

Figure 4.55: Conversion of palm oil with temperature.

Similar pyrolysis pattern was observed for the rapeseed oil. This shows that this oil degraded to similar degree as inhibited palm oil. Other complementary tests (TAN and IV) and kinetic order number analysis show that the palm and rapeseed oil had been worsely degraded, while the introduction of additive has greatly improved the degradation rate. Conversion pattern of palm + 2%F10 blend oil is shown in Figure 4.56. The fractional weight loss of aged oil has a close track to the fresh oil. Conversion pattern of palm + 1.5%F10 oil and palm + 1.5%L135 oil is similar to that of palm + 2%F10 blend oil. The similar tracks for 0 and 600 hour palm oils with additives show that the oils were not much degraded compared to inhibited palm oil and rapeseed hydraulic oil. The results obtained for stable and unstable oils indicate that the fractional weight loss versus reaction temperatures for new and used oil can also be used to indicate the oil degradation condition.

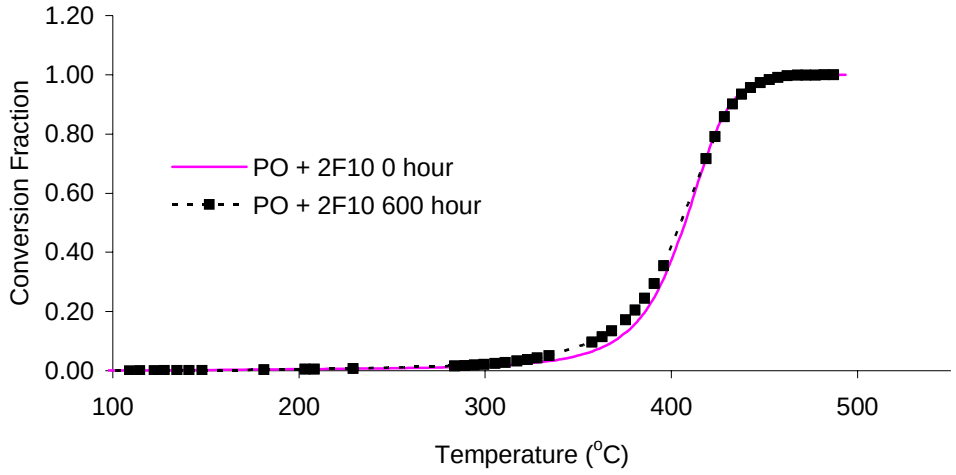

Figure 4.56: Conversion of palm oil + 2% F10 additive with temperature.

4.6.5 Activation Energy

Thermogravimetric analysis using direct Arrhenius plot method has been used by numerous researchers. Equation 2 of Appendix C was used to determine the activation energy of oil samples by direct Arrhenius plot method. In order to calculate *dx/dT*, conversion and temperature differences were calculated for each temperature. The value of *x* and *dx/dT* was calculated using Excel spreadsheet. Finally the plot of ln [(1/(1-*x*)(*dx/dT*)] versus 1/*T* for oil decomposition was made.

Figure 4.57 presents Arrhenius plot of the oil sample that was used to calculate the kinetic parameters such as activation energy and preexoponential or frequency factor. The figure shows a linear relationship of ln [(1/(1-*x*)(*dx/dT*)] versus 1/*T* . Other samples also have similar linear relationship. This result again indicates that the oil conversion reaction can be treated as a first order reaction. Thus the kinetic parameter constants at increasing temperature were determined from the graph slope with high accuracy.

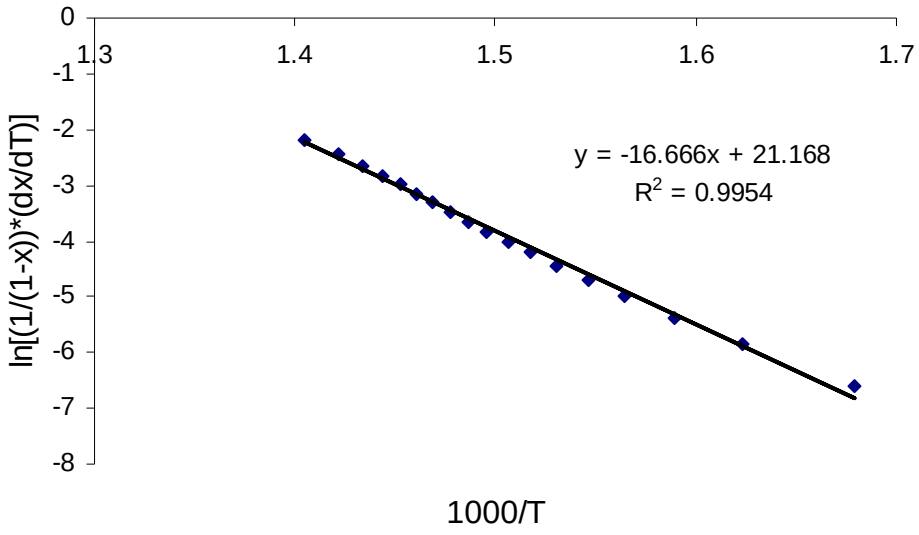

Figure 4.57: Arrhenius plot for palm oil sampled at 600 hour.

With the linear regressed of the abscissa and ordinate parameters, the slope and intercepts in the figure line indicate the values of the activation energy, E_a, and frequency factor, A, respectively. For this sample, the energy of the activation and the frequency factor were computed to be 138.57 kJ/mol and 7.80×10^9 min^{-1}, respectively.

The apparent activation energy of 0 hour palm oil was about 180 kJ/mol, while the activation energy for the blended samples was increased by 23 up to 34 kJ/mol (Table 4.24). Based on activation energy of fresh oil, the F10 additive is better than L135. The influence of same amount of F10 and L135 additives increases the activation energy by 27 and 24 kJ/mol, respectively. Increasing the F10 additive amount from 1.5% to 2% increases the activation energy from 207.77 to 214.07 kJ/mol.

The frequency factor has similar form as activation energy. Frequency factor for palm oil is the smallest while palm + 2%F10 has the highest frequency factor. Thus it can be said that additive amount also has some effect on frequency factor. Increasing the additive amount from 1.5% to 2% increases the frequency factor to 4.55×10^{15} from 1.39×10^{15} min^{-1}.

Table 4.24a: Kinetic parameter for palm with and without additives at 0 hour

Sample Id.	Sample size (mg)	Activation energy (kJ/mol)	Frequency factor (min^{-1})	Average decomposition rate (%/min)
A_0	14.880	180.56	5.48E+12	6.596339
B_0	15.539	207.77	1.39E+15	6.710903
C_0	14.733	214.07	4.55E+15	6.86378
D_0	14.903	203.47	6.85E+14	6.237263
E_0	14.581	154.22	8.96E+12	5.701796

Table 4.24b: Kinetic parameter for palm with and without additives at 600 hours

Sample Id.	Sample size (mg)	Activation energy (kJ/mol)	Frequency factor (min^{-1})	Average decomposition rate (%/min)
A_{600}	14.609	138.57	7.80E+09	4.32757
B_{600}	14.675	195.94	1.90E+14	5.97951
C_{600}	15.947	192.32	9.46E+13	5.94236
D_{600}	15.793	188.14	4.61E+13	5.80407
E_{600}	14.338	132.39	1.93E+09	4.06740

In order to ensure sample temperature uniformity, approximately same sample size (15 mg) was used in the experiment. This is to reduce the result error. It is expected that onset, 1% weight loss and final temperatures to decrease or increase if smaller or larger sample size was used, respectively. Larger sample size means smaller surface exposure per sample volume. This will make decomposition process slower.

Column 5 of Table 4.24 shows the decomposition rate of samples at 0 and 600 hour. Decomposition rate of palm oils were higher than rapeseed hydraulic oil, both for 0 and 600 hour samples. This may suggest that palm oil structure is less complex than the rapeseed oil.

When the oils were degraded for 600 hours, the decomposition rate reduced. Reduced decomposition rate suggests that the sample is more difficult to be decomposed, which further suggests that the oil was becoming more complex. The increased difficulty in decomposition could be relate also to the increased oil viscosity as discussed in Section 4.4.1. Thus based on decomposition rate, the oils

seem becoming more complex after heated. However this result contradicts with the kinetic order result.

Table 4.25 compares the activation energy calculated using direct Arrhenius method and integral method (Equations 2 and 3 of Appendix C, respectively). Except for the palm and rapeseed oils at 0 hour, the activation energies for all samples calculated using direct Arrhenius method are larger than the integral method. The activation energy values for aged samples are always smaller compared to fresh sample. This is also true for integral methods. As can be seen from the table, almost all correlation coefficients by direct Arrhenius and integral methods were close to unity.

Table 4.25: Activation energy calculated by Integral and Direct Arrhenius methods

Sample	Integral	Correlation coefficient	Direct Arrhenius	Correlation coefficient
A 0 hour	188.85	0.9989	180.56	0.9979
A 600 hours	105.34	0.9792	138.57	0.9954
B 0 hour	188.85	0.9980	207.77	0.9849
B 600 hours	158.74	0.9910	195.94	0.9973
C 0 hour	191.83	0.9971	214.07	0.9822
C 600 hours	173.09	0.9960	192.32	0.9954
D 0 hour	203.47	0.9783	203.47	0.9783
D 600 hour	154.52	0.9907	188.14	0.9940
E 0 hour	161.65	0.9908	154.22	0.9205
E 600 hours	108.20	0.9934	132.39	0.9264

4.6.6 Kinetic Order

The reaction order for the oil sample was calculated using Equation 3.3 where $n = (y - B - Cx)/z$. The result is shown in the form of bar chart in Figure 4.58. For the palm oil samples, with or without additives, fresh or aged samples the apparent order of reactions n were in the range of 0.852 to 1.46. However, for the commercial rapeseed hydraulic oil the order for the fresh and aged sample were 1.92, 1.72, respectively. The high order number of the rapeseed oil may be due to complex formulation of the oil. This corresponds to low decomposition rate as shown in Table 4.24. A high coefficient of correlation ($R^2 > 0.99$) was obtained for all oil samples.

It was found that the order decreased with heating time for all samples. This suggests that the rate of decomposition decreases with ageing. Also it is noticed that the order increases slightly with additive, the more the additive the higher the order. Interestingly, the order reduction for palm oil without additive (A) is almost double than the sample with additive. This observation further suggests that the palm oil without additive had undergone significant physical or chemical change. With the presence of additive, less changes occurred which is indicated by less order change. Indirectly the results show that the additive protected the palm oil. Not only the additive type, but additive amount also affects the order reduction. Higher amount of additive (oil C compared to oil B) reduces the order reduction.

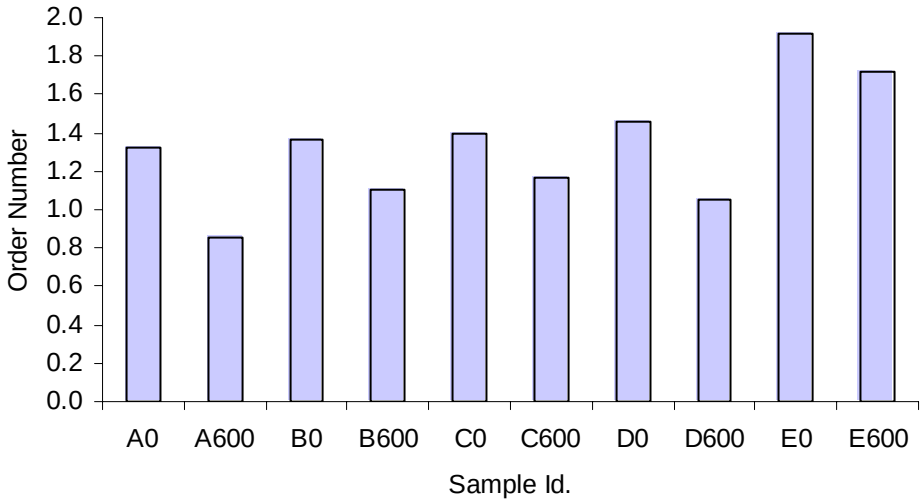

Figure 4.58: Kinetic order for all samples.

The kinetic study performed in this investigation helped the author for making quick assessment of comparative oil thermal degradation. Similar trends of onset temperature, conversion pattern and order number was observed. Similar finding was also reported by Adhvaryu *et al*. (2000) but without order number and conversion pattern results.

4.6.7 Iodine Value

Iodine value (IV) measures the number of double bonds or unsaturation level of fats and oils. Figure 4.59 shows that the IV for the palm oil before being degraded

in hydraulic sample as 59 cg I_2/g. Similar IV was reported by Noh *et al*. (2002). However after 600 hours of heating and shearing, the IV of the palm oil without additive decreased to 43 cg I_2/g. This iodine value analysis indicates the decrease in the double bond of the oil sample after 600 hours operation. The C=C double bond was damaged due to thermal oxidation. The heating and shearing process in the hydraulic system provided energy to excite the molecules. At a certain stage, the molecules had enough energy to break the bond in the chain. Mostly this happened to the unsaturated parts, which will then enable the saturated structure to form.

Commercial rapeseed at 0 hour had high IV. This is due to the high mono-unsaturated (63%) and polyunsaturated (28.4%) acids, compared to palm oil which had only 43.6% mono-unsaturated and 11.8% polyunsaturated acid components. However, rapeseed oil also had undergone significant IV reduction after being heated in the hydraulic system. This is due to its high unsaturation level which prones to oxidation.

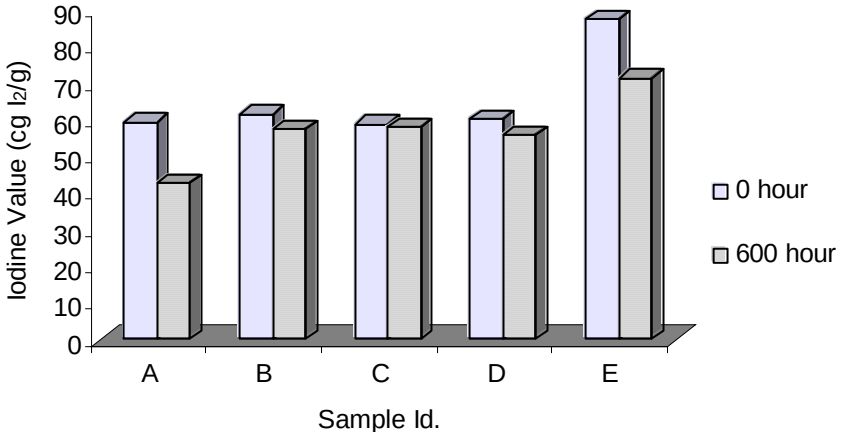

Figure 4.59: Comparison of iodine values of fresh and aged oils.

4.6.8 Infrared Spectroscopic Analysis

The main functional groups of palm oil such as carbonyl, unsaturated and saturated hydrocarbon were determined by the infrared analysis (IR). The oil samples at 0 hour and lower hour of operation show a narrow weak band around 3472 cm^{-1}. This band is usually assigned to the overtone of the glyceride ester carbonyl

adsorption. As the thermal oxidation process advances, the band becomes wider. This is due to the increase of the concentration of hydroperoxide group in oil. According to Guillen and Cabo (2002), degraded oil experienced the expansion of the O-H stretching region, which is in the wavenumber region of 3200-3700 cm^{-1}.

Other major changes can be observed from the infrared spectroscopic analysis towards the thermal oxidative test to palm oil. There is an expansion of the overtone region for C=O stretching caused by the increasing hydroperoxide structure after ageing process, decreasing intensity of C=C and absorption band for aldehyde and ketone C=O stretching vibration shifting to the lower wavenumber.

Every functional group of palm oil was represented by different frequency as shown in Table 4.26. For example, absorption bands at 3005 cm^{-1} is the C–H stretching from H–C=C structure, peaks from 2950 cm^{-1} to 2850 cm^{-1} are C–H stretching from CH_2 and CH_3 and 1236.89 cm^{-1} is C–O stretching from carbon sp^2 (Solomons and Fryhle, 2000).

Expansion region for C=O overtone is caused by the increasing hydroperoxide structure after ageing process. Theoretically, oxidation at allylic hydrogen atom can form hydroperoxide O–O–H easily. Then, the hydroperoxide structure were oxidised again to form aldehyde, ketone, alcohol and acid.

There is a decreasing intensity for C=C stretching at 3005 cm^{-1}. This is because the atoms attached to the C=C had changed from hydrogen to other functional groups such as carbonyl, alkyl, and hydroxyl after ageing process. As the result, the intensity of the C=C stretching decreases and peak for C=C becomes shorter and weaker as shown in the Figure 4.60.

The aldehyde and ketone C=O stretching vibration shift to a lower wavenumber. Absorption band for C=O stretching at 1746.48 cm^{-1} had shifted to 1745.97 cm^{-1}. The frequency of a given stretching vibration in an IR spectrum can be related to two factors. These are the masses of the bonded atoms and the relative stiffness of the bond (Solomons and Fryhle, 2000). It is well observed that the

reduced mass attached to the C=O increase, then value of the wavenumber must decrease. In this case, the molecule weight attached to C=O increased after process ageing becomes a branch complex molecule which yield the lower wavenumber.

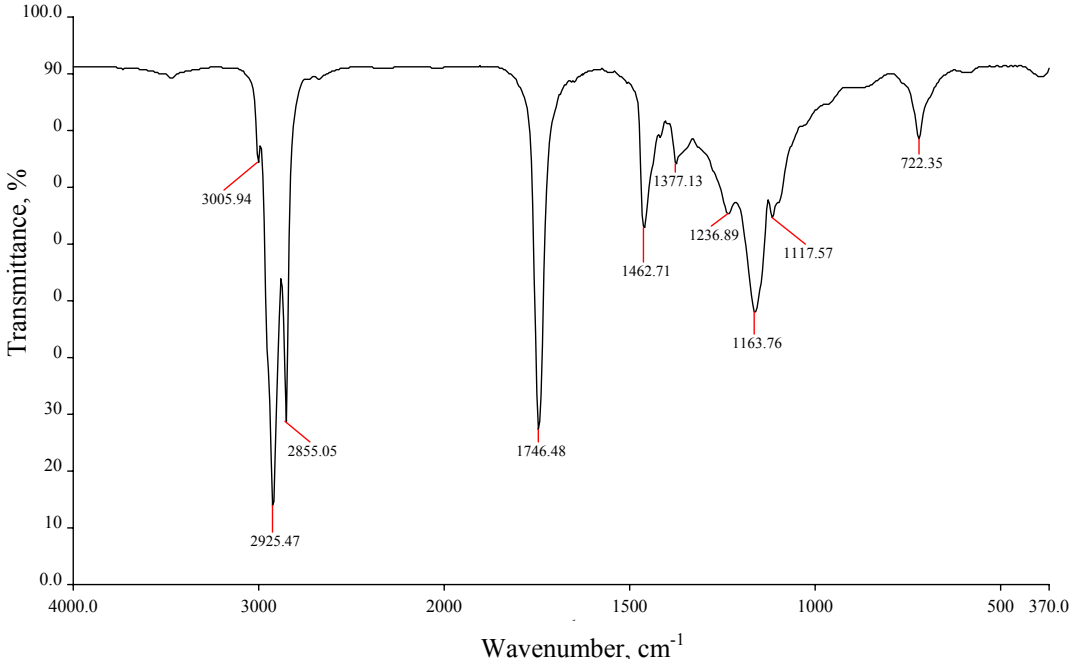

(a)

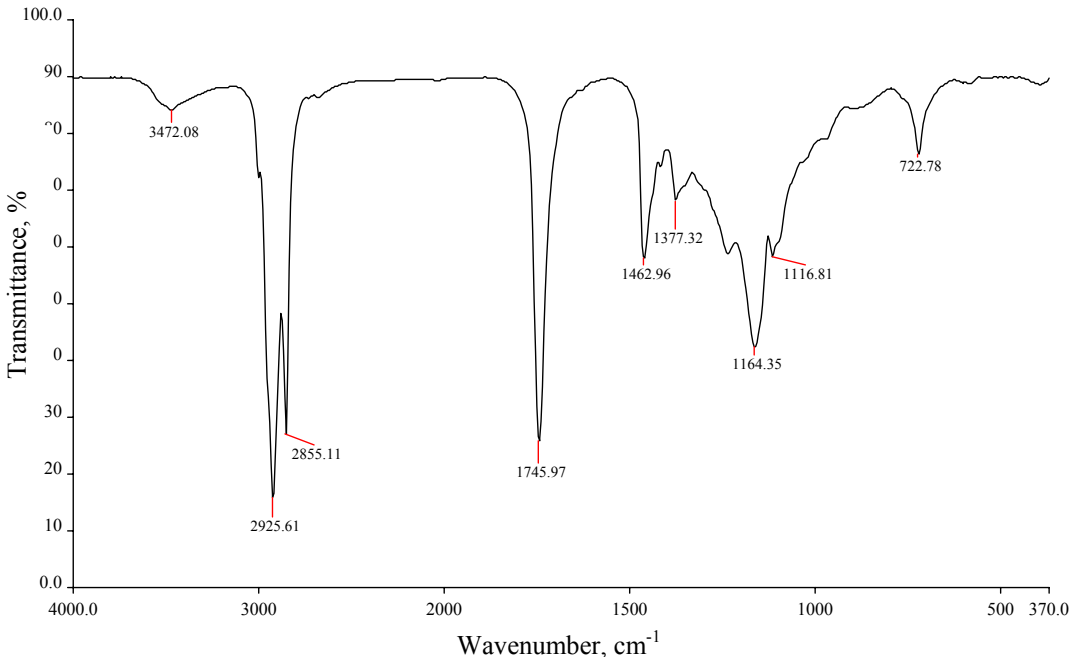

(b)

Figure 4.60: Infrared spectra for palm oil (a) at 0 hour and (b) after 600 hours of operation.

Table 4.26: Vibrational frequency and the assign of functional group for palm oil (0 hour and 600 hour)

Vibrational Frequency (cm^{-1})		Functional Group
0 hour	600 hours	
-	3472.08	Overtone C=O str and O–O–H str
3005.94	-	C–H str from H–C=C
2925.47	2925.61	C–H str from CH_2 and CH_3
2855.05	2855.11	C–H str from CH_2 and CH_3
1746.48	1745.97	C=O str
1462.71	1462.96	CH_2 and CH_3 deformation
1377.13	1377.32	CH_3 umbrella bending (symmetric bending)
1236.89	-	C–O str from Csp^2
1163.76	1164.35	C–O str
1117.57	1116.81	C–O str from Csp^3
722.35	722.78	C-H O.O.p. (Out of Plane) bending from (–HC=CH–)

4.7 Basic Performance of Hydraulic System

This section will discuss the basic hydraulic test rig performance with respect to various running parameters. Only one parameter was varied at one time. The result of this section is based on unadditived palm oil used in the hydraulic test rig. Except for specific tests, the rig was run continuously for 15 hours a day at 70 bar and 70^{o}C.

4.7.1 System Discharge

In this experiment, the system discharge (oil reentering reservoir) characteristic was investigated. The experiment was conducted at 70^{o}C and oil viscosity of 0.015 Pa.s. The pump was operated at 10 different speeds. The actual flow rate coming out from the return line was measured using measuring cylinder and stop watch. The flow meter was recalibrated with the calculated flow rate.

Figure 4.61 shows the effect of motor speed on the vane pump discharge. As the speed increases, the discharge also increases. Similar result was obtained by

Ranganathan *et al*. (2004) but with smaller discharge even conducted at higher speed. This is due to the small size of gerotor pump used in Ranganatahan's study.

The relationship between the discharge and the speed is nearly linear. As expected, the reduced discharge is observed for 150 bar operation compared to 35 bar operation. At lower speed operation the discharge difference is larger compare with at high speed ($\Delta Q_{600} > \Delta Q_{1400}$). For instance at 600, 840, 900, 1050, 1200, 1350 and 1440 rpm the discharge are 2.401, 2.394, 2.381, 2.232, 2.187, 2.150, and 2.035 l/min, respectively. The difference can be explained in the aspect of force imbalance between centrifugal and pressure force acting on pump vane. At low speed, the centrifugal force acting on the vane is low and pressure force pushes the vane further into the rotor slot (Figure 4.62). As the result, the amount of net swept is low. This effect is more for the higher pressure operation, thus suppress the discharge.

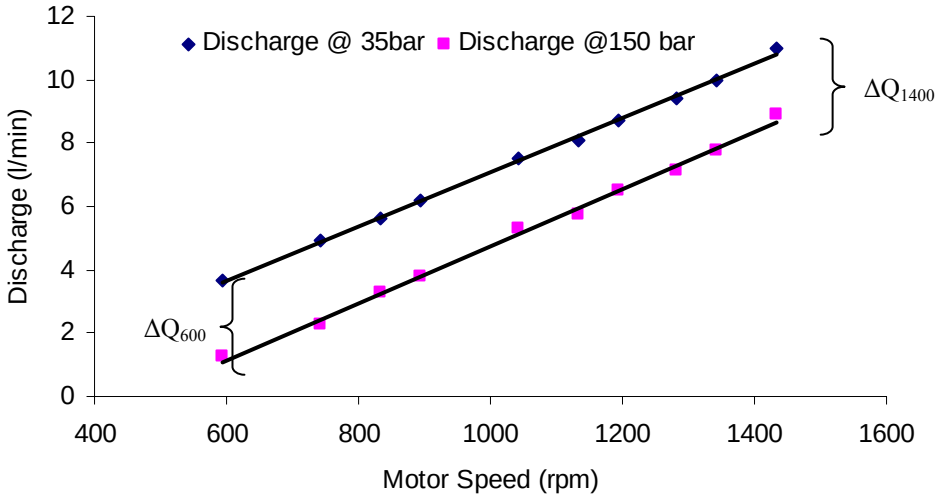

Figure 4.61: Discharge versus motor speed.

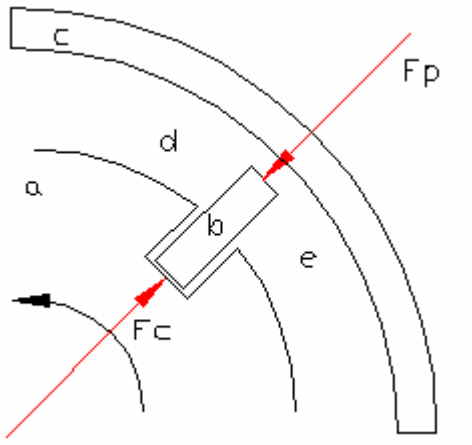

a – rotor

b – vane

c – cam ring

d – high pressure chamber

e – low pressure chamber

F_c – centrifugal force

F_p – pressure force

Figure 4.62: Schematic diagram showing centrifugal and pressure forces acting on vane.

4.7.2 Flow Rate - Pressure Relationship

Flow rate - pressure relationship when the pumping system running at 1440 rpm is shown in Figure 4.63. The system lost 8.6 l/min when the system pressure was increased from 30 to 200 bar. The result from this study shows a linear reduction of flow rate with pressure, with correlation coefficient of higher than 99% between flow rate and pressure. This contradicts with the normal curving down of flow rate due to increase in upstream pressure (Pinches and Ashby, 1989).

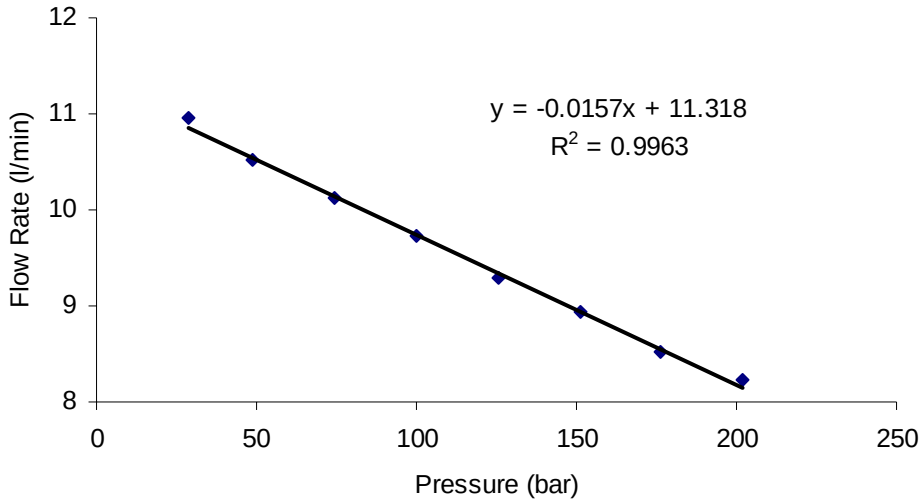

Figure 4.63: Flow rate – pressure relationship when motor running at 1440 rpm.

4.7.3 Torque Losses

Figure 4.64 shows variation of torque required to run the pump. The system was operated at 1050 rpm against 50 bar load. The rig was started at ambient temperature of 30^{o}C and the system was stopped when the reservoir temperature reached about 70^{o}C.

The data was recorded automatically using LabVIEW software every for 90 seconds. The total observation time was 130 minutes. It was observed that the high

value of torque was recorded at the starting condition. This is related to rheological property of the oil as presented in Sections 4.2 and 4.3. At 30 - 40^{o}C, the oil internal resistance is about 50 to 30 cP. The high internal resistance gave rise to high torque to transport the fluid. As the oil and the system got heated, the torque required to run the system reduces. The torque reduction pattern is similar to oil viscosity reduction pattern shown in Section 4.2.1.

This phenomenon can also be attributed to thermal properties of the fluid and the hydraulic components. At starting, the pump produced low shear rate. As already discussed earlier (rheological section), palm oil behaves non-Newtonianally at low shear rate. As shown in Figure 4.2, at low shear rate the viscosity is high, thus creating high flow resistance.

Comparing rheological and thermal factors, the more significant influence is the thermal property of the oil. Thicker oil gives rise to large shear stress. To overcome this stress, motor had to apply higher torque to run the pump. However, after 70 minutes, the oil becomes relatively thin. The oil could flow more easily and posed less stress for the pump to rotate. Hence the torque was low after 70 minutes.

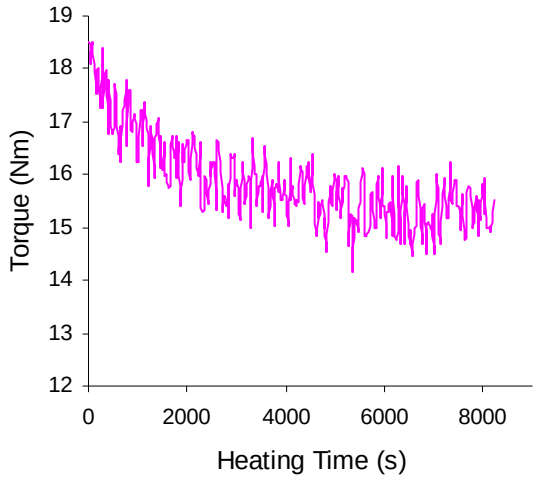

Figure 4.64: Torque versus heating time.

4.7.4 Variation of Torque Loss with Speed

Figure 4.65 shows the variation of torque loss (T_l) with motor speed from 20 Hz to 48 Hz at 50, 75, 175 and 200 bar condition. It was observed that the torque loss did not vary much with speed at low pressure environment (50 and 75 bar). However, noticeable torque loss occurred at higher pressures. The higher the pressure, the higher the torque loss. This is inline with Equation 2.33 and the models indicated in Table 2.4. The higher torque loss is due to the increase in coulomb friction. Coulomb or load dependent friction is proportional to load (Dupont, 1992), in this case pressure.

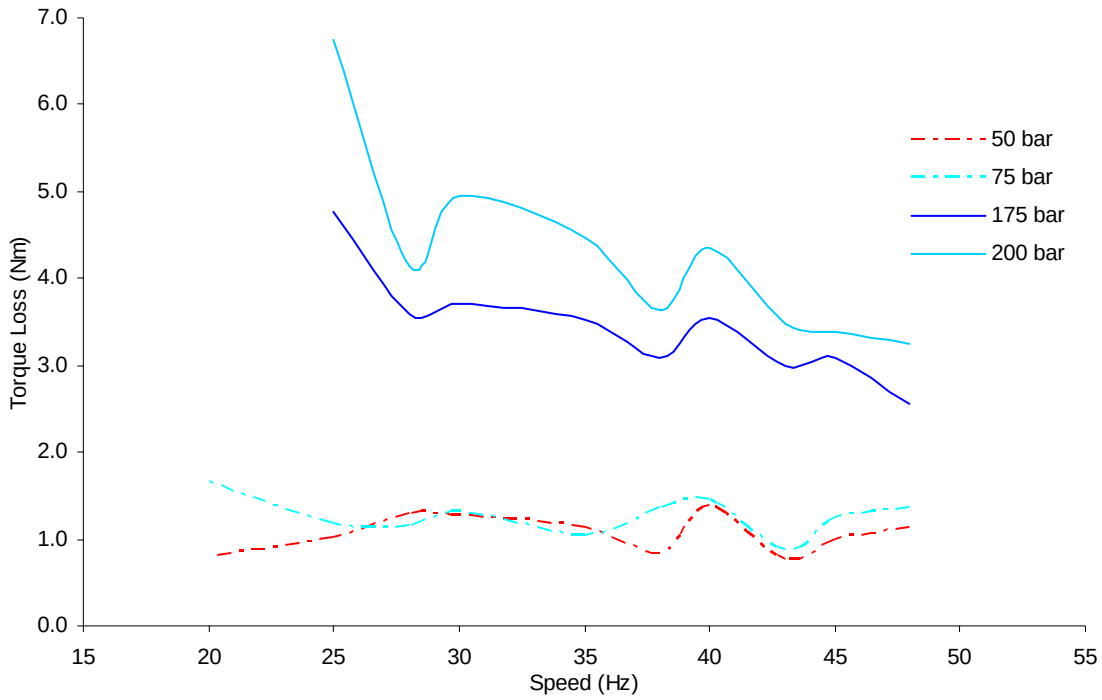

Figure 4.65: Variation of torque loss with speed.

Decrease of torque loss with increase in speed is not inline with Equation 2.32 and models shown in Table 2.4. However, McCandlish (1984) obtained similar result pattern when he used gear pump with the result of author's work. Extended work performed shows that the torque loss decrease with increase in speed is due to the variation of viscous coefficient, C_v. C_v value decreases from 428699 to 232854 and from 949668 to 541752 for test temperature of 40^{o}C and 50^{o}C cases, respectively (Table 4.35).

4.7.5 Variation of Torque Loss with Pressure

In order to investigate the influence of pressure on torque loss, the rig was run against several pressure conditions (0 to 200 bar). Figure 4.69 shows that the effect of pressure is quite significant above 120 bar. It can be seen that above 120 bar at the speed of 900 and 1200 rpm the torque loss is less at higher speed case. This result complements the result discussed in Section 4.7.4.

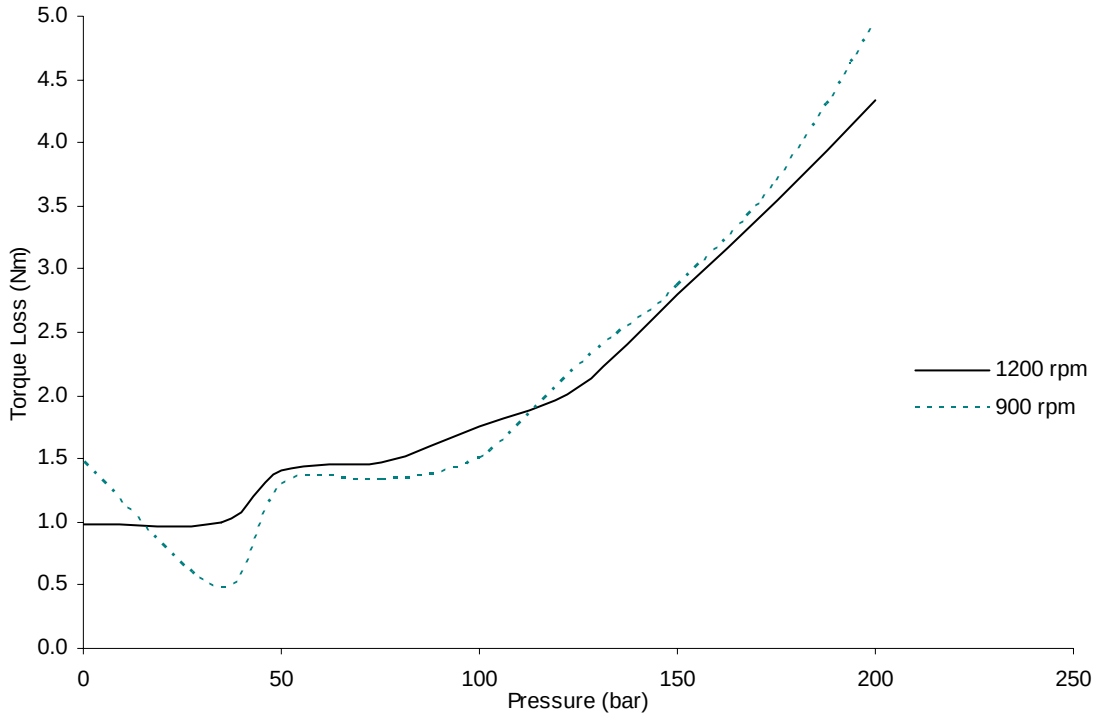

Figure 4.66: Torque loss versus pressure.

The result from this study compares well with the result of McCandlish (1984). In this study, the crossover points occur at 18 and 120 bar pressure while for McCandlish result the crossover point occur at 160 bar. This might be due to different pumps used in the study. This study used vane pump while the McCandlish referred case is the gear pump. The loss is non-linear increasing rapidly with pressure. The effect of pressure however is related to speed. Higher stiction friction was observed for lower speed case.

4.8 System Efficiency

4.8.1 Input Power versus Temperature

This test investigated the effect of temperature on the input power. The system was operated at constant speed of 1440 rpm and 50 bar pressure from 35°C up to 75°C with 5°C increment. Then test was repeated with 1200 speed at the same pressure (for 1200 rpm case, only up to 70°C).

The input power to drive the hydraulic system was calculated as Equation 2.36. Figure 4.67 shows that the power required to operate the system is decreasing with operating temperature. This is due to rheological palm oil behavior as discussed in Sections 4.2 – 4.4. As expected, the power required to operate the system at higher speed requires higher power. This results from an increase of mass flow rate.

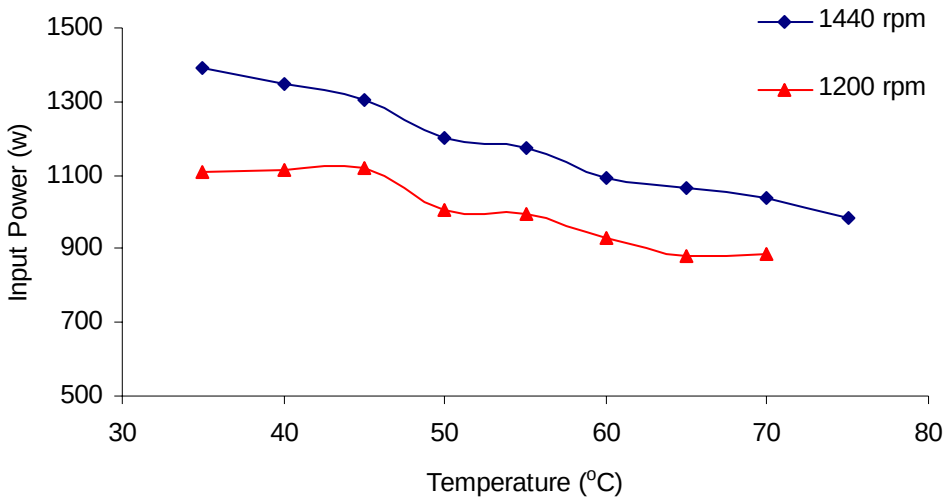

Figure 4.67: Input power versus temperature.

4.8.2 Volumetric Efficiency versus Discharge Pressure

The volumetric efficiency of the hydraulic test rig when operating at different speeds is shown in Figure 4.68. The system was operated against discharge pressure of 0 bar to 200 bar. The volumetric efficiency is defined as the actual flow rate oil flowing through the return line to the reservoir divided by amount of oil that should

flow as calculated by pump speed and pump size. The volumetric efficiency was calculated as in Equation 2.38a.

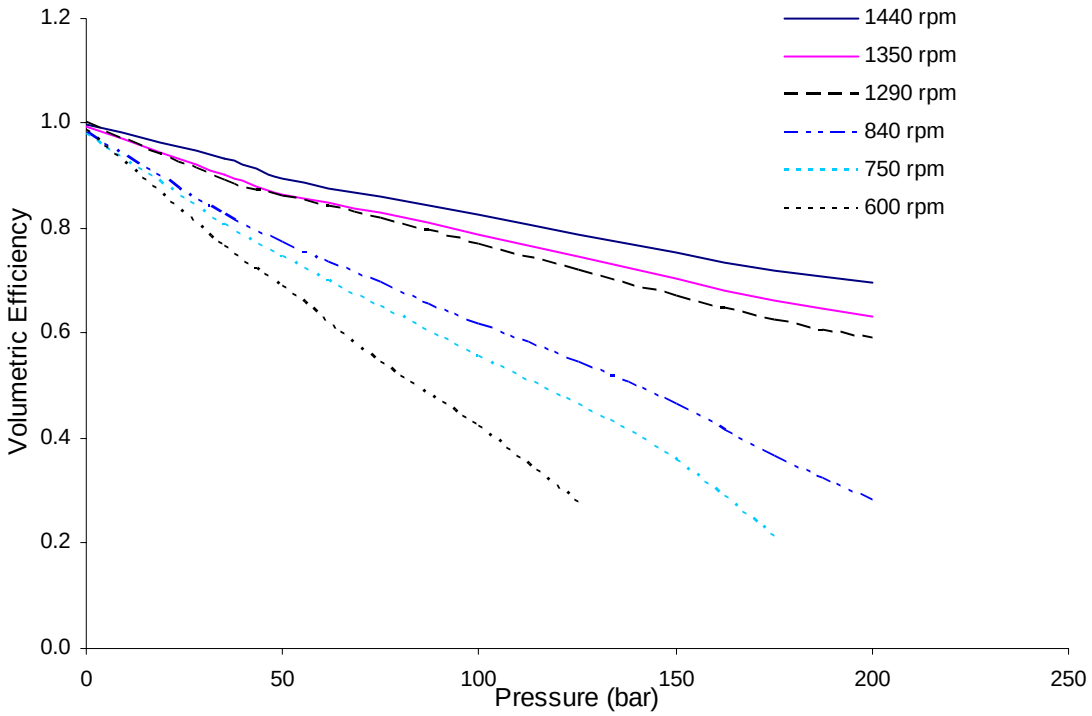

Figure 4.68: Volumetric efficiency versus discharge pressure.

The figure shows that the volumetric efficiency of the system running at speed of 1440, 1350, 1290, 840, 750 and 600 rpm decreases almost linearly with increasing pressure. The volumetric efficiency decreases with pressure due to the existence of back pressure at pump outlet. The volumetric efficiency of 1440 rpm at minimal load is 99% and at load of 200 bar is about 73%. About same volumetric efficiency was achieved for other speeds at low pressure.

However, as plotted in Figure 4.68, for low pressure operation the efficiency was reduced with reducing speed (840, 750, 600 rpm). At 600 rpm, the efficiency decreased from 98% to 26%. This means that volumetric efficiency decreased at higher rate with the reduction of speed. Furthermore, there was unstable result at high pressures for low speed operation. This is due to system capability to flow the oil against high system loading. Back pressure might result in reduced flow rate. For 600 rpm operation, the rig was unable to withstand the high load, and stalled at 150 bar.

The reduced efficiency at increasing pressure means that there is increased leakage and compressibility effect. It was observed that the external leakage is minimal even if at elevated pressures. Thus it is expected that the reduced efficiency is due to internal leakage across the pump outlet and inlet. The difference in volumetric efficiency at 200 bar between 1440 and 840 rpm cases is about 41%.

There are several factors that influence volumetric efficiency. They are internal leakage between vane and cam ring and leakage at the side plate. High pressure operation results in high temperature working condition which influences the oil viscosity. The loss in viscosity will further increase the internal and external leakage.

4.8.3 Mechanical Efficiency versus Discharge Pressure

Theoretically, mechanical efficiency is dependent on torque required to run the pump. In turn this torque depends on loading pressure and oil viscosity. The effect of pressure on mechanical efficiency is illustrated in Figure 4.69. It is clear that for all speeds mechanical efficiency increases drastically with pressure from the start of operation. This increase continues until pressure around 100 bar. After this point mechanical efficiency becomes stable at the range of 80 to 90%. Slight decrease was observed at high pressure region (180 – 200 bar).

The set temperature in this test was 70^{o}C. This means that the solenoid valve energized at this temperature and tap water flowed into shell and tube exchanger. Certain amount of heat was absorbed by cooling water. However, for higher pressures, a lot of heat was generated. Amount of heat generated was higher than amount of heat taken out from hydraulic system. Thus the oil temperature increased slightly, meaning that the oil viscosity decreased. This would reduce friction generated, and thus reduce the torque required to run the pump.

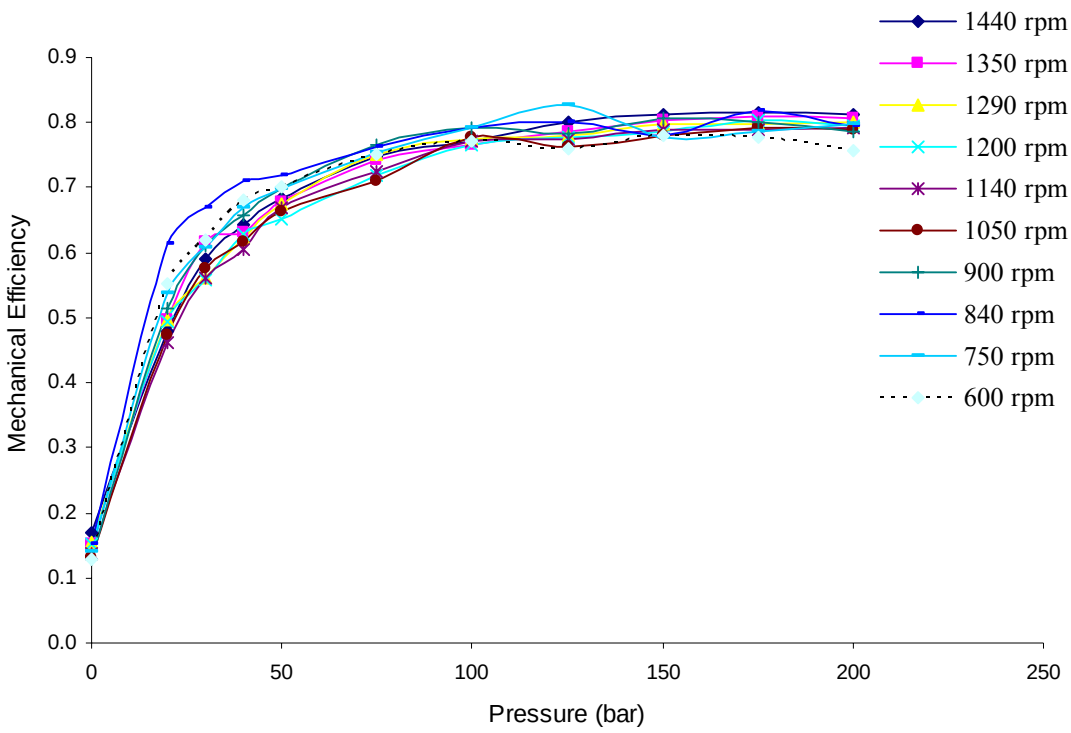

Figure 4.69: Mechanical efficiency versus discharge pressure.

4.8.4 Volumetric Efficiency versus Speed

Variation of volumetric efficiency of the hydraulic test rig when operating at different speeds is shown in Figure 4.70. Unlike Section 4.8.2, the speed in Section 4.8.4 was varying continuously from 1440 rpm (48 Hz) down to 600 rpm (20 Hz). The experiment was repeated for different discharge pressures of 35 bar to 200 bar. The figure shows that as the pump speed increases, the volumetric efficiency increases with high rate initially before reducing its rate. A similar phenomenon was observed by Sadashivappa *et.al*. (1996).

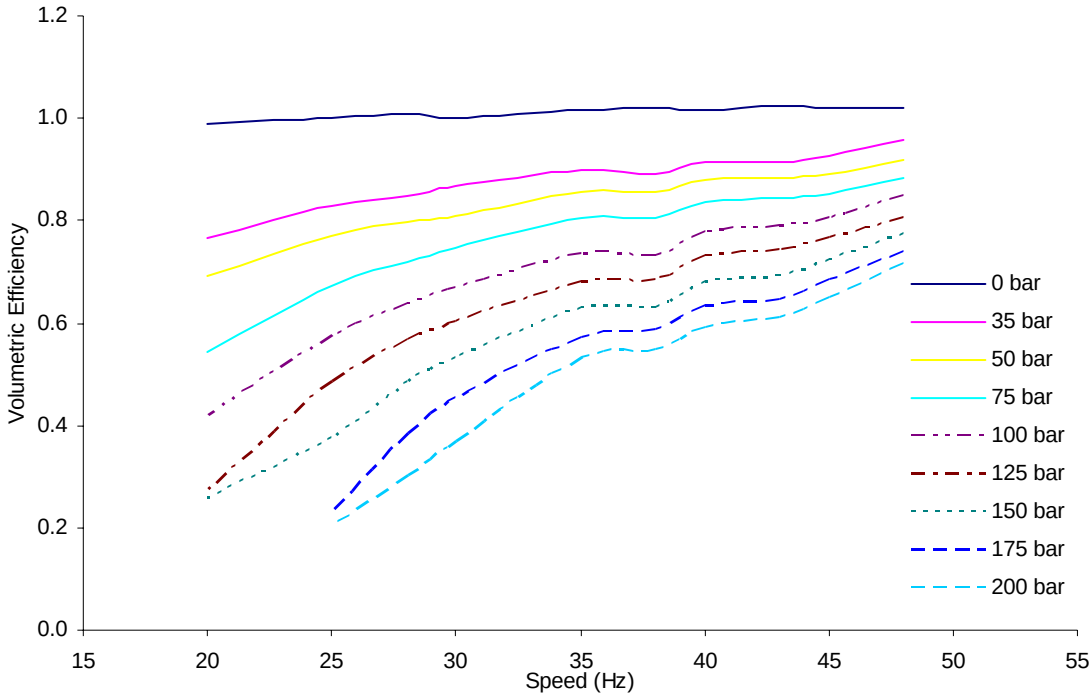

Figure 4.70: Volumetric efficiency versus speed.

The low volumetric efficiency at low speed can be attributed to centrifugal force also. Low speed creates low centrifugal force. Low centrifugal force produces low sealing effect at the cam ring. This will induce internal leakage from high pressure chamber to the low pressure chamber.

When the speed was increased, high sealing effect increased the volumetric efficiency. Increasing loading pressure resulted in higher pressure force. The imbalance between the pressure force and the centrifugal force pushed the vane back to the rotor slot slightly. This reduced the amount of oil swept. Thus the volumetric efficiency was suppressed.

It was observed from the figure that there is slight perturbation occurs at around 38 Hz. This corresponds to strange observation when running around this speed. Noticeable sound was heard from the pipe and flow control valve. When the flow meter cover was opened, it could be seen that the flow was not very smooth (Figure 4.71). This phenomenon might be attributed to the natural frequencies of the system. Every mechanical parts or machine has its own natural frequency. When the

machine is attenuated at its natural frequency (in this case speed and pressure) the system vibrates or produces disturbed flow.

(a)

(b)

Figure 4.71: Flow condition in pipe (a) normal flow and (b) disturbed flow.

4.8.5 Mechanical Efficiency versus Speed

The test was conducted at various motor speeds at 3 bar and the mechanical efficiency was noted. Then the test was repeated by 20, 30, 40, 50, 75, 100, 125, 150, 175 and 200 bar cases. The mechanical efficiency of 3 bar case was around 15%. The efficiency jumped to 50% when the pressure was increased to 20 bar. Less and less increase in efficiency was observed when the pressure was further increased up to 200 bar.

According to Equation 2.39b, mechanical efficiency should decrease with increasing speed. However, based on Figure 4.72, not much can be deduced concerning variation of mechanical efficiency with speed. The result in Figure 4.72 suggests that mechanical efficiency is independent of speed. To determine the reason for the insensitivity of mechanical efficiency, dimensionless parameters were investigated and the results are discussed in Section 4.9.

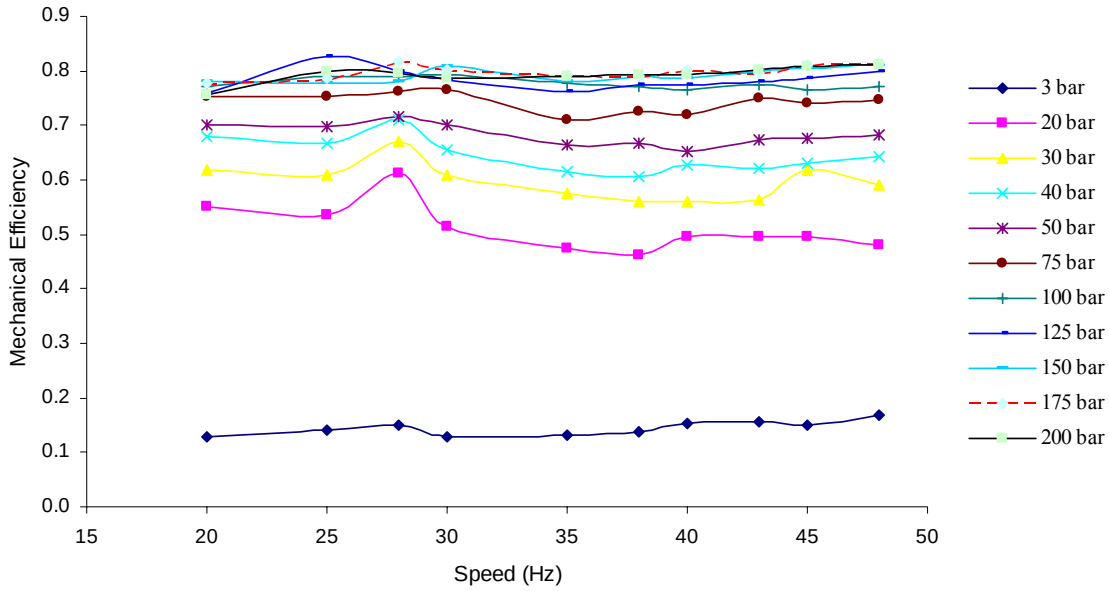

Figure 4.72: Mechanical efficiency versus speed.

4.8.6 Mechanical Efficiency versus Running Temperature

In hydraulic test rig experiment, there would be high volume fraction of dispersed gas bubble presence in the hydraulic tank and hydraulic fluid itself. This would be worse for low temperature case. Thus the presence of this gas bubble, plus the low operating temperature during starting, it is expected that the oil would further deviate from Newtonian behavior. Thus more stress would occur, and more torque is required to run the hydraulic system during starting. Finally this non-Newtonian behavior would result in reduced mechanical efficiency, especially at low temperature.

To observe this phenomenon a test was conducted. The result is depicted in Figure 4.73 where mechanical efficiency was monitored at 90 minutes interval from room temperature of temperature of 35^{o}C to around 70^{o}C with cooling system was disable. The motor was run at 1200 rpm with loading pressure of 70 bar. Data was captured and computed automatically using the built program. As running time increases, the oil temperature increases. Thus the running time can be translated to oil temperature. The result shows that under this operating condition, the relationship

between mechanical efficiency and operating temperature can be in the form of polynomial equation:

$$\eta_m = -3x10^{-5}T^2 + 0.008T + 0.419.$$

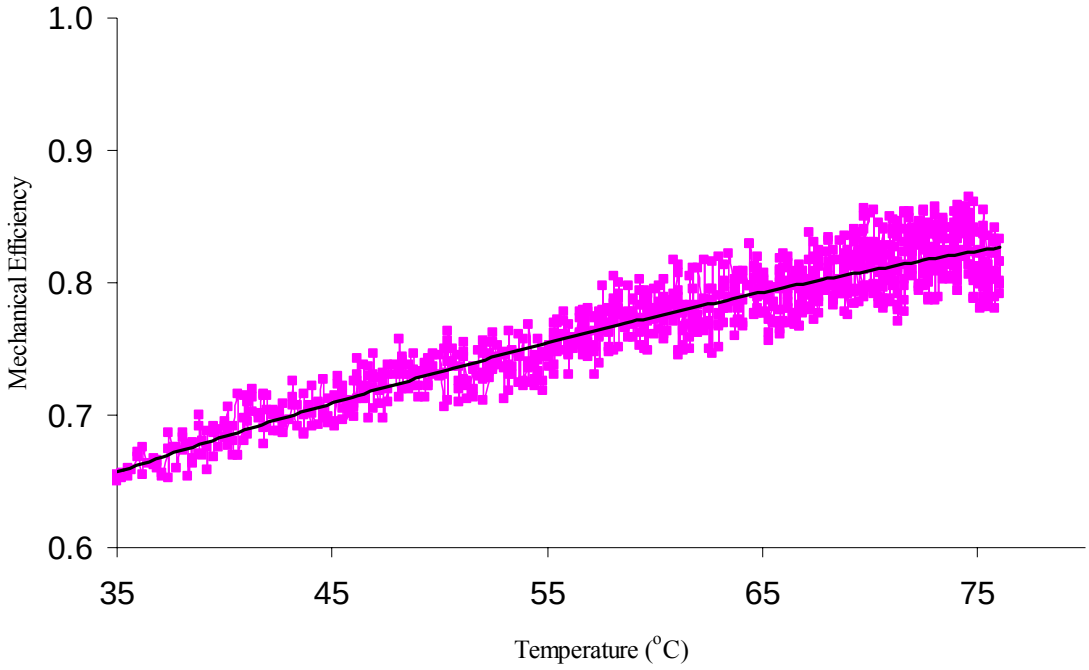

Figure 4.73: Mechanical efficiency versus temperature.

4.8.7 Effect of Oil Ageing on System Performance

Throughout the endurance test for 900 hours at 70 bar and 70°C continuously 15 hours a day, thermal heat and friction force were generated during the operation, hence degrading the oil in a rate proportional to time. The degradation process mainly affected the oil viscosity, making it more viscous, and density, making it denser. In addition to that, formation of sludge might cause some blockage and additional resistance to flow.

Figures 4.74 and 4.75 show the variation of mechanical efficiency with ageing of the palm based hydraulic fluid when it was investigated with respect to pressure and speed, respectively. The figures suggest that the mechanical efficiency

drops with the oil ageing. This is due to the increase in the palm oil internal resistance.

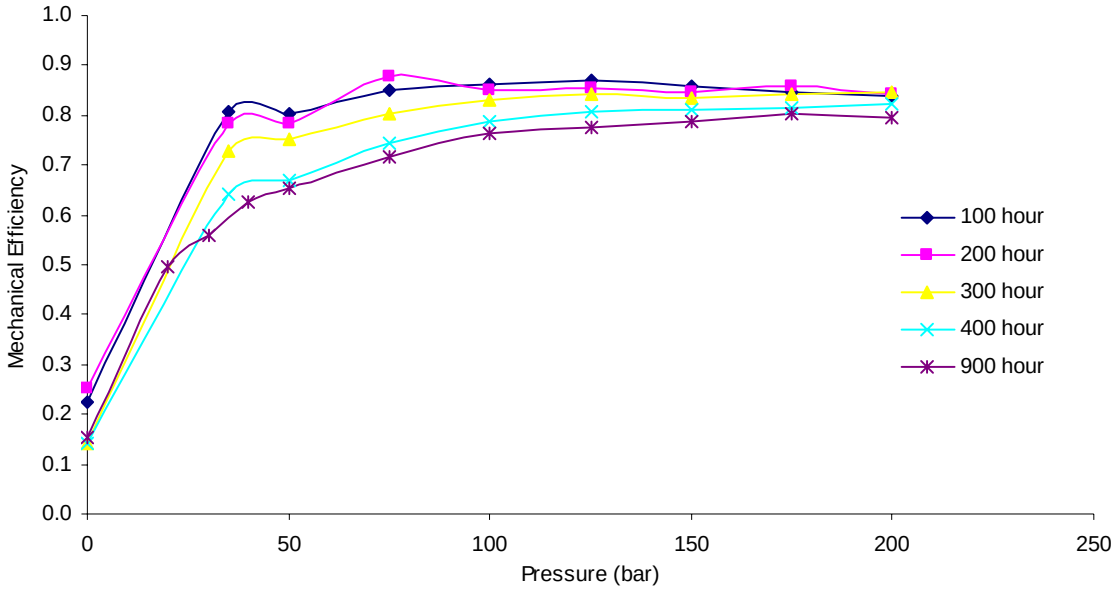

Figure 4.74: Mechanical efficiency against pressure at respective interval of time.

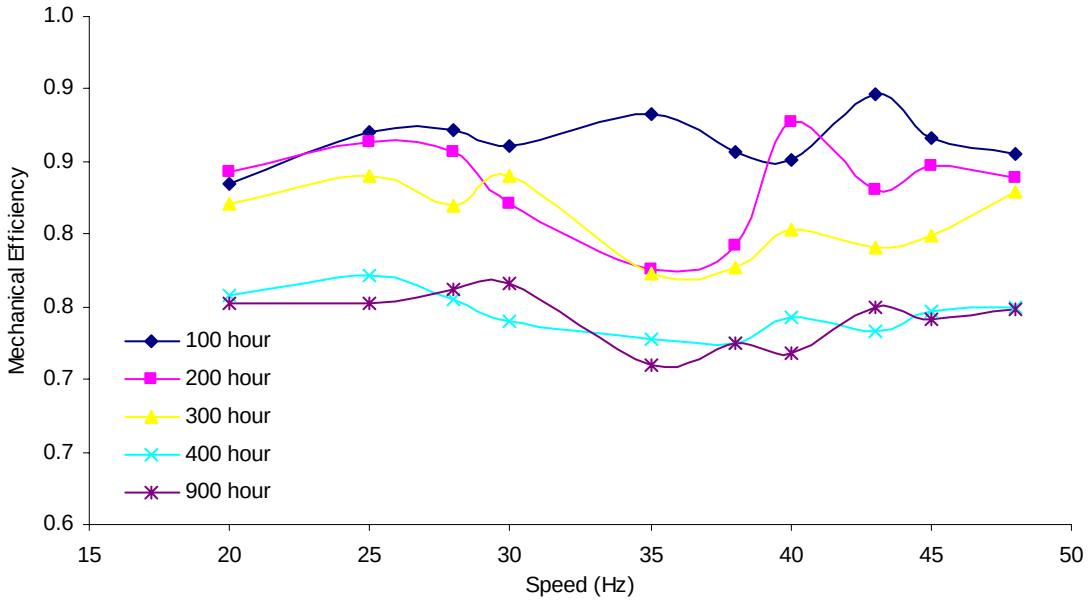

Figure 4.75: Mechanical efficiency against speed at respective interval of time.

On the other hand, Figures 4.76 and 4.77 show that volumetric efficiency increased over time. The rate of efficiency drop with pressure reduces when the oil has aged (at higher operation hour). The increase in volumetric efficiency with ageing period is due to the increased viscosity of the oil as discussed in Section 4.4.2.

Thicker oil results in less flow loss due to leakage. These results are inline with the viscosity and rheology theories as mentioned in Section 2.4.

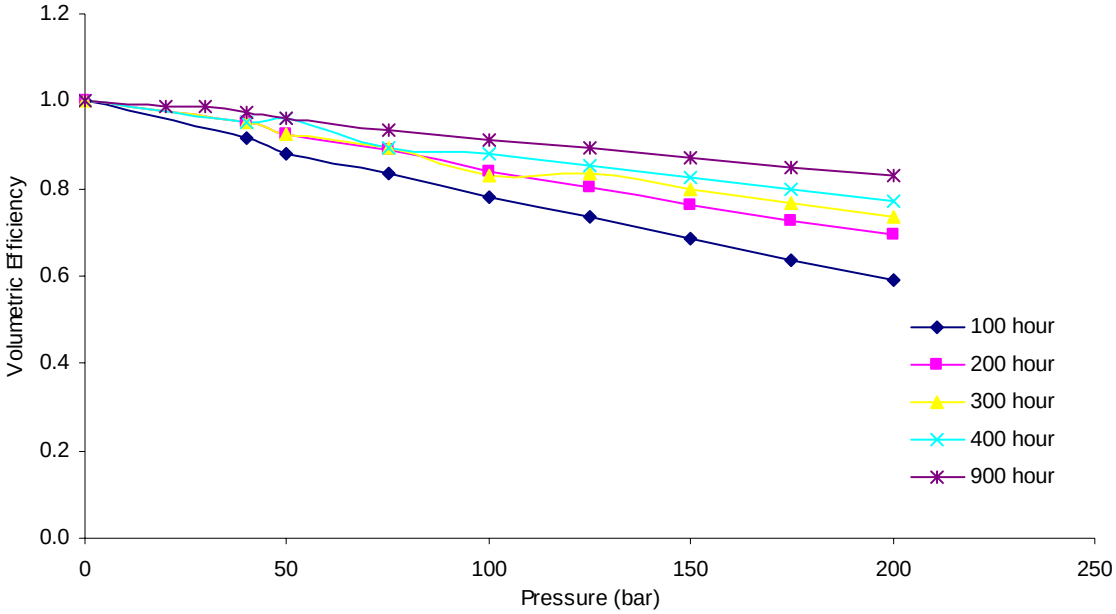

Figure 4.76: Volumetric efficiency against pressure at respective interval of time.

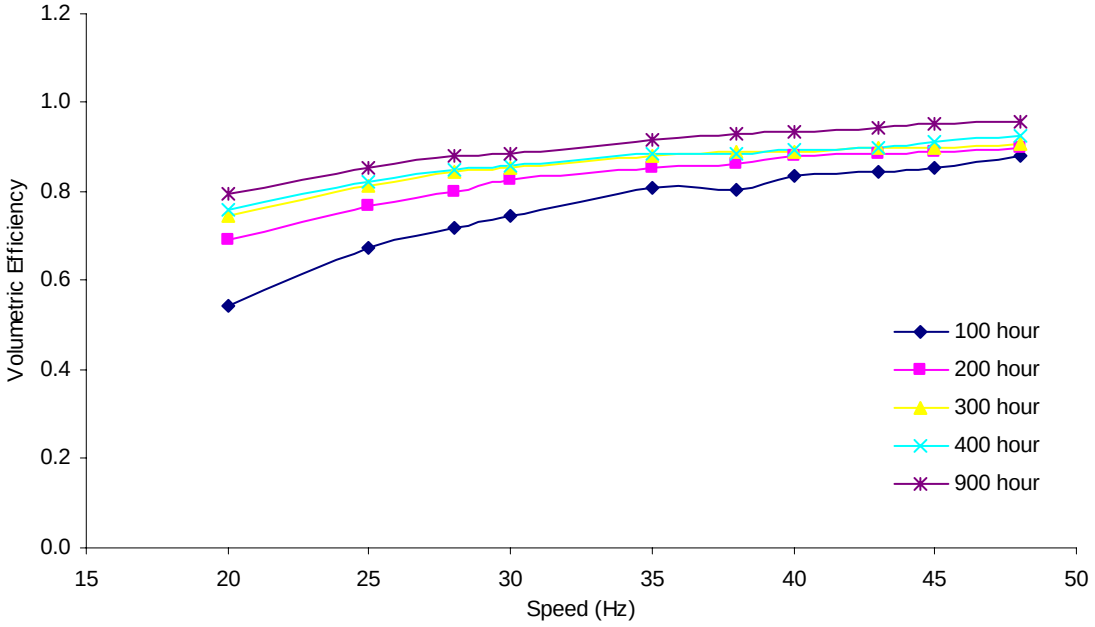

Figure 4.77: Volumetric efficiency against speed at respective interval of time.

Oil ageing was analyzed using IR. Figure 4.78 shows the infrared spectra of oil sampled at 0, 100, 400 and 900 hours. The infrared spectra obtained shows that the palm oil undergone degradation after being sheared at 70 bar and 70^{o}C. Important observation from this figure is that the peak area at 3473 cm^{-1} increases as the oil

degraded from 0 hour to 900 hour. Similar results were obtained by Sraj and Vizintin (2000) who analyzed oil sample from laboratory hydraulic systems and dredger, and they found that the oxidation products only slightly influenced the physical properties of the oil.

According to Guillen and Gabo (2000), the frequency of C-H stretching (C=C-H) at around 3006 cm^{-1} of oxidized oil slowly shifted toward smaller wavenumber. The spectra shows that C-H stretching shifted from 3005.89 cm^{-1} (0 hour) to 3004.69 cm^{-1} (900 hour).

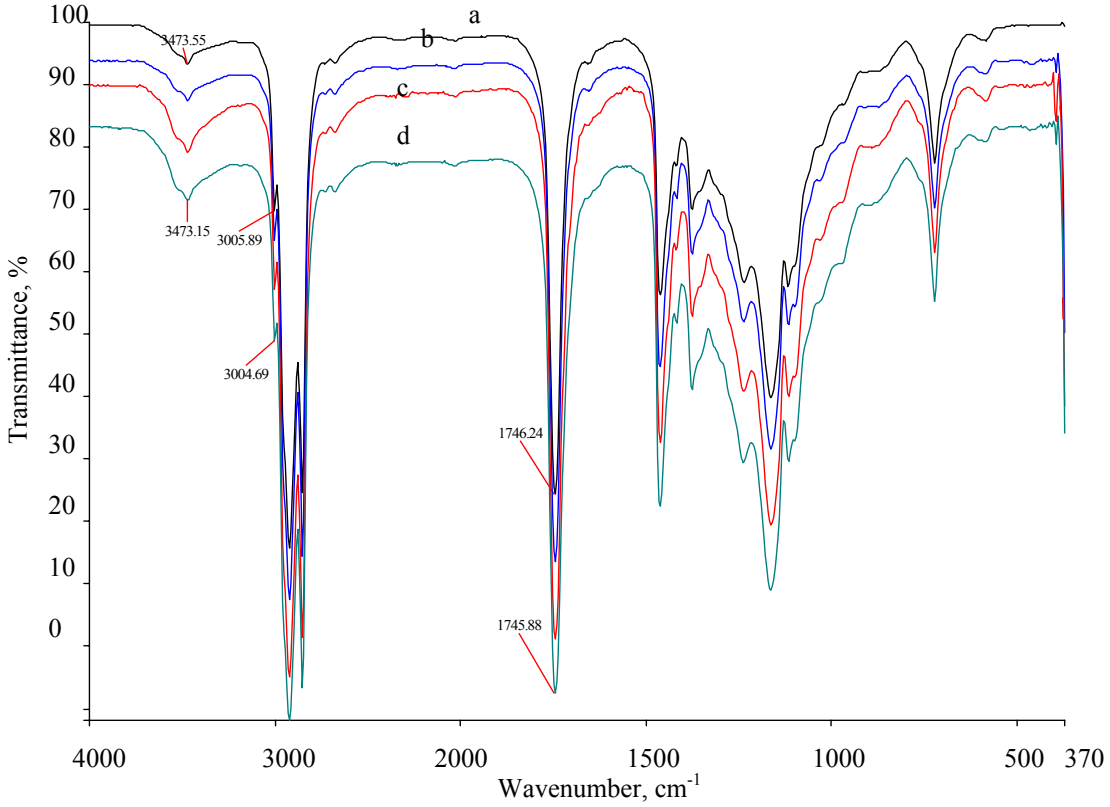

Figure 4.78: Infrared spectra of oil from test rig running intermittently at 70 bar 70°C sampled at (a) 0, (b) 100, (c) 400 and (d) 900 hour.

4.8.8 Modeling Study

4.8.8.1 Comparison of Experimental and Predicted Performance

The data was acquired and the results were calculated manually (Sections 4.8.8.1 and 4.8.8.2). Then performance of hydraulic test rig was evaluated manually. Thus, unlike Sections 4.7 and 4.8.1-4.8.7, only limited data is available in Section 4.8.8. Figure 4.79 shows the result of volumetric efficiency versus pressure. The reduction in volumetric efficiency is not at constant rate. The efficiency decreases at low rate in low pressure region, then at higher rate at higher pressure region. Similar pattern was also reported by Cheng *et al*. (1994) who studied performance of biodegradable hydraulic fluid using Rexroth piston pump system. Unlike the result in Sections 4.8.1-4.8.7, the larger drop in volumetric efficiency when pressure is increased (Figure 4.79) can be attributed to the compressibility of the fluid. The reduction in volumetric efficiency with increase in pressure is in accordance to Equation 2.38b. In-depth study in Section 4.9 does not show the increase in flow slip coefficient with increase in pressure. Thus, according to Equation 2.38b, the large volumetric efficiency drop is possibly due to compressibility effect which is influenced by the oil compressibility and foaming properties.

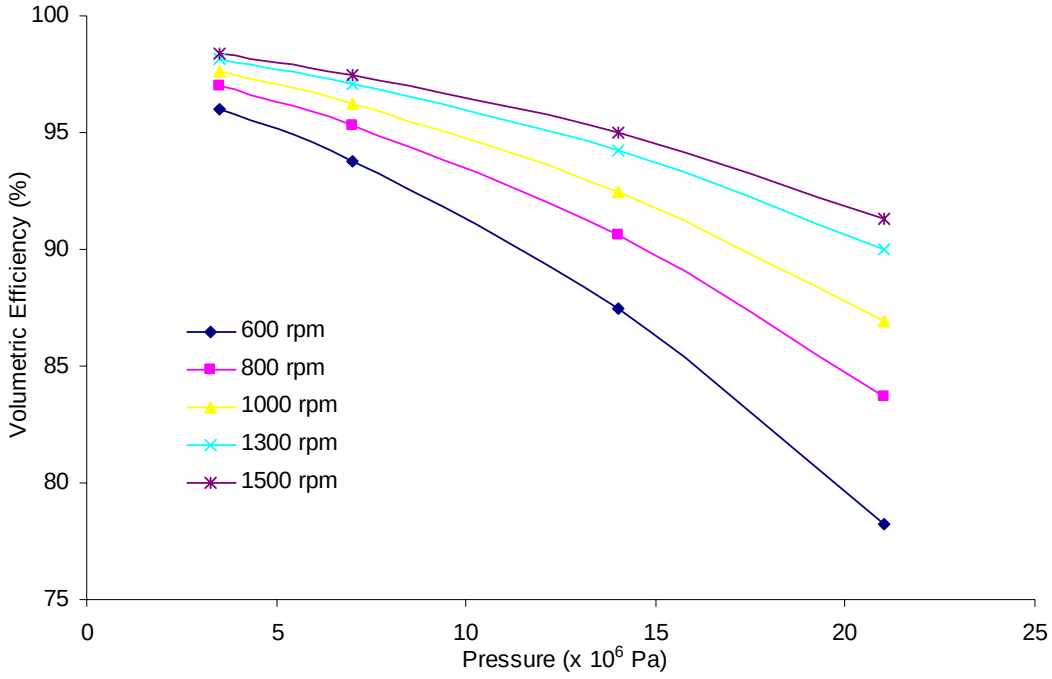

Figure 4.79: Volumetric efficiency versus pressure - experimental data.

Flow slip coefficient, C_s, was calculated for each pressure case using Equation 2.38b. Compressibility effect was neglected. Table 4.27 shows the value for C_s for 1500 rpm case as modeled by Equation 2.38b. The value for C_s obtained from the slope of Figure 4.79 is also shown.

Table 4.27: Data for Equation 2.38b model (1500 rpm case)

Pressure (Pa)	η_{vp} Actual	η_{vp} Predicted	Diff.	C_s (i)*	C_s (slope)**
$3.5x10^6$	98.4	98.4	0.0	$8.45x10^{-9}$	$3.43x10^{-9}$
$7.1x10^6$	97.5	97.4	0.1	$6.60x10^{-9}$	$5.52x10^{-9}$
$1.4x10^7$	95.1	93.9	1.2	$6.46x10^{-9}$	$8.01x10^{-9}$
$2.1x10^7$	91.2	87.6	3.6	$7.74x10^{-9}$	$1.09x10^{-8}$

* C_s (i) was calculated from Equation 2.38b model for each respective pressure.

** C_s (slope) was obtained through the slope measured at each pressure point.

μ @ 70ºC = 0.012 Pa.s

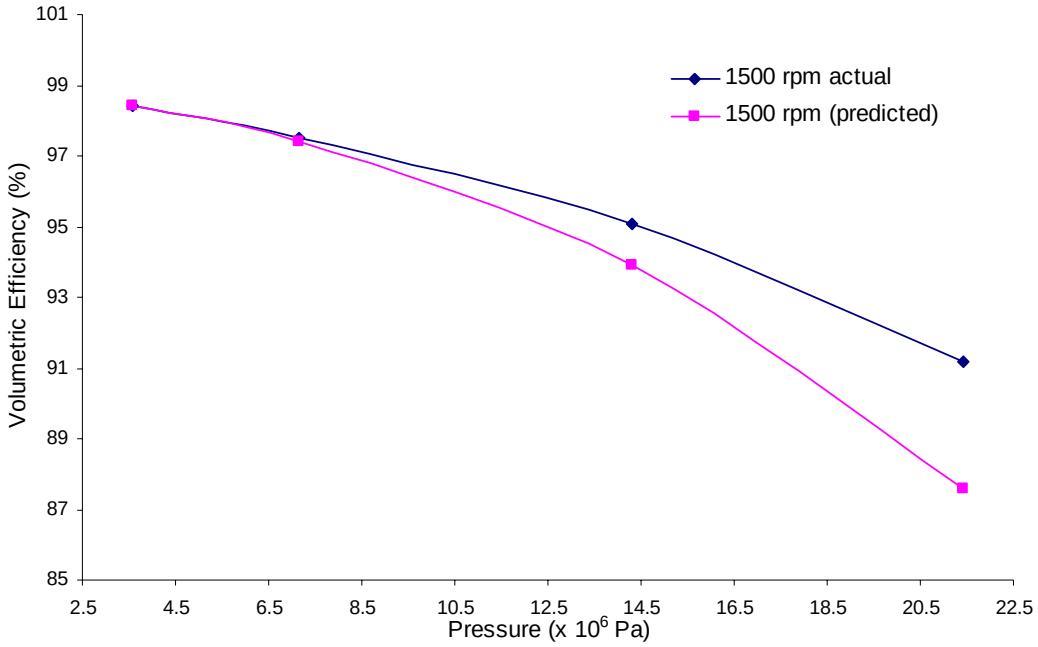

Figure 4.80: Actual and predicted volumetric efficiency modeled using Equation 2.38b.

Using the calculated C_s as $8.45x10^{-9}$, the volumetric efficiency was recalculated for 1500 rpm operation. Actual and predicted efficiencies are plotted on the same graph from $3.5x10^6$ to $21.0x10^6$ Pa. Figure 4.80 shows the actual and

predicted volumetric efficiency when running the system at 1500 rpm. The predicted volumetric efficiency agrees well with the real data at 35 bar. However, as the pressure increases, the deviation becomes larger. The predicted efficiency is always lower than the experimental efficiency. This study shows that the slip coefficient varies with pressure. If the low pressure data is used to simulate higher pressure conditions, some errors will be introduced.

The second attempt was to use Schlosser's model (Table 4.28). Based on actual volumetric efficiency, flow slip and turbulent slip coefficients of Schlosser's model were determined. Pump speed and oil viscosity as in the previous case were considered. Values calculated using simultaneous equation based on data (a) and (b) of Table 4.28 are:

Flow slip coefficient, $C_s = 2.12\text{x}10^{-9}$

Turbulent slip coefficient, $C_{st} = 6.58\text{x}10^{-5}$.

Table 4.28: Data for and result from Schlosser's model

Data	Pressure (Pa)	η_{vp} Actual	η_{vp} Predicted	Diff.
a	$3.5\text{x}10^{6}$	98.4	98.4	0.0
b	$7.1\text{x}10^{6}$	97.5	97.5	0.0
c	$1.4\text{x}10^{7}$	95.1	96.0	-0.9
d	$2.1\text{x}10^{7}$	91.2	94.7	-3.5

Using the calculated slip and turbulent slip coefficients, the predicted volumetric efficiencies for case c and d were calculated and plotted in Figure 4.81. Unlike the result in Figure 4.80, the predicted volumetric efficiency calculated using Schlosser's model yield almost a linear relationship between volumetric efficiency and pressure. The predicted efficiency is always greater than the experimental efficiency. This model yields the same volumetric efficiency for the two lowest pressure cases. In addition to that, this model also yields lower error for higher pressure cases.

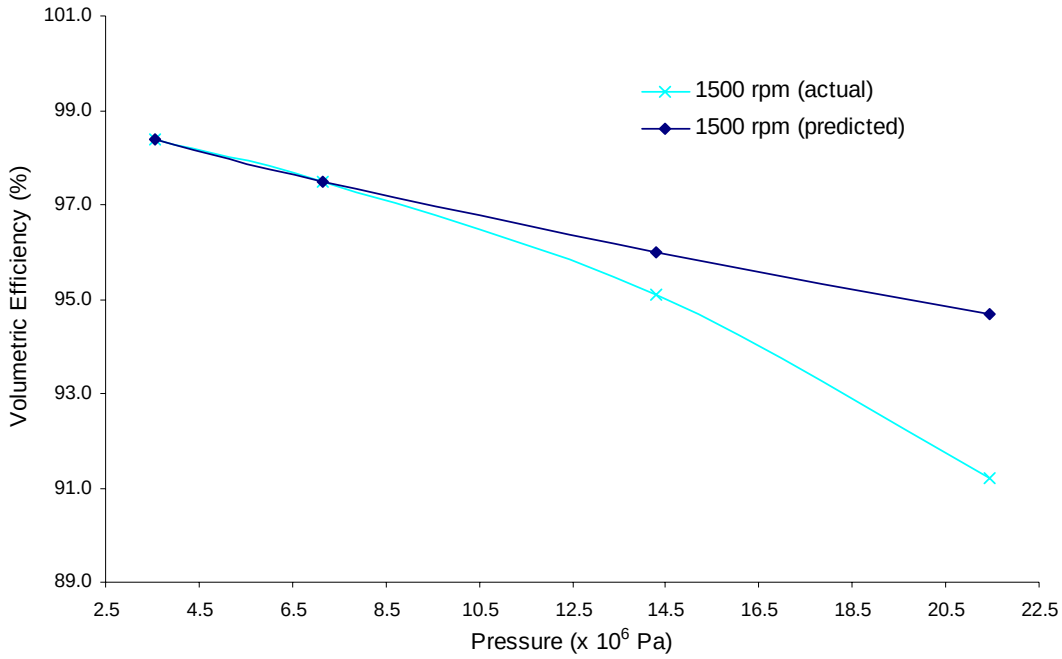

Figure 4.81: Actual and predicted volumetric efficiency modeled using Schlosser's model.

The next effort was to model the mechanical efficiency. Equation 2.39b was used to calculate friction coefficients. Using these coefficients, predicted mechanical efficiency for other pressures was calculated. Table 4.29 compares the predicted and calculated mechanical efficiencies for 1200 rpm case.

Table 4.29: Data for calculating predicted mechanical efficiency (1200 rpm case)

Pressure (Pa)	Actual mech. eff.	Predicted mech. eff.
$3.5x10^6$	78.5	78.5
$7.1x10^6$	83.8	83.8
$1.4x10^7$	85.8	86.4
$2.1x10^7$	85.4	87.4

Based on 35 bar and 70 bar cases, it was calculated that the C_c and C_v (Equation 2.39b) were found to be 6.02 and $2.98x10^5$, respectively. The model and actual mechanical efficiencies were plotted as in Figure 4.82. Using the C_c and C_v of 6.02 and $2.98x10^5$, respectively, the predicted mechanical efficiency was calculated for 600, 800, 1000, 1300 and 1500 rpm cases. The results are tabulated in Table 4.30.

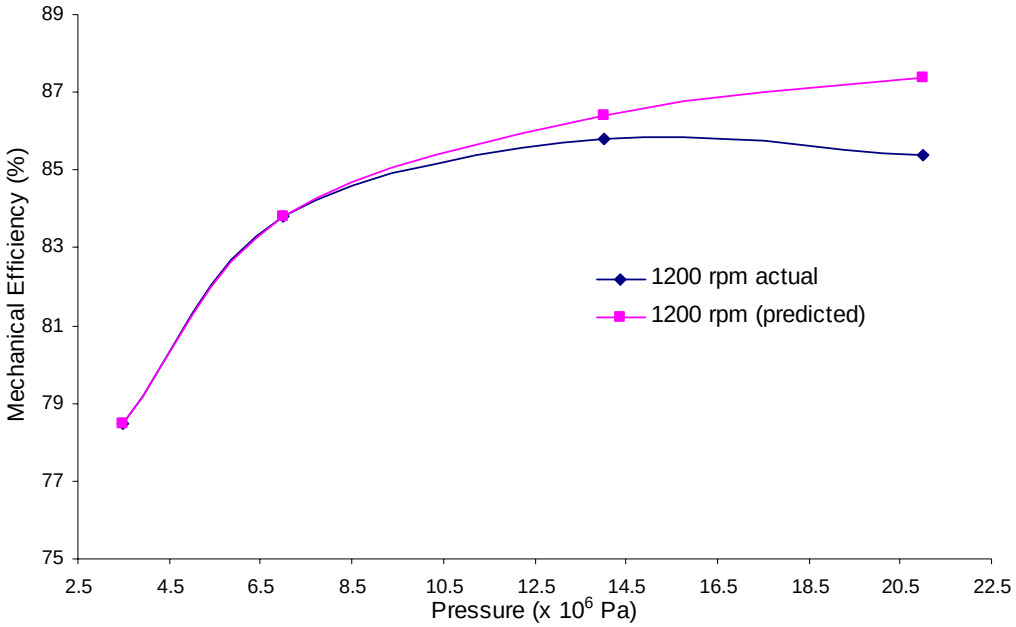

Figure 4.82: Actual and predicted mechanical efficiency modeled by Equation 2.39b.

Table 4.30: Predicted mechanical efficiency for different speed cases

Pressure (Pa)	600 rpm	800 rpm	1000 rpm	1300 rpm	1500 rpm
$3.5x10^6$	83.5	78.5	78.5	78.5	78.5
$7.1x10^6$	86.4	83.8	83.8	83.8	83.8
$1.4x10^7$	98.4	85.8	85.8	85.8	85.8
$2.1x10^7$	88.4	85.4	85.4	85.4	85.4

4.8.8.2 Constant and Variable Coefficient Linear Models

Basically the discussion in this modeling section is based on discrete testing result. In discrete testing, flow rate from four maximum and minimum pressure and speed combinations were measured. This minimum test data was used in determining predicted flow slip coefficient and system performance when the hydraulic system had undergone several hundred hours of operation.

Table 4.31 shows flow rate measured at four different conditions from discrete test. As expected the flow rate for 1440 rpm was higher than of 750 rpm. For the same speed, flow rate for higher pressure case was reduced. Predicted flow slip

coefficient was then calculated based on constant coefficient linear model and variable coefficient linear model as proposed by McCandlish and Dorey (1984).

Table 4.31: Speed, pressure and flow rate from discrete test

Test	Speed (rpm)	Pressure (bar)	Flow rate (m^3/s)
A	1440	35	$1.83x10^{-4}$
B	1440	200	$1.37x10^{-4}$
C	750	35	$8.22x10^{-5}$
D	750	200	$2.04x10^{-5}$

$$C_{sAB} = \frac{(Q_A - Q_B)}{(P_B - P_A)} \quad (\mu/D)$$
$$= 3.244x10^{-8}$$

$$C_{sCD} = \frac{(Q_C - Q_D)}{(P_D - P_C)} \quad (\mu/D)$$
$$= 4.413x10^{-8}$$

$$C_s = \frac{C_{sAB} + C_{sCD}}{2}$$
$$= 3.828x10^{-8}$$

From the above analysis, based on ratio of flow difference and pressure difference between 200 and 35 bar cases, flow slip coefficient at high and low speed were calculated as $3.244x10^{-8}$ and $4.413x10^{-8}$, respectively. The average slip coefficient for all four cases was calculated as $3.828x10^{-8}$.

Based on slip coefficients already calculated using constant coefficient linear model, slip coefficients for other speeds were calculated by means of variable coefficient linear model. Linear interpolation was performed to determine flow coefficients at 1200 rpm and 900 rpm operation. The coefficient was calculated as a function of speed by:

$$C_{s\omega} = C_{sAB} + (C_{sCD} - C_{sAB}) \frac{(w - w_A)}{(w_C - w_A)}$$

where w is the speed of interest and w_A and w_B are the speeds for test A and B, respectively (Table 4.31). From the above analysis, the interpolation step yields the

slip coefficient for 1200 rpm and 900 rpm cases as 3.651×10^{-8} and 4.159×10^{-8}, respectively.

Table 4.32 shows the comparison of predicted slip coefficients obtained using combination of constant coefficient linear model and variable coefficient linear model with actual slip coefficients obtained from test rig. The values were quite close to each other for 1439, 1200 and 900 rpm cases. This shows that the models fit to the actual experimental data. For the 600 rpm case, the error is 5.4%. This can be attributed to the smaller speed range when the constant coefficient linear model was performed. Furthermore, the variable coefficient model assumed a linear relationship between the slip coefficient and speed, while in the actual case it was found that the slip coefficient decreases at increasing rate with speed.

Table 4.32: Comparison between predicted and actual slip coefficients for four different speeds

Speed (rpm)	Predicted coefficient	Experimental coefficient
	C_s (x 10^{-7})	C_s (x 10^{-7})
1440	0.3244	0.3204
1200	0.3651	0.3698
900	0.4159	0.4139
600	0.4667	0.4428

Using the experimental flow slip coefficient for 1440 rpm 70^{o}C case as 0.3204×10^{-7}, the volumetric efficiency for ageing operation was predicted. The viscosity of 0.024 and 0.030 Pa.s were used to simulate the performance for 200 and 400 hour cases, respectively. The predicted variation of volumetric efficiency with pressure for both cases is shown in Figure 4.83.

From Figure 4.83, it is clearly shown that the actual performance is less than the predicted ones. The reduced efficiencies for aged condition indicate that the slip coefficient has increased with test rig operation time (as shown in Section 4.9.5). Theoretically the flow slip coefficient is related to internal and external leakage. However, there was no external leakage detected throughout the experiment. As discussed in Section 4.10.1, it was found out that the sliding action between vane and cam ring in the pump resulted in vane weight loss at a rate of 0.0462 mg/100 hour operation. The weight loss indicates the existence of wear. Even the weight loss was

very small, it can contribute to some internal leakage since the system was operated at 1440 rpm. The efficiency for 400 hour is higher than 200 hour due to the increased in viscosity (Equation 2.38b).

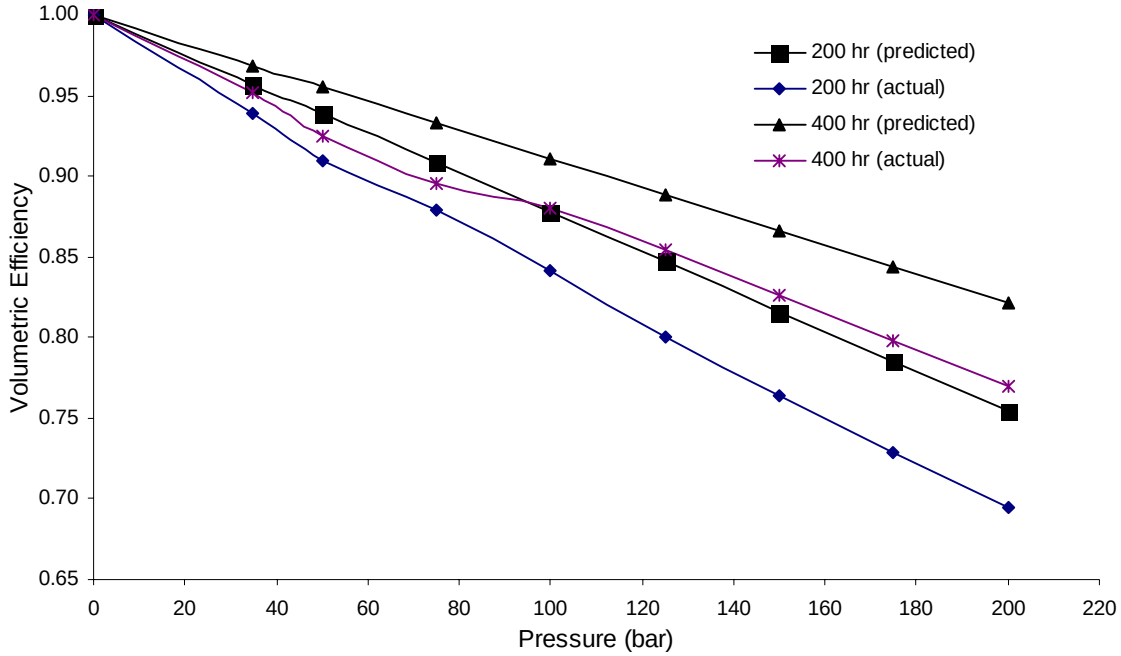

Figure 4.83: Variation of predicted and experimental volumetric efficiency with pressure.

4.9 Dimensionless Parameter Study

In many of the hydraulic models dealing with efficiencies, the parameters viscosity, speed and pressure play important role (Section 2.8). For this reason, it is of great interest to show the efficiencies with respect to these parameters. In Fluid Mechanic study, a technique which has proven very useful in reducing to a minimum number of experiments required is known as dimensional analysis (Massey, 1997).

Thus in this study parameters viscosity, speed and pressure were lumped together, with the effect of units were taken into account. Volumetric, mechanical and overall efficiencies of the hydraulic system as function of dimensionless parameters were calculated and the relationship between efficiencies and dimensionless parameters were studied.

Information extracted from the resultant figures in Appendix F is used to determine various coefficients given important parameters such as oil viscosity or temperature, pump speed and operating pressure. On the other hand, efficiencies can be determined if the coefficients are known. This method can minimize the time in determining the system efficiencies or parameter coefficients.

The hydraulic system was operated at 1200 rpm and the circulated palm oil temperature was maintained at 40^{o}C with the help of a heat exchanger. Pressure was increased from 35 bar to 200 bar. Volumetric, mechanical and overall efficiencies were calculated. Viscosity, speed and pressure were grouped together to yield a dimensionless parameter. The calculated result with respect to pressure is tabled in Table 4.33 and plotted in Figure 4.84.

In another test, the system was operated at 75 bar and the oil temperature was maintained at 40^{o}C. The varying operating condition was the pump speed. The pump speed was increased from 600 to 1440 rpm. Detailed information was tabled in Table 4.34 and plotted in Figure 4.85. Comparing Figure 4.84 and Figure 4.85, a slight variation of efficiency pattern was observed. Similar tests were conducted with some parameters maintained while other parameters changing.

Table 4.33: Efficiencies and dimensionless parameter running at 1200 rpm and varying pressures

Speed (Hz)	Pressure (bar)	Volumetric Eff.	Mechanical Eff.	Overall Eff.	$\mu W_p/P_p$ x10^{-7}
40	35	0.968	0.664	0.655	13.28
	50	0.945	0.761	0.733	9.30
	75	0.914	0.777	0.725	6.20
	100	0.893	0.803	0.731	4.65
	125	0.870	0.790	0.701	3.72
	150	0.846	0.857	0.739	3.10
	175	0.821	0.844	0.706	2.66
	200	0.800	0.845	0.689	2.32

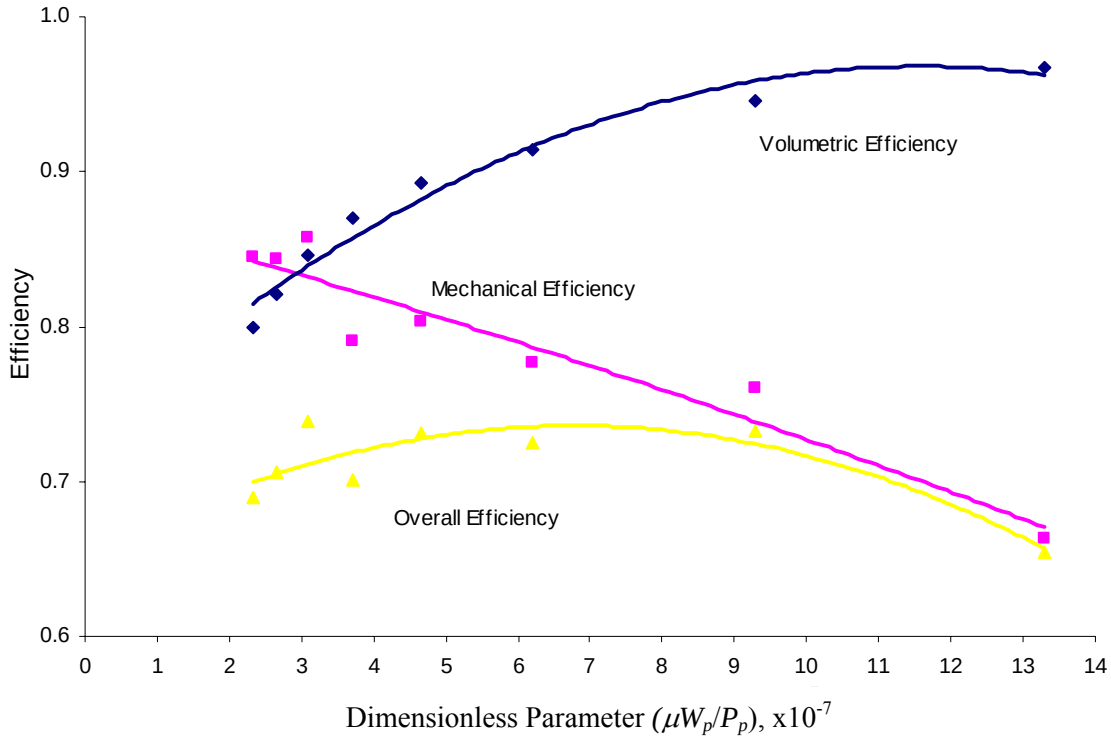

Figure 4.84: Efficiencies and dimensionless parameter running at 1200 rpm, 40°C and varying pressures.

Table 4.34: Efficiencies and dimensionless parameter running at 75 bar and varying speeds

Pressure (bar)	Speed (rpm)	Volumetric Eff.	Mechanical Eff.	Overall Eff.	$\mu W_p/P_p$ x10^{-7}
75	1440	0.936	0.795	0.759	7.44
	1350	0.929	0.781	0.739	6.97
	1290	0.921	0.797	0.748	6.66
	1200	0.914	0.777	0.725	6.20
	1140	0.905	0.752	0.694	5.89
	1050	0.896	0.752	0.687	5.42
	900	0.865	0.794	0.701	4.65
	840	0.854	0.764	0.666	4.34
	750	0.834	0.792	0.674	3.87
	600	0.779	0.777	0.617	3.10

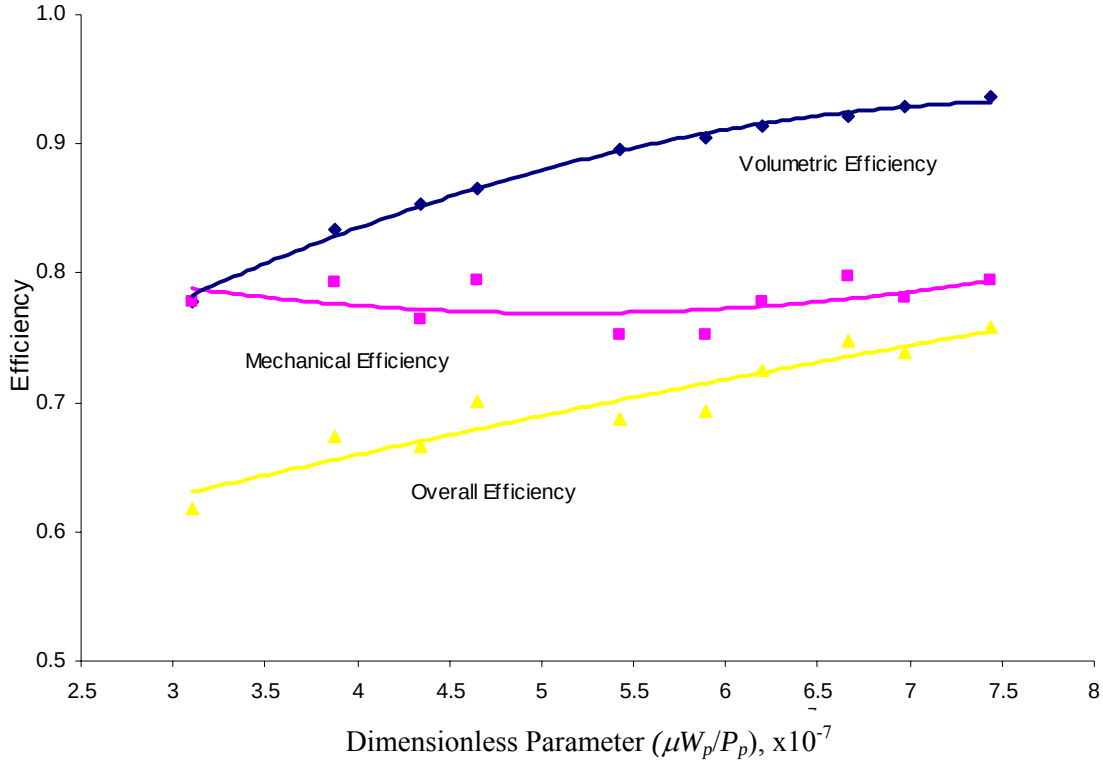

Figure 4.85: Efficiencies and dimensionless parameter running at 75 bar, 40°C and varying speeds.

4.9.1 Flow Slip Coefficient

Volumetric efficiency as shown in Equation 2.38b can be written as Equation 4.9 when the compressibility effect is ignored,

$$\eta_{vp} = 1 - C_s \frac{P_p}{2\pi\mu W_p}. \qquad 4.9$$

This equation is analogous to y=mx +C equation. If η_{vp} is proportional to $\frac{P_p}{2\pi\mu W_p}$, then the slope represents the C_s.

A test at 75 bar with varying speeds was conducted at palm oil temperature of 40°C, 50°C and 60°C. Then volumetric efficiency versus dimensionless parameter $P_p/\mu W_p$ was plotted (Figure 4.86). The graph shows that the volumetric efficiency varies linearly with the dimensionless parameter with different sloping for different temperature cases. Based on Equation 4.9, the slip coefficients were obtained. The

C_ss for 40°C, 50°C and 60°C cases were calculated as 0.8359×10^{-8}, 0.6533×10^{-8} and 0.6144×10^{-8}, respectively.

The experiment was then repeated at same running speed but varying pressure. Volumetric efficiency versus dimensionless parameter $P_p/\mu W_p$ was plotted as in Figure 4.87. From the slopes, the C_ss for 40°C, 50°C and 60°C cases were 0.4628×10^{-8}, 0.4104×10^{-8} and 0.3938×10^{-8}, respectively. Based on these two cases, it can be concluded that the slip coefficient for the test rig is decreasing with increasing temperature. The comparison shows that the influence of speed is greater than the influence of pressure on slip coefficient change. This supports the results in Sections 4.8.2 and 4.8.4.

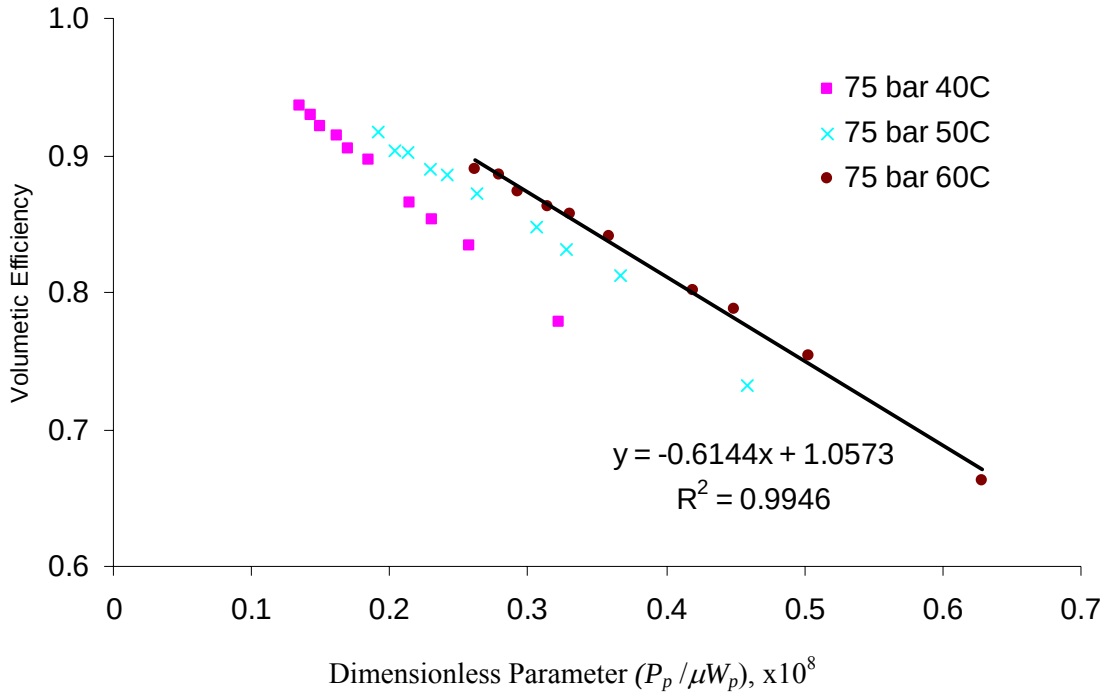

Figure 4.86: Volumetric efficiency versus dimensionless parameter – constant pressure.

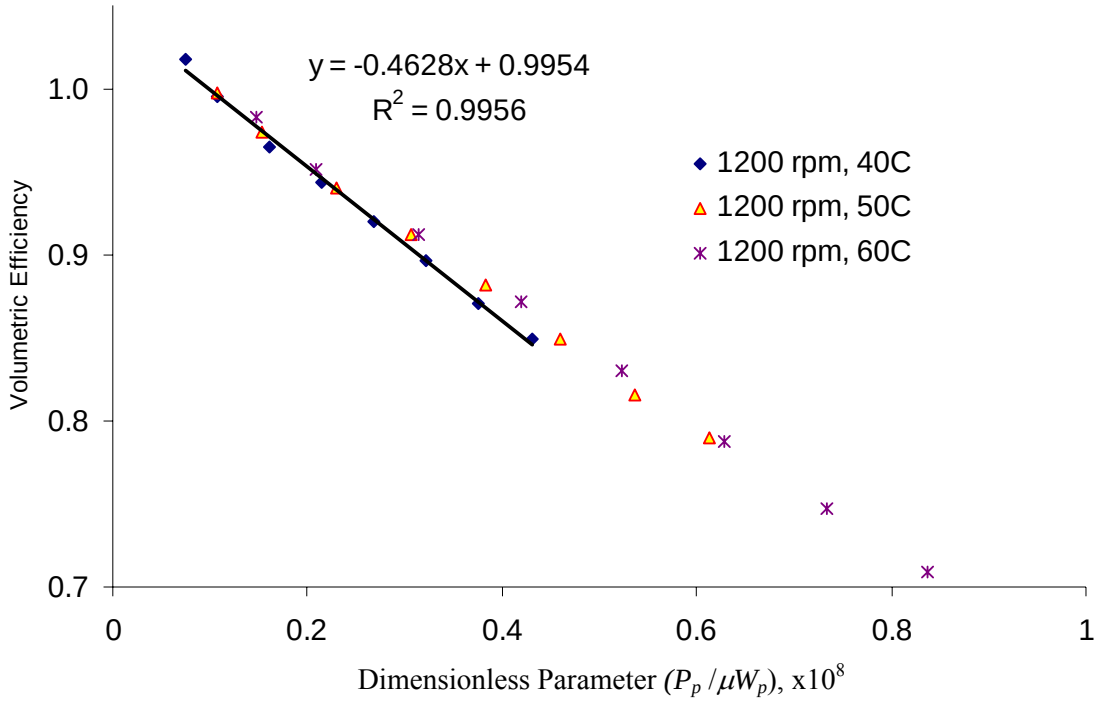

Figure 4.87: Volumetric efficiency versus dimensionless parameter – constant speed.

4.9.2 Coulomb Friction Coefficient

Dividing both numerator and denumerator of Equation 2.39b by pressure term and change to convenient units, Equation 2.39b can be written as

$$\eta_{mp} = \frac{1}{1 + C_c + C_v \mu W_p / P_p}. \qquad 4.10$$

Graph of mechanical efficiency versus dimensionless parameter $\mu W_p/P_p$ was plotted as in Figure 4.88 for 1200 rpm and 60°C case.

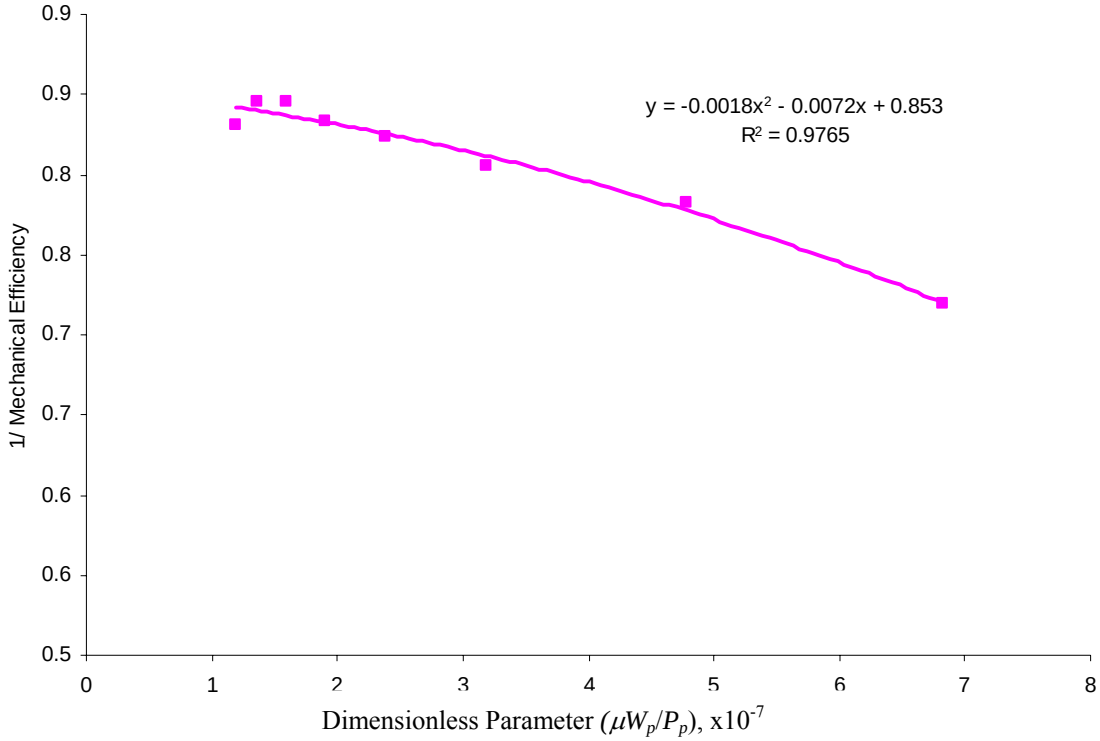

Figure 4.88: Mechanical efficiency versus dimensionless parameter – 1200 rpm and 60°C.

When the dimensionless parameter reduces to zero, the value for mechanical efficiency is 85.3%. Referring to Equation 4.10, dimensionless parameter reduces to zero means that

$$\eta_{mp} = \frac{1}{1 + C_c}. \qquad 4.11$$

Equating this reduced equation to value 0.853, the coulomb friction coefficient is calculated as 0.1723. This result compares well with the result of the gear pump of McCandlish (1984). This coulomb or load dependent friction is proportional to load.

4.9.3 Viscous Friction Coefficient

Equation 2.39b can also be written as

$$\frac{1}{\eta_{mp}} = \frac{P_p + C_c P + C_v \mu W_p}{P_p}. \qquad 4.12$$

Dividing the numerator and denumerator with pressure term, it can be simplified as

$$\frac{1}{\eta_{mp}} = (1 + C_c) + C_v \mu W_p / P_p . \qquad 4.13$$

The viscous coefficient can be obtained from the slope of $1/\eta_{mp}$ versus $\mu W_p/P_p$ graph. In order to determine the viscous friction coefficient, a test was conducted at 40°C. Speed of the pump was maintained at 1440 rpm. Pressure was varied from 35 bar to 210 bar. Actual torque was recorded and theoretical torque was calculated. Then the test was determined for 1200, 900 and 600 rpm cases.

From graph in Figure 4.89 and referring to Equation 4.13, the viscous friction coefficient for 1440, 1200, 900 and 600 rpm cases was determined as 2.37×10^5, 2.73×10^5, 3.21×10^5 and 3.47×10^5, respectively. The C_v as conducted on gear pump at 1500 rpm was 2.05×10^5 (McCandlish, 1984).

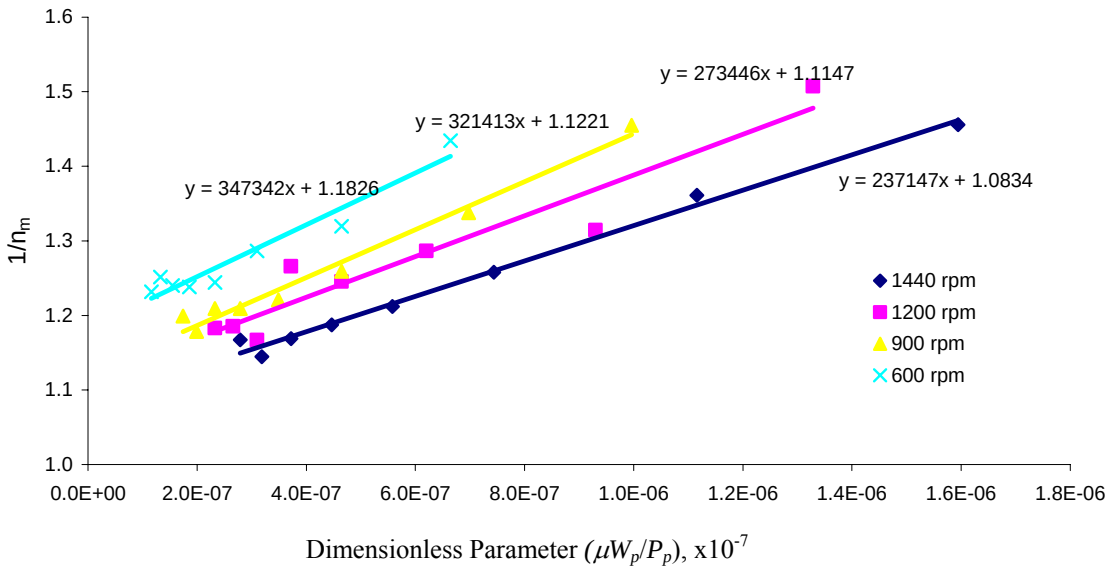

Figure 4.89: Determination of viscous coefficient.

4.9.4 Dimensionless Parameter Study for 100 hour case

Extensive tests were conducted to investigate of how the hydraulic system built performs after it was running on palm oil for 100 hours. Sections 4.9.1 – 4.9.3 show an example of how flow slip, coulomb and viscous friction coefficients were determined. Appendix F provides some of the graphs used in determining the coefficients. The results for 100 hour case are summarized in Table 4.35. The table depicts the effect of various operating conditions of hydraulic system running on palm oil on the flow slip, coulomb friction and viscous friction coefficients.

Based on results presented in the Table 4.35 it can be deduced and summarized that:

a. As the temperature increases, flow slip coefficient increases.
b. There is no clear relationship can be made between coulomb friction coefficient and temperature.
c. As pressure increases, flow slip coefficient decreases.
d. As speed decreases, viscous friction coefficient increases.
e. As speed increases, coulomb friction decreases.

Running the system at 1200 rpm and the test conducted at various increasing temperature (Table 4.35a) results in increasing slip coefficient (summary a). This can be easily explained by viscometric property of the palm oil. When temperature increases, viscosity decreases (discussed in Section 4.2). This will induce more fluid slippage through hydraulic component cleavage. If the hydraulic system uses petroleum based oil, the slip coefficient will increase at higher rate due to its lower viscosity index.

From observation d above, it can be said that viscous friction coefficient is a speed-dependent parameter. Thus viscous friction is affected by fluid rheology and speed of fluid flow. However, pressure effect on viscous friction is not very clear. It is expected that there is indirect interrelation effect of pressure, fluid rheology and speed.

Table 4.35: Summary of coefficient values for 100 hour interval

a) At constant speed 1200 rpm

Temperature (ºC)	C_s X10^{-8}	C_c	C_v
40	0.4628	0.1457	264812
50	0.4104	0.1119	713792
60	0.3938	0.1723	361866
70	0.3698	0.1660	156152

b) At temperature 40ºC

Speed (rpm)	C_s X10^{-8}	C_c	C_v
1440	0.4743	0.0839	232854
1200	0.4628	0.1457	264812
900	0.4425	0.1545	323887
600	0.4276	0.2291	428699

c) At temperature 50ºC

Speed (rpm)	C_s X10^{-8}	C_c	C_v
1440	0.4153	0.1091	541752
1200	0.4104	0.1119	713792
900	0.4034	0.1700	724889
600	0.4882	0.2614	949668

d) At temperature 60ºC

Speed (rpm)	C_s X10^{-8}	C_c	C_v
1440	0.3735	0.1220	245602
1200	0.3938	0.1723	361866
900	0.4038	0.1686	269161
600	0.4991	0.3151	

e) At temperature 70ºC

Speed (rpm)	C_s X10^{-8}	C_c	C_v
1440	0.3204	0.1464	388460
1200	0.3698	0.1660	156152
900	0.4139	0.1823	70086
600	0.4428	0.2557	

f) At constant pressure 75 bar

Temperature (ºC)	C_s X10^{-8}	C_c	C_v
40	0.8359	0.1213	
50	0.6533	0.2064	249131
60	0.6144	0.1755	
70	0.6966	0.3755	

g) At temperature 40ºC

Pressure (bar)	C_s X10^{-8}	C_c	C_v
35	1.3997	0.0129	82282
75	0.8359	0.1213	
125	0.6964	0.1659	
200	0.5666	0.2341	

h) At temperature 50ºC

Pressure (bar)	C_s X10^{-8}	C_c	C_v
35	0.9333	0.4286	162543
75	0.6533	0.2064	249131
125	0.6136	0.2968	
200	0.5930	0.2599	

i) At temperature 60ºC

Pressure (bar)	C_s X10^{-8}	C_c	C_v
35	0.7874	0.9161	
75	0.6144	0.1755	
125	0.5579	0.2989	
200	0.5373	0.0398	

j) At temperature 70ºC

Pressure (bar)	C_s X10^{-8}	C_c	C_v
35	0.7968	0.0570	359651
75	0.6966	0.3765	
125	0.6480		
200	0.6117	0.7123	

There is a contradict observation between result in Table 4.35b and 4.35e. Flow slip coefficient decreases in case of running the system at various speeds while maintaining the palm oil temperature at 40^{o}C. On the other hand, the table shows that the flow slip coefficient constantly decreases as the test was conducted at increasing

speed while maintaining palm oil temperature at 70^{o}C. Based on literature report, no other researcher has studied this aspect. This experimental results show that temperature has significant influence on flow slip coefficient. This maybe due to the fact that temperature affects the oil viscosity and also expansion of metal. Both the viscosity and metal expansion affect the leakage flow.

4.9.5 Effect of Ageing Time on Flow and Friction Coefficients

Table 4.36 summarizes the coefficient values determined when the hydraulic system had been operating on palm oil for 100, 200, 300, 400 and 900 hour. The detailed information can be obtained from Appendix F.

Table 4.36: Summary of coefficients values against operating hour

Duration (hour) Temperature 70ºC	100	200	300	400	900
			Slip Coefficient, C_s		
Speed (Hz)					
48	0.3204	0.4308	0.4889	0.4009	0.5527
40	0.3698	0.4373	0.4379	0.4451	0.5073
30	0.4139	0.4453	0.4365	0.4502	0.5186
20	0.4428	0.5357	0.5449	0.5750	0.5490
Pressure (bar)					
35 (30)	0.7968	0.9941	0.9220	1.3258	1.5911
75 (50)	0.6966	0.7103	0.6293	0.7337	1.2075
125 (100)	0.6480	0.6453	0.6410	0.7433	0.8616
200 (150)	0.6117	0.6242	0.6502	0.7490	0.7497
			Friction Coefficient, C_c		
Pressure (bar)					
35 (30)	0.0421	0.2410	0.2423	0.5270	0.4938
75 (50)	0.1824	0.1833	0.1795	0.2949	0.3590
125 (100)	0.1483	0.1830	0.2307	0.2669	0.2495
200 (150)	0.3553	0.2988	0.2710	0.3035	0.3172
			Viscous Coefficient, C_v		
Speed (Hz)					
48	284910	195724	239357	416755	289161
40	180441	167536	254147	457057	329483
30	-	366838	231882	509958	384121
20	-	101063	211802	726828	435348

* Pressure in bracket only applicable to 900 hour sample.

Figure 4.90 shows the variation of flow slip coefficient as calculated from 100, 200, 300, 400, 900 hour of 1200 rpm and 70^{o}C data. The figure shows that the coefficient increases with test rig running time, or as palm oil degrades. The increase of flow slip coefficient can be attributed to the wear and clearances of hydraulic component, which is studied in Section 4.10. On the other hand, coulomb friction and viscous friction coefficient show fluctuated values over time.

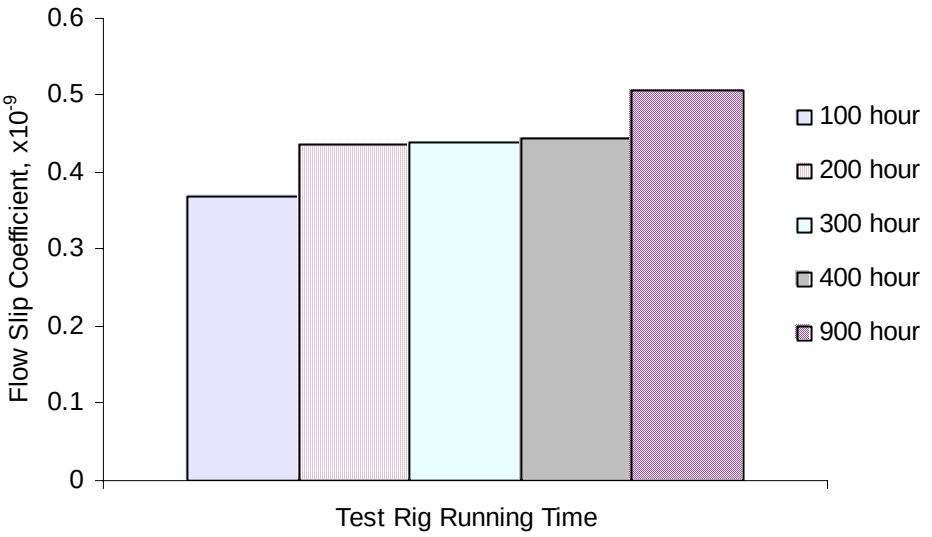

Figure 4.90: Variation of flow slip coefficient with test rig running time.

A check on the variation of flow slip coefficient with oil viscosity was made. As in bench test, the oil viscosity in hydraulic test rig also increased with test rig running time. Figure 4.91 indicates that as viscosity increases, flow slip coefficient also increases. Theoretically there is no direct relation between viscosity and flow slip coefficient (Equation 2.38b). However, as test rig running time increases viscosity also increases. One of the factors that influence the viscosity increase is the increase in contaminants level. This contaminants level can affect the components wear which in turn influence the flow slip coefficient.

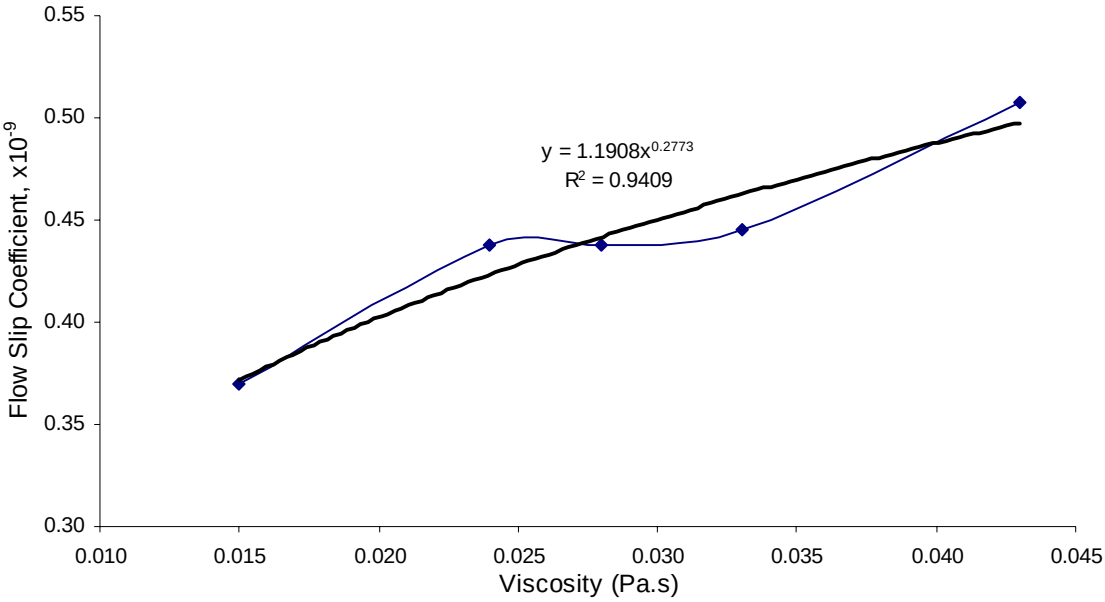

Figure 4.91: Variation of flow slip coefficient with oil viscosity.

4.10 Hydraulic Components Wear

The effect of lubricating capability of the palm oil was evaluated by considering the wear of moving and stationery components. In this study the concentration was on the vane pump which is the heart of hydraulic system. Prior to installation into hydraulic test rig, the pump was dismantled. The pump was again dismantled at 500 hours and at the end of operation period (900 hour). Figure 4.92 shows the picture of the dismantled pump at 900 hour.

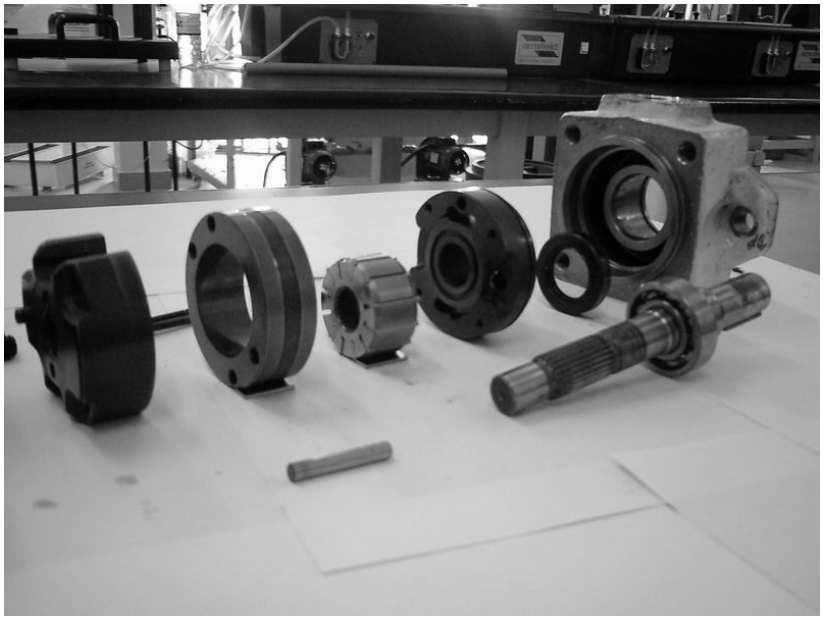

Figure 4.92: Appearance of vane pump dismantled at 900 hour.

The vane pump mechanical structures consist of a rotor with passages for the vanes to slide in and out. The rotor, which contains radial slots, is splined to the drive shaft and rotates inside a cam ring. Each slot contains a vane designed to mate with the surface of the cam ring as the rotor turns. The main pump components investigated was vane, cam ring, rotor and side bushing. The wear of the components was based on the weight loss, appearance of component surface and surface roughness.

4.10.1 Weight Loss

Throughout the pump operation, friction and collision between metal compartments and decrement in lubrication resulted in metal cavitation wear and erosion wear, especially on the vanes, cam ring, bushings and rotor. Sliding actions produced by two surfaces in relative motion are prime reason for critical wear areas. Referring to Figure 4.92, these types of interfaces in the vane pump are as follow:

- The contact between the vane tips and the cam ring.
- The contact between the vanes and rotor.
- The contact between the vanes, rotor and side bushings.

Weight loss of 12 vanes is shown in Figure 4.93. Under the operating condition of 500 hours, the vanes had been sliding against harder material, cam ring, for about 5650 km (the peripheral distance has been converted to equivalent linear distance). At high rotational speed of 1200 rpm, centrifugal force forces the vane towards cam ring. At high pressure chamber, the two materials maybe separated by a thin layer of palm oil. On the other hand, at suction chamber the vane may be rubbing hard on the inside of cam ring surface. As a result 0.12% of the vane had been worn. Another 0.01% wear occur during 500 - 900 hour.

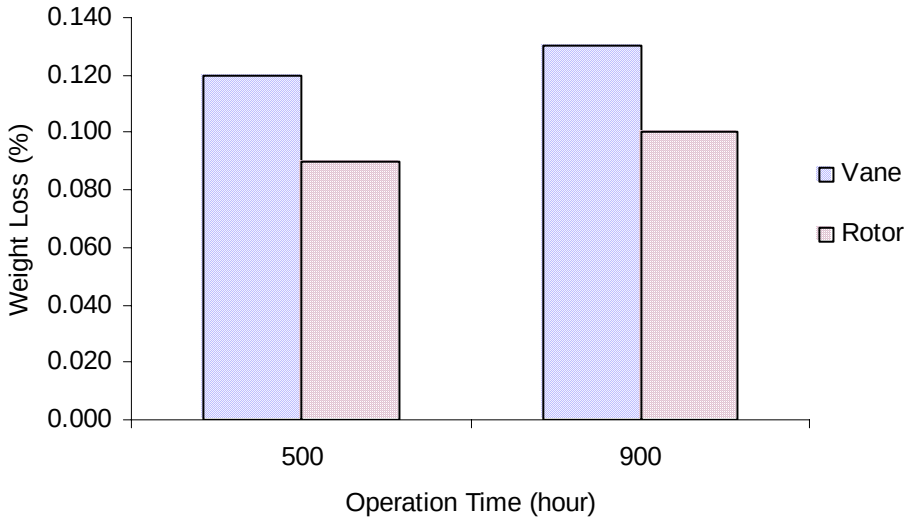

Figure 4.93: Weight loss of vane and rotor.

Surprisingly the rotor also experienced significant wear (Figure 4.93). However the amount of wear of rotor was less than that of vane. The wear might occur at the sliding surface with side bushings. The wear might also occur at the slots where the vane moving in and out.

Figure 4.94 shows the percentage weight loss of cam ring and bushing. Normally the major weight loss occurred at a vane pump are vane and cam ring. However, in this study the weight loss of cam ring was minimal. About 0.012% weight loss occurred during 0 - 500 hour period and further 0.003% loss occurred during 500 - 900 hour period. The figure also shows the percentage weight loss of bushing. Only about 0.004% weight loss occurred during 0 - 500 hours and no further weight loss measured during 500 - 900 hours operation.

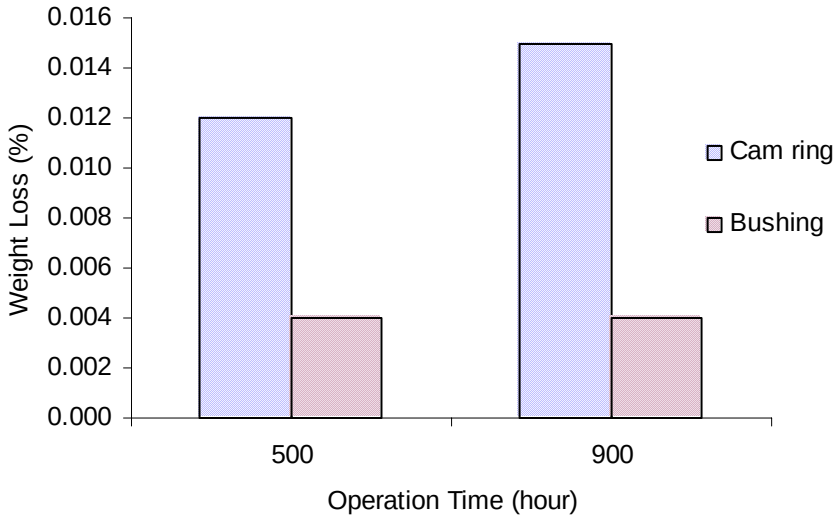

Figure 4.94: Weight loss of cam ring and bushing.

For the weight loss profile for vane, cam ring and rotor it is observed that most of the wear occurred during 0 - 500 hour period compared to 500 - 900 hour period. Thus it can be said that most of the wear occurred during running in period during the first several hundred hours. The highest loss occur to the vanes which slide against cam ring at equivalent sliding speed of up to 3.2 ms^{-1}. The wear may be attributed to impurities and increased viscosity of the palm oil.

4.10.2 Components Appearance

Figures 4.95a and 4.95b shows the pictures of side bushing, before and after the operation, respectively. In general, the components were still in good condition. Visually, there was no significant wear observed on the components. Good close-up shows slight erosion wear.

Figure 4.95a: Side bushing of a new pump.

Figure 4.95b: Side bushing of used pump (900 hours).

4.10.3 SEM Micrographs

Philip XL40 SEM was used to obtain metal micrographs. Figure 4.96 shows the vane part under examination. Several micrographs were taken at vane tip. Figures 4.97a -4.97d show the micrograph of vane tip after 900 hours. Figure 4.97a shows the edge of vane tip (magnification 110x). The pitting was not observed at this location at 0 and 500 hour operation. This micrograph indicates that cavitation might have occurred during 500 – 900 hour operation.

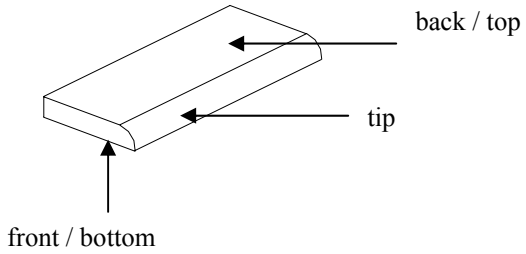

Figure 4.96: Vane configuration under study.

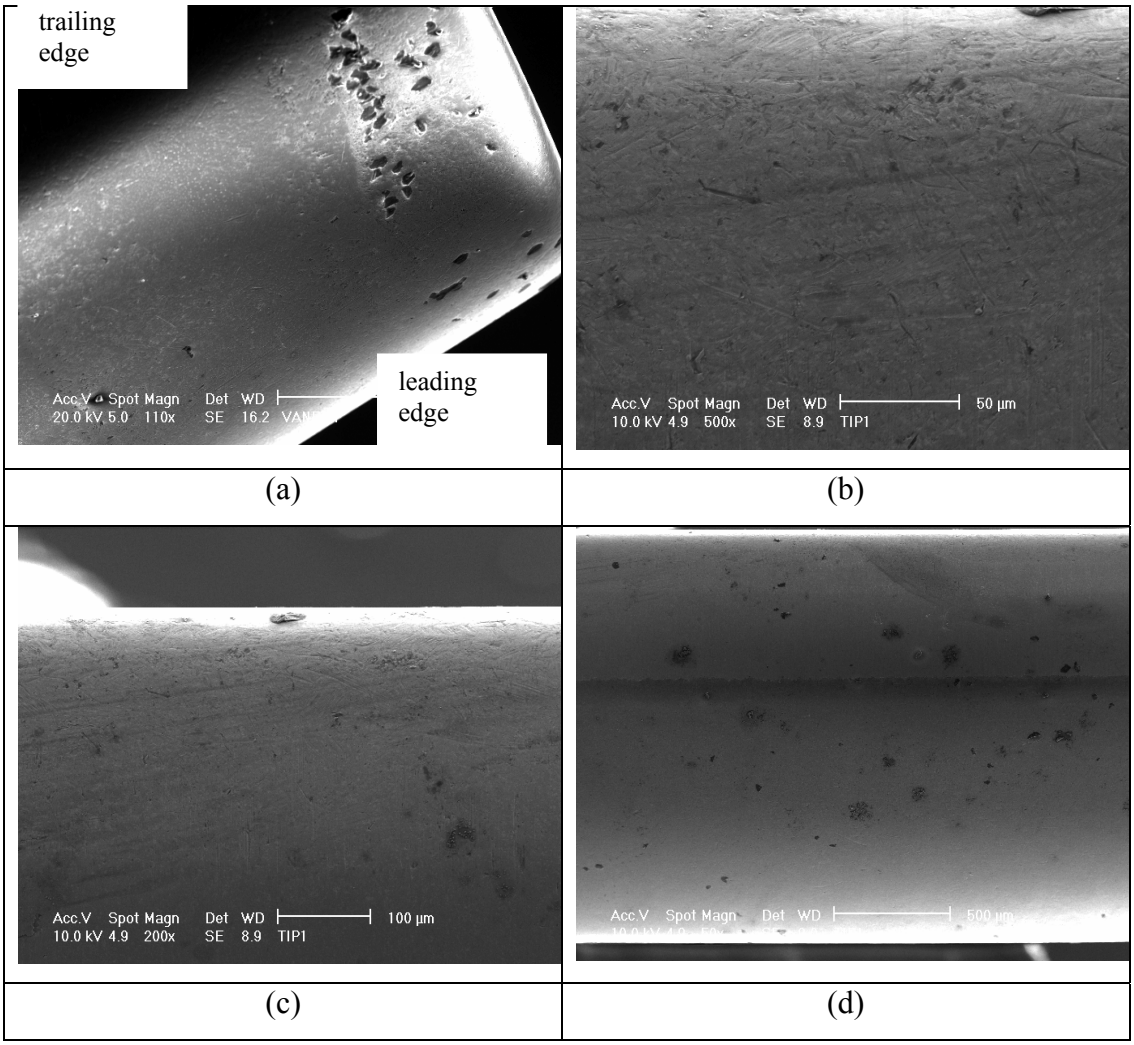

Figure 4.97: Micrograph of vane tip (900 hours).

During one-quarter revolution of rotor rotation, the volume increases between the rotor and cam ring (Figure 4.98: from position a → b). The resulting volume expansion causes a reduction of pressure. This is the suction process, which causes fluid to flow through the inlet port and fill the void. When the palm oil becomes

thicker (as presented in Section 4.4.2), the oil flow rate to fill this void decreases, drops the chamber pressure. The trailing edge of the vane experienced the worst pressure drop. This induces the cavitation to occur. Figure 4.97a shows that pittings are more severe in the trailing edge compared to leading edge.

As the rotor rotates through the second quarter revolution (Figure 4.98: section c→ d), the surface of the cam ring pushes the vanes back into their slots and the trapped volume is reduced. This positively ejects the trapped fluid through the discharge port. In this process positive pressure exists in the chamber and thus cavitation does not occur.

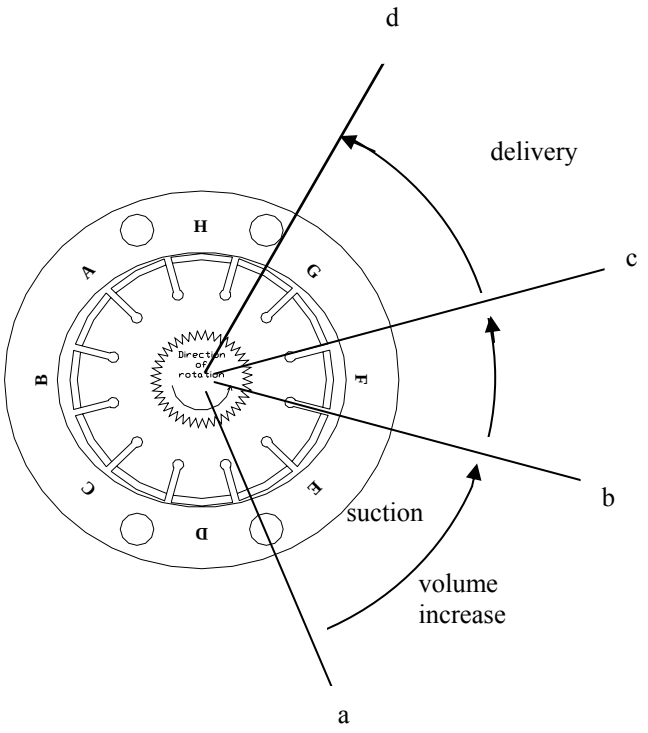

Figure 4.98: Movement and rotation of vane and rotor in cam ring.

Figures 4.97b – 4.97d show the micrographs of vane tip at middle parts with different magnifications. No pitting sign was observed even after 500 times magnification. Figures 4.99a and 4.99b show the appearances of vane top at 0 hour and 900 hour, respectively. With the same magnification, wear lines were observed at 900 hours. Beside the wear lines, no peculiar sign was observed.

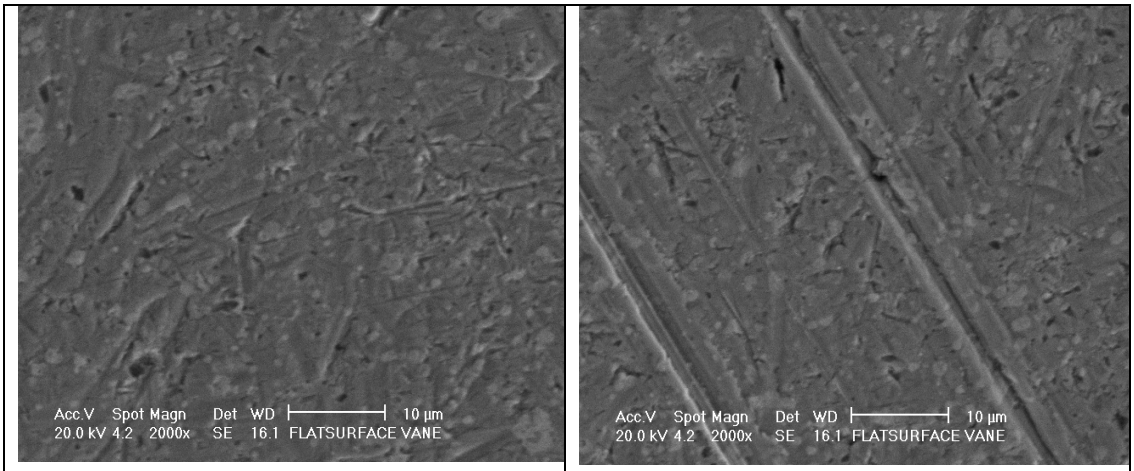

(a) (b)

Figure 4.99: Appearances of vane top at (a) 0 hour and (b) 900 hour.

4.10.4 Surface Roughness

Taylor Hobson Form Talysurf 6 was used to measure metal surface roughness. Figure 4.100 shows the example of roughness profile of vane tip. Table 4.37 shows the surface roughness summary of the internal surface of cam ring. For the analysis purposes the investigated surface was divided into sections A, B, C, D, E, F, G and H (Notation is as in Figure 4.98). The surface roughness of each section at 0, 500 and 900 hours are shown. For each surface, the surface roughness decreased with running hour. The surface roughness between 500 – 0 hour period was compared to 900 - 500 hour. Interestingly, the results show that the highest percentage of smoothing occurs at sections D and H.

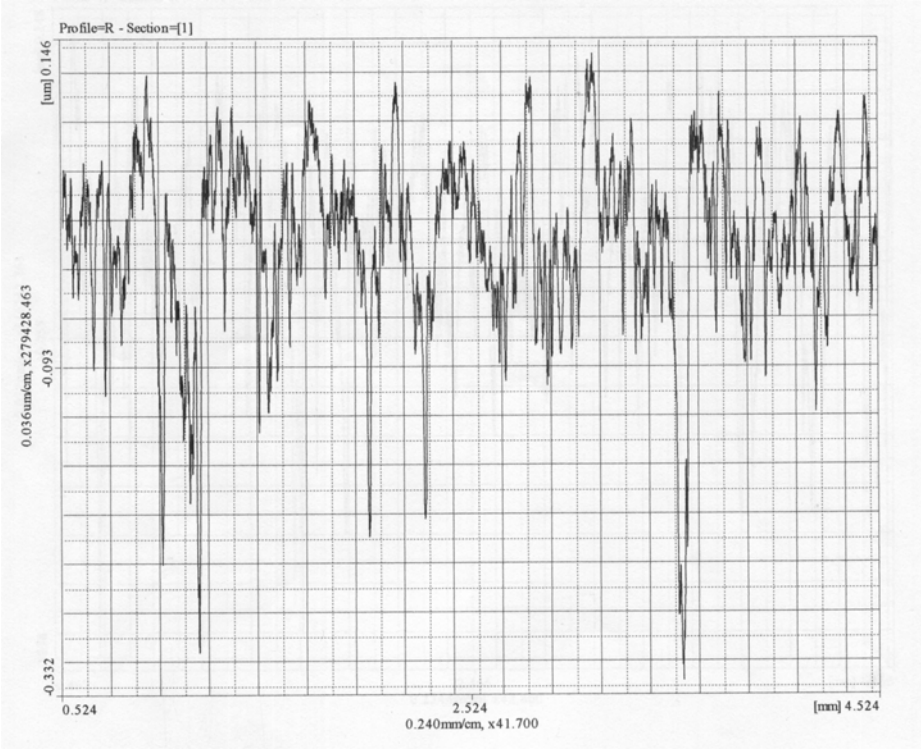

Figure 4.100: Roughness profile of vane tip

Further studies show that sections D and H are the initial suction sections (not F and B as initial thought). The onset of suction process seems to pose severe wear. Referring to Figure 4.100, section D may not be exposed to suction port yet. However the chamber volume opening has occurred. This might creates sudden pressure drop. Negative pressure in the outer section while high centrifugal force from the core might result in tremendous wear.

Least surface roughness change occurred at section F (B and C being equal). At section F the oil chamber volume starts to decrease. Referring to Figure 4.98, the delivery port has not yet opened. Thus the pressure in F and G sections build up. The pressure force pushes the vane inward and thus less vane-to-cam ring contact occurs here.

Table 4.38 also shows that the change of surface roughness of vane. Tip of the vane experienced more surface roughness than the flat surface of the top and bottom. The table compares the surface roughness of vane surfaces (notation is as in Figure 4.98).

Tables 4.37 and 4.38 also show that more surface roughness change occurred during 0 - 500 hour period compared to 500 - 900 hour period. Percentage of smoothing indicates the percentage of surface roughness change during 0 - 500 hour compared to the overall surface roughness change during 0 – 900 hour. These surface roughness results complement the weight loss results discussed in Section 4.10.1.

Table 4.37: Surface roughness of the internal surface of cam ring

Running hour	Sections							
	A	B	C	D	E	F	G	H
0	0.134	0.119	0.099	0.136	0.142	0.106	0.110	0.135
500	0.087	0.085	0.081	0.094	0.089	0.088	0.089	0.090
900	0.067	0.068	0.072	0.088	0.068	0.077	0.083	0.088
Δ500-0	0.047	0.034	0.018	0.042	0.053	0.018	0.021	0.045
Δ900-0	0.067	0.051	0.027	0.048	0.074	0.029	0.027	0.047
% smoothing	0.701	0.667	0.667	0.875	0.716	0.621	0.778	0.957

Table 4.38: Surface roughness of the vane

Running hour	Sections		
	vane tip	vane bottom	vane top
0	0.108	0.070	0.062
500	0.077	0.055	0.051
900	0.061	0.046	0.046
Δ500-0	0.031	0.015	0.011
Δ900-0	0.047	0.024	0.016
% smoothing	0.660	0.625	0.688

CHAPTER 5

CONCLUSIONS AND RECOMMENDATIONS

5.1 Introduction

The aim of the project was to investigate the feasibility of using palm oil as energy transport media in hydraulic system. The objectives of the study as mentioned in Chapter 1 have been achieved.

Performance of palm based oil as hydraulic fluid was investigated, both in bench tests and in the built hydraulic test rig. In the initial part of the study a novel hydraulic test rig was developed and built. Parallel to the hydraulic system development, palm based oil was formulated and tested in bench test.

The bench test condition was set to follow closely international standard test criteria and simulating hydraulic system environment. For this reason the test is labeled as ‘simulated bench test’.

The experimental work consisted of two major parts: bench test and actual hydraulic test. In the bench test, thermal stability of palm oil and its blends was evaluated. The purpose of the bench test was to predict the oil performance when it was used in hydraulic system. The best palm oil blends were then tested in the built hydraulic test rig (Section 4.6). The test temperature was set $55^{o}C$ to simulate the maximum practical operating temperature. The thermal and rheological performances of the blends were investigated in thorough.

The performance of hydraulic system when running on palm oil with out additive was then performed at 70 bar and elevated temperature of 70^{o}C. Variations of torque and flow losses, mechanical and volumetric efficiencies with a number of operating conditions were studied. Simple dimensional analysis study was used in determining flow slip, viscous and coulomb friction coefficients. Attempt to relate these performances and parameters to wear of components and ageing of palm oil were made.

Beside the experimental work performed, the analysis has been made in three major areas as follows:

i. Lubricating capability of the oils was evaluated based on the oils rheological properties. For most of the oils, flow diagrams were established. Several rheological models were used and relevant flow parameters were determined.

ii. Thermal stability of the oil was evaluated mainly on acid content. In the aspect of thermal kinetics, onset temperature and activation energy were determined.

iii. Power transmission capability was based on volumetric and mechanical efficiencies. Effect of ageing of palm oil on the performance was investigated. The changes of flow slip, viscous and coulomb friction coefficients were observed.

5.2 Summarizing Conclusions

i. The built hydraulic test rig was successfully in evaluating the thermal stability of palm based oils and determining the hydraulic system performance when palm oil was used as hydraulic fluid. The built test rig has additional capability than the system used in ASTM D2882 and BS281 since the built test rig is capable of determining hydraulic performances.

ii. In most cases rheological, TAN, IV and TGA thermogram analysis yield similar outcome related to changes of oil properties when the oil was degraded either in bench test or hydraulic system test. This shows that the bench test is very relevant

in predicting the oil performance in the hydraulic system. However the exception is that the flow behavior index increases with test period for bench test and hydraulic test running continuously, while the index decreases when the hydraulic test running intermittently at 70 bar and 70^{o}C (harsher condition).

iii. Basic RBD palm oil is not suitable to be used as hydraulic fluid. Significance acid content (more than 2 mg KOH/g) was accumulated in both bench and hydraulic system test due to thermal-oxidation factor. The acid content can be detrimental to hydraulic components especially hydraulic seal.

iv. Good additives to be blended with palm oil have been determined from both bench test and hydraulic test (continuous running at 55^{o}C). It was found out that F10 and L135 additives, both from Ciba Geigy International USA, far surpass other additives. The recommended treat level for F10 additive is between 1.5% to 2.0%, while for L135% is 1.5%. Higher usage of additive level may not be economical.

v. Rheological properties of palm oil can be best represented by Cross and Carreau models. This is followed by Herschel-Bulkley, modified power law and Ostwald de-Waele models. This is applied to new palm oil samples and also aged samples after being used in hydraulic test rig.

vi. After the hydraulic test rig was ran for 900 hours, the volumetric efficiency increases for about 27% when operated at 200 bar due to the increase in palm oil viscosity. On the other hand, the mechanical efficiency drops to about 10%. However, for real application use, detrimental effects due to the aged oil should be considered. In the aspect of tribology, more than 60% wear occurred during the first 500 hours of operation where the vanes experienced the most severe wear.

5.3 Recommendations for Future Work

This project is believed to be the first in investigating the use of palm based oil as hydraulic fluid. Thus there is a large spectrum of areas that can be further explored. The following work is suggested:

i. Locally, palm oil has been transesterified into trimethylolpropane by researchers in Universiti Putra Malaysia. The product from those researchers can be tested in the built test rig. The thermal performance of this product can be compared to the thermal performance of the best blends determined in this study.

ii. The test of two palm oil blends and Shell Tellus oil at 70^{o}C and 70 bar was halted due test rig problems. One of the problems was due to the pump malfunction. It is recommended that the Yuken pump used in this study to be changed to Vickers 104C pump.

iii. It is recommended that the data acquisition of the test rig be improved in order that transient test can be performed. Bottlenecking of signals at ADAM 4520 should be avoided by using better ADAM module or by providing separate controls for rig no. 1 and rig no. 2. Another option is to use multiple channel cards.

iv. Since the palm oils under studied show fast increase in acid level, it is suggested that corrosion study should be performed. Compatibility of hydraulic components especially hydraulic seal with the used oil should also be checked.

v. For comparison, the performance of mineral oil running at 70 bar, 70^{o}C and with the same running period should be performed. Palm oil with identified additive is to be used in the hydraulic test rig. It is recommended to use 1.5% L135 and 1.5% F10 additives. High temperature and high pressure condition should be applied. Then direct performance comparison can be evaluated.

Benefits Report Guidelines

A. Purpose

The purpose of the Benefits Report is to allow the IRPA Panels and their supporting experts to assess the benefits derived from IRPA-funded research projects.

B. Information Required

The Project Leader is required to provide information on the results of the research project, specifically in the following areas:

- Direct outputs of the project;
- Organisational outcomes of the project; and
- Sectoral/national impacts of the project.

C. Responsibility

The Benefits Report should be completed by the Project Leader of the IRPA-funded project.

D. Timing

The Benefits Report is to be completed within three months of notification by the IRPA Secretariat. Only IRPA-funded projects identified by MPKSN are subject to this review. Generally, the Secretariat will notify Project Leaders of selected projects within 18 months of project completion.

E. Submission Procedure

One copy of this report is to be mailed to :

IRPA Secretariat
Ministry of Science, Technology and the Environment
14th, Floor, Wisma Sime Darby
Jalan Raja Laut
55662 Kuala Lumpur

Benefit Report

1. Description of the Project

A. Project identification

1. Project number : 09-02-06-0007 AE007 (Vot 74033)
2. Project title : Performance Investigation of Energy Transport Media as Influenced by Crop Based Properties.
3. Project leader : Prof Dr Farid Nasir Ani

B. Type of research

Indicate the type of research of the project (Please see definitions in the Guidelines for completing the Application Form)

☐ Scientific research (fundamental research)

☒ Technology development (applied research)

☐ Product/process development (design and engineering)

☐ Social/policy research

C. Objectives of the project

1. Socio-economic objectives

Which socio-economic objectives are adressed by the project? (Please indentify the sector, SEO Category and SEO Group under which the project falls. Refer to the Malaysian R&D Classification System brochure for the SEO Group code)

Sector : **Science and Engineering**

SEO Category : **Natural Science, Technologies and Engineering (S50100)**

SEO Group and Code : **Applied Science and Technologies (S50106)**

2. Fields of research

Which are the two main FO: Categories, FOR Groups, and FOR Areas of your project? (Please refer to the Malaysia R&D Classification System brochure for the FOR Group Code)

a. Primary field of research

FOR Category : **Engineering Science (F10700)**

FOR Group and Code : **F10701 –Mechanical and Industrial Engineering**
FOR Area : **Mechanical Engineering**

b. Secondary field of research

FOR Category : **Engineering Science (F10700)**

FOR Group and Code : **Chemical Engineering (F10702)**

FOR Area : **Chemical/physical modification**

D. Project duration

What was the duration of the project ?

36 Months

E. Project manpower

How many man-months did the project involve?

65 Man-months

F. Project costs

What were the total project expenses of the project?

RM 249,980.00

G. Project funding

Which were the funding sources for the project?

Funding sources	Total Allocation (RM)
IRPA	**249,980.00**

II. Direct Outputs of the Project

A. Technical contribution of the project

1. **What was the achieved direct output of the project :**

For scientific (fundamental) research projects?

- ☐ Algorithm
- ☐ Structure
- ☒ Data
- ☐ Other, please specify : _____

For technology development (applied research) projects :

- ☒ Method/technique
- ☐ Demonstrator/prototype
- ☐ Other, please specify : _____

For product/process development (design and engineering) projects:

- ☒ Product/component
- ☐ Process
- ☐ Software
- ☐ Other, please specify : _____

2. How would you characterise the quality of this output?

- ☐ Significant breakthrough
- ☒ Major improvement
- ☐ Minor improvement

B. Contribution of the project to knowledge

1. How has the output of the project been documented?

- [/] Detailed project report
- [ ] Product/process specification documents
- [ ] Other, please specify : _____

2. Did the project create an intellectual property stock?

- [ ] Patent obtained
- [ ] Patent pending
- [/] Patent application will be filed
- [ ] Copyright

3. What publications are available?

- [ ] Articles (s) in scientific publications How Many: _____
- [/] Papers(s) delivered at conferences/seminars How Many: _____
- [ ] Book
- [ ] Other, please specify : _____

4. How significant are citations of the results?

- [ ] Citations in national publications How Many: _____
- [/] Citations in international publications How Many: _____
- [ ] None yet
- [ ] Not known

lll. Organisational Outcomes of the Project

A. Contribution of the project to expertise development

1. How did the project contribute to expertise?

- [x] PhD degrees — How Many: 1
- [ ] MSc degrees — How Many: _____
- [ ] Research staff with new specialty — How Many: _____
- [ ] Other, please specify: _____

2. How significant is this expertise?

- [x] One of the key areas of priority for Malaysia
- [ ] An important area, but not a priority one

B. Economic contribution of the project?

1. How has the economic contribution of the project materialised?

- [ ] Sales of manufactured product/equipment
- [ ] Royalties from licensing
- [x] Cost savings
- [ ] Time savings
- [ ] Other, please specify : _____

2. How important is this economic contribution ?

- [ ] High economic contribution — Value: RM_____
- [ ] Medium economic contribution — Value: RM_____
- [x] Low economic contribution — Value: RM_____

3. When has this economic contribution materialised?

- [x] Already materialised
- [ ] Within months of project completion
- [ ] Within three years of project completion
- [ ] Expected in three years or more
- [ ] Unknown

C Infrastructural contribution of the project

1. What infrastructural contribution has the project had?

- [x] New equipment — Value: **RM 25,750.00**
- [ ] New/improved facility — Investment : RM _____
- [ ] New information networks
- [ ] Other, please specify: _____

2. How significant is this infrastructural contribution for the organisation?

- [ ] Not significant/does not leverage other projects
- [ ] Moderately significant
- [x] Very significant/significantly leverages other projects

D. Contribution of the project to the organisation's reputation

1. How has the project contributed to increasing the reputation of the organisation

- [ ] Recognition as a Centre of Excellence
- [ ] National award
- [ ] International award
- [ ] Demand for advisory services
- [ ] Invitations to give speeches on conferences
- [ ] Visits from other organisations
- [ ] Other, please specify: _____

2. How important is the project's contribution to the organisation's reputation ?

- [ ] Not significant
- [ ] Moderately significant
- [x] Very significant

1V. National Impacts of the Project

A. Contribution of the project to organisational linkages

1. Which kinds of linkages did the project create?

- [ ] Domestic industry linkages
- [ ] International industry linkages
- [x] Linkages with domestic research institutions, universities
- [ ] Linkages with international research institutions, universities

2. What is the nature of the linkages?

- [ ] Staff exchanges
- [ ] Inter-organisational project team
- [ ] Research contract with a commercial client
- [x] Informal consultation
- [ ] Other, please specify: _____

B. Social-economic contribution of the project

1. Who are the direct customer/beneficiaries of the project output?

Customers/beneficiaries:	Number:
_____	_____
_____	_____
_____	_____

2. How has/will the socio-economic contribution of the project materialised ?

- [ ] Improvements in health
- [ ] Improvements in safety
- [ ] Improvements in the environment
- [x] Improvements in energy consumption/supply
- [ ] Improvements in international relations
- [ ] Other, please specify: _____

3. How important is this socio-economic contribution?

- [ ] High social contribution
- [x] Medium social contribution
- [ ] Low social contribution

4. When has/will this social contribution materialised?

- [ ] Already materialised
- [ ] Within three years of project completion
- [x] Expected in three years or more
- [ ] Unknown

Date: **Signature:**

End of Project Report Guidelines

A. Purpose

The purpose of the End of Project is to allow the IRPA Panels and their supporting group of experts to assess the results of research projects and the technology transfer actions to be taken.

B. Information Required

The following Information is required in the End of Project Report :

- Project summary for the Annual MPKSN Report;
- Extent of achievement of the original project objectives;
- Technology transfer and commercialisation approach;
- Benefits of the project, particularly project outputs and organisational outcomes; and
- Assessment of the project team, research approach, project schedule and project costs.

C. Responsibility

The End of Project Report should be completed by the Project Leader of the IRPA-funded project.

D. Timing

The End of Project Report should be submitted within three months of the completion of the research project.

E. Submission Procedure

One copy of the End of Project is to be mailed to :

IRPA Secretariat
Ministry of Science, Technology and the Environment
14th Floor, Wisma Sime Darby
Jalan Raja Laut
55662 Kuala Lumpur

End of Project Report

A. Project number : 09-02-06-0007 AE007 (Vot 74033)

Project title : Performance Investigation of Energy Transport Media as Influenced by Crop Based Properties.

Project leader: Prof Dr Farid Nasir Ani

Tel: 607-5534650 **Fax: 607-5566159**

B. Summary for the MPKSN Report (for publication in the Annual MPKSN Report, please summarise the project objectives, significant results achieved, research approach and team structure)

Project Objectives

The objectives of this project are to design and build suitable mechanical test rig for oil performance evaluation. It is also included in the objectives to determine power transmission, corrosion protection, lubrication, mechanical and volumetric performance of the oil. Performance comparison between this environmentally adapted oil and conventional mineral oil will be made. On other side, the project conducted too study mechanical and chemical properties of local crops. Base oil stability will be evaluated. Finally, the objective is to improve the oil properties through additives formulation.

Significant results achieved:

1. Hydraulic test rig with DAS and online feedback contol system.
2. Data of palm oil hydraulic fluid.

The research approach was carried by following steps:

1. Literature search.
2. Screening of vegetable oil. Physical properties tests.
3. Chemical testing and analysis.
4. Improvement of oil properties.
5. Hydraulic system design and fabrication.
6. Operational oil performance.
7. Theoretical/Computer Modelling Validation.
8. Conduct profit analysis.
9. Field testing
10. Analysis of data/results.
11. Preparation of reports/publication of research findings.

The project team structure:-

1. Professor Farid Nasir Bin Hj. Ani
2. Wan Mohd Nursani Wan Nik.
3. Prof. Dr. Hamdan Suhaimi.
4. Assoc. Prof. Dr. Mustaffa Nawawi, Science Fac, UTM
5. Wan Hasamudin Wan Ghani, MPOB
6. Yahaya b. Abdul Ghani, PRSS

C. Objectives achievement

- **Original project objectives** (Please state the specific project objectives as described in Section ll of the Application Form).

1. To design and build suitable mechanical test rig for oil performance evaluation.
2. To determine power transmission, corrosion protection, lubrication, mechanical and volumetric performance of the oil. Performance comparison between this environmentally adapted oil and conventional mineral oil will be made.
3. To study mechanical and chemical properties of local crops. Base oil stability will be evaluated.
4. To improve the oil properties through additives formulation.

- **Objectives Achieved** (Please state the extent to which the project objectives were achieved)

1. To design and build suitable mechanical test rig for oil performance evaluation.
2. To determine power transmission, corrosion protection, lubrication, mechanical and volumetric performance of the oil. Performance comparison between this environmentally adapted oil and conventional mineral oil will be made.
3. To study mechanical and chemical properties of local crops. Base oil stability will be evaluated.
4. To improve the oil properties through additives formulation.

- **Objectives not achieved** (Please identify the objectives that were not achieved and give reasons)

-nil-

D. **Technology Transfer/Commercialisation Approach** (Please describe the approach planned to transfer/commercialise the results of the project)

1. Local oil, lubricant producers - Research findings will help them to produce product or improve their current products. Knowledge will be disseminated through seminar/conference and advisory services.
2. MPOB - By working together with this research institution, this research is complementing the work done by the MPOB scientist.

E. Benefits of the Project (Please identify the actual benefits arising from the project as defined in Section lll of the Application Form. For examples of outputs, organisational outcomes and sectoral/national impacts, please refer to Section lll of the Guidelines for the Application of R&D Funding under IRPA)

- **Outputs of the project and potential beneficiaries** (Please describe as specifically as possible the outputs achieved and provide an assessment of their significance to users)

  1. Comprehensive information on performance of the improved product.
  2. Mechanical efficiencies of machineries using the studied local crops.
  3. Formulations of industrial products using local crop oil.
  4. Comparative data between local crop and crops used in USA and Europe

- **Organisational Outcomes** (Please describe as specifically as possible the organisational benefits arising from the project and provide an assessment of their significance)

  1. PhD degrees -1
  2. Research staff with specialization in energy transport fluid
  3. Improved laboratory facilities

- **National Impacts** (If known at this point in time, please describes specifically as possible the potential sectoral/national benefits arising from the project and provide an assessment of their significance)

  1. PhD degrees -1
  2. Research staff with specialization in energy transport fluid
  3. Improved laboratory facilities
  4. Closed collaboration between UTM, KUT, UM, PRSS and MPOB.
  5. Linkages with research institutes and universities in USA, UK and other parts of Europe.
  6. Improvement in environment- use/modification of environmentally friendly product
  7. Improvement in health - use of nontoxic fluid
  8. Improvement in safety - use of high flash point energy transport media
  9. Farmers in Agro-based sectors such as palm and coconut will gain economic benefits from sale of the crops. Increase in use/sale of local based crop.
  10. Improvement in job opportunities for the cultivation, harvesting and processing of crop oil.

F. Assessment of project structure

- **Project Team** (Please provide an assessment of how the project team performed and highlight any significant departures from plan in either structure or actual man-days utilised)

  The project team performed successfully with the objectives of the project.

- **Collaborations** (Please describe the nature of collaborations with other research organisations and/or industry)

  Collaborations with other research organizations such as MPOB, UPM and UM etc. were good in the sense that they giving advices and analyzing of samples.

G. Assessment of Research Approach (Please highlight the main steps actually performed and indicate any major departure from the planned approach or any major difficulty encountered)

The main steps actually performed as planned.

H. Assessment of the Project Schedule (Please make any relevant comment regarding the actual duration of the project and highlight any significant variation from plan)

The actual duration of the project was as planned with insignificant variation from plan.

I. Assessment of Project Costs (Please comment on the appropriateness of the original budget and highlight any major departure from the planned budget)

Major departure from the planned budget are in J- series ie. paying of research officers.

J. Additional Project Funding Obtained (In case of involvement of other funding sources, please indicate the source and total funding provided)

No other funding sources.

K. Other Remarks (Please include any other comment which you feel is relevant for the evaluation of this project)

The project achieved it objectives, producing a doctorate officer, a test rig and data regarding the use of palm oil as hydraulic fluids.

Date : **Signature :**

APPENDIX A

Derivation of shear rate, shear stress, torque and viscosity terms

Referring to Figure A1 below, assuming that the oil flows in a steady pattern and in steady state condition in annular passage between disposable chamber and spindle, equation of motion in the tangent direction can be reduced to (Bird *et al.*, 2001):

$$0 = \frac{d}{dx}\left(\frac{1}{x}\frac{d}{dx}\left(xv_\theta\right)\right). \qquad 1$$

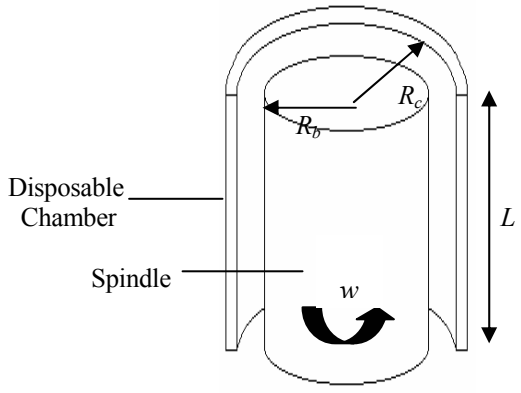

Figure A1: Schematic of coaxial viscometer.

Solving Equation 1,

$$\int 0dx = \int d\left[\frac{1}{x}\frac{d}{dx}\left(xv\right)\right]$$

$$1 + c_1 = \frac{1}{x}\frac{d}{dx}\left(xv\right)$$

$$\left(1 + c_1\right)\int xdx = \int d\left(xv\right)$$

$$\left(\frac{1 + c_1}{2}\right)x^2 = xv + c_2 \qquad 2$$

Taking the boundary conditions and assuming no slip condition, velocity of oil sample is

at moving spindle is wR_b and at stagnant disposable chamber is zero:

$$At \quad x = R_b \quad , \quad v = R_b w$$

$$\left(\frac{1+c_1}{2}\right){R_b}^2 = R_b\left(R_b w\right) + c_2$$

$$\left(\frac{1+c_1}{2}\right){R_b}^2 = {R_b}^2 w + c_2 \qquad 3$$

$$At \quad x = R_c \quad , \quad v = 0$$

$$\left(\frac{1+c_1}{2}\right){R_c}^2 = 0 + c_2$$

$$c_2 = \left(\frac{1+c_1}{2}\right){R_c}^2 \qquad 4$$

Solving the above equations,

$$(4) \text{ into } (3) \quad , \quad \left(\frac{1+c_1}{2}\right){R_b}^2 = {R_b}^2 w + \left(\frac{1+c_1}{2}\right){R_c}^2$$

$$\left(\frac{1+c_1}{2}\right)\left({R_b}^2 - {R_c}^2\right) = {R_b}^2 w$$

$$\frac{1+c_1}{2} = \frac{{R_b}^2 w}{{R_b}^2 - {R_c}^2} \qquad 5$$

$$(5) \text{ into } (4) \quad , \quad c_2 = \left(\frac{{R_b}^2 w}{{R_b}^2 - {R_c}^2}\right){R_c}^2$$

$$c_2 = \frac{{R_b}^2 {R_c}^2 w}{{R_b}^2 - {R_c}^2} \qquad 6$$

$$(5)\&(6) \text{ into } (2) \quad , \quad \frac{{R_b}^2 w}{{R_b}^2 - {R_c}^2} x^2 = xv + \frac{{R_b}^2 {R_c}^2 w}{{R_b}^2 - {R_c}^2}$$

$$xv = \frac{{R_b}^2 w x^2}{{R_b}^2 - {R_c}^2} - \frac{{R_b}^2 {R_c}^2 w}{{R_b}^2 - {R_c}^2}$$

$$xv = \frac{{R_b}^2 w}{{R_b}^2 - {R_c}^2}\left(x^2 - {R_c}^2\right)$$

The velocity at any point in the oil sample can be shown as

$$v = \frac{R_b{}^2 w}{R_b{}^2 - R_c{}^2}\left(x - \frac{R_c{}^2}{x}\right) \qquad 7$$

Shear stress for Newtonian fluids in the cylinder (cylinder type disposable chamber) coordinates can be shown as below (Bird *et al.*, 2001):

$$\tau_{x\theta} = \tau_{\theta x} = -\eta\left[x\frac{d}{dx}\left(\frac{v_\theta}{x}\right) + \frac{1}{x}\frac{dv_x}{d\theta}\right]. \qquad 8$$

With second term goes to zero, shear stress can be shown as below:

$$\begin{aligned}
\tau_{x\theta} = \tau_{\theta x} &= -\eta\left[x\frac{d}{dx}\left(\frac{R_b{}^2 w}{x\left(R_b{}^2 - R_c{}^2\right)}\left(x - \frac{R_c{}^2}{x}\right)\right) + 0\right] \\
&= -\eta\left[x\frac{d}{dx}\left(\frac{R_b{}^2 w}{x\left(R_b{}^2 - R_c{}^2\right)}\left(x - \frac{R_c{}^2}{x}\right)\right)\right] \\
&= -\eta\left[x\left(\frac{R_b{}^2 w}{\left(R_b{}^2 - R_c{}^2\right)}\left(\frac{2R_c{}^2}{x^3}\right)\right)\right] \\
&= -\eta\left[\frac{2R_b{}^2 R_c{}^2 w}{x^2\left(R_b{}^2 - R_c{}^2\right)}\right] \\
&= \eta\left[\frac{2R_b{}^2 R_c{}^2 w}{x^2\left(R_c{}^2 - R_b{}^2\right)}\right]
\end{aligned}$$

Thus shear stress can be shown as

$$\tau_{x\theta} = \tau_{\theta x} = \eta\left[\frac{2R_b{}^2 R_c{}^2 w}{x^2\left(R_c{}^2 - R_b{}^2\right)}\right] \qquad 9$$

Since shear stress-shear rate from basic fluid mechanics can be shown as

Shear stress = viscosity x shear rate 10

$$\text{Therefore, } \gamma = \frac{2R_b{}^2 R_c{}^2 w}{x^2\left(R_c{}^2 - R_b{}^2\right)} \qquad 11$$

Torque , $m = \tau_{r\theta} \times \text{Area} \times \text{moment arm}$

$$= \tau_{r\theta} \times (2\pi R_b L) \times R_b$$

$$\tau_{r\theta} = \frac{m}{2\pi R_b{}^2 L} \qquad 12$$

Combining Equations 10, 11 and 12,

$$\eta = \frac{\left(\frac{m}{2\pi R_b{}^2 L}\right)}{\left(\frac{2R_b{}^2 R_c{}^2 w}{x^2\left(R_c{}^2 - R_b{}^2\right)}\right)}$$

$$= \frac{m\left(R_c{}^2 - R_b{}^2\right)x^2}{4\pi w L R_c{}^2 R_b{}^4}$$

if $x = R_b$,

$$\eta = \frac{m\left(R_c{}^2 - R_b{}^2\right)}{4\pi w L R_c{}^2 R_b{}^2} \qquad 13$$

where

c_1, c_2 = constants
m = *%/100 x 673.7*
L = 3.553 cm
R_b = 0.874 cm
R_c = 0.953 cm
w = 2π/60 x *rpm*
π = 22/7

APPENDIX B

Pictures during development of hydraulic test rig:

Overall LabVIEW program for running the test rig:

Figure B1: Basic loose components.

Figure B2: Fabrication of hydraulic power pack.

Figure B3: Fabrication of hydraulic reservoir.

Figure B4: Electrical control.

Figure B5: Complete hydraulic test rig.

Figure B6: PC control of the test rig.

APPENDIX C

Activation energy relationship

Substituting Equation 2.3 into Equation 2.2 yields

$$\frac{dx}{dT} = \frac{A}{B}\exp\left(\frac{-E_a}{RT}\right)\ (1\text{-}x)\ . \qquad 1$$

In this study, two models were used to evaluate the kinetic parameters of the oil samples. By direct Arrhenius plot method for the non-isothermal kinetic parameters with constant heating rate ($B = dT/dt$), Equation 1 was rearranged to

$$\ln\left[\frac{1}{(1-x)}\frac{dx}{dT}\right] = \ln\frac{A}{B} - \frac{E_a}{RT}. \qquad 2$$

The plot $\ln[(1/(1\text{-}x)(dx/dT)]$ versus $1/T$ should give a straight line with slope $-E_a/R$ gives the activation energy E_a.

The integration method determines the overall reaction from conversion versus temperature curves. Rearranging, integrating and using a natural logarithm, Equation 1 yields

$$\ln\left(-\ln(1-x)\right) = \ln\left[\frac{ART^2}{BE_a}\left(1-\frac{2RT}{E_a}\right)\right] - \frac{E_a}{RT}\ . \qquad 3$$

The plot $\ln [-\ln(1\text{-}x)]$ versus $1/T$ should yield a straight line with slope $-E_a/R$, where the activation energy E_a can be calculated.

APPENDIX D

Mathematica programs:

Program #D1: Determination of Andrade constants

Program #D2: Oswald de-Waele model

Program #D3: Cross model

Program #D4: Proposed modified Power Law model

Program #D5: 3-dimensional model

APPENDIX E

Determination of R^2 and MSE for Al-Zahrani and Al-Fariss's and proposed generalized rheological models.

APPENDIX F

Loss coefficients values

Loss Coefficients Value for 100 hour.

At temperature 40 ºC (μ = 0.037 Pa.s)

Speed (Hz)	C_s (x 10^{-7})	C_c	C_v	Pressure (bar)	C_s (x 10^{-7})	C_c	C_v
48	0.4743	0.0834	237147	35	1.3977	0.3668	96854
40	0.4628	0.1147	273446	75	0.8359	0.3004	-27217
30	0.4425	0.1221	321413	125	0.6964	0.2560	-111242
20	0.4276	0.1826	347342	200	0.5666	0.2761	-400207

At temperature 50 ºC (μ = 0.026 Pa.s)

Speed (Hz)	C_s (x 10^{-7})	C_c	C_v	Pressure (bar)	C_s (x 10^{-7})	C_c	C_v
48	0.4153	0.0770	550830	35	0.9333	0.5609	161433
40	0.4104	0.1102	701356	75	0.6533	0.2905	224780
30	0.4034	0.1142	737035	125	0.6136	0.2859	-98660
20	0.4882	0.1683	924179	200	0.5930	0.2783	-386402

At temperature 60 ºC (μ = 0.019 Pa.s)

Speed (Hz)	C_s (x 10^{-7})	C_c	C_v	Pressure (bar)	C_s (x 10^{-7})	C_c	C_v
48	0.3735	0.1015	252119	35	0.7874	0.5208	-268237
40	0.3938	0.1359	346915	75	0.6144	0.3124	-306173
30	0.4038	0.1360	332500	125	0.5579	0.2542	-414827
20	0.4991	0.1692	624812	200	0.5373	0.2748	-824920

At temperature 70 ºC (μ = 0.015 Pa.s)

Speed (Hz)	C_s (x 10^{-7})	C_c	C_v	Pressure (bar)	C_s (x 10^{-7})	C_c	C_v
48	0.3204	0.0982	284910	35	0.7968	0.0421	362620
40	0.3698	0.1469	180441	75	0.6966	0.1824	-115388
30	0.4139	0.1907	-111763	125	0.6480	0.1483	-25704
20	0.4428	0.2006	-117805	200	0.6117	0.3553	-2000000

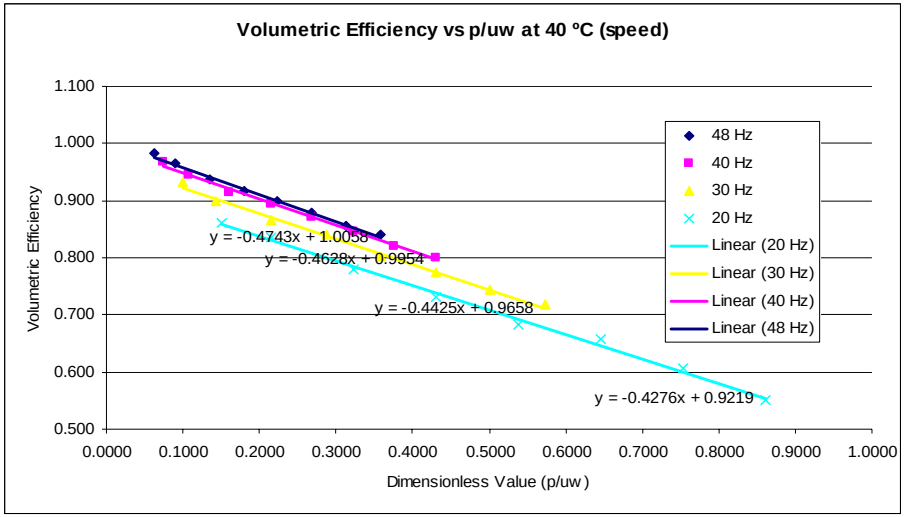
Volumetric Efficiency vs p/uw at 40 ºC (speed)
Volumetric Efficiency
Dimensionless Value (p/uw)
y = -0.4743x + 1.0058
y = -0.4628x + 0.9954
y = -0.4425x + 0.9658
y = -0.4276x + 0.9219
48 Hz
40 Hz
30 Hz
20 Hz
Linear (20 Hz)
Linear (30 Hz)
Linear (40 Hz)
Linear (48 Hz)

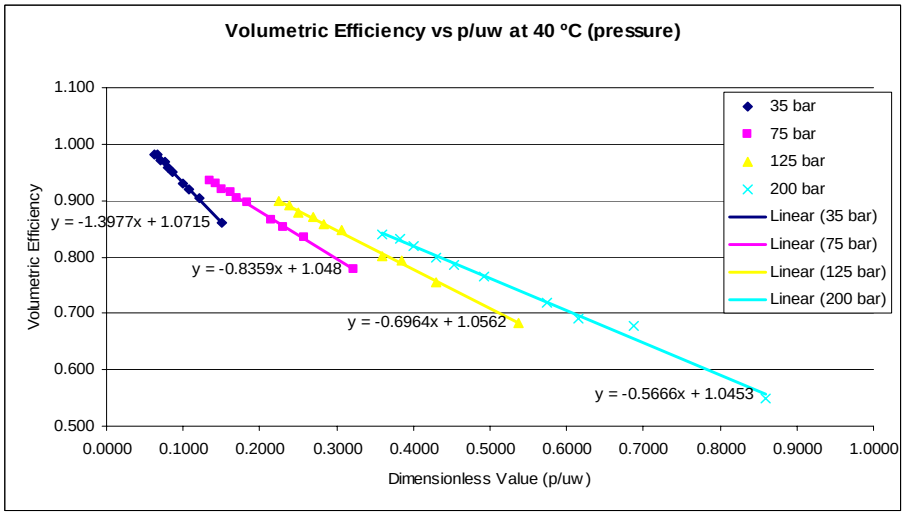
Volumetric Efficiency vs p/uw at 40 ºC (pressure)
Volumetric Efficiency
Dimensionless Value (p/uw)
y = -1.3977x + 1.0715
y = -0.8359x + 1.048
y = -0.6964x + 1.0562
y = -0.5666x + 1.0453
35 bar
75 bar
125 bar
200 bar
Linear (35 bar)
Linear (75 bar)
Linear (125 bar)
Linear (200 bar)

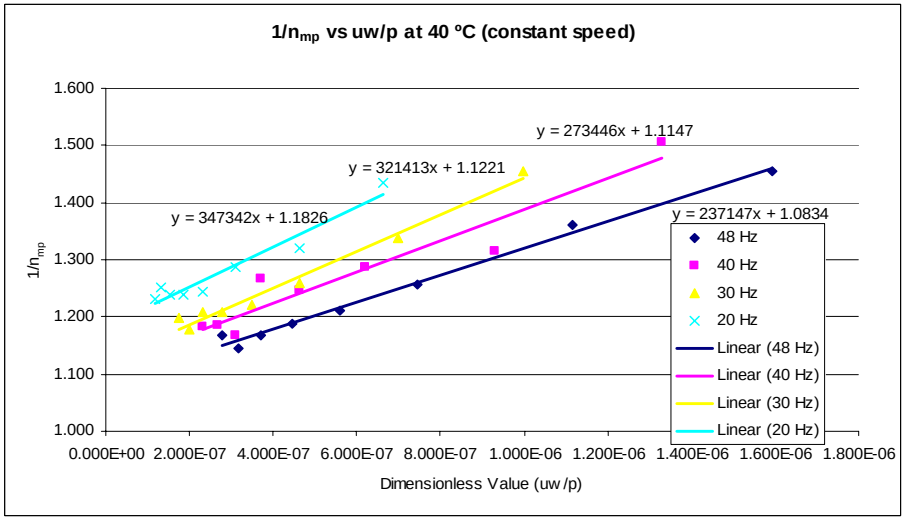
1/n_mp vs uw/p at 40 ºC (constant speed)
1/n_mp
Dimensionless Value (uw/p)
y = 273446x + 1.1147
y = 321413x + 1.1221
y = 347342x + 1.1826
y = 237147x + 1.0834
48 Hz
40 Hz
30 Hz
20 Hz
Linear (48 Hz)
Linear (40 Hz)
Linear (30 Hz)
Linear (20 Hz)

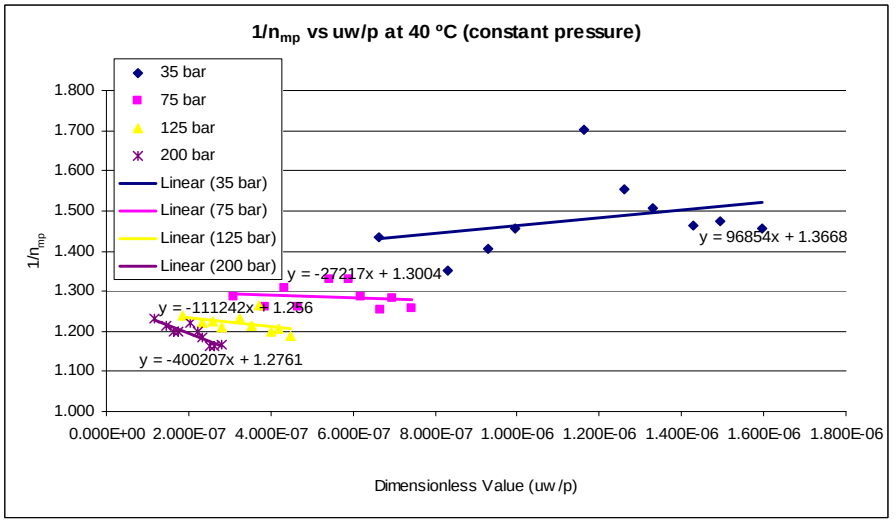
1/n_mp vs uw/p at 40 ºC (constant pressure)
1/n_mp
Dimensionless Value (uw/p)
y = 96854x + 1.3668
y = -27217x + 1.3004
y = -111242x + 1.256
y = -400207x + 1.2761
35 bar
75 bar
125 bar
200 bar
Linear (35 bar)
Linear (75 bar)
Linear (125 bar)
Linear (200 bar)

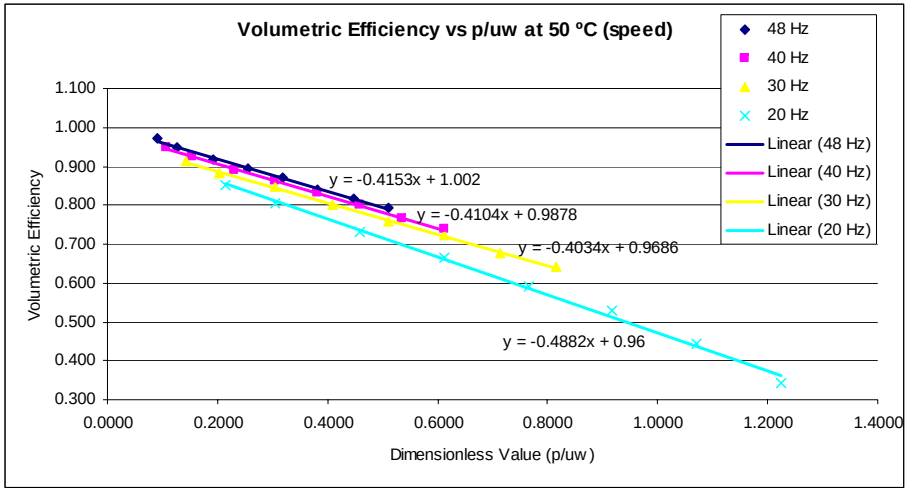
Volumetric Efficiency vs p/uw at 50 °C (speed)
Volumetric Efficiency
Dimensionless Value (p/uw)
48 Hz
40 Hz
30 Hz
20 Hz
Linear (48 Hz)
Linear (40 Hz)
Linear (30 Hz)
Linear (20 Hz)
y = -0.4153x + 1.002
y = -0.4104x + 0.9878
y = -0.4034x + 0.9686
y = -0.4882x + 0.96
1.100
1.000
0.900
0.800
0.700
0.600
0.500
0.400
0.300
0.0000
0.2000
0.4000
0.6000
0.8000
1.0000
1.2000
1.4000

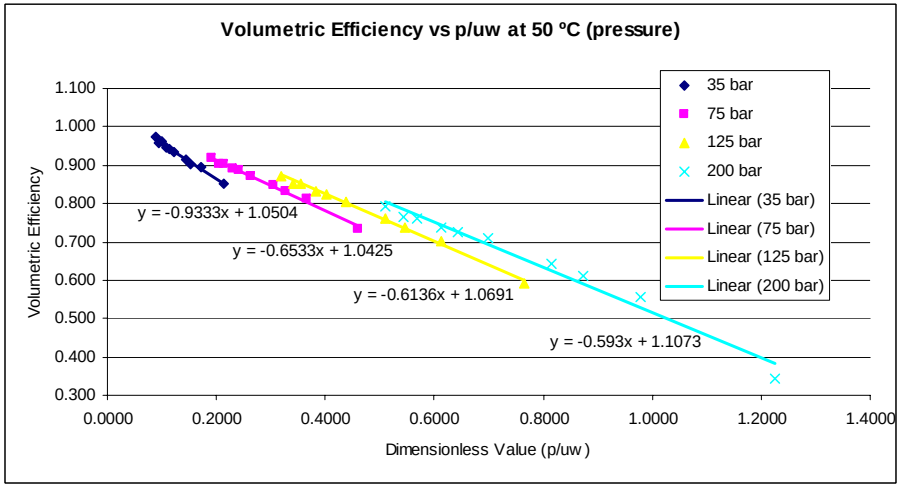
Volumetric Efficiency vs p/uw at 50 °C (pressure)
Volumetric Efficiency
Dimensionless Value (p/uw)
35 bar
75 bar
125 bar
200 bar
Linear (35 bar)
Linear (75 bar)
Linear (125 bar)
Linear (200 bar)
y = -0.9333x + 1.0504
y = -0.6533x + 1.0425
y = -0.6136x + 1.0691
y = -0.593x + 1.1073
1.100
1.000
0.900
0.800
0.700
0.600
0.500
0.400
0.300
0.0000
0.2000
0.4000
0.6000
0.8000
1.0000
1.2000
1.4000

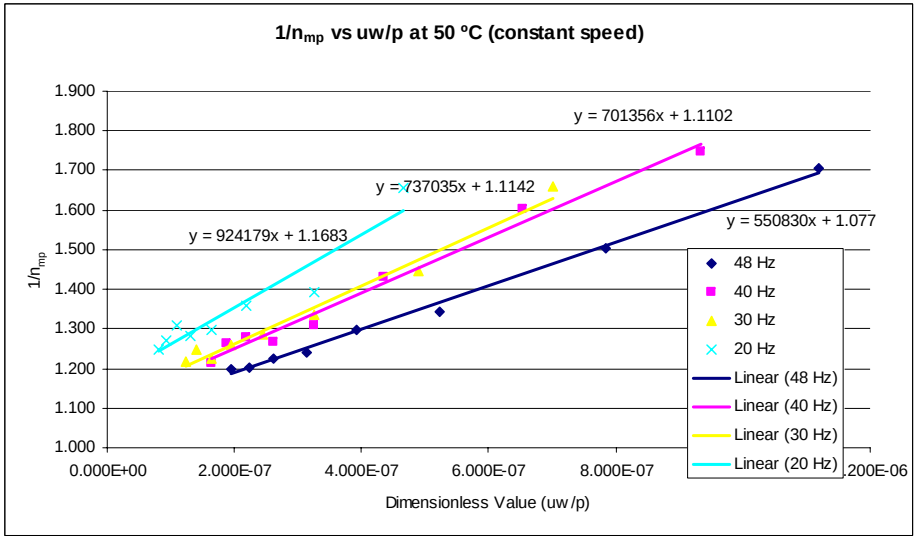
1/n_mp vs uw/p at 50 °C (constant speed)
1/n_mp
Dimensionless Value (uw/p)
48 Hz
40 Hz
30 Hz
20 Hz
Linear (48 Hz)
Linear (40 Hz)
Linear (30 Hz)
Linear (20 Hz)
y = 701356x + 1.1102
y = 737035x + 1.1142
y = 924179x + 1.1683
y = 550830x + 1.077
1.900
1.800
1.700
1.600
1.500
1.400
1.300
1.200
1.100
1.000
0.000E+00
2.000E-07
4.000E-07
6.000E-07
8.000E-07
1.000E-06
1.200E-06

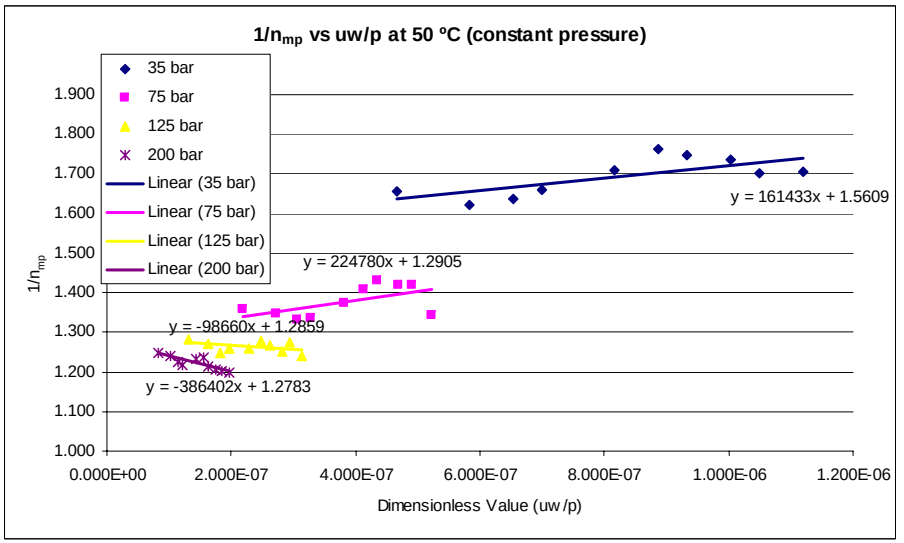
1/n_mp vs uw/p at 50 °C (constant pressure)
1/n_mp
Dimensionless Value (uw/p)
35 bar
75 bar
125 bar
200 bar
Linear (35 bar)
Linear (75 bar)
Linear (125 bar)
Linear (200 bar)
y = 161433x + 1.5609
y = 224780x + 1.2905
y = -98660x + 1.2859
y = -386402x + 1.2783
1.900
1.800
1.700
1.600
1.500
1.400
1.300
1.200
1.100
1.000
0.000E+00
2.000E-07
4.000E-07
6.000E-07
8.000E-07
1.000E-06
1.200E-06

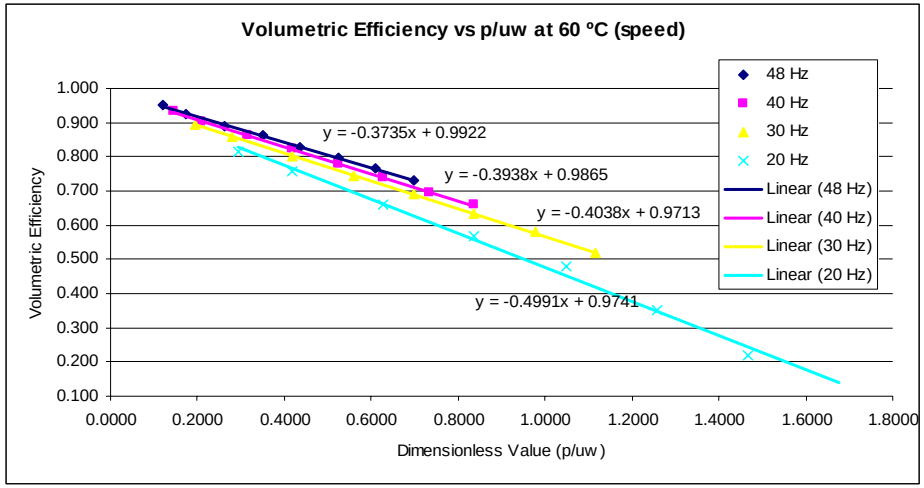
Volumetric Efficiency vs p/uw at 60 °C (speed)
Volumetric Efficiency
Dimensionless Value (p/uw)
y = -0.3735x + 0.9922
y = -0.3938x + 0.9865
y = -0.4038x + 0.9713
y = -0.4991x + 0.9741
48 Hz
40 Hz
30 Hz
20 Hz
Linear (48 Hz)
Linear (40 Hz)
Linear (30 Hz)
Linear (20 Hz)

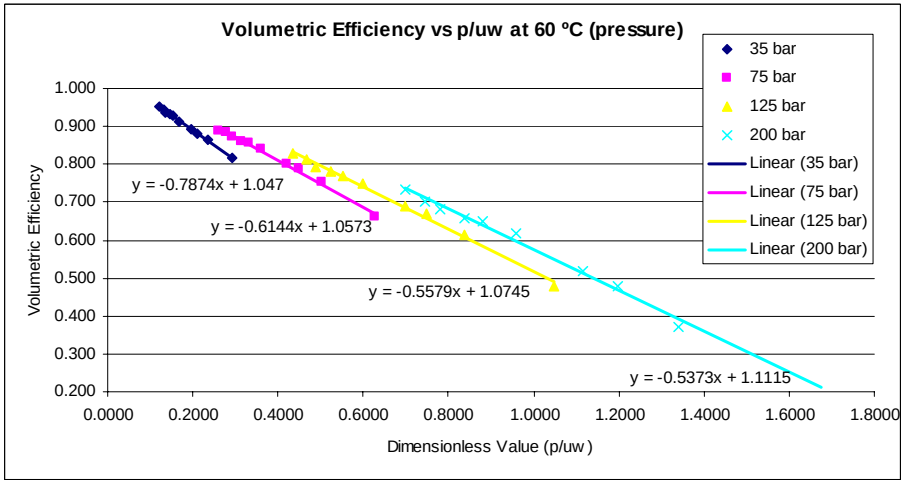
Volumetric Efficiency vs p/uw at 60 °C (pressure)
Volumetric Efficiency
Dimensionless Value (p/uw)
y = -0.7874x + 1.047
y = -0.6144x + 1.0573
y = -0.5579x + 1.0745
y = -0.5373x + 1.1115
35 bar
75 bar
125 bar
200 bar
Linear (35 bar)
Linear (75 bar)
Linear (125 bar)
Linear (200 bar)

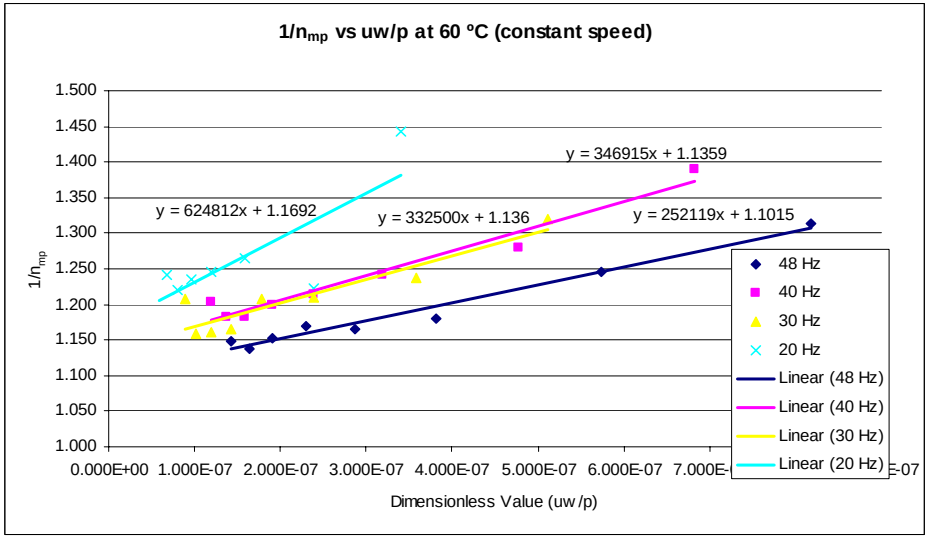
1/n_mp vs uw/p at 60 °C (constant speed)
1/n_mp
Dimensionless Value (uw/p)
y = 346915x + 1.1359
y = 624812x + 1.1692
y = 332500x + 1.136
y = 252119x + 1.1015
48 Hz
40 Hz
30 Hz
20 Hz
Linear (48 Hz)
Linear (40 Hz)
Linear (30 Hz)
Linear (20 Hz)

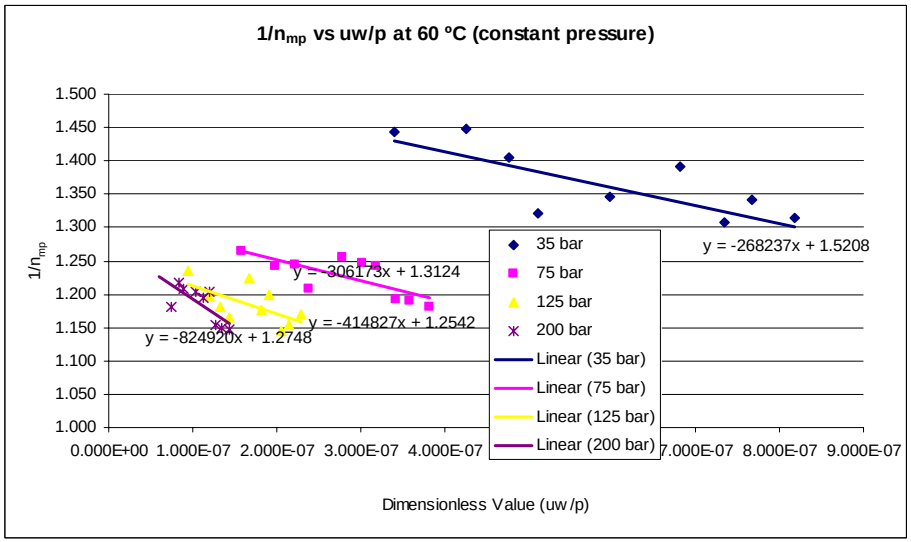
1/n_mp vs uw/p at 60 °C (constant pressure)
1/n_mp
Dimensionless Value (uw/p)
y = -268237x + 1.5208
y = -306173x + 1.3124
y = -414827x + 1.2542
y = -824920x + 1.2748
35 bar
75 bar
125 bar
200 bar
Linear (35 bar)
Linear (75 bar)
Linear (125 bar)
Linear (200 bar)

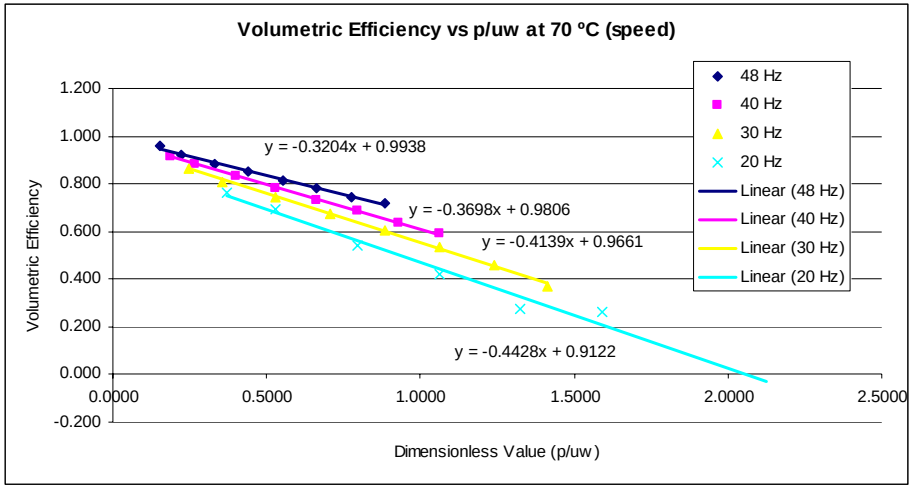
Volumetric Efficiency vs p/uw at 70 °C (speed)
Volumetric Efficiency
Dimensionless Value (p/uw)
y = -0.3204x + 0.9938
y = -0.3698x + 0.9806
y = -0.4139x + 0.9661
y = -0.4428x + 0.9122
48 Hz
40 Hz
30 Hz
20 Hz
Linear (48 Hz)
Linear (40 Hz)
Linear (30 Hz)
Linear (20 Hz)

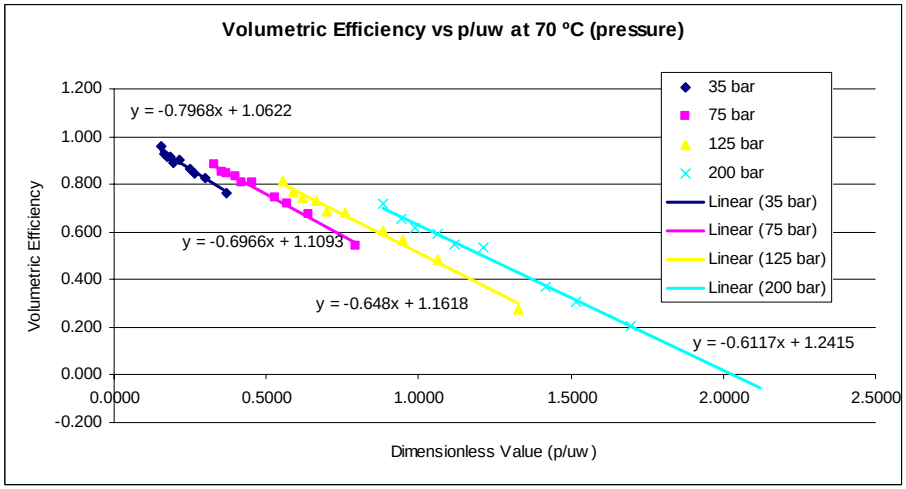
Volumetric Efficiency vs p/uw at 70 °C (pressure)
Volumetric Efficiency
Dimensionless Value (p/uw)
y = -0.7968x + 1.0622
y = -0.6966x + 1.1093
y = -0.648x + 1.1618
y = -0.6117x + 1.2415
35 bar
75 bar
125 bar
200 bar
Linear (35 bar)
Linear (75 bar)
Linear (125 bar)
Linear (200 bar)

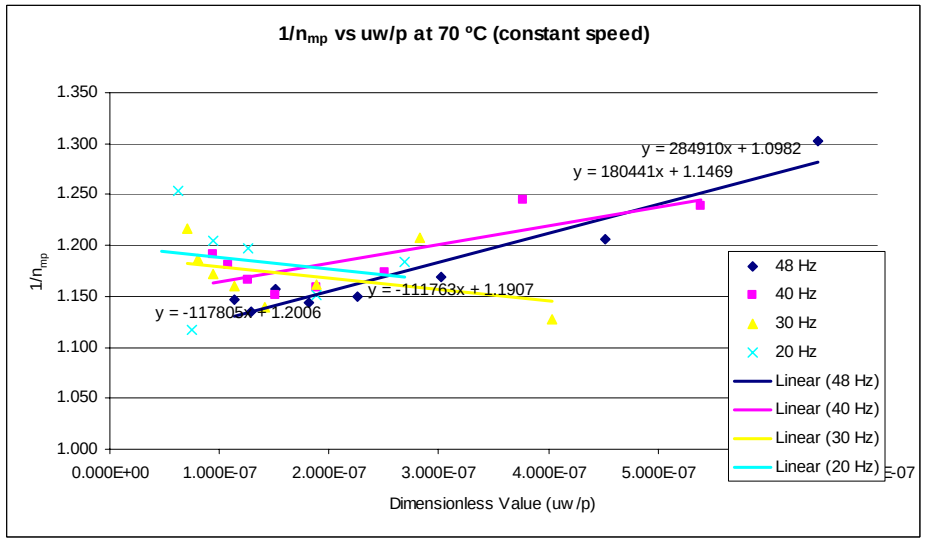
1/nmp vs uw/p at 70 °C (constant speed)
1/nmp
Dimensionless Value (uw/p)
y = 284910x + 1.0982
y = 180441x + 1.1469
y = -111763x + 1.1907
y = -117805x + 1.2006
48 Hz
40 Hz
30 Hz
20 Hz
Linear (48 Hz)
Linear (40 Hz)
Linear (30 Hz)
Linear (20 Hz)

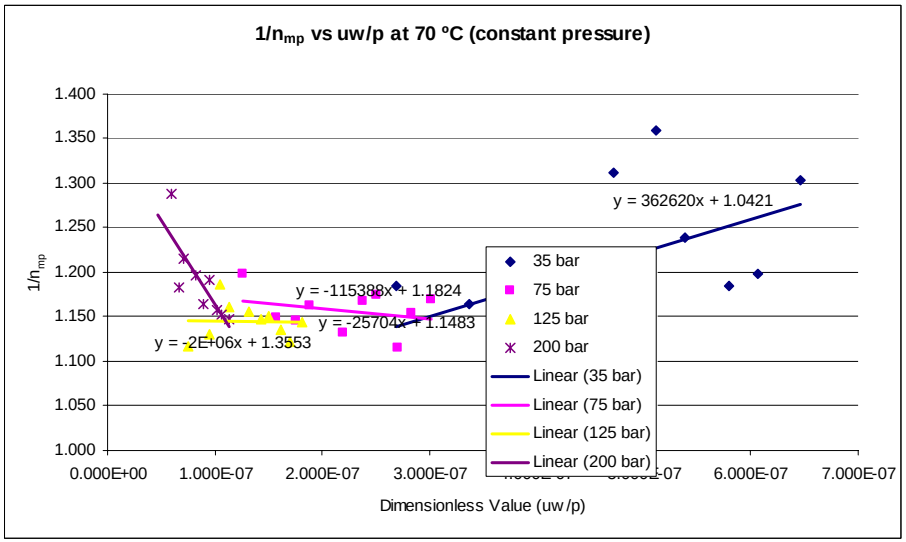
1/nmp vs uw/p at 70 °C (constant pressure)
1/nmp
Dimensionless Value (uw/p)
y = 362620x + 1.0421
y = -115388x + 1.1824
y = -25704x + 1.1483
y = -2E+06x + 1.3553
35 bar
75 bar
125 bar
200 bar
Linear (35 bar)
Linear (75 bar)
Linear (125 bar)
Linear (200 bar)

Loss Coefficients Value for 200 Hour.

At temperature 40 ºC (μ = 0.067 Pa.s)

Speed (Hz)	C_s (x 10^{-7})	C_c	C_v	Pressure (bar)	C_s (x 10^{-7})	C_c	C_v
48	0.6289	0.0705	222856	35	2.2030	0.4749	80451
40	0.5910	0.1085	241415	75	1.3172	0.3114	50962
30	0.5418	0.1250	259498	125	0.9708	0.2054	84403
20	0.5823	0.1294	386151	200	0.8186	0.1965	3595

At temperature 50 ºC (μ = 0.045 Pa.s)

Speed (Hz)	C_s (x 10^{-7})	C_c	C_v	Pressure (bar)	C_s (x 10^{-7})	C_c	C_v
48	0.5203	0.0758	277940	35	1.5208	0.5813	7361.8
40	0.5163	0.1147	271735	75	0.8892	0.2960	25652
30	0.5205	0.1618	175249	125	0.7795	0.2396	-25158
20	0.5312	0.2028	225454	200	0.6527	0.2340	-192989

At temperature 60 ºC (μ = 0.032 Pa.s)

Speed (Hz)	C_s (x 10^{-7})	C_c	C_v	Pressure (bar)	C_s (x 10^{-7})	C_c	C_v
48	0.4845	0.0602	348712	35	1.2410	0.5583	-2791.1
40	0.4947	0.1040	380467	75	0.7690	0.2830	45786
30	0.4825	0.1099	513100	125	0.7111	0.2899	-184422
20	0.5398	0.1420	690220	200	0.6793	0.2729	-472915

At temperature 70 ºC (μ = 0.024 Pa.s)

Speed (Hz)	C_s (x 10^{-7})	C_c	C_v	Pressure (bar)	C_s (x 10^{-7})	C_c	C_v
48	0.4308	0.0925	195724	35	0.9941	0.2410	48028
40	0.4451	0.1355	167536	75	0.7103	0.1833	47263
30	0.4453	0.1012	366838	125	0.6453	0.1830	-143094
20	0.5357	0.1983	101063	200	0.6242	0.2988	-859199

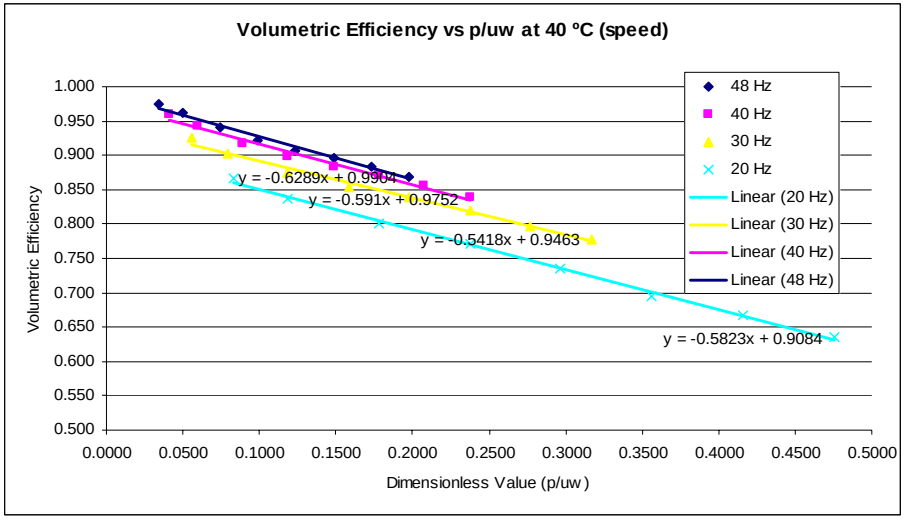
Volumetric Efficiency vs p/uw at 40 ºC (speed)
Volumetric Efficiency
Dimensionless Value (p/uw)
48 Hz
40 Hz
30 Hz
20 Hz
Linear (20 Hz)
Linear (30 Hz)
Linear (40 Hz)
Linear (48 Hz)
y = -0.6289x + 0.9904
y = -0.591x + 0.9752
y = -0.5418x + 0.9463
y = -0.5823x + 0.9084

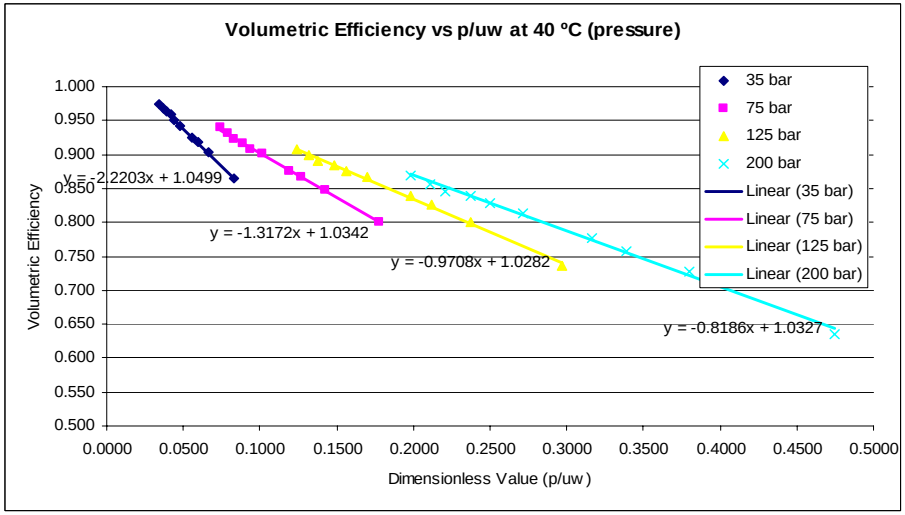
Volumetric Efficiency vs p/uw at 40 ºC (pressure)
Volumetric Efficiency
Dimensionless Value (p/uw)
35 bar
75 bar
125 bar
200 bar
Linear (35 bar)
Linear (75 bar)
Linear (125 bar)
Linear (200 bar)
y = -2.2203x + 1.0499
y = -1.3172x + 1.0342
y = -0.9708x + 1.0282
y = -0.8186x + 1.0327

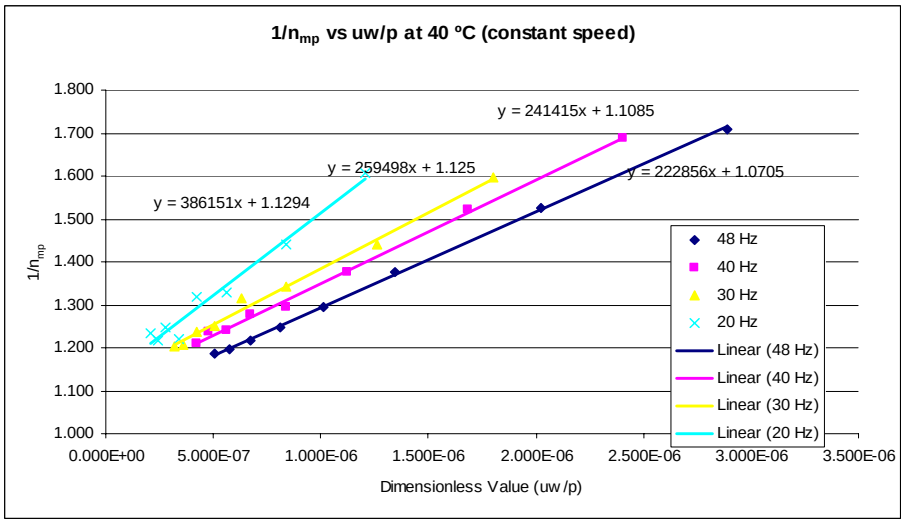
1/n_mp vs uw/p at 40 ºC (constant speed)
1/n_mp
Dimensionless Value (uw/p)
48 Hz
40 Hz
30 Hz
20 Hz
Linear (48 Hz)
Linear (40 Hz)
Linear (30 Hz)
Linear (20 Hz)
y = 241415x + 1.1085
y = 259498x + 1.125
y = 222856x + 1.0705
y = 386151x + 1.1294

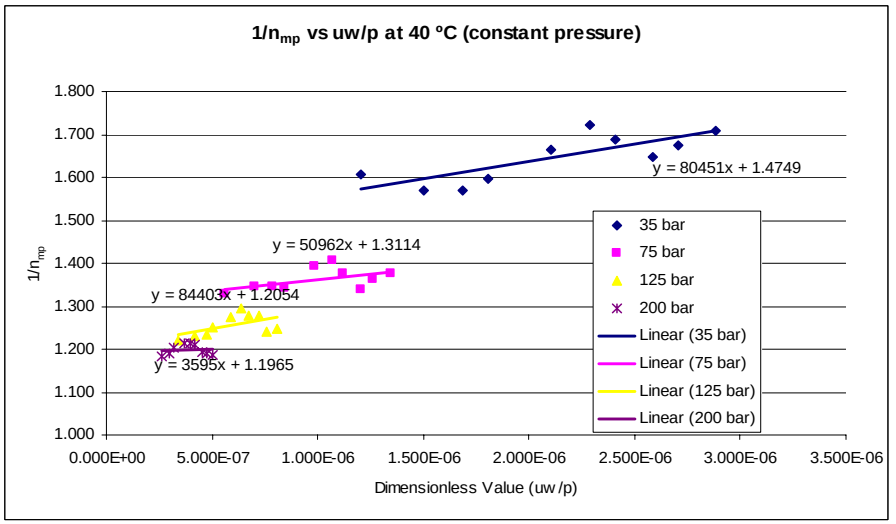
1/n_mp vs uw/p at 40 ºC (constant pressure)
1/n_mp
Dimensionless Value (uw/p)
35 bar
75 bar
125 bar
200 bar
Linear (35 bar)
Linear (75 bar)
Linear (125 bar)
Linear (200 bar)
y = 80451x + 1.4749
y = 50962x + 1.3114
y = 84403x + 1.2054
y = 3595x + 1.1965

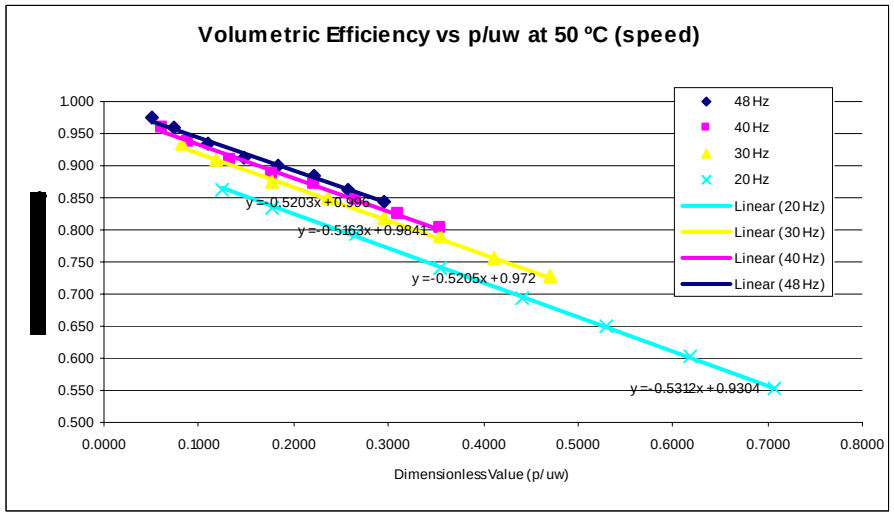
Volumetric Efficiency vs p/uw at 50 ºC (speed)
48 Hz
40 Hz
30 Hz
20 Hz
Linear (20 Hz)
Linear (30 Hz)
Linear (40 Hz)
Linear (48 Hz)
y = -0.5203x + 0.996
y = -0.5163x + 0.9841
y = -0.5205x + 0.972
y = -0.5312x + 0.9304
1.000
0.950
0.900
0.850
0.800
0.750
0.700
0.650
0.600
0.550
0.500
0.0000
0.1000
0.2000
0.3000
0.4000
0.5000
0.6000
0.7000
0.8000
Dimensionless Value (p/uw)

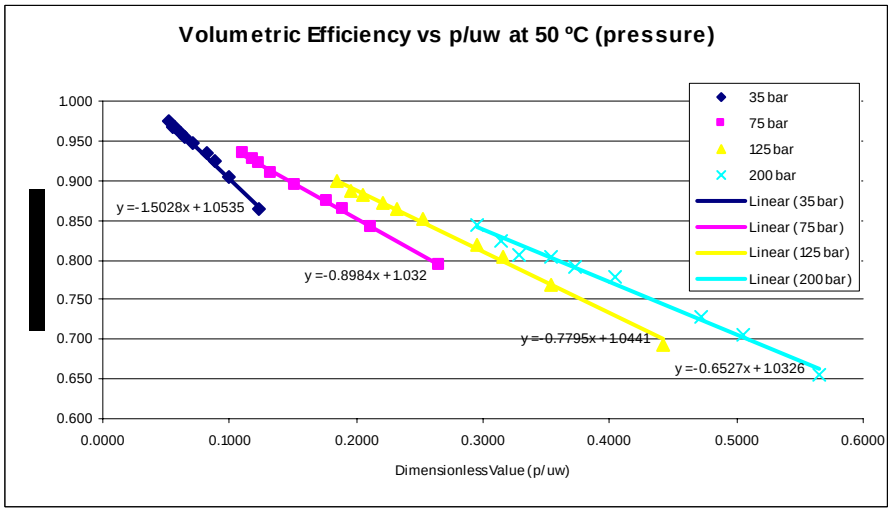
Volumetric Efficiency vs p/uw at 50 ºC (pressure)
35 bar
75 bar
125 bar
200 bar
Linear (35 bar)
Linear (75 bar)
Linear (125 bar)
Linear (200 bar)
y = -1.5028x + 1.0535
y = -0.8984x + 1.032
y = -0.7795x + 1.0441
y = -0.6527x + 1.0326
1.000
0.950
0.900
0.850
0.800
0.750
0.700
0.650
0.600
0.0000
0.1000
0.2000
0.3000
0.4000
0.5000
0.6000
Dimensionless Value (p/uw)

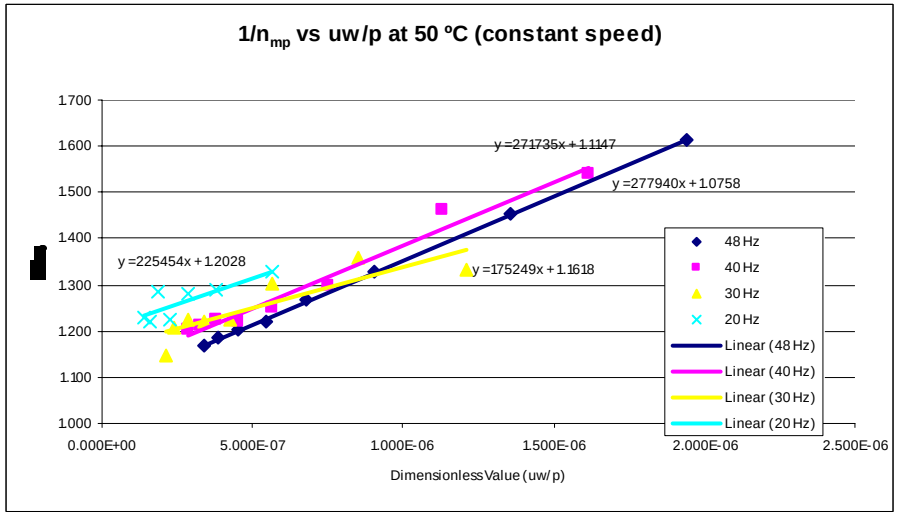
1/n_mp vs uw/p at 50 ºC (constant speed)
48 Hz
40 Hz
30 Hz
20 Hz
Linear (48 Hz)
Linear (40 Hz)
Linear (30 Hz)
Linear (20 Hz)
y = 271735x + 1.1147
y = 277940x + 1.0758
y = 225454x + 1.2028
y = 175249x + 1.1618
1.700
1.600
1.500
1.400
1.300
1.200
1.100
1.000
0.000E+00
5.000E-07
1.000E-06
1.500E-06
2.000E-06
2.500E-06
Dimensionless Value (uw/p)

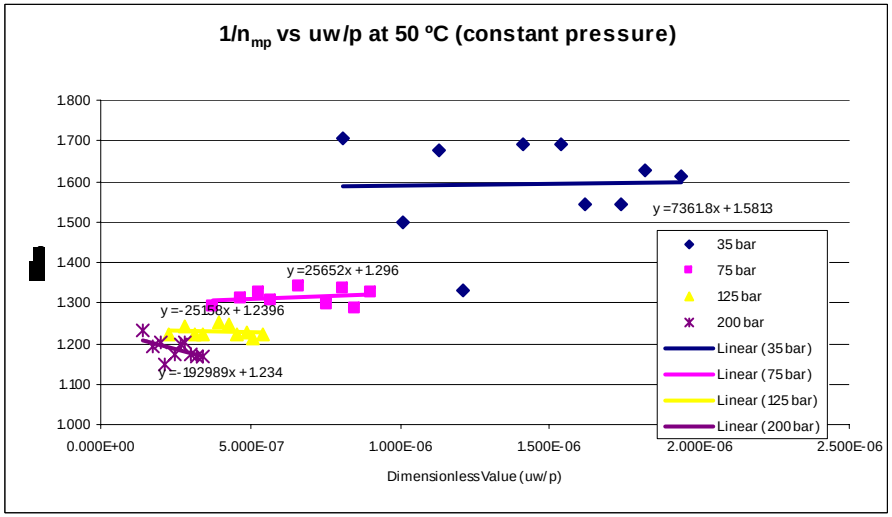
1/n_mp vs uw/p at 50 ºC (constant pressure)
35 bar
75 bar
125 bar
200 bar
Linear (35 bar)
Linear (75 bar)
Linear (125 bar)
Linear (200 bar)
y = 73618x + 1.5813
y = 25652x + 1.296
y = -25158x + 1.2396
y = -192989x + 1.234
1.800
1.700
1.600
1.500
1.400
1.300
1.200
1.100
1.000
0.000E+00
5.000E-07
1.000E-06
1.500E-06
2.000E-06
2.500E-06
Dimensionless Value (uw/p)

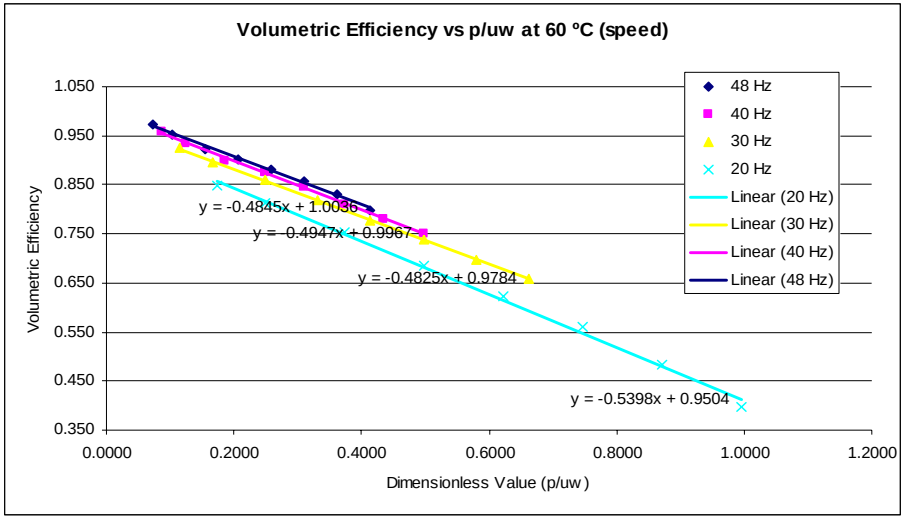
Volumetric Efficiency vs p/uw at 60 ºC (speed)
Volumetric Efficiency
Dimensionless Value (p/uw)
1.050
0.950
0.850
0.750
0.650
0.550
0.450
0.350
0.0000
0.2000
0.4000
0.6000
0.8000
1.0000
1.2000
y = -0.4845x + 1.0036
y = -0.4947x + 0.9967
y = -0.4825x + 0.9784
y = -0.5398x + 0.9504
48 Hz
40 Hz
30 Hz
20 Hz
Linear (20 Hz)
Linear (30 Hz)
Linear (40 Hz)
Linear (48 Hz)

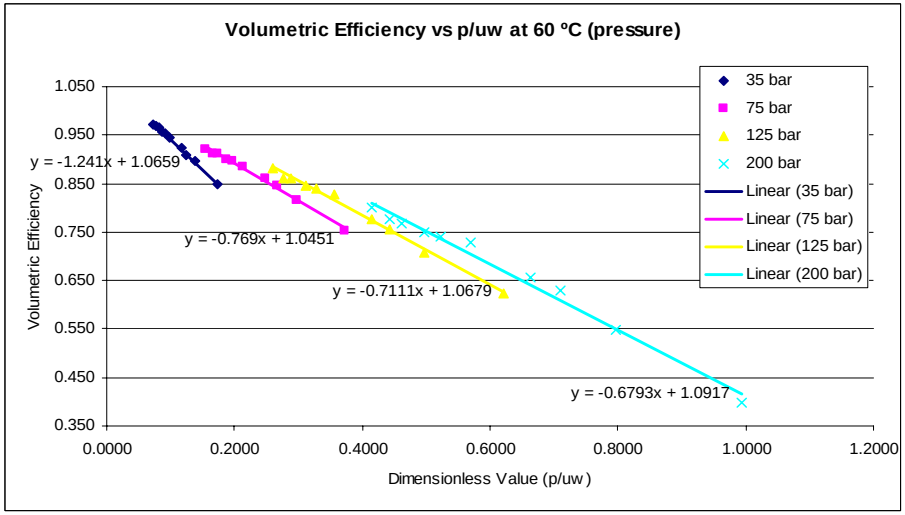
Volumetric Efficiency vs p/uw at 60 ºC (pressure)
Volumetric Efficiency
Dimensionless Value (p/uw)
1.050
0.950
0.850
0.750
0.650
0.550
0.450
0.350
0.0000
0.2000
0.4000
0.6000
0.8000
1.0000
1.2000
y = -1.241x + 1.0659
y = -0.769x + 1.0451
y = -0.7111x + 1.0679
y = -0.6793x + 1.0917
35 bar
75 bar
125 bar
200 bar
Linear (35 bar)
Linear (75 bar)
Linear (125 bar)
Linear (200 bar)

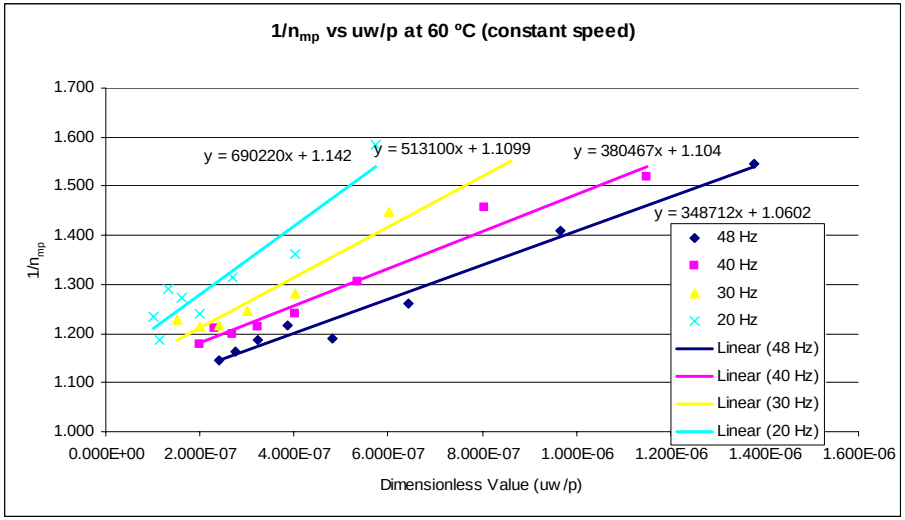
1/n_mp vs uw/p at 60 ºC (constant speed)
1/n_mp
Dimensionless Value (uw/p)
1.700
1.600
1.500
1.400
1.300
1.200
1.100
1.000
0.000E+00
2.000E-07
4.000E-07
6.000E-07
8.000E-07
1.000E-06
1.200E-06
1.400E-06
1.600E-06
y = 690220x + 1.142
y = 513100x + 1.1099
y = 380467x + 1.104
y = 348712x + 1.0602
48 Hz
40 Hz
30 Hz
20 Hz
Linear (48 Hz)
Linear (40 Hz)
Linear (30 Hz)
Linear (20 Hz)

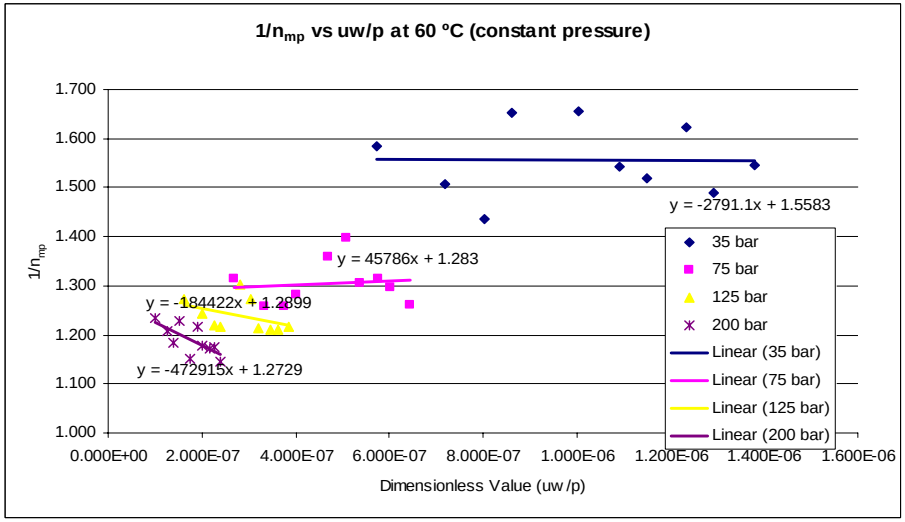
1/n_mp vs uw/p at 60 ºC (constant pressure)
1/n_mp
Dimensionless Value (uw/p)
1.700
1.600
1.500
1.400
1.300
1.200
1.100
1.000
0.000E+00
2.000E-07
4.000E-07
6.000E-07
8.000E-07
1.000E-06
1.200E-06
1.400E-06
1.600E-06
y = -2791.1x + 1.5583
y = 45786x + 1.283
y = -184422x + 1.2899
y = -472915x + 1.2729
35 bar
75 bar
125 bar
200 bar
Linear (35 bar)
Linear (75 bar)
Linear (125 bar)
Linear (200 bar)

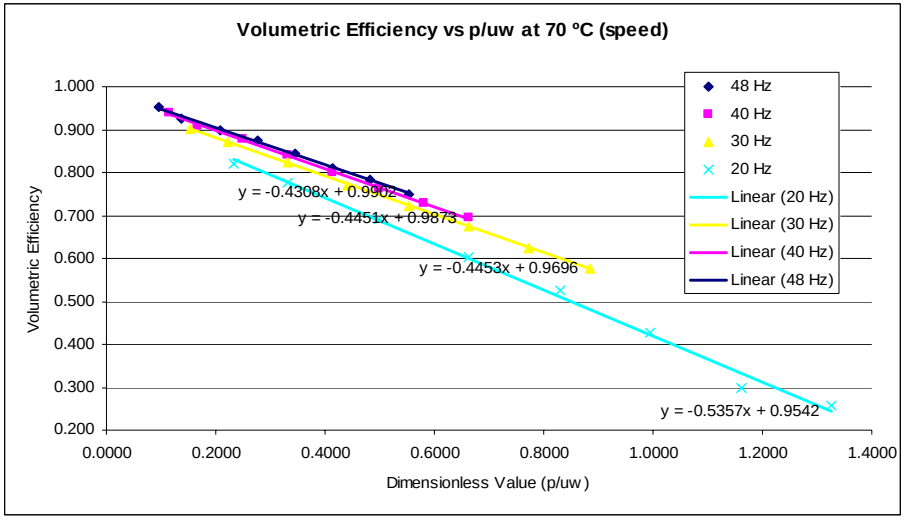
Volumetric Efficiency vs p/uw at 70 ºC (speed)
Volumetric Efficiency
Dimensionless Value (p/uw)
y = -0.4308x + 0.9902
y = -0.4451x + 0.9873
y = -0.4453x + 0.9696
y = -0.5357x + 0.9542
48 Hz
40 Hz
30 Hz
20 Hz
Linear (20 Hz)
Linear (30 Hz)
Linear (40 Hz)
Linear (48 Hz)

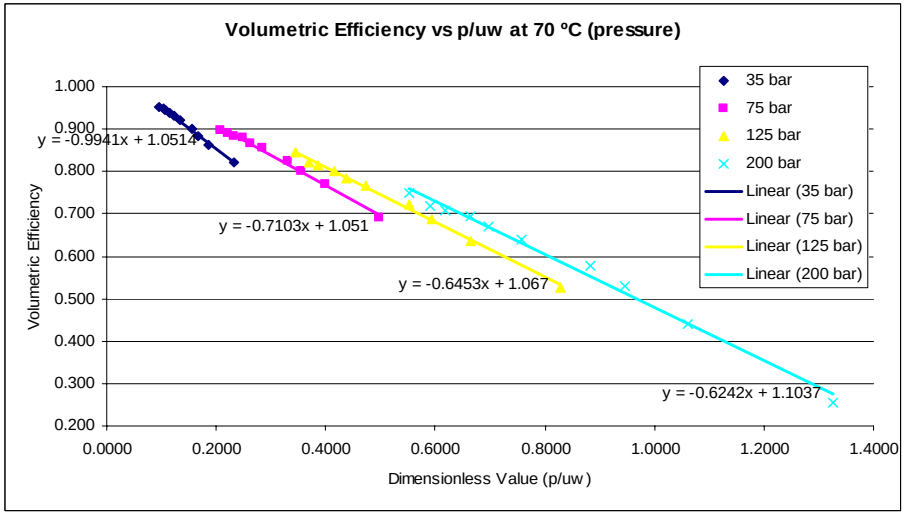
Volumetric Efficiency vs p/uw at 70 ºC (pressure)
Volumetric Efficiency
Dimensionless Value (p/uw)
y = -0.9941x + 1.0514
y = -0.7103x + 1.051
y = -0.6453x + 1.067
y = -0.6242x + 1.1037
35 bar
75 bar
125 bar
200 bar
Linear (35 bar)
Linear (75 bar)
Linear (125 bar)
Linear (200 bar)

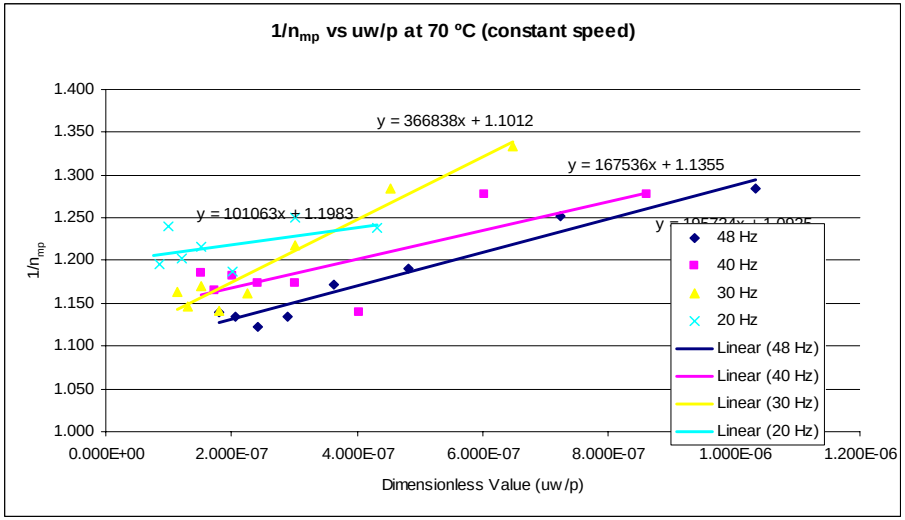
1/n_mp vs uw/p at 70 ºC (constant speed)
1/n_mp
Dimensionless Value (uw/p)
y = 366838x + 1.1012
y = 167536x + 1.1355
y = 101063x + 1.1983
48 Hz
40 Hz
30 Hz
20 Hz
Linear (48 Hz)
Linear (40 Hz)
Linear (30 Hz)
Linear (20 Hz)

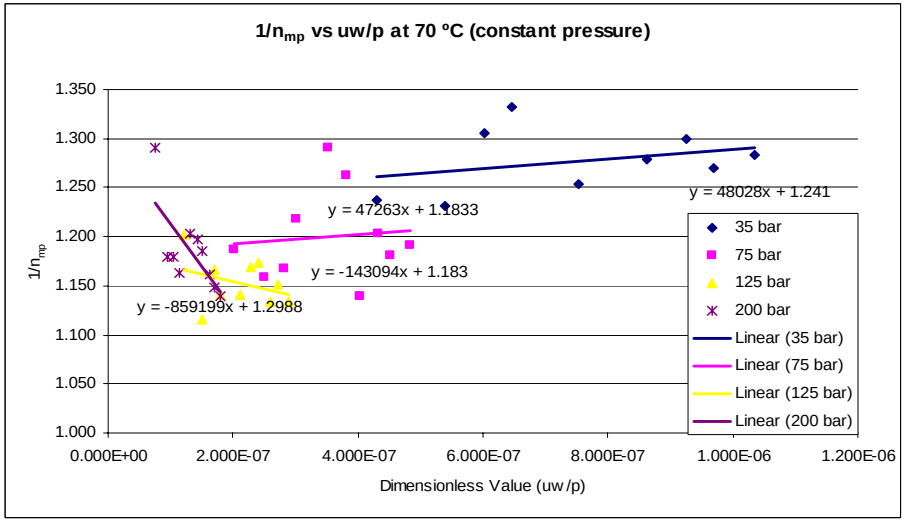
1/n_mp vs uw/p at 70 ºC (constant pressure)
1/n_mp
Dimensionless Value (uw/p)
y = 48028x + 1.241
y = 47263x + 1.1833
y = -143094x + 1.183
y = -859199x + 1.2988
35 bar
75 bar
125 bar
200 bar
Linear (35 bar)
Linear (75 bar)
Linear (125 bar)
Linear (200 bar)

Loss Coefficients Value for 300 hour.

At temperature 40 ºC (μ = 0.080 Pa.s)

Speed (Hz)	C_s (x 10^{-7})	C_c	C_v	Pressure (bar)	C_s (x 10^{-7})	C_c	C_v
48	0.6251	0.0837	230230	35	3.2096	0.6306	70083
40	0.5837	0.1051	260972	75	1.8271	0.3570	63146
30	0.4823	0.1092	324466	125	1.1185	0.2981	19413
20	0.4963	0.1339	411010	200	0.9145	0.2728	-83695

At temperature 50 ºC (μ = 0.053 Pa.s)

Speed (Hz)	C_s (x 10^{-7})	C_c	C_v	Pressure (bar)	C_s (x 10^{-7})	C_c	C_v
48	0.5282	0.0843	177824	35	1.8627	0.4359	46612
40	0.4875	0.1031	215333	75	1.0267	0.2405	54917
30	0.4537	0.1127	224803	125	0.7451	0.1901	40729
20	0.4836	0.1272	348590	200	0.6759	0.2530	-228865

At temperature 60 ºC (μ = 0.032 Pa.s)

Speed (Hz)	C_s (x 10^{-7})	C_c	C_v	Pressure (bar)	C_s (x 10^{-7})	C_c	C_v
48	0.4265	0.0750	296467	35	1.2141	0.4113	91029
40	0.4565	0.1010	364592	75	0.6639	0.2471	114614
30	0.4191	0.1514	252718	125	0.6461	0.2440	-77246
20	0.4875	0.1840	283836	200	0.5630	0.2137	-134865

At temperature 70 ºC (μ = 0.024 Pa.s)

Speed (Hz)	C_s (x 10^{-7})	C_c	C_v	Pressure (bar)	C_s (x 10^{-7})	C_c	C_v
48	0.4889	0.0870	239357	35	0.9220	0.2423	140068
40	0.4379	0.1293	254147	75	0.6293	0.1795	138221
30	0.4365	0.1344	231882	125	0.6410	0.2307	-207271
20	0.5449	0.1894	211802	200	0.6502	0.2710	-582735

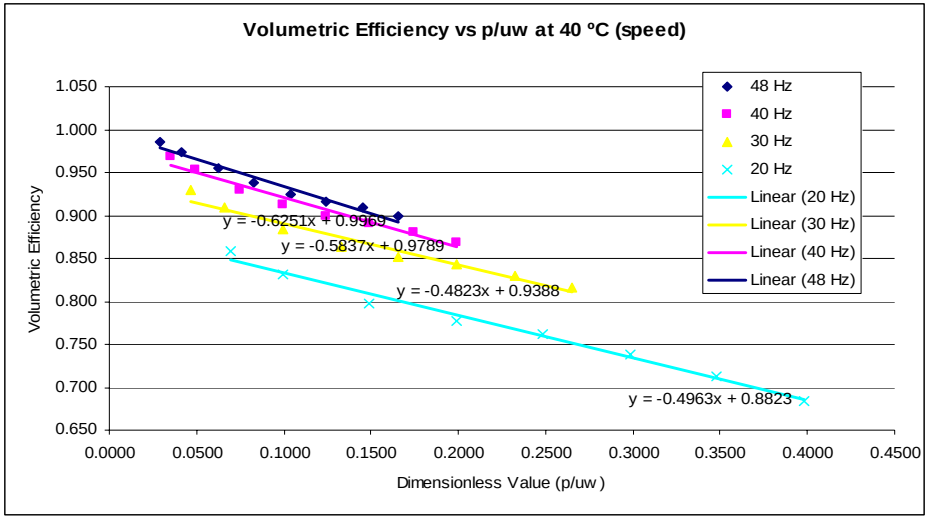
Volumetric Efficiency vs p/uw at 40 °C (speed)
Volumetric Efficiency
Dimensionless Value (p/uw)
48 Hz
40 Hz
30 Hz
20 Hz
Linear (20 Hz)
Linear (30 Hz)
Linear (40 Hz)
Linear (48 Hz)
y = -0.6251x + 0.9969
y = -0.5837x + 0.9789
y = -0.4823x + 0.9388
y = -0.4963x + 0.8823

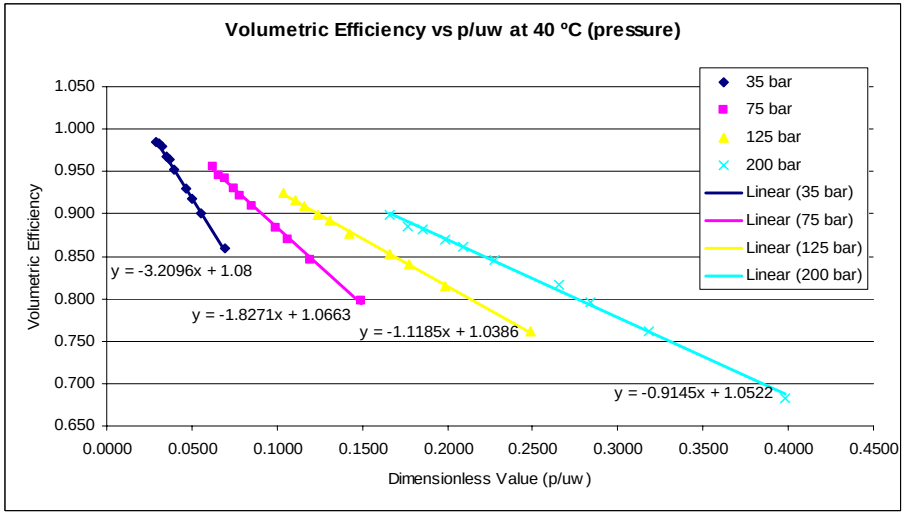
Volumetric Efficiency vs p/uw at 40 °C (pressure)
Volumetric Efficiency
Dimensionless Value (p/uw)
35 bar
75 bar
125 bar
200 bar
Linear (35 bar)
Linear (75 bar)
Linear (125 bar)
Linear (200 bar)
y = -3.2096x + 1.08
y = -1.8271x + 1.0663
y = -1.1185x + 1.0386
y = -0.9145x + 1.0522

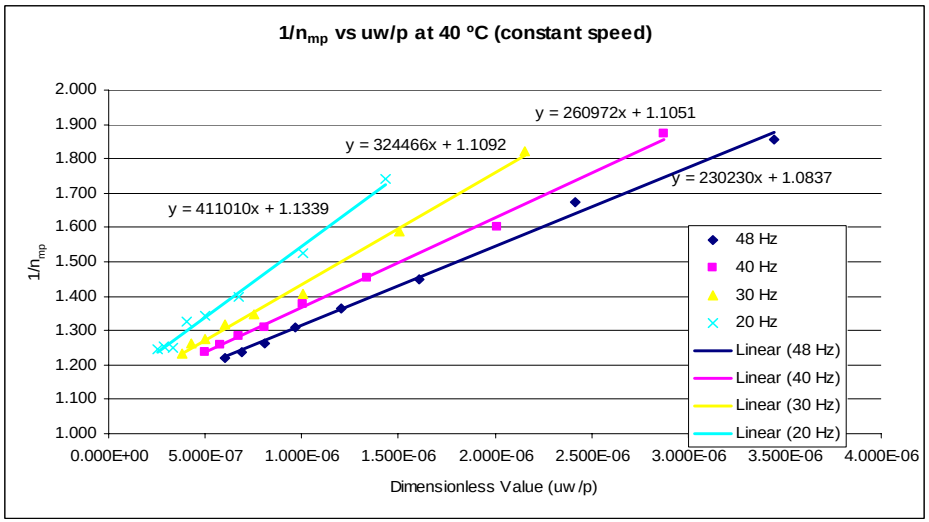
1/n_mp vs uw/p at 40 °C (constant speed)
1/n_mp
Dimensionless Value (uw/p)
48 Hz
40 Hz
30 Hz
20 Hz
Linear (48 Hz)
Linear (40 Hz)
Linear (30 Hz)
Linear (20 Hz)
y = 260972x + 1.1051
y = 324466x + 1.1092
y = 230230x + 1.0837
y = 411010x + 1.1339

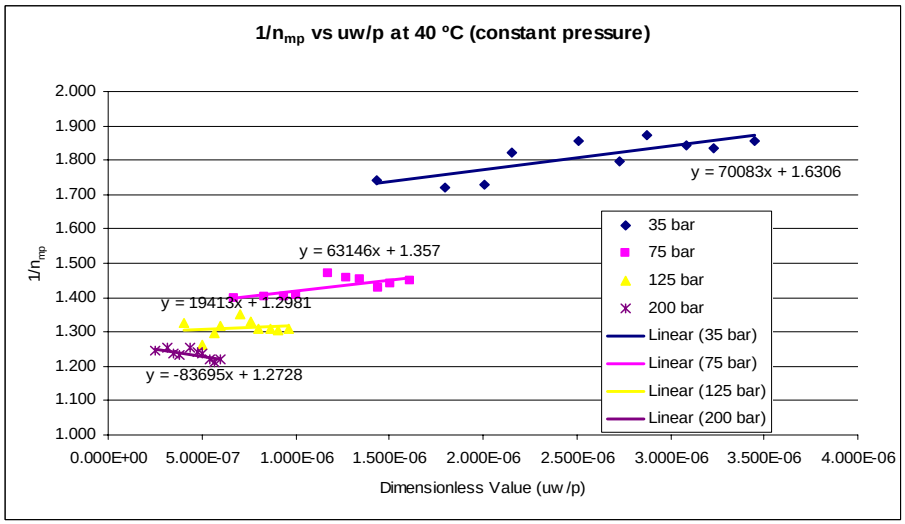
1/n_mp vs uw/p at 40 °C (constant pressure)
1/n_mp
Dimensionless Value (uw/p)
35 bar
75 bar
125 bar
200 bar
Linear (35 bar)
Linear (75 bar)
Linear (125 bar)
Linear (200 bar)
y = 70083x + 1.6306
y = 63146x + 1.357
y = 19413x + 1.2981
y = -83695x + 1.2728

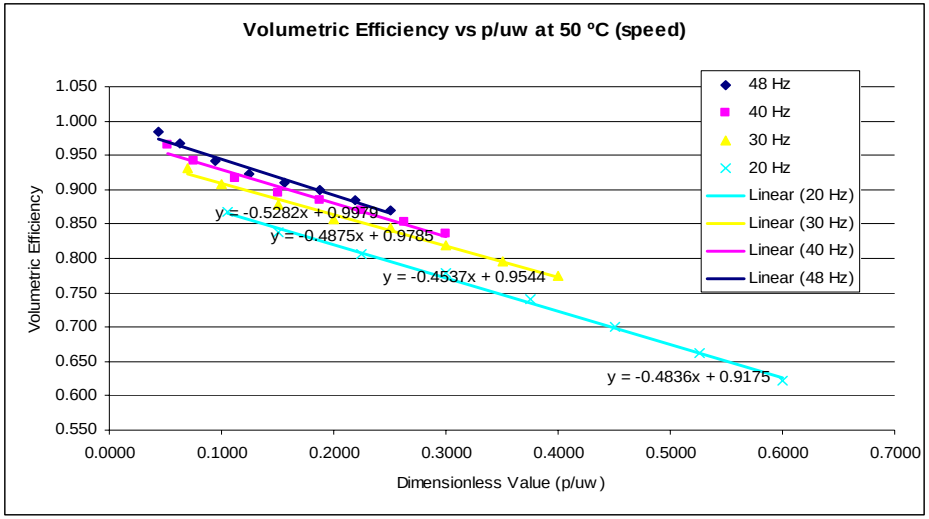
Volumetric Efficiency vs p/uw at 50 °C (speed)
Volumetric Efficiency
Dimensionless Value (p/uw)
48 Hz
40 Hz
30 Hz
20 Hz
Linear (20 Hz)
Linear (30 Hz)
Linear (40 Hz)
Linear (48 Hz)
y = -0.5282x + 0.9979
y = -0.4875x + 0.9785
y = -0.4537x + 0.9544
y = -0.4836x + 0.9175

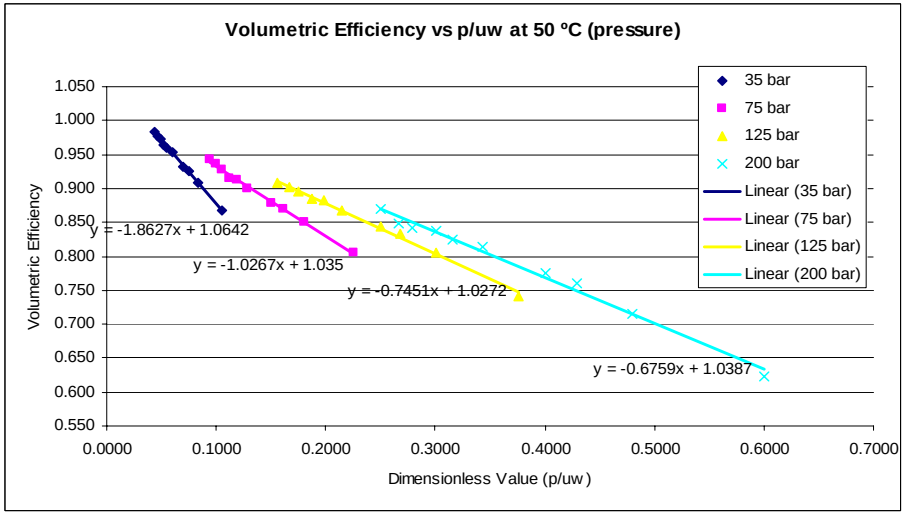
Volumetric Efficiency vs p/uw at 50 °C (pressure)
Volumetric Efficiency
Dimensionless Value (p/uw)
35 bar
75 bar
125 bar
200 bar
Linear (35 bar)
Linear (75 bar)
Linear (125 bar)
Linear (200 bar)
y = -1.8627x + 1.0642
y = -1.0267x + 1.035
y = -0.7451x + 1.0272
y = -0.6759x + 1.0387

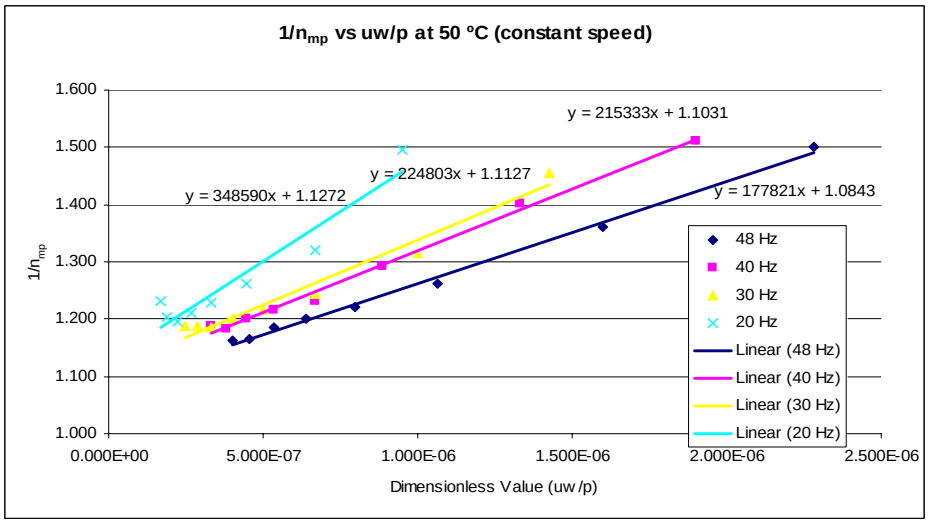
1/nmp vs uw/p at 50 °C (constant speed)
1/nmp
Dimensionless Value (uw/p)
48 Hz
40 Hz
30 Hz
20 Hz
Linear (48 Hz)
Linear (40 Hz)
Linear (30 Hz)
Linear (20 Hz)
y = 215333x + 1.1031
y = 224803x + 1.1127
y = 348590x + 1.1272
y = 177821x + 1.0843

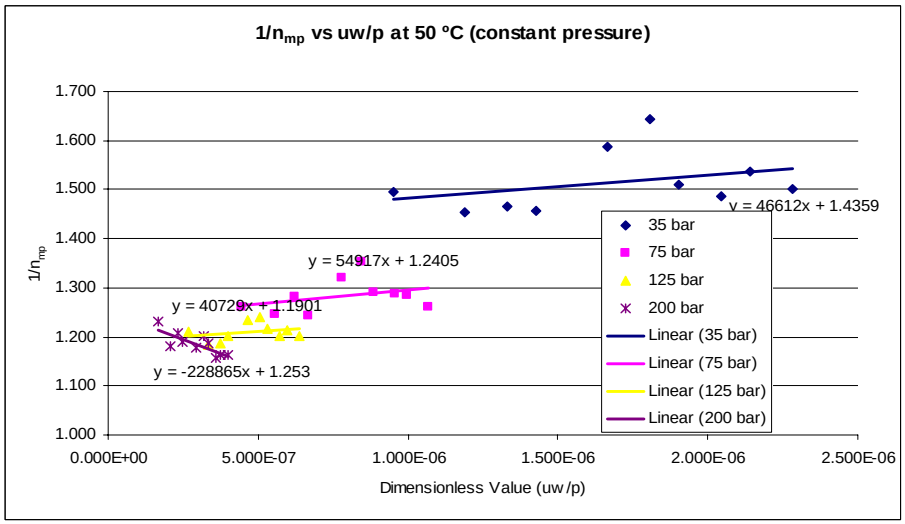
1/nmp vs uw/p at 50 °C (constant pressure)
1/nmp
Dimensionless Value (uw/p)
35 bar
75 bar
125 bar
200 bar
Linear (35 bar)
Linear (75 bar)
Linear (125 bar)
Linear (200 bar)
y = 46612x + 1.4359
y = 54917x + 1.2405
y = 40729x + 1.1901
y = -228865x + 1.253

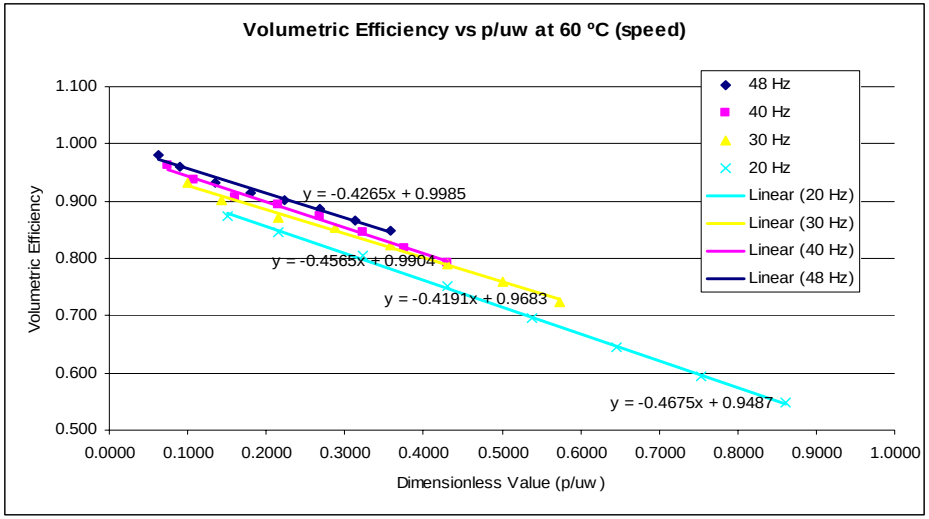
Volumetric Efficiency vs p/uw at 60 ºC (speed)
Volumetric Efficiency
Dimensionless Value (p/uw)
y = -0.4265x + 0.9985
y = -0.4565x + 0.9904
y = -0.4191x + 0.9683
y = -0.4675x + 0.9487
48 Hz
40 Hz
30 Hz
20 Hz
Linear (20 Hz)
Linear (30 Hz)
Linear (40 Hz)
Linear (48 Hz)

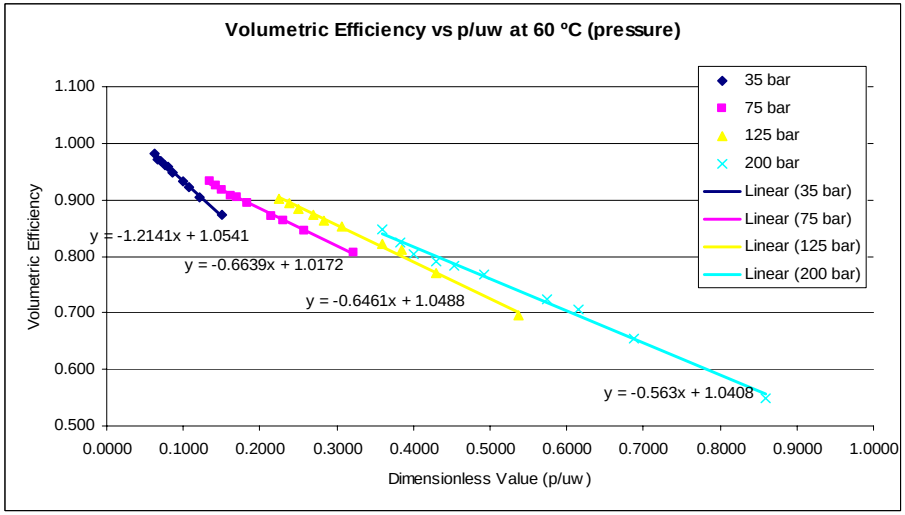
Volumetric Efficiency vs p/uw at 60 ºC (pressure)
Volumetric Efficiency
Dimensionless Value (p/uw)
y = -1.2141x + 1.0541
y = -0.6639x + 1.0172
y = -0.6461x + 1.0488
y = -0.563x + 1.0408
35 bar
75 bar
125 bar
200 bar
Linear (35 bar)
Linear (75 bar)
Linear (125 bar)
Linear (200 bar)

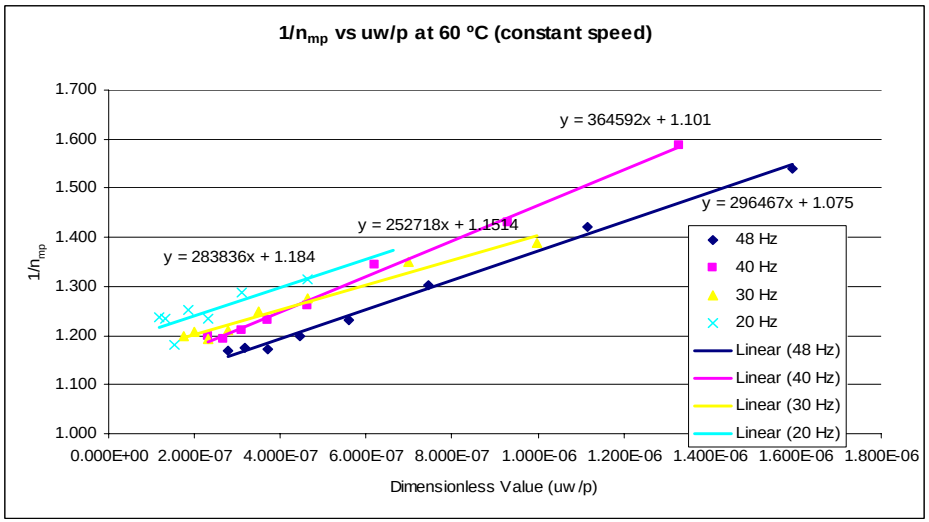
1/n_mp vs uw/p at 60 ºC (constant speed)
1/n_mp
Dimensionless Value (uw/p)
y = 364592x + 1.101
y = 296467x + 1.075
y = 252718x + 1.1514
y = 283836x + 1.184
48 Hz
40 Hz
30 Hz
20 Hz
Linear (48 Hz)
Linear (40 Hz)
Linear (30 Hz)
Linear (20 Hz)

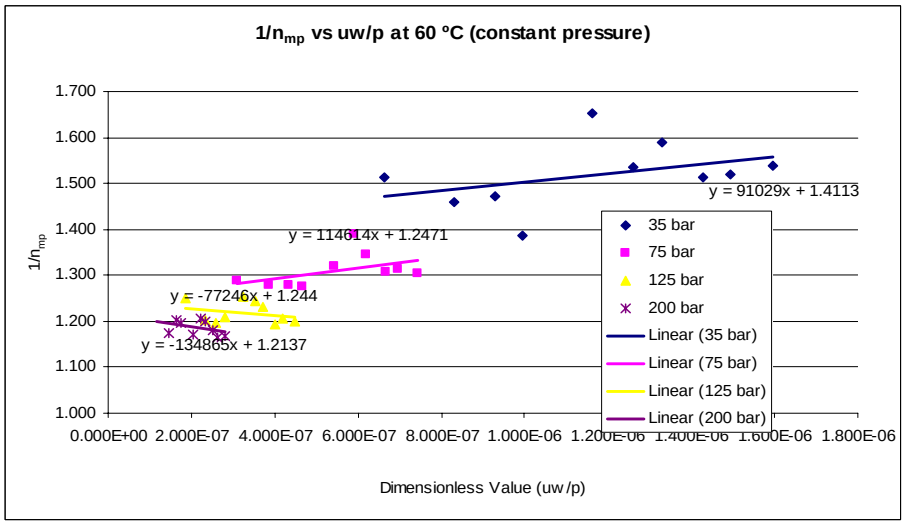
1/n_mp vs uw/p at 60 ºC (constant pressure)
1/n_mp
Dimensionless Value (uw/p)
y = 91029x + 1.4113
y = 114614x + 1.2471
y = -77246x + 1.244
y = -134865x + 1.2137
35 bar
75 bar
125 bar
200 bar
Linear (35 bar)
Linear (75 bar)
Linear (125 bar)
Linear (200 bar)

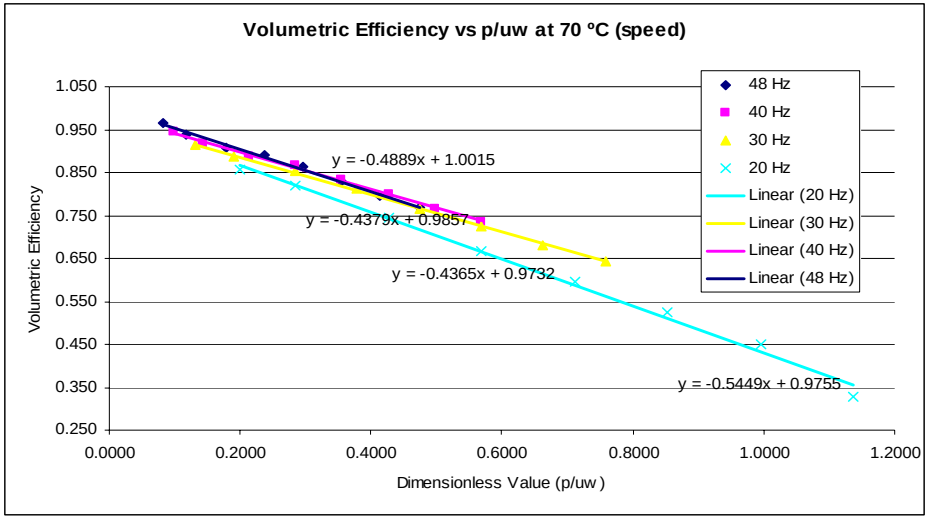
Volumetric Efficiency vs p/uw at 70 ºC (speed)
Volumetric Efficiency
Dimensionless Value (p/uw)
y = -0.4889x + 1.0015
y = -0.4379x + 0.9857
y = -0.4365x + 0.9732
y = -0.5449x + 0.9755
48 Hz
40 Hz
30 Hz
20 Hz
Linear (20 Hz)
Linear (30 Hz)
Linear (40 Hz)
Linear (48 Hz)

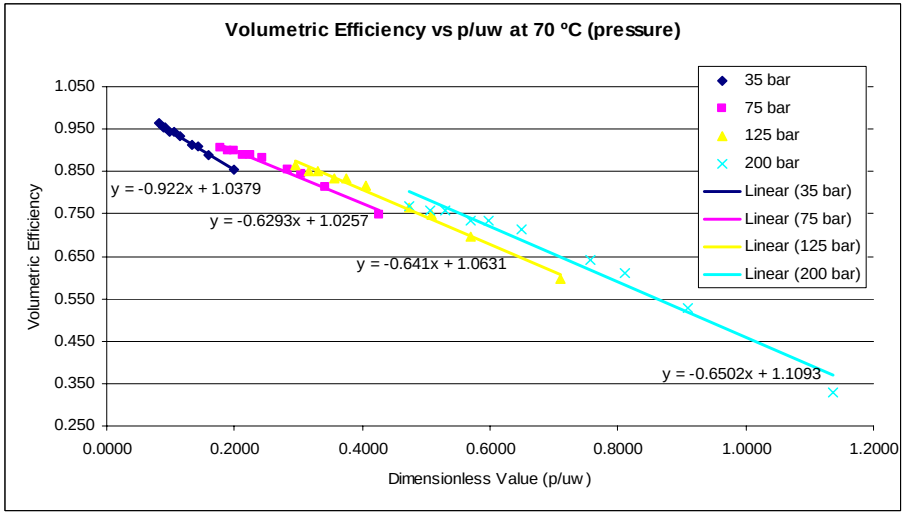
Volumetric Efficiency vs p/uw at 70 ºC (pressure)
Volumetric Efficiency
Dimensionless Value (p/uw)
y = -0.922x + 1.0379
y = -0.6293x + 1.0257
y = -0.641x + 1.0631
y = -0.6502x + 1.1093
35 bar
75 bar
125 bar
200 bar
Linear (35 bar)
Linear (75 bar)
Linear (125 bar)
Linear (200 bar)

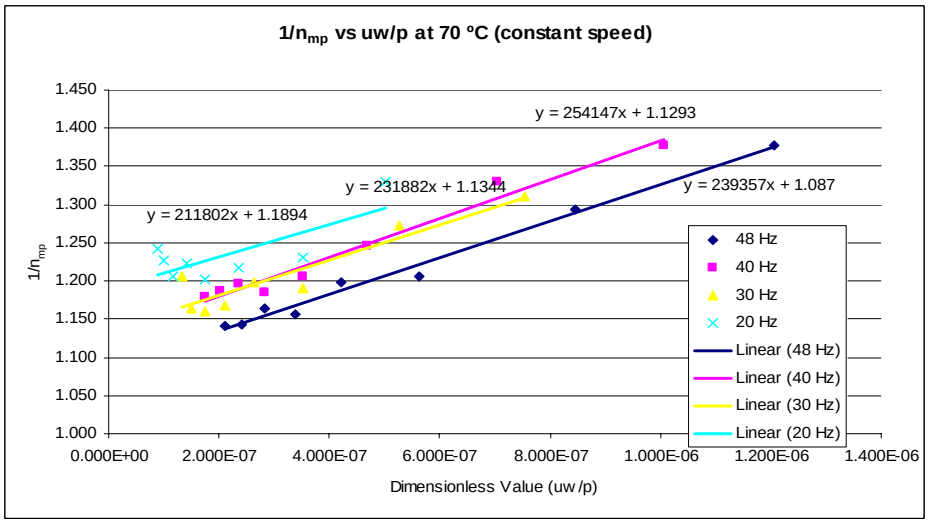
1/n_mp vs uw/p at 70 ºC (constant speed)
1/n_mp
Dimensionless Value (uw/p)
y = 254147x + 1.1293
y = 231882x + 1.1344
y = 239357x + 1.087
y = 211802x + 1.1894
48 Hz
40 Hz
30 Hz
20 Hz
Linear (48 Hz)
Linear (40 Hz)
Linear (30 Hz)
Linear (20 Hz)

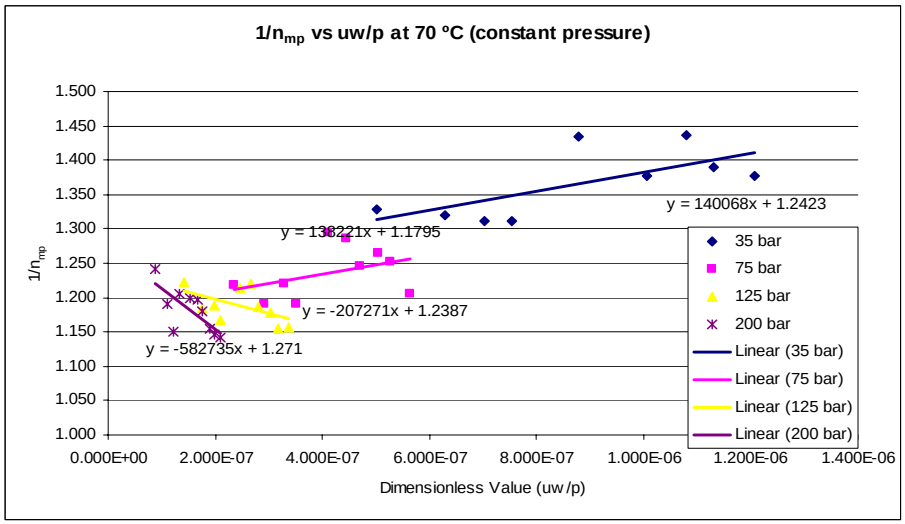
1/n_mp vs uw/p at 70 ºC (constant pressure)
1/n_mp
Dimensionless Value (uw/p)
y = 140068x + 1.2423
y = 138221x + 1.1795
y = -207271x + 1.2387
y = -582735x + 1.271
35 bar
75 bar
125 bar
200 bar
Linear (35 bar)
Linear (75 bar)
Linear (125 bar)
Linear (200 bar)

Loss Coefficients Value for 400 hour

At temperature 70 °C (μ = 0.033 Pa.s)

Speed (Hz)	C_s (x 10^{-7})	C_c	C_v	Pressure (bar)	C_s (x 10^{-7})	C_c	C_v
48	0.4009	0.0672	416755	35	1.3258	0.5270	72287
40	0.4373	0.1031	457057	75	0.7337	0.2949	98213
30	0.4502	0.1253	509958	125	0.7433	0.2669	-77722
20	0.5750	0.1471	726828	200	0.7490	0.3035	-479625

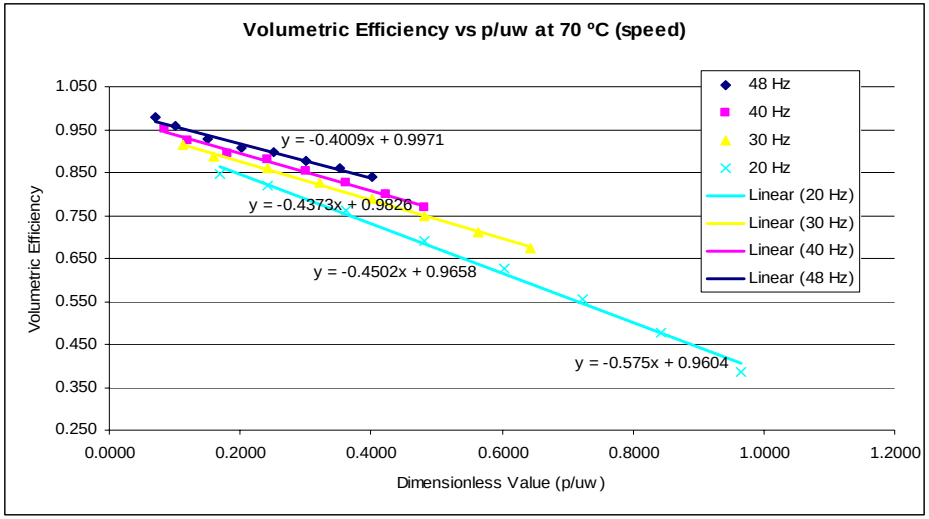
Volumetric Efficiency vs p/uw at 70 °C (speed)
Volumetric Efficiency
Dimensionless Value (p/uw)
y = -0.4009x + 0.9971
y = -0.4373x + 0.9826
y = -0.4502x + 0.9658
y = -0.575x + 0.9604
48 Hz
40 Hz
30 Hz
20 Hz
Linear (20 Hz)
Linear (30 Hz)
Linear (40 Hz)
Linear (48 Hz)

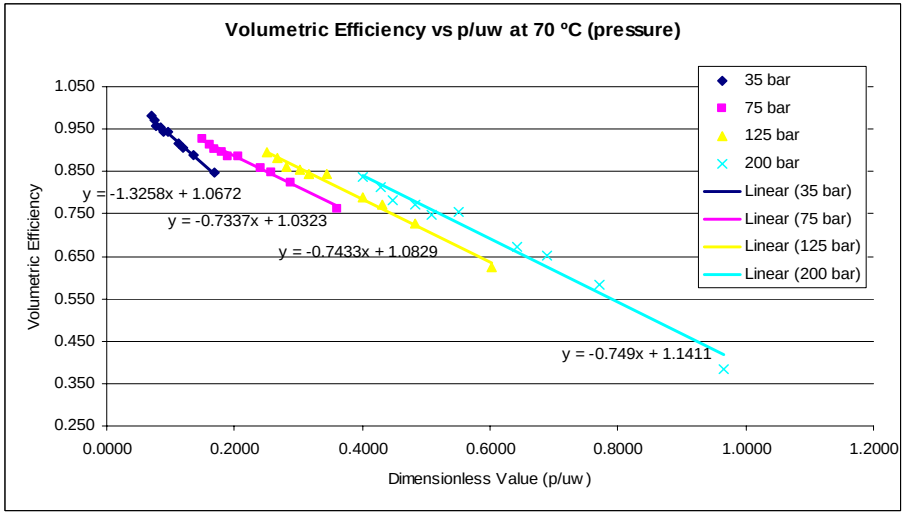
Volumetric Efficiency vs p/uw at 70 °C (pressure)
Volumetric Efficiency
Dimensionless Value (p/uw)
y = -1.3258x + 1.0672
y = -0.7337x + 1.0323
y = -0.7433x + 1.0829
y = -0.749x + 1.1411
35 bar
75 bar
125 bar
200 bar
Linear (35 bar)
Linear (75 bar)
Linear (125 bar)
Linear (200 bar)

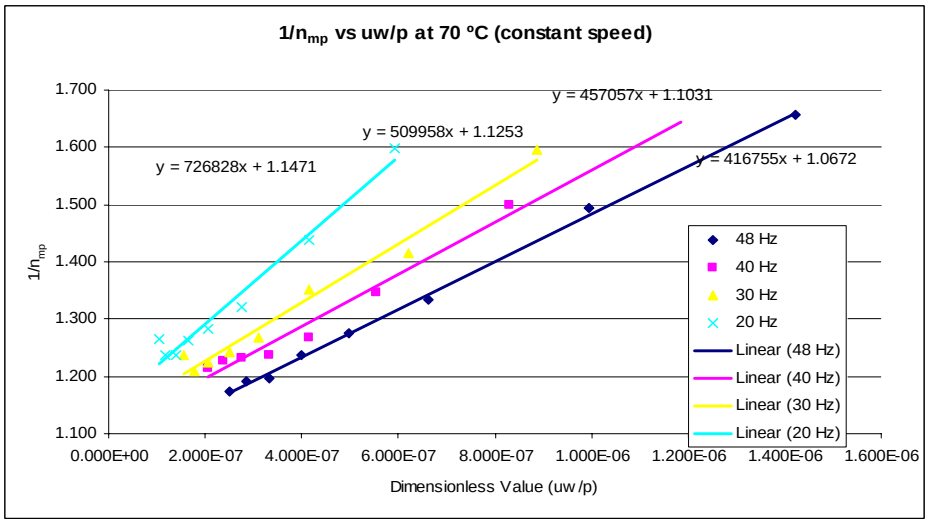
1/n_mp vs uw/p at 70 °C (constant speed)
1/n_mp
Dimensionless Value (uw/p)
y = 457057x + 1.1031
y = 509958x + 1.1253
y = 726828x + 1.1471
y = 416755x + 1.0672
48 Hz
40 Hz
30 Hz
20 Hz
Linear (48 Hz)
Linear (40 Hz)
Linear (30 Hz)
Linear (20 Hz)

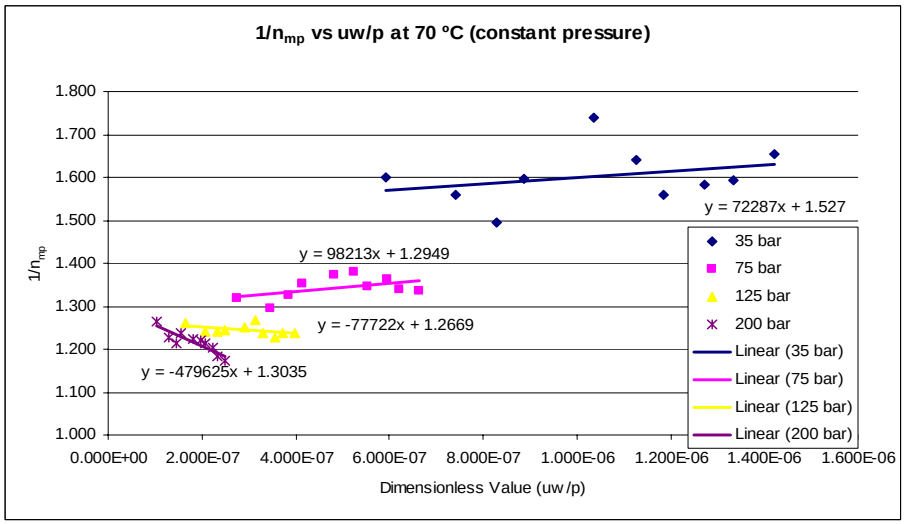
1/n_mp vs uw/p at 70 °C (constant pressure)
1/n_mp
Dimensionless Value (uw/p)
y = 72287x + 1.527
y = 98213x + 1.2949
y = -77722x + 1.2669
y = -479625x + 1.3035
35 bar
75 bar
125 bar
200 bar
Linear (35 bar)
Linear (75 bar)
Linear (125 bar)
Linear (200 bar)

Loss Coefficients Value for 900 hour.

At temperature 40ºC (μ = 0.137 Pa.s)

Speed (Hz)	C_s (x 10^{-7})	C_c	C_v	Pressure (bar)	C_s (x 10^{-7})	C_c	C_v
48	0.6351	0.0888	158417	30	6.2183	0.8570	48775
40	0.7380	0.1200	189550	50	4.2181	0.6138	64913
30	0.8225	0.0859	241416	100	2.4919	0.3829	17348
20	0.7988	0.1591	302254	150	1.9592	0.3556	-32328
				200	1.6658	0.3114	-37605

At temperature 50ºC (μ = 0.086 Pa.s)

Speed (Hz)	C_s (x 10^{-7})	C_c	C_v	Pressure (bar)	C_s (x 10^{-7})	C_c	C_v
48	0.7298	0.1091	233968	30	3.4502	0.8271	81537
40	0.7009	0.1232	293923	50	2.4407	0.5985	86579
30	0.6523	0.1475	313873	100	1.5724	0.3827	28429
20	0.7108	0.1905	430068	150	1.2480	0.3703	-75151
				200	1.0899	0.3289	-102030

At temperature 60ºC (μ = 0.059 Pa.s)

Speed (Hz)	C_s (x 10^{-7})	C_c	C_v	Pressure (bar)	C_s (x 10^{-7})	C_c	C_v
48	0.6337	0.1050	231722	30	2.2173	0.5873	87073
40	0.5944	0.1467	287682	50	1.6203	0.3929	105672
30	0.5807	0.1226	348098	100	1.0825	0.3175	18559
20	0.5819	0.1781	427460	150	0.8896	0.3250	-129908
				200	0.7750	0.3183	-201251

At temperature 70ºC (μ = 0.043 Pa.s)

Speed (Hz)	C_s (x 10^{-7})	C_c	C_v	Pressure (bar)	C_s (x 10^{-7})	C_c	C_v
48	0.5227	0.1046	289161	30	1.5911	0.4938	116539
40	0.5073	0.1548	329483	50	1.2075	0.3590	110418
30	0.5186	0.1386	384121	100	0.8616	0.2495	80229
20	0.5490	0.2070	435348	150	0.7497	0.3172	-168366
				200	0.6924	0.3325	-301731

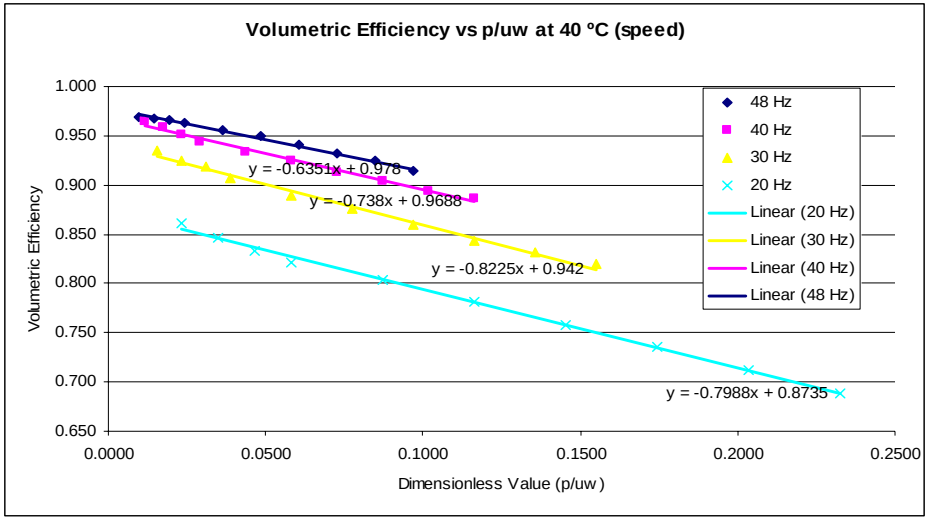
Volumetric Efficiency vs p/uw at 40 °C (speed)
Volumetric Efficiency
Dimensionless Value (p/uw)
y = -0.6351x + 0.978
y = -0.738x + 0.9688
y = -0.8225x + 0.942
y = -0.7988x + 0.8735
48 Hz
40 Hz
30 Hz
20 Hz
Linear (20 Hz)
Linear (30 Hz)
Linear (40 Hz)
Linear (48 Hz)

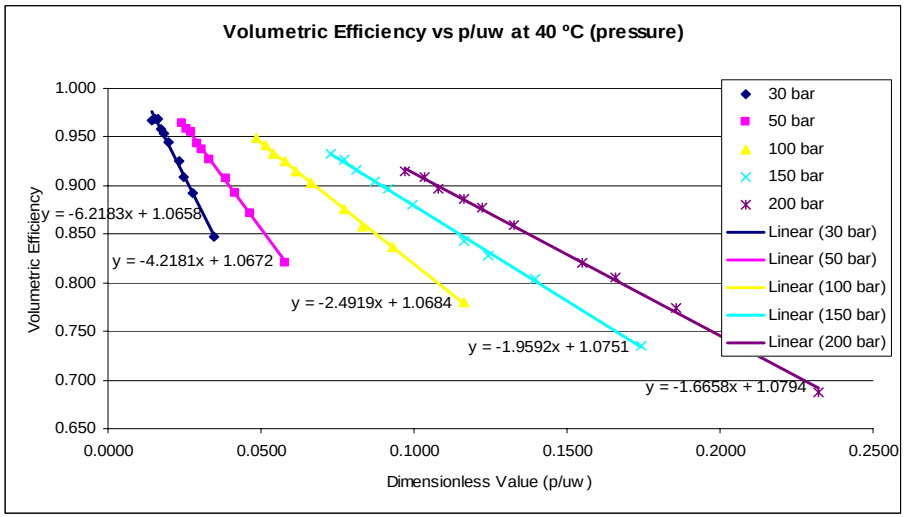
Volumetric Efficiency vs p/uw at 40 °C (pressure)
Volumetric Efficiency
Dimensionless Value (p/uw)
y = -6.2183x + 1.0658
y = -4.2181x + 1.0672
y = -2.4919x + 1.0684
y = -1.9592x + 1.0751
y = -1.6658x + 1.0794
30 bar
50 bar
100 bar
150 bar
200 bar
Linear (30 bar)
Linear (50 bar)
Linear (100 bar)
Linear (150 bar)
Linear (200 bar)

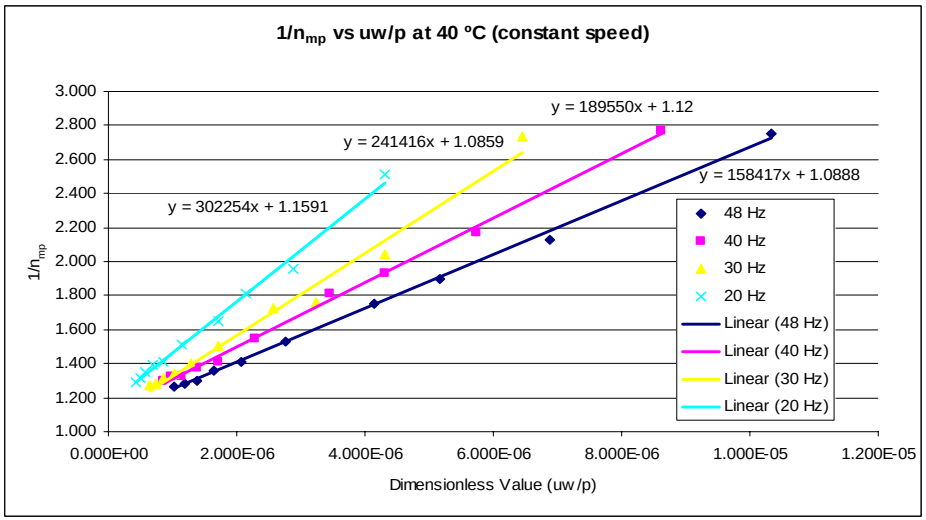
1/n_mp vs uw/p at 40 °C (constant speed)
1/n_mp
Dimensionless Value (uw/p)
y = 189550x + 1.12
y = 241416x + 1.0859
y = 158417x + 1.0888
y = 302254x + 1.1591
48 Hz
40 Hz
30 Hz
20 Hz
Linear (48 Hz)
Linear (40 Hz)
Linear (30 Hz)
Linear (20 Hz)

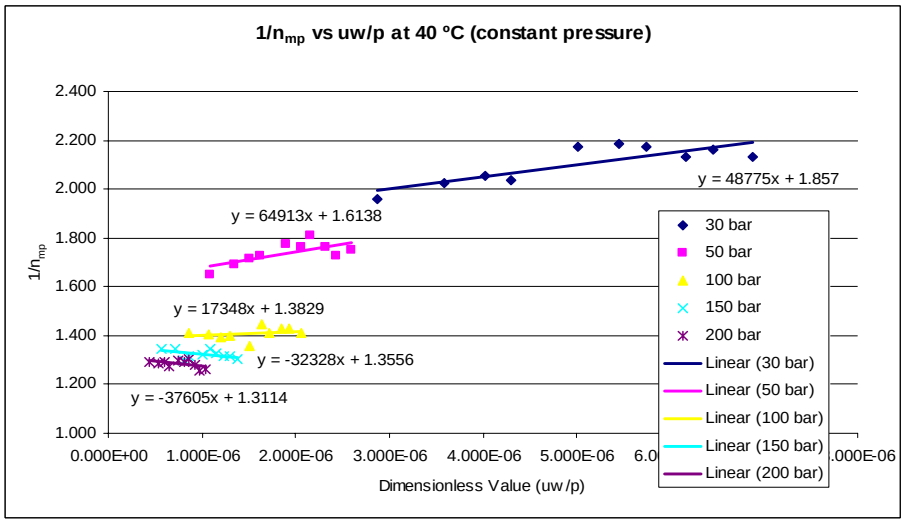
1/n_mp vs uw/p at 40 °C (constant pressure)
1/n_mp
Dimensionless Value (uw/p)
y = 48775x + 1.857
y = 64913x + 1.6138
y = 17348x + 1.3829
y = -32328x + 1.3556
y = -37605x + 1.3114
30 bar
50 bar
100 bar
150 bar
200 bar
Linear (30 bar)
Linear (50 bar)
Linear (100 bar)
Linear (150 bar)
Linear (200 bar)

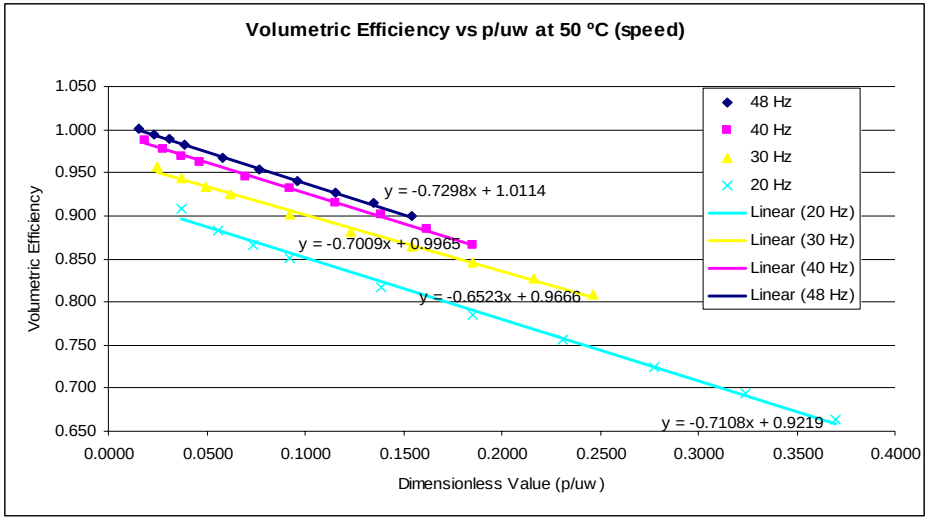
Volumetric Efficiency vs p/uw at 50 °C (speed)
Volumetric Efficiency
Dimensionless Value (p/uw)
y = -0.7298x + 1.0114
y = -0.7009x + 0.9965
y = -0.6523x + 0.9666
y = -0.7108x + 0.9219
48 Hz
40 Hz
30 Hz
20 Hz
Linear (20 Hz)
Linear (30 Hz)
Linear (40 Hz)
Linear (48 Hz)

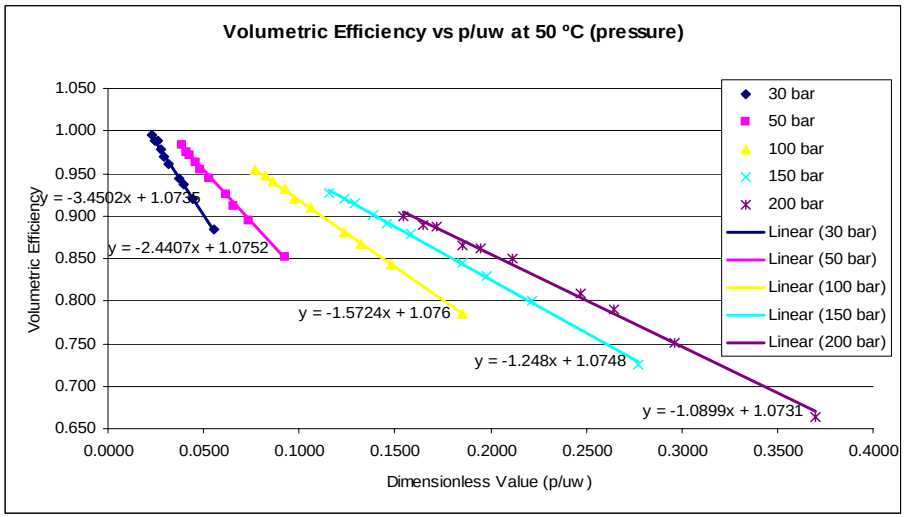
Volumetric Efficiency vs p/uw at 50 °C (pressure)
Volumetric Efficiency
Dimensionless Value (p/uw)
y = -3.4502x + 1.0735
y = -2.4407x + 1.0752
y = -1.5724x + 1.076
y = -1.248x + 1.0748
y = -1.0899x + 1.0731
30 bar
50 bar
100 bar
150 bar
200 bar
Linear (30 bar)
Linear (50 bar)
Linear (100 bar)
Linear (150 bar)
Linear (200 bar)

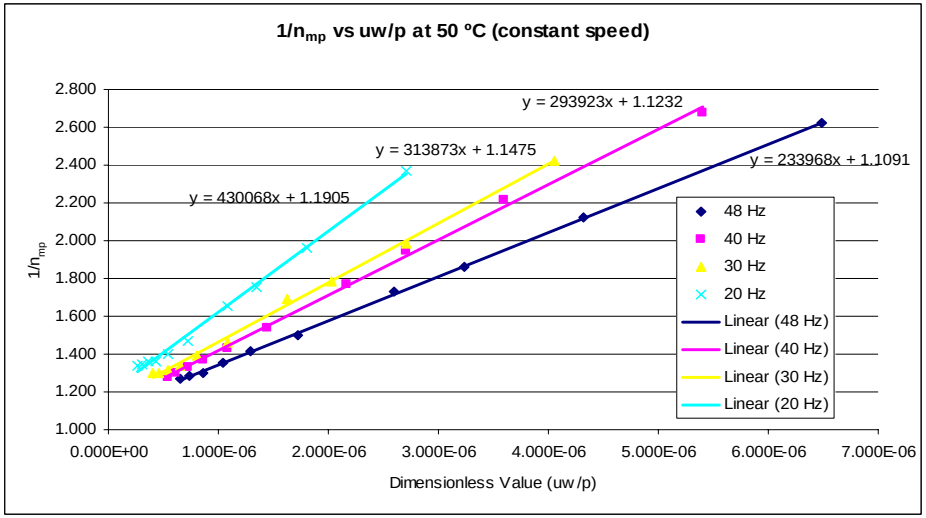
1/n_mp vs uw/p at 50 °C (constant speed)
1/n_mp
Dimensionless Value (uw/p)
y = 293923x + 1.1232
y = 313873x + 1.1475
y = 233968x + 1.1091
y = 430068x + 1.1905
48 Hz
40 Hz
30 Hz
20 Hz
Linear (48 Hz)
Linear (40 Hz)
Linear (30 Hz)
Linear (20 Hz)

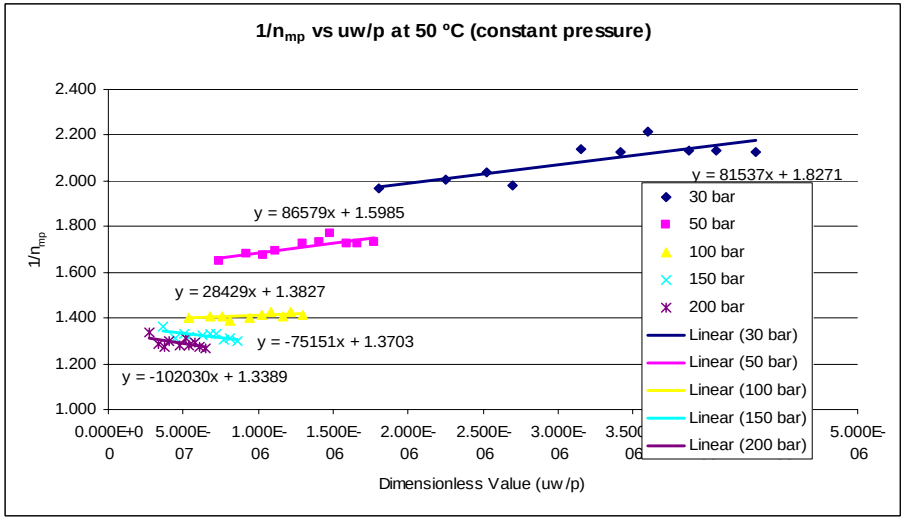
1/n_mp vs uw/p at 50 °C (constant pressure)
1/n_mp
Dimensionless Value (uw/p)
y = 81537x + 1.8271
y = 86579x + 1.5985
y = 28429x + 1.3827
y = -75151x + 1.3703
y = -102030x + 1.3389
30 bar
50 bar
100 bar
150 bar
200 bar
Linear (30 bar)
Linear (50 bar)
Linear (100 bar)
Linear (150 bar)
Linear (200 bar)

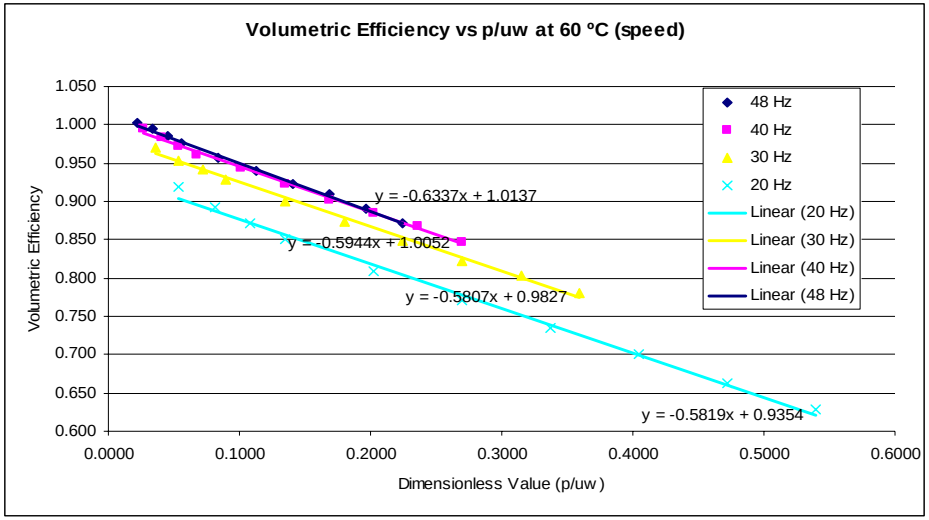
Volumetric Efficiency vs p/uw at 60 °C (speed)
Volumetric Efficiency
Dimensionless Value (p/uw)
y = -0.6337x + 1.0137
y = -0.5944x + 1.0052
y = -0.5807x + 0.9827
y = -0.5819x + 0.9354
48 Hz
40 Hz
30 Hz
20 Hz
Linear (20 Hz)
Linear (30 Hz)
Linear (40 Hz)
Linear (48 Hz)

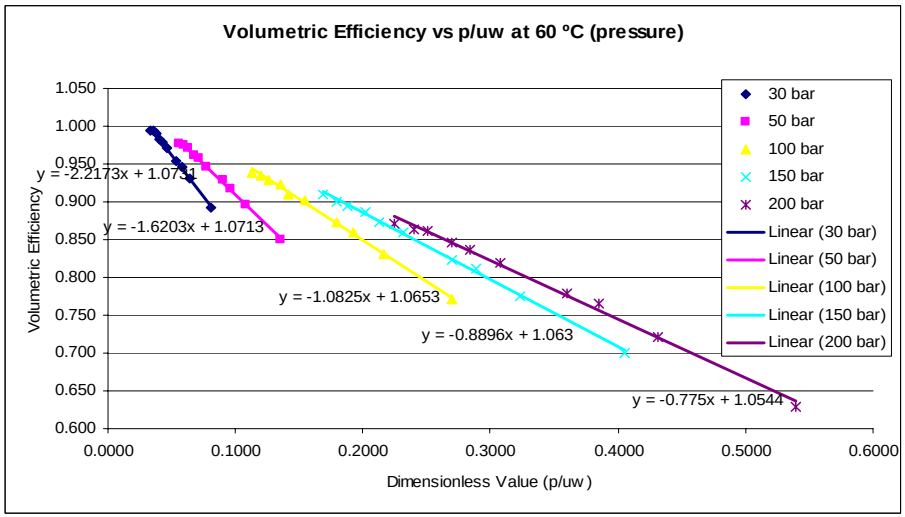
Volumetric Efficiency vs p/uw at 60 °C (pressure)
Volumetric Efficiency
Dimensionless Value (p/uw)
y = -2.2173x + 1.0731
y = -1.6203x + 1.0713
y = -1.0825x + 1.0653
y = -0.8896x + 1.063
y = -0.775x + 1.0544
30 bar
50 bar
100 bar
150 bar
200 bar
Linear (30 bar)
Linear (50 bar)
Linear (100 bar)
Linear (150 bar)
Linear (200 bar)

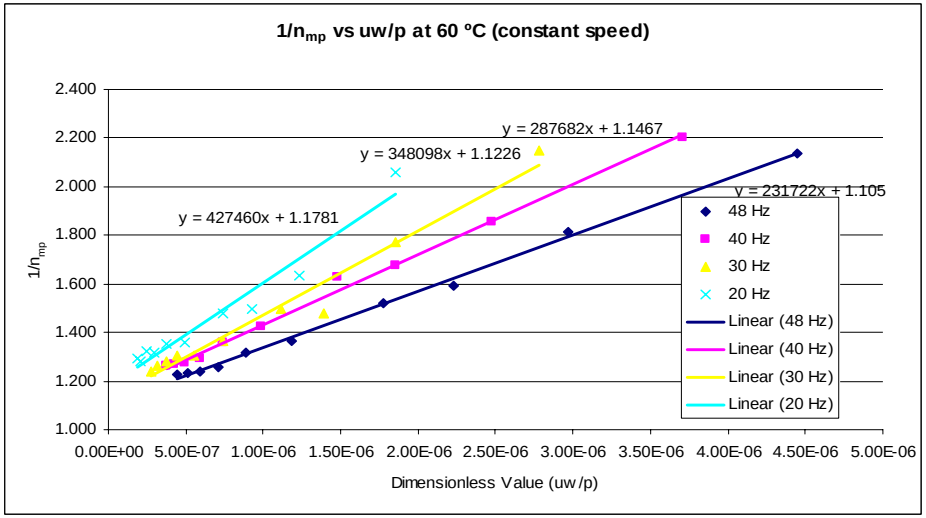
1/n_mp vs uw/p at 60 °C (constant speed)
1/n_mp
Dimensionless Value (uw/p)
y = 427460x + 1.1781
y = 348098x + 1.1226
y = 287682x + 1.1467
y = 231722x + 1.105
48 Hz
40 Hz
30 Hz
20 Hz
Linear (48 Hz)
Linear (40 Hz)
Linear (30 Hz)
Linear (20 Hz)

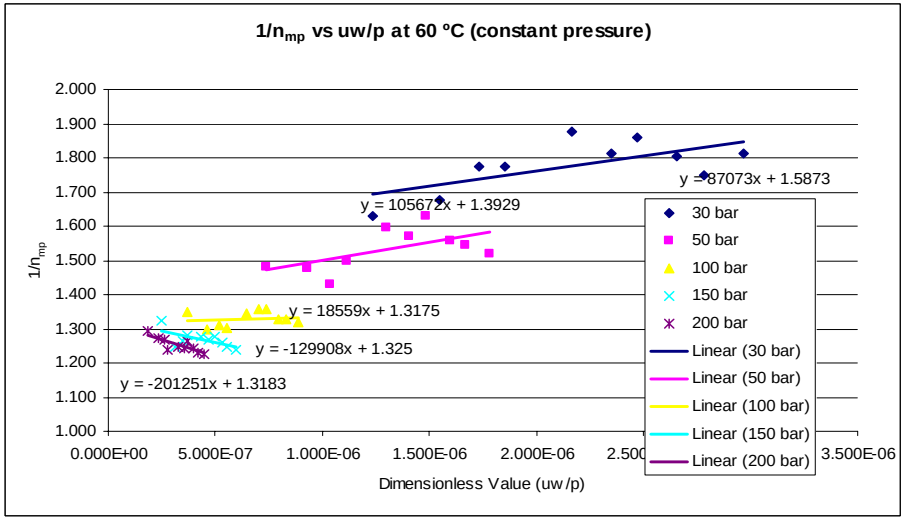
1/n_mp vs uw/p at 60 °C (constant pressure)
1/n_mp
Dimensionless Value (uw/p)
y = 87073x + 1.5873
y = 105672x + 1.3929
y = 18559x + 1.3175
y = -129908x + 1.325
y = -201251x + 1.3183
30 bar
50 bar
100 bar
150 bar
200 bar
Linear (30 bar)
Linear (50 bar)
Linear (100 bar)
Linear (150 bar)
Linear (200 bar)

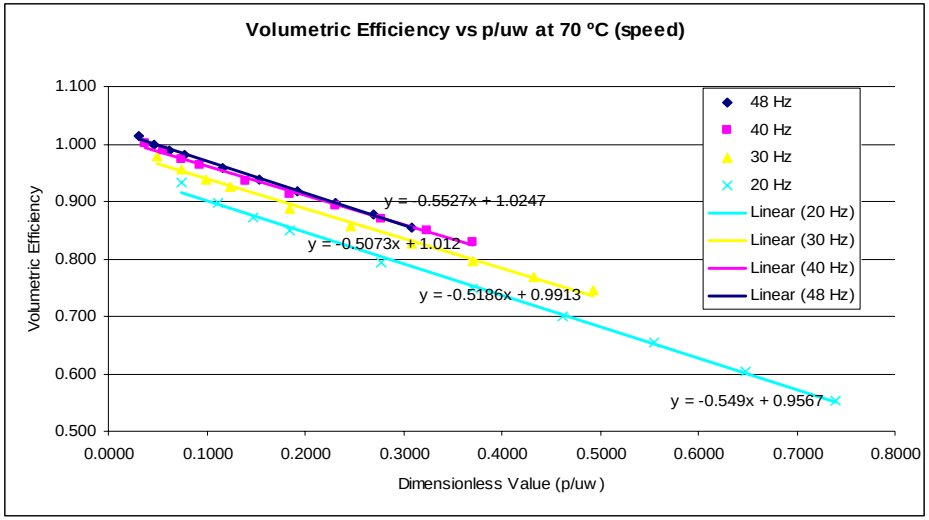
Volumetric Efficiency vs p/uw at 70 °C (speed)
Volumetric Efficiency
Dimensionless Value (p/uw)
1.100
1.000
0.900
0.800
0.700
0.600
0.500
0.0000
0.1000
0.2000
0.3000
0.4000
0.5000
0.6000
0.7000
0.8000
y = -0.5527x + 1.0247
y = -0.5073x + 1.012
y = -0.5186x + 0.9913
y = -0.549x + 0.9567
48 Hz
40 Hz
30 Hz
20 Hz
Linear (20 Hz)
Linear (30 Hz)
Linear (40 Hz)
Linear (48 Hz)

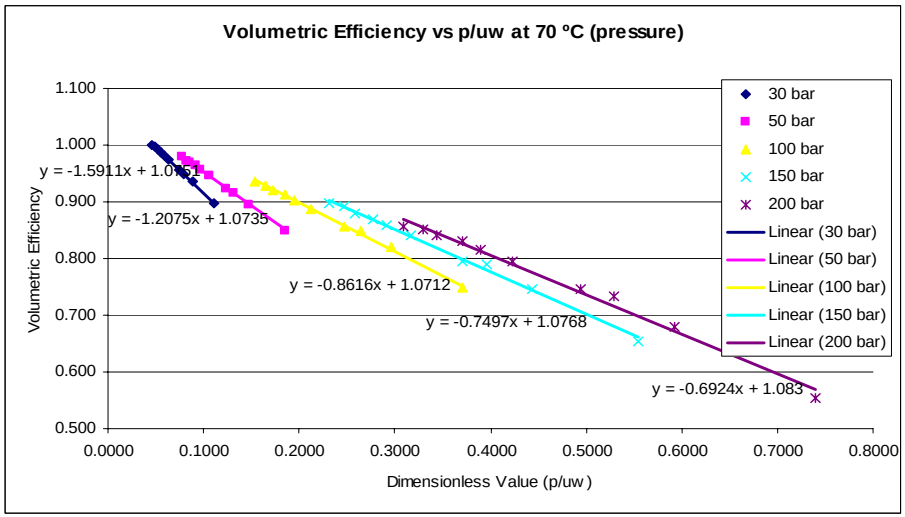
Volumetric Efficiency vs p/uw at 70 °C (pressure)
Volumetric Efficiency
Dimensionless Value (p/uw)
1.100
1.000
0.900
0.800
0.700
0.600
0.500
0.0000
0.1000
0.2000
0.3000
0.4000
0.5000
0.6000
0.7000
0.8000
y = -1.5911x + 1.0751
y = -1.2075x + 1.0735
y = -0.8616x + 1.0712
y = -0.7497x + 1.0768
y = -0.6924x + 1.083
30 bar
50 bar
100 bar
150 bar
200 bar
Linear (30 bar)
Linear (50 bar)
Linear (100 bar)
Linear (150 bar)
Linear (200 bar)

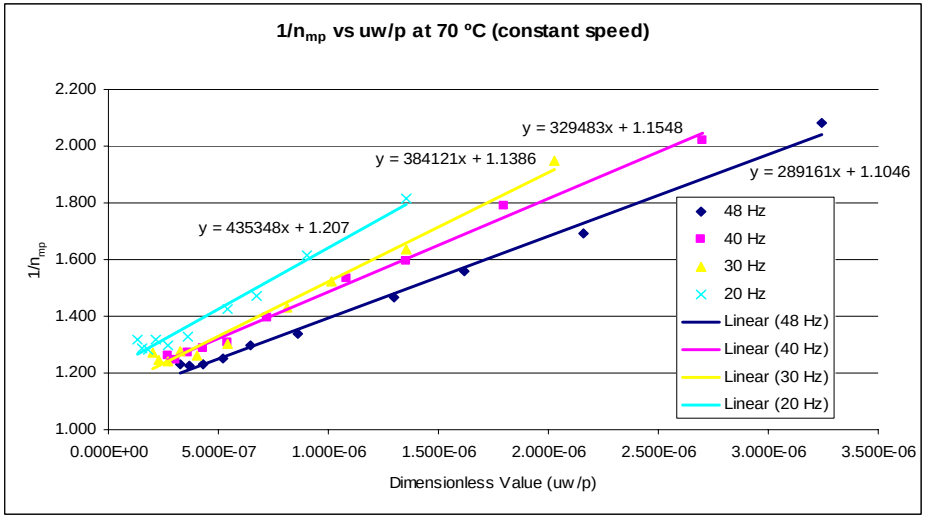
1/n_mp vs uw/p at 70 °C (constant speed)
1/n_mp
Dimensionless Value (uw/p)
2.200
2.000
1.800
1.600
1.400
1.200
1.000
0.000E+00
5.000E-07
1.000E-06
1.500E-06
2.000E-06
2.500E-06
3.000E-06
3.500E-06
y = 329483x + 1.1548
y = 384121x + 1.1386
y = 289161x + 1.1046
y = 435348x + 1.207
48 Hz
40 Hz
30 Hz
20 Hz
Linear (48 Hz)
Linear (40 Hz)
Linear (30 Hz)
Linear (20 Hz)

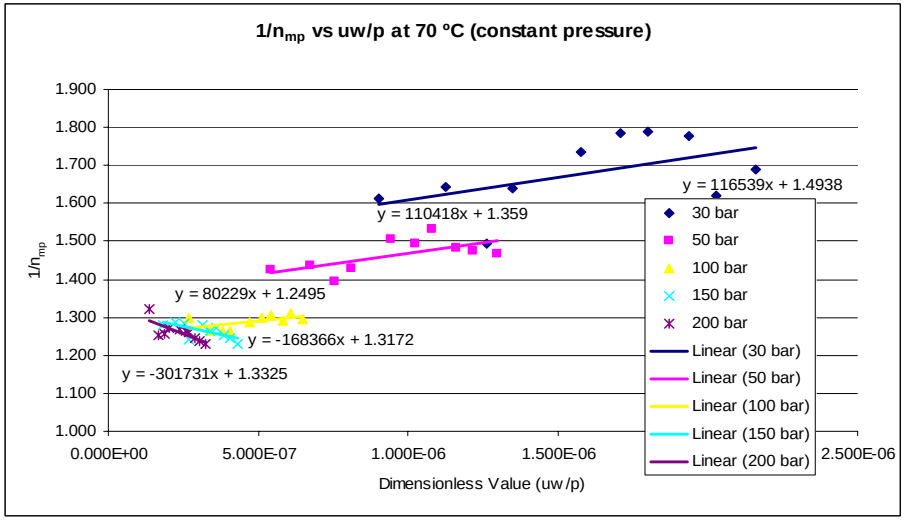
1/n_mp vs uw/p at 70 °C (constant pressure)
1/n_mp
Dimensionless Value (uw/p)
1.900
1.800
1.700
1.600
1.500
1.400
1.300
1.200
1.100
1.000
0.000E+00
5.000E-07
1.000E-06
1.500E-06
2.500E-06
y = 116539x + 1.4938
y = 110418x + 1.359
y = 80229x + 1.2495
y = -168366x + 1.3172
y = -301731x + 1.3325
30 bar
50 bar
100 bar
150 bar
200 bar
Linear (30 bar)
Linear (50 bar)
Linear (100 bar)
Linear (150 bar)
Linear (200 bar)

UNIVERSITI TEKNOLOGI MALAYSIA
Research Management Centre

PRELIMINARY IP SCREENING & TECHNOLOGY ASSESSMENT FORM

(To be completed by Project Leader submission of Final Report to RMC or whenever IP protection arrangement is required)

1. **PROJECT TITLE IDENTIFICATION** :

Performance Investigation of Energy Transport Media as Influenced by Crop Based Properties.

Vote No: 74033

2. **PROJECT LEADER** :

Name : Prof Dr Farid Nasir Ani

Address :

Jabatan Termo-Bendalir, Fakulti Kejuruteraan Mekanikal, Universiti Teknologi Malaysia, 81310 Skudai, Johor Darul Takzim.

Tel : 607-5534650 Fax : 607-5566159 e-mail : ***farid@fkm.utm.my***

3. **DIRECT OUTPUT OF PROJECT** *(Please tick where applicable)*

Scientific Research	Applied Research	Product/Process Development
☐ Algorithm	☑ Method/Technique	☑ Product / Component
☐ Structure	☐ Demonstration / Prototype	☐ Process
☑ Data		☐ Software
☐ Other, please specify	☐ Other, please specify	☐ Other, please specify
_____	_____	_____
_____	_____	_____
_____	_____	_____

4. INTELLECTUAL PROPERTY *(Please tick where applicable)*

☐	Not patentable	☐	Technology protected by patents
☐	Patent search required	☐	Patent pending
☐	Patent search completed and clean	☐	Monograph available
☑	Invention remains confidential	☐	Inventor technology champion
☐	No publications pending	☐	Inventor team player
☐	No prior claims to the technology	☐	Industrial partner identified

5. LIST OF EQUIPMENT BOUGHT USING THIS VOT

	Unit	Price/unit	Total Price (RM)
1. 128MB Memory Card	1	190.00	190.00
2. Battery NB-ILH	1	200.00	200.00
3. Pen Drive Apacer USB	1	222.00	222.00
4. Ammonia Unit Detector	1	850.00	850.00
5. Power Backup Battery (UPS)	1	930.00	930.00
6. Regulator Concoa	1	1,280.00	1,280.00
7. Riello Diesel Feul Burner	1	1,885.00	1,885.00
8. Canon IXUS Digital Camera	1	1,950.00	1,950.00
9. Pv2Ri Pump	1	1,960.00	1,960.00
10. Komputer Peribadi	1	2,752.00	2,752.00
11. Electrical Control Equiupments	1	4,700.00	4,700.00
12. Komputer Intel Pentium 4	1	5,888.00	5,888.00
13. Perisian Lab View Fds	1	6,812.00	6,812.00
14. Equipment for Pneumatic and Liquid Line	1	8,350.00	8,350.00
		Total	**25,750.00**

6. STATEMENT OF ACCOUNT

a) APPROVED FUNDING RM :

b) TOTAL SPENDING RM :

c) BALANCE RM :

7. TECHNICAL DESCRIPTION AND PERSPECTIVE

Please tick an executive summary of the new technology product, process, etc., describing how it works. Include brief analysis that compares it with competitive technology and signals the one that it may replace. Identify potential technology user group and the strategic means for exploitation.

a) Technology Description

Current energy transport fluid is of petroleum type. The oil is toxic, nonbiodegradable, and of limited source. It can not be assured in any application that the energy transport fluid does not leak, thus posing undesirable effect on the environment. Intensive researches in Europe and United States of America have produced energy transport fluids that pose less environmentally pollutant characteristics than conventional petroleum based oils. The development of the environmentally friendly fluid was resulted from coordinated efforts by universities, government bodies, product manufacturers and independent testing institutes. To date there are arrays of ester based hydraulic fluid products, an example of energy transport fluid, in the market (more than 20 different ester based oils). However, the studied crops are only the types available in the respective countries. Malaysia, to develop value added product from its natural resource, has to initiate its own basic research. At present, research in this area in Malaysia is minimal. Two engine oil brands in Malaysia are produced ‘on license’ and researched by foreign institutions. So, due to lack of comprehensive data and expertise in Malaysia, this project is crucial. Critical performance criteria such as power transmission, lubricating capability and base oil stability have to be investigated. Based fluid to be studied must come from local crop.

b) Market Potential

The project still need further research especially the hydraulic palm oil need to run more than 3000 hours to meet the international standard requirements.

c) Commercialisation Strategies

1. Collaborations with the local industries and the ministry of environment and various related departments is necessary in order to excess to information and the research carried out.
2. Universiti Teknologi Malaysia will invite the entrepreneurs and government agencies in demonstrating this product.
3. Participation in National and International Exhibition, such as INATEX Exhibition, ITEX Exhibition, and Geneva International Exhibition.

Signature of Projet Leader :- Date :-

_____ _____

8 RESEARCH PERFORMANCE EVALUATION

a) FACULTY RESEARCH COORDINATOR

Research Status	( )	( )	( )	( )	( )	( )
Spending	( )	( )	( )	( )	( )	( )
Overall Status	( )	( )	( )	( )	( )	( )
	Excellent	Very Good	Good	Satisfactory	Fair	Weak

Comment/Recommendations :

……

……..

…… Name : ……

Signature and stamp of JKPP Chairman Date : ……

b) RMC EVALUATION

Research Status	( )	( )	( )	( )	( )	( )
Spending	( )	( )	( )	( )	( )	( )
Overall Status	( )	( )	( )	( )	( )	( )
	Excellent	Very Good	Good	Satisfactory	Fair	Weak

Comments :-

_____

_____

_____

Recommendations :

Needs further research
Patent application recommended

Market without patent

No tangible product. Report to be filed as reference

…….. Name : ……

Signature and Stamp of Dean / Deputy Dean Date : ……

Research Management Centre